Title
Structural and Functional Characterization of the Tetrahymena Telomerase Holoenzyme

Author
Chan, Henry

Publication Date
2017

Peer reviewed|Thesis/dissertation

UNIVERSITY OF CALIFORNIA

Los Angeles

Structural and Functional Characterization of the *Tetrahymena* Telomerase Holoenzyme

A dissertation submitted in partial satisfaction of the

requirements for the degree Doctor of Philosophy

in Biochemistry and Molecular Biology

by

Henry Chan

2017

ABSTRACT OF THE DISSERTATION

Structural and Functional Characterization of the *Tetrahymena* Telomerase Holoenzyme

by

Henry Chan

Doctor of Philosophy in Biochemistry and Molecular Biology

University of California, Los Angeles, 2017

Professor Juli F. Feigon, Chair

This dissertation describes the structural characterization of the telomerase holoenzyme from the ciliate *Tetrahymena thermophila* using a combination of X-ray crystallography, cryogenic electron microscopy, and nuclear magnetic resonance spectroscopy. Telomerase is the ribonucleoprotein complex that iteratively reverse transcribes telomeric repeats to the ends of linear chromosomes in actively replicating eukaryotic cells. Previous biochemical and genetic studies of *Tetrahymena* telomerase holoenzyme identified the components TERT (the reverse transcriptase), TR (the internal RNA template), and six other accessory proteins (p65, Teb1, p50, p75, p45, and p19). Of these, p50, p75, p45, and p19 were largely uncharacterized and possessed no known homology to other proteins. A major focus of this work was to study p75-45-p19 which was known to form a trimeric complex. In the course of this work, crystal structures of p19 and the p45 C-terminal domain were solved and shown to be structurally homologous to the Ten1 and Stn1 proteins of the Replication Protein A (RPA)-like telomeric Ctc1-Stn1-Ten1 (CST) complex that is found in plants, vertebrates, and yeast, leading to the conclusion that p75-p45-p19 is *Tetrahymena* CST. In addition, the ongoing structural characterization of the p75 protein is discussed, in which a

specific interaction between p75 and p50 is identified. The work in this thesis also contributed to the overall structural characterization of the entire holoenzyme through an electron microscopy (EM) collaboration with the Zhou lab where negative stain and cryogenic EM (cryo-EM) structures of *Tetrahymena* telomerase were solved to 25 and 9 Å resolution respectively. These EM structures led to the characterization and unambiguous placement of all of the then known subunits including the placement of a homology model of the p75-p45-p19 trimeric core, based on the structure of p19 and the structure of the RPA trimeric core, into the cryo-EM structure, further confirming the characterization of p75-p45-p19 as *Tetrahymena* CST. The cryo-EM structure also led to the identification of two new subunits Teb2 and Teb3 by mass spectrometry, which were determined to form another trimeric RPA-like subcomplex, TEB, with Teb1. The identification and characterization of these TEB proteins led to the discovery that Teb2 and Teb3 are shared subunits with *Tetrahymena* RPA and of a new RPA-like protein, Rlp2, which forms an alternative complex with Teb3.

The dissertation of Henry Chan is approved.

Robert Clubb

Feng Guo

Juli F. Feigon, Committee Chair

University of California, Los Angeles

2017

Dedicated to my mother.

TABLE OF CONTENTS

LIST OF FIGURES

Chapter 5:

Chapter 6 (reprinted):

LIST OF TABLES

ACKNOWLEDGEMENTS

First and foremost, I would like to thank my advisor, Professor Juli Feigon, for her guidance, mentorship, and help during my tenure as a graduate student. The work presented in this dissertation would not be possible without her continuous support. The training, resources, and motivation she has provided was invaluable and has made me a better scientist.

Furthermore, I would like to thank Professors Doug Black, Steven Clarke, Robert Clubb, and Feng Guo for serving as my committee members. Their continual guidance, comments, and suggestions are greatly appreciated.

Other current and past members of the Feigon Lab have also played an instrumental role in my development as a scientist. I would like to thank Dr. Jiansen Jiang, a joint postdoc between the Feigon Lab and the Zhou Lab for his expertise in electron microscopy as well as his numerous helpful scientific contributions, suggestions, and discussions. Dr. Edward Miracco, a former postdoc, for his mentorship as well as his early work on the *Tetrahymena* telomerase holoenzyme. Dr. Robert Peterson our resident NMR expert and facilities manager, along with postdoc Dr. Lukas Susac have provided with invaluable help and instruction on NMR. I would also like to thank the current and former postdocs of the Feigon lab, Dr. Darian Cash, Dr. Catherine Eichhorn, Dr. Yaqiang Wang, Dr. Mahavir Singh, Dr. Meijong Kang, Dr. Zhonghua Wang, Dr. Jing Xue, Dr. Yuan Yang, Dr. Wendan Ren, Dr. Ritwika Basu and Dr. Elon Hartman for their companionship as well as contribution to my scientific growth.

In addition, I've had the pleasure of collaborating with the Collins lab at University of California Berkeley; professor Kathy Collins and her former student Dr. Heather Upton were always extremely knowledgeable and helpful regarding anything *Tetrahymena* or telomerase. I would also like to

acknowledge Professor Joseph Loo and Dr. Rachel Loo for their collaboration and expertise in mass spectrometry.

Special acknowledgements to undergraduate researcher Jamie Baron and to former rotation students Jeannette Bowler, Jessica Davis, and Scott McConnell for their assistance and exceptional work.

The crystallography in this work would not be possible without the exceptional dedication and competence of the UCLA crystallization core run by Dr. Duilio Cascio, Dr. Michael Sawaya, and Michael Collazo. Particularly Duilio for all of his expertise, hands on help, and informative discussions. Utilization of crystallization resources from the Eisenberg lab maintained by Professor David Eisenberg and Dr. Dan Anderson was also extremely valuable and greatly appreciated.

I would like to acknowledge the Cellular and Molecular Biology Training Grant program at UCLA which is supported by the Ruth L. Kirschstein National Research Service Award GM007185 and the Dissertation Year Fellowship at UCLA.

I would like to thank Professor Milton Saier at University of California San Diego who gave me my first opportunity to do research. His outlook and integrity in science and life continue to inspire me on a daily basis.

I would like to thank my grandparents, aunts, uncles, cousins, brother and parents for their support. I especially wish to acknowledge my mother who raised my brother and me almost entirely on her own and has always supported me and pushed me to achieve my goals.

Finally, I would like to thank the friends and colleagues that I have met at UCLA. Everyone that I have met has taught me something and impacted my life positively. In particular, my good friends, D.C., J.G., M.H., B.K., K.T. and N.W.

Chapter 2 contains a reprint of the published manuscript: Jiang J, Miracco EJ, Hong K, Eckert B, Chan H, Cash DD, Min B, Zhou ZH, Collins K, Feigon J: The architecture of *Tetrahymena* telomerase holoenzyme. *Nature* 2013, 496(7444):187-192; copyright 2013 with permission from Nature Publishing Group.

Chapter 3 is a reprint of the published manuscript: Jiang J, Chan H, Cash DD, Miracco EJ, Ogorzalek Loo RR, Upton HE, Cascio D, O'Brien Johnson R, Collins K, Loo JA et al: Structure of *Tetrahymena* telomerase reveals previously unknown subunits, functions, and interactions. *Science* 2015, 350(6260):aab4070; copyright 2015 with permission from the American Association for the Advancement of Science.

Chapter 6 is a reprint of the published manuscript: Chan H, Wang Y, Feigon J: Progress in Human and *Tetrahymena* Telomerase Structure. *Annu Rev Biophys* 2017, 46:199-225; copyright 2017 with permission from Annual Reviews.

VITA

Education

M.S. Biology, (UCSD)	Jun 2010
B.S. Molecular Biology, UCSD	Jun 2008

Research and Work Experience

Graduate researcher, Feigon Lab, UCLA	Sept 2011 – Jun 2017
Research associate, Inhibrx	Jun 2010 – Aug 2011
Student researcher, Saier Lab, UCSD	Jan 2008 – Jun 2010

Honors and Awards

Dissertation Year Fellowship, UCLA	Sep 2016 – Jun 2017
Audree Fowler Fellowship in Protein Science, UCLA	Jan 2016
Ernest F. Hare, Jr. Memorial Scholarship, UCLA	Nov 2015
Outstanding Poster Presentation UCLA-MBI retreat	Apr 2015
Ruth L. Kirschstein Pre-Doctoral National Research Service Award	Jul 2012 – Jun 2015
Excellence in Second Year Academics and Research Award, UCLA	Apr 2013
Chancellor's Prize, UCLA	Sep 2011
Regent's Scholar, USCD	Sep 2004 – Jun 2008

PUBLICATIONS

Chan H, Wang Y, Feigon J: Progress in Human and *Tetrahymena* Telomerase Structure. *Annu Rev Biophys* 2017, 46:199-225.

Upton HE, Chan H, Feigon J, Collins K: Shared Subunits of *Tetrahymena* Telomerase Holoenzyme and Replication Protein A Have Different Functions in Different Cellular Complexes. *J Biol Chem* 2017, 292(1):217-228.

Feigon J, Chan H, Jiang J: Integrative structural biology of *Tetrahymena* telomerase - insights into catalytic mechanism and interaction at telomeres. *FEBS J* 2016, 283(11):2044-2050.

Jiang J, Chan H, Cash DD, Miracco EJ, Ogorzalek Loo RR, Upton HE, Cascio D, O'Brien Johnson R, Collins K, Loo JA, Zhou ZH, Feigon J: Structure of *Tetrahymena* telomerase reveals previously unknown subunits, functions, and interactions. *Science* 2015, 350(6260):aab4070.

Jiang J, Miracco EJ, Hong K, Eckert B, Chan H, Cash DD, Min B, Zhou ZH, Collins K, Feigon J: The architecture of *Tetrahymena* telomerase holoenzyme. *Nature* 2013, 496(7444):187-192.

Lopez-de Los Santos Y, Chan H, Cantu VA, Rettner R, Sanchez F, Zhang Z. Saier MH Jr, Soberon X: Genetic engineering of the phosphocharrier protein NPr of the *Escherichia coli* phosphotransferase system selectively improves sugar uptake activity: *J Biol Chem* 2012, 287(35):29931-9.

Lam VH, Lee JH, Silverio A, Chan H, Gomolplitinant KM, Povolotsky TL, Orlava E, Sun EI, Welliver CH, Saier MH Jr: Pathways of transport protein evolution: recent advances. *Biol Chem* 2011, 392(1-2):5-12.

Chan H, Babayan V, Blyumin E, Gandhi C, Hak K, Harake D, Kumar K, Lee P, Li TT, Liu HY, Lo TC, Meyer CJ, Stanford S, Zamora KS, Saier MH Jr: *J Mol Microbiol Biotechnol* 2010, 19(1-2):5-104.

CHAPTER ONE

Introduction

Overview

Actively replicating eukaryotic cells face two challenges at the ends of their linear chromosomes which threaten the integrity of their genome. The first is that the ends of their chromosomal DNA are vulnerable to degradation and fusion by DNA acting enzymes (**Figure 1.1a**). The second is that multiple rounds of DNA replication lead to progressive shortening of their linear chromosomes, also known as the 'end replication problem' [1] (**Figure 1.1b**). To address these problems, chromosome ends are packaged into protective structures called telomeres and their length is maintained in part by the enzyme telomerase [2-5].

Telomeres are comprised of the telomeric DNA at the ends of linear eukaryotic chromosomes and telomeric DNA binding proteins [2, 6-8]. Telomeric DNA are hundreds to several thousand base-pairs of tandem G-rich repeats that are processed to end in a single stranded 3' overhang [9, 10]. These non-coding repeats act as a buffer against the end replication problem and can allow the cell to replicate until the 'Hayflick limit' is reached [11-14]; the point at which telomeric DNA becomes too short leading to cellular senescence and/or apoptosis [15]. The double stranded and single stranded telomeric repeats are packaged into telomeres by specific telomeric DNA binding protein complexes that protect telomeric DNA from degradation by DNA-exonucleases and non-homologous end joining (NHEJ) by DNA repair enzymes [16, 17] (**Figure 1.1a**). Telomeres also participate in regulating the maintenance of its own telomeric DNA length through the recruitment or inhibition of telomerase [7, 8].

Telomerase is the ribonucleoprotein enzyme complex that uses an internal telomerase RNA (TR) [18] and a telomerase reverse transcriptase (TERT) [19] for the reverse transcription of telomeric repeats (GGTTAG in humans and GGGTTG in *Tetrahymena*) to the 3' ends of linear chromosomes, thus reversing the progressive shortening that occurs during DNA replication (**Figure 1.2**). Together, TERT and TR comprise the 'catalytic core' of telomerase, which are the minimum components necessary for telomeric repeat addition *in vitro* [20, 21].

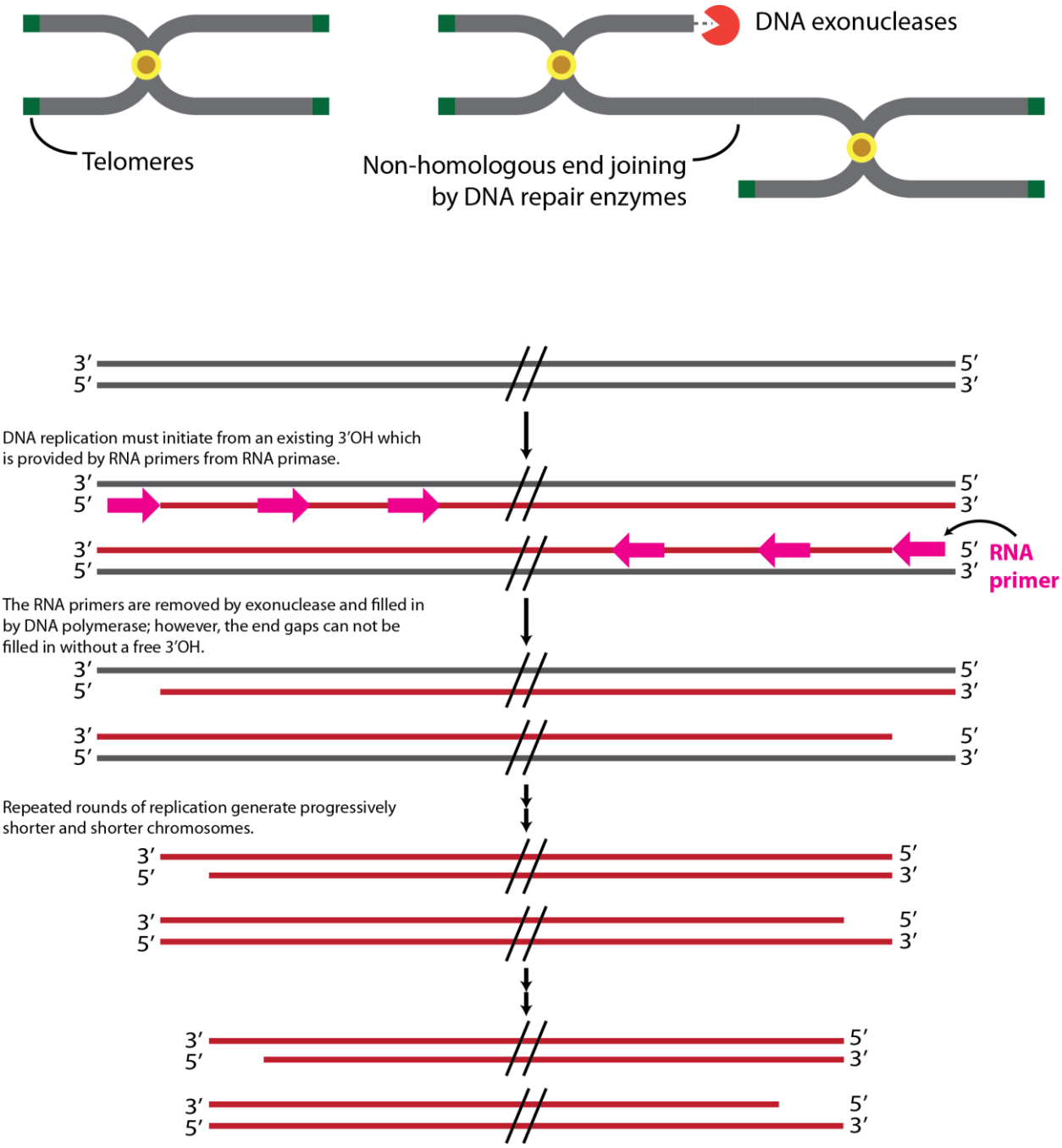

Figure 1.1. Telomere end protection and end replication problem. (*a*) Telomeres are protective nucleoprotein structures located at the ends of linear chromosomes. Unprotected chromosome ends are subject to degradation by DNA exonucleases as well as chromosome end to end fusion by DNA repair enzymes. (*b*) Initiation of DNA synthesis requires an RNA primer due to the requirement of DNA polymerase for a free 3' hydroxyl for DNA synthesis. The end gaps left by the RNA primers cannot be filled in and lead to a shortened daughter strand at the 5' end. Repeated replication of shortened strands lead to progressively shorter chromosomes in daughter cells.

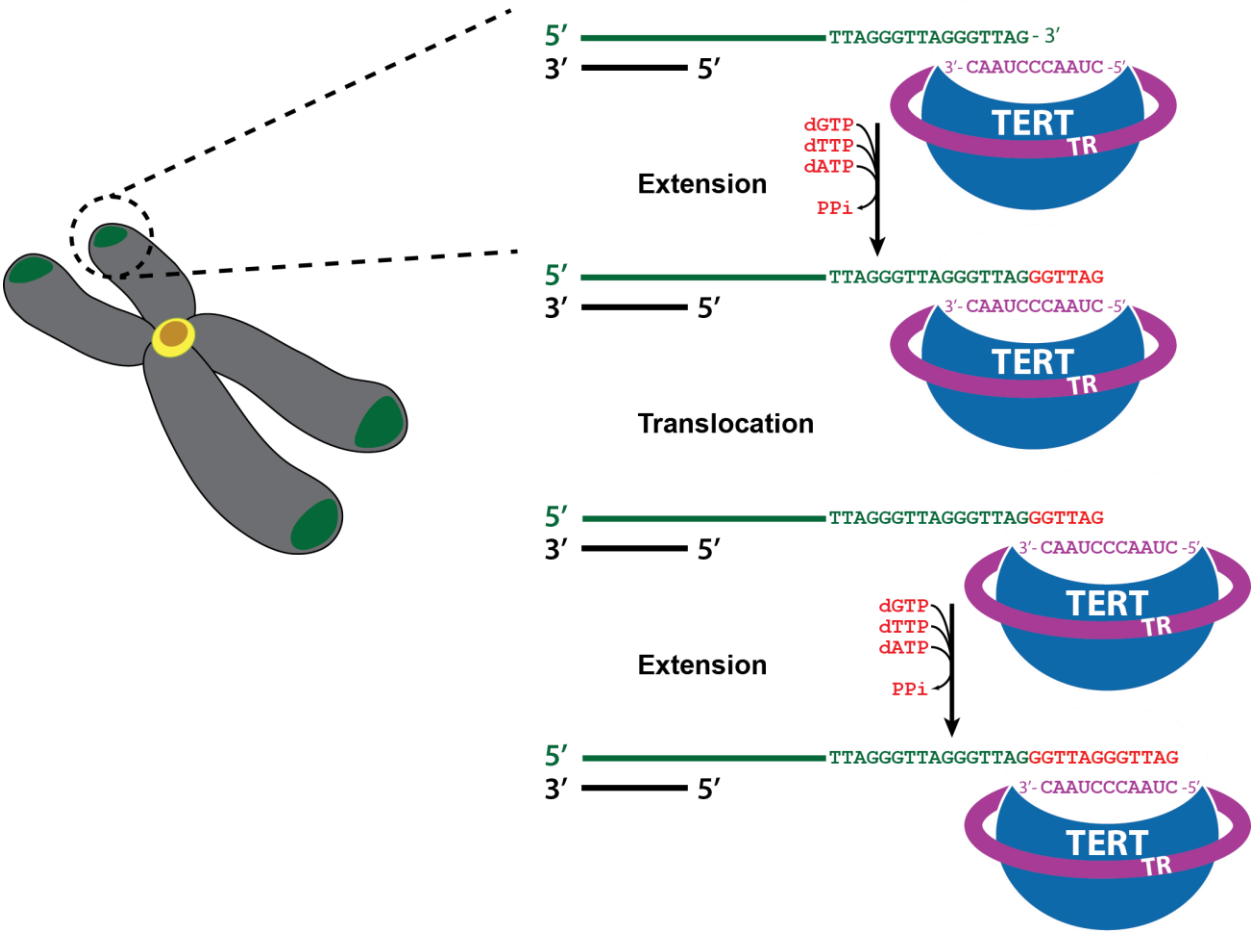

Figure 1.2. Extension of telomeric 3' overhang by telomerase. Telomerase lengthens telomeres through the reverse transcription of the telomerase RNA template onto the 3' single stranded ends of linear chromosomes. After the successful extension of a single telomeric repeat, telomerase shifts register by one whole repeat in a process known as translocation. After this step, which is considered the enzymatic bottleneck for repeat addition processivity, extension can reinitiate.

Due to the direct correlation between telomeres and telomerase and the ability of the cell to maintain sustained or 'immortal' replication, research in telomeres and telomerase is of active interest to the study of cancer (90% of cancers have upregulated telomerase activity) and cellular aging [22-27]. Additionally, mutations in telomerase proteins, telomerase RNA, and telomere associated proteins are linked to a wide variety of inherited diseases; such as dyskeratosis congenita and other progeria-like diseases of rapid aging [7, 22, 28-30].

Overview of *Tetrahymena* and human telomerase-telomere interactions

Human telomeres are packaged by the shelterin complex which is comprised of: RAP1, TRF1 and TRF2 which bind double-stranded telomeric DNA (dstDNA) as homodimers, the single-stranded telomeric DNA (sstDNA) binding POT1, and TPP1 and TIN2 which serve as mediators for shelterin assembly and telomerase recruitment [2, 31-35] (**Figure 1.3a**). Telomerase is recruited primarily by a direct interaction between the TEN (TERT essential N-terminal) domain and TPP1 [35-37]. Human TERT and TR, along with the H/ACA RNP complex, important for TR biogenesis and maturation, form the human 'telomerase RNP core' [8, 38-43]. After sufficient telomere extension, the CST complex (formed from Ctc1, Stn1, and Ten1) is recruited by TPP1:POT1 for the recruitment of DNA polymerase-alpha primase (pol-α) for complementary strand synthesis [44-46]. CST is also thought to act as a terminator for telomerase activity [45, 47].

Telomerase activity was first detected in *Tetrahymena thermophila* [48, 49], a ciliated single celled eukaryotic organism that possesses a germline micronucleus and a somatic macronucleus [50]. This somatic macronucleus which performs the transcriptional duties for the cell can possess ~20,000 telomere capped mini-chromosomes, making *Tetrahymena* an excellent model organism for studying telomerase and source of endogenous enzyme [50]. *Tetrahymena* telomeric DNA are packaged at their 3' singled stranded overhang by the four protein complex Pot1, Tpt1, Pat1 and Pat2 [51-53] (**Figure 1.3b**). These proteins protect the chromosome ends and prevent runaway

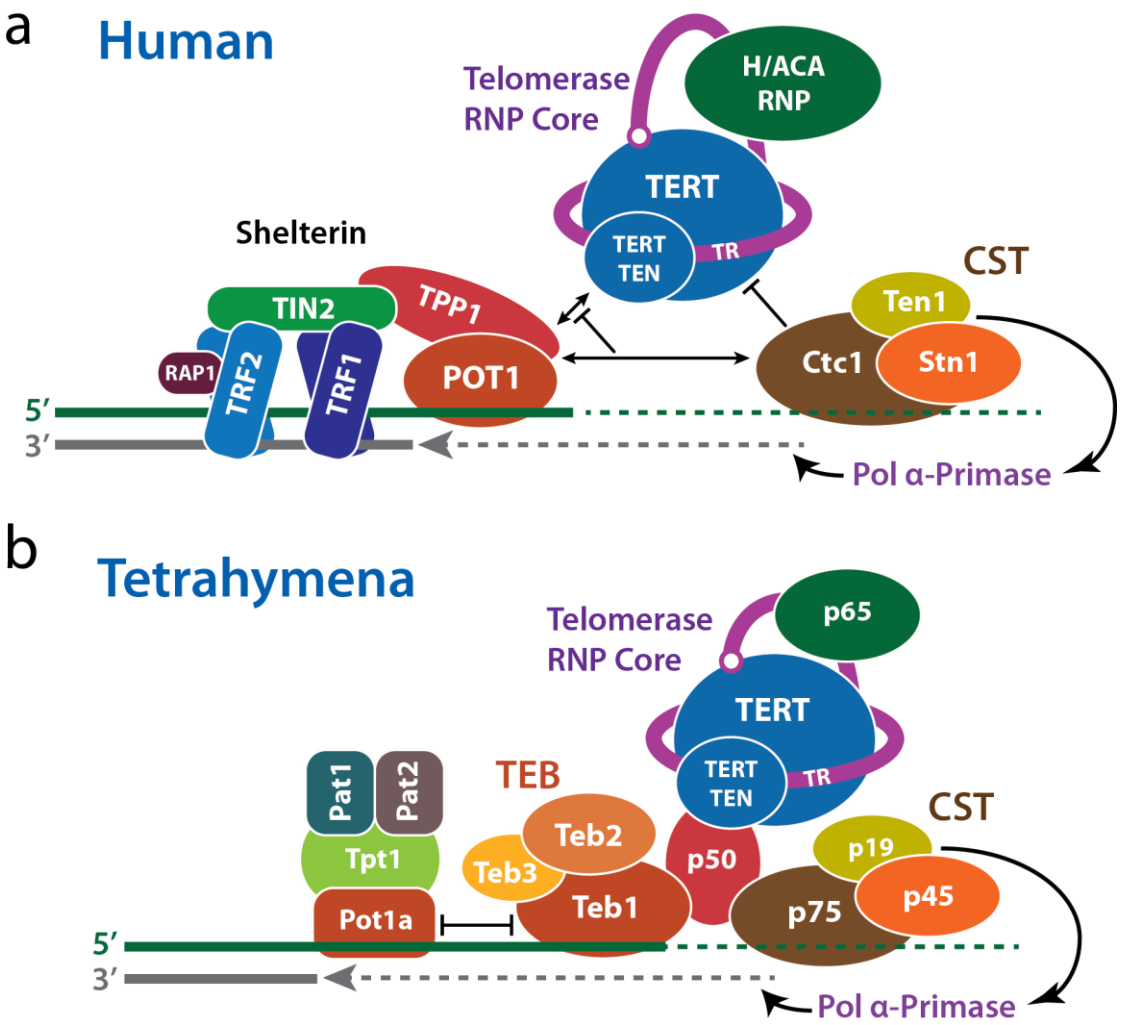

Figure 1.3. Overview of Human and *Tetrahymena* telomerase and interaction at telomeres. (*a*) Human telomeres are packaged by the six protein component shelterin comprising: RAP1, dstDNA binding TRF2 & TRF1, hub and recruitment proteins TIN2 & TPP1, and dstDNA binding POT1. The telomerase RNP core comprising TERT, TR, and the H/ACA RNP is recruited to the 3'overhang by a direct interaction between the TERT TEN domain and TPP1. After sufficient telomere repeat elongation, CST is recruited by TPP1-POT1 for termination of telomerase activity and stimulation of pol-α primase for C-strand synthesis. (*b*) *Tetrahymena* sstDNA is packaged by the Pot1-Tpt1-Pat1-Pat2 complex. TEB (Teb1-Teb2-Teb3) binding to sstDNA facilitates the association and recruitment of telomerase to telomeres. The central hub p50 bridges the interaction to the RNP core (TERT-TR-p65) via a direct interaction with the TERT TEN domain. *Tetrahymena* CST (p75-p45-p19) is constitutively associated to the holoenzyme via an interaction with p50 and facilitates recruitment of pol-α primase.

telomere elongation by telomerase [52]. The *Tetrahymena* telomerase holoenzyme is comprised of one telomerase RNA (TR), one telomerase reverse transcriptase (TERT), and eight other accessory protein subunits [54-58] (**Figure 1.3b**), two of which Teb2 and Teb3 were discovered in the course of this work. Previously, these accessory proteins were not thought to have direct orthologues to human telomerase. However, the work presented in this thesis and recent work from the Feigon lab indicates otherwise. p65 is the TR chaperone that assists in assembly of the *Tetrahymena* telomerase RNP core, comprising TERT, TR and p65 [56, 59, 60]. Recruitment to telomeres is mediated by TEB:p50, which we propose to be the functional orthologue of POT1:TPP1 [54, 56, 61-63]. We identified TEB to be an RPA-like trimeric complex, comprising Teb1, Teb2 and Teb3, that is specific for sstDNA. It bridges the RNP core to telomeres via an interaction with p50, which associates with TERT via an interaction with the TERT TEN domain [54, 55, 61, 63]. The remaining proteins p75-p45-p19 were known to form a trimeric complex that was determined here to be *Tetrahymena* CST by solving the crystal structure of p19 and the p45 C-terminal domain. These proteins are involved in DNA polymerase α-primase (pol-α) recruitment [54, 64]. Unlike most other organisms, the *Tetrahymena* telomerase 'holoenzyme' appears to be 'constitutively' assembled with its recruitment and sstDNA binding factors as well as the CST complex [61, 65].

Motivation

Telomerase has long been a challenging target for structural and molecular biology. The components that constitute a stable 'holoenzyme' have historically been difficult to define, while apparent divergence amongst different organisms in the accessory proteins (components other than TERT and TER) make parallel studies in model organisms difficult to interpret and generalize relative to humans. In addition, telomerase proteins are notoriously difficult to express and purify and are often conformationally flexible or prone to aggregation when purified to concentrations relevant for structural biology. Thus, many structural aspects of the mechanism of telomerase activity, translocation, function, and recruitment remain unexplained. The goal of my thesis work

was to determine the structure and function of *Tetrahymena* telomerase accessory proteins p19, p45, and p75. This work also led to the discovery of the TEB complex and insights into how these complexes interact with p50, the central hub of *Tetrahymena* telomerase interaction with telomerase subcomplexes as well as recruitment to telomeres.

Thesis Synopsis

The work presented in this thesis seeks to structurally characterize the *Tetrahymena* telomerase holoenzyme, with an emphasis on the accessory proteins, primarily using a combined structural biology approach with electron microscopy (EM), x-ray crystallography, and nuclear magnetic resonance (NMR) spectroscopy.

Chapter 2 presents the published manuscript which describes the first EM structure of a telomerase holoenzyme [55]. This work, performed primarily by postdocs Jiansen Jiang and Edward Miracco, determined the 25 Å negative stain EM structure of the *Tetrahymena* telomerase holoenzyme with the locations of each of the then known subunits (TERT, TR, p65, Teb1, p50, p75, p45, p19) as determined by affinity labelling. This work was in collaboration with the Zhou lab (for EM) and the Collins lab (for *Tetrahymena* strains and activity assays). My contribution to this work was the localization of the TR Stem-loop2 (SL2) in the 25 Å negative stain EM structure of the holoenzyme. MS2 coat protein was used to pulldown telomerase holoenzyme at a modified SL2 hairpin on the TR. The MS2 coat protein dimer was visible by negative stain 2D class averages and facilitated placement and orientation of known elements of the TR relative to the SL2 along with the TERT TRBD-RT-CTE ring relative to the TERT TRBD, which binds SL2, into the 25 Å map. A detailed description of the protocol used is described after the paper reprint.

Chapter 3 presents the published manuscript describing the 9 Å cryo-EM structure of the *Tetrahymena* telomerase holoenzyme in collaboration with Professor Hong Zhou and postdoc Jiansen Jiang (for EM) [54]. In this work, a model, which utilized the unambiguous docking of crystal, NMR, and homologous structures into the EM density was, built for 8 of the 9 proteins

subunits and the TR of the holoenzyme. This work led to the discovery of two new proteins by EM and mass spectrometry, Teb2 and Teb3, which form an RPA-like heterotrimer with Teb1. The previously uncharacterized p75, p45, and p19 proteins were identified as *Tetrahymena* CST. Important contacts and interactions proposed by the model were validated by activity assays performed by our collaborators in the Collins lab. My contributions to this work was preparing the holoenzyme samples for cryo-EM and for the mass spectrometry which was performed in collaboration with the Loo lab, for which I assisted in the data analysis. In addition, I solved crystal structures of p19 and the p45 C-terminal domain, leading to their identification as the Ten1 and Stn1 subunits of *Tetrahymena* CST.

Chapter 4 describes ongoing structural investigation into the *Tetrahymena* telomerase protein p75. Identification of the previously uncharacterized p75, p45, and p19 subunits as *Tetrahymena* CST greatly improved our understanding of these accessory proteins. Namely, the comparisons of the p19 and p45 crystal structures to other known Ten1 and Stn1 structures aided greatly in gaining this insight, while docking models of the 9 Å cryo-EM structure provided an unprecedented view into the architecture of the trimeric complex. However, the largest subunit of the CST complex (Ctc1 in vertebrates, p75 in *Tetrahymena*) remains the most mysterious. Based on the proposed homology of p75 to Ctc1, the N-terminal domain of p75 (p75N) was identified and purified for study by NMR. Additionally, inspired by EM and biochemical data, a small fragment of p50 that binds to p75N was identified which could explain in part the interaction of CST with the holoenzyme. This p75N:p50 complex will aid in the structural investigation of this interaction by NMR and crystallography.

Chapter 5 describes the identification and partial characterization of a new RPA protein in *Tetrahymena*, Rlp2 (RPA like protein 2). As discussed above, we identified two new RPA32-like and RPA14-like subunits, Teb2 and Teb3, in *Tetrahymena* telomerase holoenzyme as part of the RPA-like telomerase TEB complex. In lieu of other RPA32 and RPA14 homologs in the *Tetrahymena*

proteome and their expression levels relative to other telomerase proteins, it was proposed and confirmed that Teb2 and Teb3 were shared subunits between the RPA70-like Teb1, Rpa1, and Rlp1, to each form distinct RPA-like heterotrimers TEB, RPA, and RTT respectively [66]. Separately, Rlp2 was identified as an RPA32 homolog that binds to Teb3 but not to Teb1. Preliminary domain and interaction characterization for Rlp2 is described.

Chapter 6 presents the published review on the structural biology of *Tetrahymena* and human telomerase [56]. It reviews the current literature with an emphasis on *Tetrahymena* telomerase structures in the context of relating to and understanding human telomerase structure and function. Owing to the divergence of the *Tetrahymena* telomerase proteins from human telomerase proteins, analogous functions and interactions were previously difficult to identify. However, recently solved high resolution structures and the 9 Å cryo-EM structure of *Tetrahymena* telomerase reveal that the majority of telomerase subunits, subdomains, and subcomplexes have direct analogs. In addition, the constitutively assembled nature of the *Tetrahymena* telomerase holoenzyme provides an unprecedented opportunity to study analogous interactions which are transient in vertebrates, as illustrated in **Figure 1.3**. Parallel findings and trends among different organisms present in the RNP core, CST subcomplex, telomere binding, and telomerase recruitment proteins are discussed. [My written contributions to this review are the Introduction, the section on DNA handling and telomerase recruitment, the CST section, and Future prospects. Figures contributed are 1, 6 & 7, and partial contribution to Figure 5.]

REFERENCES

1. Levy MZ, Allsopp RC, Futcher AB, Greider CW, Harley CB: Telomere end-replication problem and cell aging. *J Mol Biol* 1992, 225(4):951-960.

2. Stewart JA, Chaiken MF, Wang F, Price CM: Maintaining the end: roles of telomere proteins in end-protection, telomere replication and length regulation. *Mutat Res* 2012, 730(1-2):12-19.

3. Blackburn EH, Epel ES, Lin J: Human telomere biology: A contributory and interactive factor in aging, disease risks, and protection. *Science* 2015, 350(6265):1193-1198.

4. Croy JE, Wuttke DS: Themes in ssDNA recognition by telomere-end protection proteins. *Trends Biochem Sci* 2006, 31(9):516-525.

5. Martinez P, Blasco MA: Replicating through telomeres: a means to an end. *Trends Biochem Sci* 2015, 40(9):504-515.

6. Egan ED, Collins K: Biogenesis of telomerase ribonucleoproteins. *RNA* 2012, 18(10):1747-1759.

7. Nandakumar J, Cech TR: Finding the end: recruitment of telomerase to telomeres. *Nature Reviews Molecular Cell Biology* 2013, 14(2):69-82.

8. Schmidt JC, Cech TR: Human telomerase: biogenesis, trafficking, recruitment, and activation. *Genes Dev* 2015, 29(11):1095-1105.

9. Podlevsky JD, Bley CJ, Omana RV, Qi X, Chen JJ: The telomerase database. *Nucleic Acids Research* 2008, 36(Database issue):D339-343.

10. Podlevsky JD, Chen JJ: Evolutionary perspectives of telomerase RNA structure and function. *RNA Biology* 2016, 13(8):720-732.

11. Shay JW, Wright WE: Hayflick, his limit, and cellular ageing. *Nature Reviews Molecular Cell Biology* 2000, 1(1):72-76.

12. Hayflick L: Recent Advances in the Cell Biology of Aging. *Mechanisms of Ageing and Development* 1980, 14(1-2):59-79.

13. Effros RB, Walford RL: T cell cultures and the Hayflick limit. *Hum Immunol* 1984, 9(1):49-65.

14. Bremermann HJ: Reliability of proliferation controls. The Hayflick limit and its breakdown in cancer. *J Theor Biol* 1982, 97(4):641-662.

15. Rousseau P, Autexier C: Telomere biology: Rationale for diagnostics and therapeutics in cancer. *RNA Biol* 2015, 12(10):1078-1082.

16. Riha K, Heacock ML, Shippen DE: The role of the nonhomologous end-joining DNA double-strand break repair pathway in telomere biology. *Annu Rev Genet* 2006, 40:237-277.

17. Doksani Y, de Lange T: The Role of Double-Strand Break Repair Pathways at Functional and Dysfunctional Telomeres. *Csh Perspect Biol* 2014, 6(12).

18. Blackburn EH, Greider CW, Szostak JW: Telomeres and telomerase: the path from maize, *Tetrahymena* and yeast to human cancer and aging. *Natural Medicines* 2006, 12(10):1133-1138.

19. Lingner J, Hughes TR, Shevchenko A, Mann M, Lundblad V, Cech TR: Reverse transcriptase motifs in the catalytic subunit of telomerase. *Science* 1997, 276(5312):561-567.

20. Podlevsky JD, Chen JJ: It all comes together at the ends: Telomerase structure, function, and biogenesis. *Mutation Research* 2012, 730(1-2):3-11.

21. Collins K: Single-stranded DNA repeat synthesis by telomerase. *Curr Opin Chem Biol* 2011, 15(5):643-648.

22. Armanios M, Blackburn EH: The telomere syndromes. *Nature Reviews Genetics* 2012, 13(10):693-704.

23. Artandi SE, DePinho RA: Telomeres and telomerase in cancer. *Carcinogenesis* 2010, 31(1):9-18.

24. Bernardes de Jesus B, Blasco MA: Telomerase at the intersection of cancer and aging. *Trends in Genetics* 2013, 29(9):513-520.

25. Fujii H, Shao L, Colmegna I, Goronzy JJ, Weyand CM: Telomerase insufficiency in rheumatoid arthritis. *Proc Natl Acad Sci U S A* 2009, 106(11):4360-4365.

26. Marrone A, Walne A, Dokal I: Dyskeratosis congenita: telomerase, telomeres and anticipation. *Curr Opin Genet Dev* 2005, 15(3):249-257.

27. Shay JW: Role of Telomeres and Telomerase in Aging and Cancer. *Cancer Discov* 2016, 6(6):584-593.

28. Fogarty PF, Yamaguchi H, Wiestner A, Baerlocher GM, Sloand E, Zeng WS, Read EJ, Lansdorp PM, Young NS: Late presentation of dyskeratosis congenita as apparently acquired aplastic anaemia due to mutations in telomerase RNA. *Lancet* 2003, 362(9396):1628-1630.

29. Jaskelioff M, Muller FL, Paik JH, Thomas E, Jiang S, Adams AC, Sahin E, Kost-Alimova M, Protopopov A, Cadinanos J *et al*: Telomerase reactivation reverses tissue degeneration in aged telomerase-deficient mice. *Nature* 2011, 469(7328):102-106.

30. Sarek G, Marzec P, Margalef P, Boulton SJ: Molecular basis of telomere dysfunction in human genetic diseases. *Nat Struct Mol Biol* 2015, 22(11):867-874.

31. De Lange T: Telomere-related genome instability in cancer. *Cold Spring Harb Symp Quant Biol* 2005, 70:197-204.

32. Hockemeyer D, Collins K: Control of telomerase action at human telomeres. *Nat Struct Mol Biol* 2015, 22(11):848-852.

33. Wang F, Podell ER, Zaug AJ, Yang Y, Baciu P, Cech TR, Lei M: The POT1-TPP1 telomere complex is a telomerase processivity factor. *Nature* 2007, 445(7127):506-510.

34. Xin H, Liu D, Wan M, Safari A, Kim H, Sun W, O'Connor MS, Songyang Z: TPP1 is a homologue of ciliate TEBP-beta and interacts with POT1 to recruit telomerase. *Nature* 2007, 445(7127):559-562.

35. Zhong FL, Batista LF, Freund A, Pech MF, Venteicher AS, Artandi SE: TPP1 OB-fold domain controls telomere maintenance by recruiting telomerase to chromosome ends. *Cell* 2012, 150(3):481-494.

36. Nandakumar J, Bell CF, Weidenfeld I, Zaug AJ, Leinwand LA, Cech TR: The TEL patch of telomere protein TPP1 mediates telomerase recruitment and processivity. *Nature* 2012, 492(7428):285-289.

37. Sexton AN, Youmans DT, Collins K: Specificity requirements for human telomere protein interaction with telomerase holoenzyme. *J Biol Chem* 2012, 287(41):34455-34464.

38. Li L, Ye K: Crystal structure of an H/ACA box ribonucleoprotein particle. *Nature* 2006, 443(7109):302-307.

39. Rashid R, Liang B, Baker DL, Youssef OA, He Y, Phipps K, Terns RM, Terns MP, Li H: Crystal structure of a Cbf5-Nop10-Gar1 complex and implications in RNA-guided pseudouridylation and dyskeratosis congenita. *Mol Cell* 2006, 21(2):249-260.

40. Venteicher AS, Abreu EB, Meng Z, McCann KE, Terns RM, Veenstra TD, Terns MP, Artandi SE: A human telomerase holoenzyme protein required for Cajal body localization and telomere synthesis. *Science* 2009, 323(5914):644-648.

41. Tycowski KT, Shu MD, Kukoyi A, Steitz JA: A conserved WD40 protein binds the Cajal body localization signal of scaRNP particles. *Mol Cell* 2009, 34(1):47-57.

42. Mahmoudi S, Henriksson S, Weibrecht I, Smith S, Soderberg O, Stromblad S, Wiman KG, Farnebo M: WRAP53 is essential for Cajal body formation and for targeting the survival of motor neuron complex to Cajal bodies. *PLoS Biol* 2010, 8(11):e1000521.

43. Egan ED, Collins K: An enhanced H/ACA RNP assembly mechanism for human telomerase RNA. *Mol Cell Biol* 2012, 32(13):2428-2439.

44. Casteel DE, Zhuang S, Zeng Y, Perrino FW, Boss GR, Goulian M, Pilz RB: A DNA polymerase-{alpha}{middle dot}primase cofactor with homology to replication protein A-32 regulates DNA replication in mammalian cells. *J Biol Chem* 2009, 284(9):5807-5818.

45. Chen LY, Redon S, Lingner J: The human CST complex is a terminator of telomerase activity. *Nature* 2012, 488(7412):540-544.

46. Qi HY, Zakian VA: The Saccharomyces telomere-binding protein Cdc13p interacts with both the catalytic subunit of DNA polymerase alpha and the telomerase-associated Est1 protein. *Gene Dev* 2000, 14(14):1777-1788.

47. Chen LY, Lingner J: CST for the grand finale of telomere replication. *Nucleus* 2013, 4(4):277-282.

48. Greider CW, Blackburn EH: The telomere terminal transferase of *Tetrahymena* is a ribonucleoprotein enzyme with two kinds of primer specificity. *Cell* 1987, 51(6):887-898.

49. Greider CW, Blackburn EH: Identification of a specific telomere terminal transferase activity in *Tetrahymena* extracts. *Cell* 1985, 43(2 Pt 1):405-413.

50. *Tetrahymena Thermophila*, vol. 109; 2012.

51. Premkumar VL, Cranert S, Linger BR, Morin GB, Minium S, Price C: The 3 ' Overhangs at *Tetrahymena thermophila* Telomeres Are Packaged by Four Proteins, Pot1a, Tpt1, Pat1, and Pat2. *Eukaryot Cell* 2014, 13(2):240-245.

52. Linger BR, Morin GB, Price CM: The Pot1a-associated proteins Tpt1 and Pat1 coordinate telomere protection and length regulation in *Tetrahymena*. *Mol Biol Cell* 2011, 22(21):4161-4170.

53. Jacob NK, Lescasse R, Linger BR, Price CM: *Tetrahymena* POT1a regulates telomere length and prevents activation of a cell cycle checkpoint. *Mol Cell Biol* 2007, 27(5):1592-1601.

54. Jiang J, Chan H, Cash DD, Miracco EJ, Ogorzalek Loo RR, Upton HE, Cascio D, O'Brien Johnson R, Collins K, Loo JA *et al*: Structure of *Tetrahymena* telomerase reveals previously unknown subunits, functions, and interactions. *Science* 2015, 350(6260):aab4070.

55. Jiang J, Miracco EJ, Hong K, Eckert B, Chan H, Cash DD, Min B, Zhou ZH, Collins K, Feigon J: The architecture of *Tetrahymena* telomerase holoenzyme. *Nature* 2013, 496(7444):187-192.

56. Chan H, Wang Y, Feigon J: Progress in Human and *Tetrahymena* Telomerase Structure. *Annu Rev Biophys* 2017, 46:199-225.

57. Witkin KL, Prathapam R, Collins K: Positive and negative regulation of *Tetrahymena* telomerase holoenzyme. *Mol Cell Biol* 2007, 27(6):2074-2083.

58. Feigon J, Chan H, Jiang J: Integrative structural biology of *Tetrahymena* telomerase - insights into catalytic mechanism and interaction at telomeres. *FEBS J* 2016, 283(11):2044-2050.

59. Singh M, Wang Z, Koo BK, Patel A, Cascio D, Collins K, Feigon J: Structural basis for telomerase RNA recognition and RNP assembly by the holoenzyme La family protein p65. *Molecular Cell* 2012, 47(1):16-26.

60. Robart AR, Collins K: Investigation of human telomerase holoenzyme assembly, activity, and processivity using disease-linked subunit variants. *J Biol Chem* 2010, 285(7):4375-4386.

61. Upton HE, Hong K, Collins K: Direct single-stranded DNA binding by Teb1 mediates the recruitment of *Tetrahymena thermophila* telomerase to telomeres. *Mol Cell Biol* 2014, 34(22):4200-4212.

62. Hong K, Upton H, Miracco EJ, Jiang J, Zhou ZH, Feigon J, Collins K: *Tetrahymena* telomerase holoenzyme assembly, activation, and inhibition by domains of the p50 central hub. *Molecular and Cellular Biology* 2013, 33(19):3962-3971.

63. Zeng Z, Min B, Huang J, Hong K, Yang Y, Collins K, Lei M: Structural basis for *Tetrahymena* telomerase processivity factor Teb1 binding to single-stranded telomeric-repeat DNA. *Proceedings of the National Academy of Sciences of the United States of America* 2011, 108(51):20357-20361.

64. Wan B, Tang T, Upton H, Shuai J, Zhou Y, Li S, Chen J, Brunzelle JS, Zeng Z, Collins K *et al*: The *Tetrahymena* telomerase p75-p45-p19 subcomplex is a unique CST complex. *Nat Struct Mol Biol* 2015, 22(12):1023-1026.

65. Min B, Collins K: An RPA-related sequence-specific DNA-binding subunit of telomerase holoenzyme is required for elongation processivity and telomere maintenance. *Mol Cell* 2009, 36(4):609-619.

66. Upton HE, Chan H, Feigon J, Collins K: Shared Subunits of *Tetrahymena* Telomerase Holoenzyme and Replication Protein A Have Different Functions in Different Cellular Complexes. *J Biol Chem* 2017, 292(1):217-228.

CHAPTER TWO

The architecture of *Tetrahymena* telomerase holoenzyme

(Localizing Stem-loop II of *Tetrahymena* Telomerase)

ARTICLE

doi:10.1038/nature12062

The architecture of *Tetrahymena* telomerase holoenzyme

Jiansen Jiang[1,2,3]*, Edward J. Miracco[2]*, Kyungah Hong[4], Barbara Eckert[4], Henry Chan[2], Darian D. Cash[2], Bosun Min[4], Z. Hong Zhou[1,3], Kathleen Collins[4] & Juli Feigon[2,3]

Telomerase adds telomeric repeats to chromosome ends using an internal RNA template and a specialized telomerase reverse transcriptase (TERT), thereby maintaining genome integrity. Little is known about the physical relationships among protein and RNA subunits within a biologically functional holoenzyme. Here we describe the architecture of *Tetrahymena thermophila* telomerase holoenzyme determined by electron microscopy. Six of the seven proteins and the TERT-binding regions of telomerase RNA (TER) have been localized by affinity labelling. Fitting with high-resolution structures reveals the organization of TERT, TER and p65 in the ribonucleoprotein (RNP) catalytic core. p50 has an unanticipated role as a hub between the RNP catalytic core, p75–p19–p45 subcomplex, and the DNA-binding Teb1. A complete *in vitro* holoenzyme reconstitution assigns function to these interactions in processive telomeric repeat synthesis. These studies provide the first view of the extensive network of subunit associations necessary for telomerase holoenzyme assembly and physiological function.

Telomerase is a unique endogenous eukaryotic reverse transcriptase (RT) required for maintenance of linear chromosome ends and is a highly regulated determinant of cellular ageing, stem cell renewal and tumorigenesis[1,2]. TER contains a region of sequence complementarity to the telomeric repeat that is used as a template for addition of successive repeats to the 3′ end of chromosomes, for example addition of the repeat TTAGGG in humans. The specialized telomerase catalytic cycle of telomeric repeat synthesis has been extensively investigated for the human enzyme and biochemically similar enzymes from model organisms such as the telomere-rich ciliate *Tetrahymena thermophila*[3]. Whereas only TERT and TER are required for telomerase catalytic activity *in vitro*, the physiologically functional holoenzyme is a multi-subunit RNP[4,5]. Affinity purification, mass spectrometry and subunit tagging assays have identified eight telomerase-specific, reciprocally co-purifying subunits of *Tetrahymena* telomerase holoenzyme, each essential for telomere length maintenance[6,7] (Fig. 1a). Three of these subunits are required for *in vivo* assembly of a catalytically active RNP: TERT, TER and the La-family protein p65[7]. The p65 La and RRM1 domains increase p65 affinity for TER, but only the carboxy-terminal xRRM2 domain (Fig. 1a) is critical for the TER folding that enhances TERT RNP assembly *in vitro* and *in vivo*[8–11]. Two TER regions, loop 4 (L4) next to the p65 xRRM2 interaction site and the TERT high-affinity binding element (TBE) 5′ to the template (Fig. 1a), bind to the TERT high-affinity RNA binding domain (TRBD)[12–14]. The TERT TRBD, RT domain and C-terminal extension (CTE) form a ring that encircles an active site cavity, with a fourth TERT amino-terminal (TEN) domain (Fig. 1a) positioned in a TER-dependent but otherwise unknown location[15–19].

Little is known about the configuration and roles of the five additional *Tetrahymena* telomerase holoenzyme proteins required for *in vivo* telomere elongation (p75, p50, p45, p19 and Teb1; Fig. 1a); only Teb1 has a known domain structure. Like the paralogous large subunit of the single-stranded DNA (ssDNA) binding factor replication protein A, Teb1 has four OB-fold domains, NABC (Fig. 1a); A and B bind ssDNA with high affinity and C is necessary for holoenzyme association[6,20,21]. Teb1 is required for the particularly high DNA product interaction stability of an endogenously assembled *Tetrahymena* telomerase holoenzyme, evident as high repeat addition processivity (RAP) *in vitro*[6,20,21]. The holoenzyme subunits p75, p19 and p45, here designated 7-1-4, form a subcomplex that remains assembled upon micrococcal nuclease-induced dissociation of the other holoenzyme subunits *in vitro*[6,21]. Little is known about p50, which seems substoichiometric on silver-stained gels of affinity purified holoenzyme[6].

Here we report the native electron microscopy structure and a complete *in vitro* reconstitution of *Tetrahymena* telomerase holoenzyme. This first physical and functional network architecture of a telomerase holoenzyme provides unprecedented detail about the structure of the RNP catalytic core and reveals the organization of holoenzyme subunits that confer processivity and bridge telomerase to telomeres.

Overall structure and localization of subunits

Tetrahymena telomerase holoenzymes were prepared for electron microscopy (Supplementary Fig. 1) by affinity purification[6] from 10 different strains bearing N- or C-terminal 3×Flag (F) and tandem protein A (ZZ) tags (ZZF or FZZ, respectively) on TERT or other holoenzyme subunits (Supplementary Table). Comparison of the class averages from negative staining electron microscopy images of telomerase purified using TERT–FZZ (TERT-F telomerase, which results from cleavage of the ZZ tag) to those from cryo-electron microscopy images (Fig. 1b and Supplementary Fig. 2a, b) shows that the negative stain did not change the structure within experimental resolution. In addition to the predominant ('stable') conformation of the complete holoenzyme particle, constituting 31% of the total particles, the class averages show additional particle subpopulations of varying conformation and subunit composition (described below and Supplementary Fig. 2). The class averages from both negative staining electron microscopy images and cryo-electron microscopy

[1]Department of Microbiology, Immunology and Molecular Genetics, University of California, Los Angeles, California 90095, USA. [2]Department of Chemistry and Biochemistry, University of California, Los Angeles, California 90095, USA. [3]California Nanosystems Institute, University of California, Los Angeles, California 90095, USA. [4]Department of Molecular and Cell Biology, University of California, Berkeley, California 94720, USA.
*These authors contributed equally to this work.

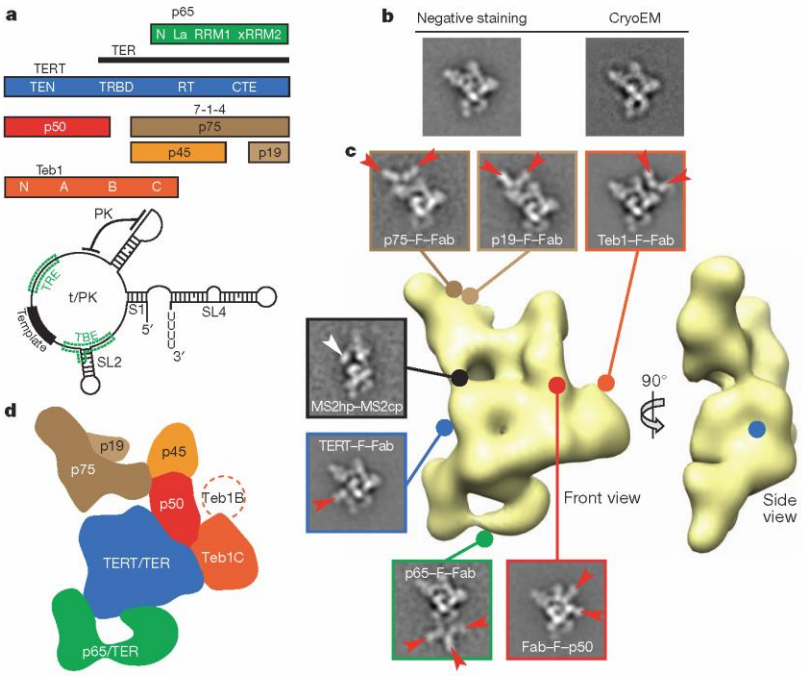

Figure 1 | Electron microscopy reconstruction of *Tetrahymena* telomerase holoenzyme and subunit localization. **a**, Holoenzyme subunits and domains (top) and TER secondary structure (below). **b**, Representative class averages of negative staining electron microscopy and cryo-electron microscopy images of TERT–F telomerase. **c**, 3D reconstruction of Teb1–F telomerase (front and side views) and class averages of affinity-labelled telomerase particles. Lines with circle heads indicate attachment point of Fab (red arrows) and MS2cp (white arrow). Side-lengths of class averages in this and subsequent figures are 350 Å. **d**, Subunit schematic (front view).

images show a strongly preferred orientation (Supplementary Fig. 2). To overcome the problems of preferred orientation and structural variability, the electron microscopy image acquisition and three-dimensional (3D) reconstructions were carried out using an automated random conical tilt (RCT) method[22] (Supplementary Fig. 3). The 3D structures of TERT–F and Teb1–F telomerase holoenzymes are indistinguishable (Supplementary Fig. 4a), and Teb1–FZZ gave higher yields of holoenzyme. A 3D structure (Fig. 1c) of the ~500 kDa Teb1–F telomerase holoenzyme from 3D reconstruction of 2,220 particles with a resolution of ~25 Å (Supplementary Fig. 4b) demonstrates well-ordered holoenzyme density occupying about 200 × 150 × 80 Å.

To locate each protein subunit within the overall holoenzyme structure, telomerase was purified from strains harbouring FZZ-tagged TERT, p75, p65, p45, p19 or Teb1 in place of the corresponding untagged protein[6]. During purification, the ZZ portion of the tag was removed by proteolytic cleavage, leaving only the short F tag that was labelled using the antigen-binding fragment (Fab) derived from monoclonal anti-Flag antibody (see Methods). Each tagged protein can bind up to three Fabs, as illustrated in some of the class averages and 3D maps (Fig. 1c and Supplementary Fig. 5), which pinpoint to a single spot and localize the binding site of Fab unambiguously. Affinity purification of the biologically functional C-terminally tagged p50 (p50–FZZ) does not enrich sufficient holoenzyme for silver staining detection in SDS–PAGE, probably due to proteolysis between the C-terminal tag location and the region of p50 required for holoenzyme assembly[6]. Instead we used N-terminally ZZF-tagged p50 (ZZF–p50) expressed in partial replacement of the endogenous locus, which did purify holoenzyme to homogeneity (Supplementary Fig. 6). All holoenzyme protein subunits were localized by Fab labelling except p45, which was identified by process of elimination (see Methods). In addition, we affinity purified telomerase from a strain with biologically functional tagged TER harbouring a small hairpin tag (MS2hp), which is recognized by the MS2 coat protein (MS2cp), appended to TER stem 2 (S2)[23] (Fig. 1c and Supplementary Fig. 5g). The MS2cp dimer bound to this tag appears as extra density in the class averages and thus provides the approximate location of the TBE 5′ to the template (Fig. 1a).

The positions of the TERT and Teb1 C termini and the p50 N terminus could be precisely mapped in the 3D reconstructions of the respective Fab-labelled telomerase particles (Supplementary Fig. 5a–c), whereas a less precise location of the C termini of p65, p75 and p19 (which due to low purification yield did not give sufficient particles for RCT data collection) was obtained from the class averages (Supplementary Table, Fig. 1c and Supplementary Fig. 5d–f). Approximate subunit boundaries (schematized in Fig. 1d) could be modelled after fitting the holoenzyme density with known TERT[15–18], TER[8,24–26], p65[8] and Teb1[20] high-resolution domain structures combined with comparisons of class averages and 3D reconstructions across different complexes as described below. These data reveal that, in the 'front' view in Fig. 1c (schematized in Fig. 1d) with p65 at the bottom, TERT occupies the centre of the particle and 7-1-4 subunits form the top. Teb1 projects from the middle layer to the right. The p50 subunit is also part of the middle layer, networked between TERT, 7-1-4 and Teb1 (Fig. 1c, d). Numerous inter-subunit appositions generate an intricate and highly contoured surface.

The structure of the RNP catalytic core

Based on the determined subunit locations we fit the crystal and NMR structures of TER and protein domains in the electron microscopy density map of Teb1–F telomerase to generate a model of the entire RNP catalytic core (Fig. 2a and Supplementary Video). The RT and CTE domains of *Tetrahymena* TERT were homology modelled[27] from the *Tribolium castaneum* TERT crystal structure[18] and combined with the crystal structures of *Tetrahymena* partial TRBD[15] and TEN[16] domains as described in Methods. The modelled TERT TRBD-RT-CTE fits in only one orientation (Fig. 2a, b and Supplementary Fig. 7a, b). The position of the TERT CTE is consistent with the location of the C terminus identified in the 3D reconstruction of TERT–F–Fab telomerase (Fig. 1c and Supplementary Fig. 5a)[17]. The TEN domain was placed into density remaining after determination of subunit boundaries of the adjacent Teb1C and p50, and oriented based on the homology model of human TERT[28]. The modelled *Tetrahymena* TERT TRBD interacts with the CTE, which is consistent with the *Tribolium* TERT crystal structures[17,18] and isolated human TERT domain interactions[19]. There is electron microscopy density linking the TEN and CTE regions and the TEN and TRBD regions, which could correspond to the ~70 amino acids of potentially unstructured

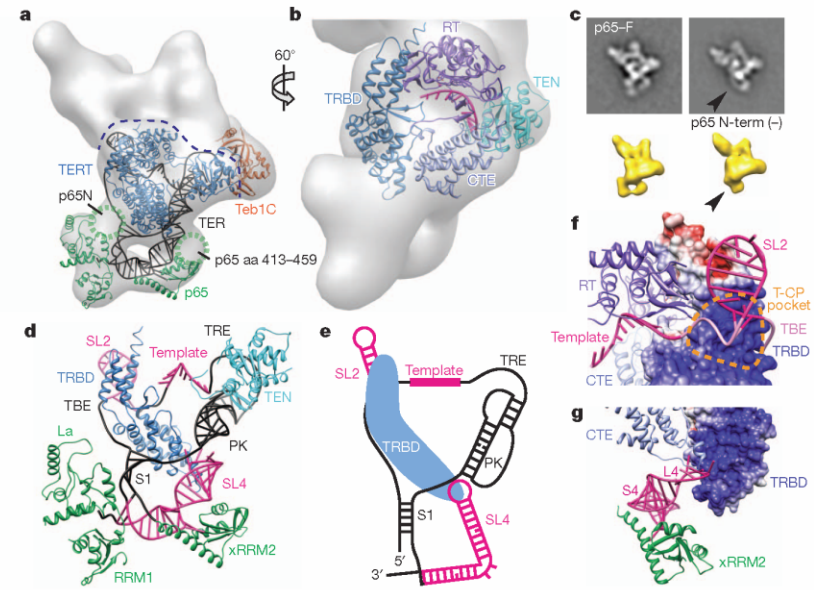

Figure 2 | Structure of the RNP catalytic core. **a**, 3D reconstruction of Teb1–F telomerase with TERT, p65 and TER (black), plus Teb1C modelled into the electron microscopy density. The dashed line indicates the top boundary of TERT/TER. **b**, Zoomed and rotated view of **a** showing TERT domains TEN, CTE, TRBD and RT, with TER template and essential Mg^{2+} at the active site in magenta. **c**, Class averages of p65–F telomerase (top) and 3D reconstructions (bottom) of TERT–F telomerase with p65 (left) and p65 missing N-terminal density (right, black arrows). **d**, TER model structure (well determined, magenta; remaining, black) and interactions with TERT TRBD and TEN and p65 La, RRM1, and xRRM2 domains. **e**, Secondary structure schematic of TER with TRBD. **f**, Modelled interaction between TBE (pink) and TRBD T-CP pocket. **g**, Modelled interactions of distal SL4 with CTE and bottom of TRBD. In **f**, **g**, TRBD is shown as GRASP surface.

TEN-TRBD linker[29,30] and adjacent TRBD sequence missing from high-resolution structures[15,16], which crosslinks to ssDNA and improves template boundary definition[19,31].

The C terminus of p65 is at the bottom of the particle, below TERT (Fig. 1d and Supplementary Fig. 5d). In the class averages and 3D reconstructions we observed particle subpopulations lacking part of the density at the bottom left of the particle (Fig. 2c and Supplementary Figs 2, 3c and 5d), which must arise from loss of p65 N-terminal domain(s) due to partial proteolysis of this subunit common during holoenzyme purification[6] and/or consequent loss of positional constraints on the remaining La and RRM1 domains. The structure of the p65 C-terminal domain xRRM2–stem 4 (S4) complex[8] could therefore be localized and fit to the density present in all the 3D reconstructions (Fig. 2a, d and Supplementary Fig. 7c, d). The remaining parts of S1–SL4 and p65 La and RRM1 could then be modelled (see Methods). The p65 N-terminal domain (near S1) and the long β2–β3 loop within xRRM2 that was deleted in the crystal structure could occupy the remaining unmodelled density (Fig. 2a)[8,26]. Together these fittings provide the overall topology of p65–TER interaction (Fig. 2a, d).

Tetrahymena TER contains two major domains, the template/pseudoknot (t/PK) and SL4, which are connected by S1 (Fig. 1a). Starting with the defined locations of the template in the active site of TERT[18], S2 by MS2cp labelling, and SL4 in complex with p65 xRRM2[8] (Fig. 2d, magenta), and considering topological restrictions based on the length of the single-stranded regions of TER, a model structure of the PK, and S1, we traced a potential trajectory of the entire TER (Fig. 2a, d, e) fit into the remaining electron microscopy density. The template recognition element (TRE) seems to be close to the TEN domain, as implicated biochemically[32], and the bottom of the PK is close to L4 (Fig. 2a, d). The locations of TER elements in the model are consistent with the large body of biochemical data on TER structure and function[4,5,33,34]. Of particular significance are the well-determined locations of the two TRBD binding elements, the TBE and L4[9,10,13,32], which we find bind to two distinct regions of the TRBD, near the top left and bottom of the TERT ring, respectively (Fig. 2b, d, e).

Remarkably, only the apical loop of SL4 connects to the density assigned to TERT, resulting in a U-shape at the bottom of the holoenzyme formed by TER S1/SL4 bound by p65. (Fig. 2a, d, e). The interaction of distal SL4 with TERT explains how it can stimulate telomerase activity when added to the t/PK in *trans*[35,36] and how binding of p65 xRRM2 to S4 mediates hierarchical assembly of p65–TER with TERT[8–10]. The electron microscopy structure and model reveal that the TRBD bridges the TBE and L4, which are ~40 Å apart. In the model, distal SL4 approaches the 3′ end of the PK, consistent with reported high fluorescence resonance energy transfer (FRET) between L4 and an internal PK position[37]. Although detailed interactions await a high-resolution structure, in the model the TBE contacts the TRBD in the T-pocket and CP-motif region (T-CP pocket) (Fig. 2f), which is consistent with biochemical data[12,14,15], and distal SL4 is flanked by the CTE and TRBD (Fig. 2g), potentially contributing to folding of TERT around TER.

p50 anchors the accessory proteins

The catalytic activity associated with telomerase purified using ZZF–p50 has low RAP, in contrast with the high-RAP activity enriched by the much lower yield of holoenzyme purified by p50–FZZ (Fig. 3a). The Fab labelling showed that the N terminus of p50 and the C terminus of Teb1 are relatively close together (Fig. 1c and Supplementary Fig. 5b, c). Comparison of the class averages of F–p50 and Teb1–F telomerase shows that all F–p50 telomerase particles lack density for Teb1 and reveals the boundary of Teb1 by difference map (Fig. 3b). The boundary of p50 was further defined by comparing class averages from a small subclass of particles containing only the RNP catalytic core, which was observed only in the MS2cp-bound MS2hp telomerase, with class averages containing p50 (Fig. 3c). Superpositions of 3D reconstructions of Fab–F–p50 and Teb1–F telomerase on TERT–F telomerase lacking Teb1 (see below) show that Fab bound to the N terminus of F–p50 occupies the same space as Teb1 (Fig. 3d). Together, these results identify the locations of Teb1 and p50, show that p50 interacts directly with the RNP catalytic core, and reveal that Teb1 is in close proximity to the N terminus of p50 and to TERT. The holoenzyme structure therefore explains the low-RAP activity of purified N-terminally tagged p50 (Fig. 3a), because enzyme purification by the N-terminal ZZF–p50 tag disrupts Teb1 binding. Beyond density assigned to the RNP catalytic core, Teb1, and p50, the remaining density in the top part of the 3D map is occupied by the 7-1-4 subcomplex. Taken together, 3D reconstructions reveal a central location for p50 in holoenzyme architecture, as an interaction hub between TERT, 7-1-4 and Teb1 (schematized in Fig. 3f).

Assigning function to subunit architecture

In parallel with structural analysis, we developed a method for holoenzyme reconstitution from entirely recombinant subunits. RNP catalytic

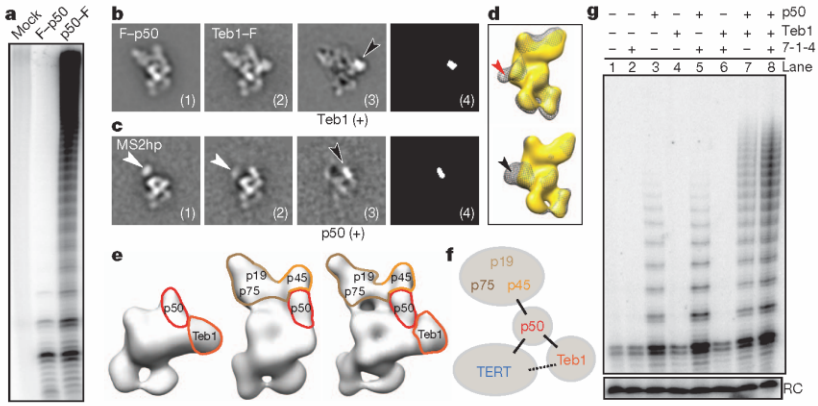

Figure 3 | p50 anchors TERT, 7-1-4 and Teb1. **a**, Primer extension assay of Flag antibody purifications from cell extracts lacking a tagged subunit (mock) or with F–p50 or p50–F. **b**, Class averages of F–p50 telomerase (1), Teb1–F telomerase (2), difference map by subtracting (1) from (2) (seen in 3), and map of statistically significant ($>4\,\sigma$) regions in the difference map (4). Black arrow points to Teb1 density. **c**, MS2hp telomerase class averages containing MS2cp without p50 (1), with p50 (2), difference map (3), and statistically significant regions (4) as in **b**. White and black arrows point to MS2cp and p50 densities, respectively. 7-1-4 is not seen in these class averages. **d**, Back view of 3D reconstructions of TERT–F telomerase lacking Teb1 (gold) overlaid with (top) Fab–F–p50 (grey mesh) and (bottom) Teb1–F telomerase (grey mesh) showing that Fab (red arrow) occupies the same site as Teb1 (black arrow). **e**, 3D reconstructions of TERT–F telomerase lacking 7-1-4 (left), lacking Teb1 (middle), and holoenzyme (right). **f**, Schematic of subunit interactions. **g**, Primer extension assay of the RNP catalytic core (TERT-TER-p65) reconstituted with additional combinations of 7-1-4, p50, and/or Teb1BC. Reactions were for 5 min. RC is a radiolabelled oligonucleotide added to telomerase products as a precipitation recovery control.

core with TERT–F was preassembled in rabbit reticulocyte lysate (RRL) and then combined with RRL-expressed p50 and/or 7-1-4 and/or bacterially expressed Teb1BC (see Methods)[21] (Fig. 3g). Direct primer-extension assays showed that addition of 7-1-4 or Teb1 alone did not alter the low-RAP product synthesis profile of the RNP catalytic core, but addition of p50 alone stimulated enzyme activity and the synthesis of multi-repeat products (Fig. 3g, lane 3). For p50-containing enzymes, 7-1-4 alone increased the amount of product (Fig. 3g, lane 5), Teb1 alone increased product length (lane 7), and their combination into complete holoenzyme was synergistic for increased activity level and long product synthesis (lane 8). These *in vitro* biochemical activities of p50, 7-1-4 and Teb1 were evident within a 5-min reaction time that allowed all product DNAs to be resolved by gel electrophoresis (Fig. 3g) or with the additional time and concentration of dGTP that supported very long product synthesis (Supplementary Fig. 8). The p50-dependent activity of 7-1-4 and Teb1 explains the presence of p50 in virtually all of the electron microscopy structures.

Previous reconstitution assays combined RRL-assembled recombinant RNP catalytic core, bacterially expressed Teb1 and endogenously assembled *Tetrahymena* proteins that remained bound to p45–F after micrococcal nuclease treatment of purified holoenzyme[20,21,38]. We found that the 7-1-4 complex isolated by this method does not completely dissociate p50, which as a full-length protein co-migrates with p45–F (Supplementary Fig. 6). The presence of residual p50 accounts for the reconstitution of holoenzyme-like catalytic activity by complementation of the RNP catalytic core and Teb1 in previous assays[20,21,38]. Reconstitutions using entirely recombinant holoenzyme subunits demonstrate a p50-dependent influence of 7-1-4 or Teb1 on RNP catalytic activity (Fig. 3g), consistent with their locations in the electron microscopy structures (Fig. 3e, f).

Teb1 domains are positionally flexible

All telomerase preparations except for those with tagged Teb1 have ~5% of particles missing density for Teb1 in the class averages and 3D reconstructions (Fig. 3e and Supplementary Fig. 2). This is not surprising, because Teb1 is sensitive to proteolysis and dissociation during holoenzyme affinity purification[6]. To identify specific Teb1 domains in the structures, we constructed strains in which TERT was C-terminally tagged at its endogenous locus with only tandem protein A domains (TERT–ZZ) and an N-terminally F-tagged Teb1C or Teb1BC was expressed from an integrated transgene. Holoenzyme particles isolated by tandem affinity purification of TERT–ZZ/F–Teb1C or TERT–ZZ/F–Teb1BC had the expected high RAP (Fig. 4a) and virtually identical class averages and 3D reconstructions to each other and to those from purified Teb1–F (Fig. 4b–d and Supplementary Fig. 4a). Because Teb1C mediates Teb1 association with other holoenzyme proteins[21] and the N-terminal tag on Teb1BC absolutely requires the associated holoenzyme to contain Teb1B, we conclude that the Teb1B domain is positionally flexible and therefore did not appear in the class averages and 3D reconstructions. Similarly, for Teb1–FZZ purified particles, which could contain all of the Teb1NABC domains, only Teb1C is visible in the majority of class averages. Teb1C was modelled into the electron microscopy density map (Fig. 2a) based on the position of the C terminus identified by Fab labelling and the best fit with the shape of the electron microscopy density. The orientation around the *y* axis is not definitive. We observed a small set of class averages (containing <5% of the particles) of F–Teb1BC and Teb1–F telomerases that show a weak extra density above Teb1C (Fig. 4c, d), which we assign to Teb1B. The conformational flexibility of Teb1 NAB domains relative to Teb1C is consistent with structural studies of the paralogous large subunit of replication protein A, which has three DNA-binding OB-fold domains that become ordered relative to each other only upon binding to ssDNA[39].

7-1-4 subcomplex has multiple orientations

Neither high-resolution structures nor exact biological functions of the 7-1-4 subunits are known. Both the electron microscopy structures and previous biochemical data[6,21] indicate they constitute a stably assembled subcomplex. Because no class averages lacking an individual 7-1-4 subunit were observed, inter-subunit boundaries could only be inferred from the class averages and Fab labelling of the C termini of p19 and p75, which showed that these two subunits are close together. In all class averages and 3D reconstructions, the major class of particles had a 7-1-4 conformation with p75 positioned across the top of the RNP catalytic core (Fig. 1c and Supplementary Fig. 2) in the stable conformation (Fig. 5). All telomerase samples show other positions of 7-1-4 in which it hinges away from the RNP catalytic core while maintaining a physical connection to p50 (Fig. 5 and Supplementary Fig. 3c). In these other conformations, the region of the class averages where 7-1-4 is located appears 'fuzzier'

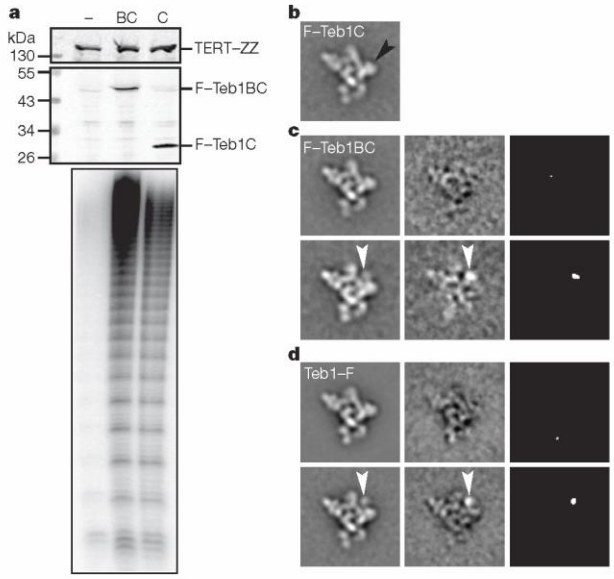

Figure 4 | Contribution of Teb1 domains to holoenzyme structure and activity. **a**, Cell extract western blots and two-step purified enzyme primer extension assays of F–Teb1BC (BC, lane 2) and F–Teb1C (C, lane 3) telomerase. Cell extract with TERT–ZZ alone (–, lane 1) is a negative control for specificity of F–Teb1BC and F–Teb1C binding to Flag antibody. **b–d**, Comparison of class averages (left column) of F–Teb1C (**b**), F–Teb1BC (**c**) and Teb1–F (**d**) telomerases. Density assigned to Teb1B (white arrows) was seen in <5% of particles, whereas density for Teb1C (black arrow in **b**) occupies a fixed position in all particles. Class averages without and with Teb1B density are represented by the upper and lower rows of **c** and **d**, respectively. Difference maps (middle column) by subtracting **b** from the respective class averages and maps of statistically significant ($>4\sigma$) regions in the difference maps (right column) in **c** and **d** show Teb1B density (white arrows).

than the rest of the particle, consistent with conformational variability in this part of telomerase holoenzyme. In ~10% of class averages from every purification, including those with tagged p75 or p45, no 7-1-4 density is visible, indicating that some 7-1-4 positions are not well defined relative to the RNP catalytic core (Fig. 3e and Supplementary Fig. 2). Binding of MS2cp to MS2hp holoenzyme seems to favour p75 displacement from the stable position (Fig. 1c and Supplementary Fig. 5g). Analysis of the various conformations indicates that 7-1-4 is rotating as an intact substructure (Fig. 5). Telomerase product DNA can be ultraviolet crosslinked to p45 as well as the TERT TEN domain[31,40], which suggests that at least some orientations of 7-1-4 must bring p45 close to DNA.

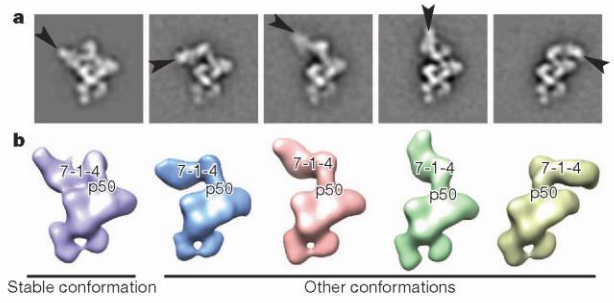

Figure 5 | Positional dynamics of 7-1-4. **a**, Teb1–F telomerase class averages with p75 indicated (black arrows). **b**, 3D reconstructions of Teb1–F telomerase showing different positions of 7-1-4.

Implications for holoenzyme assembly and function

TERT and TER comprise a minimal set of telomerase subunits for repeat synthesis *in vitro*[5,41], but despite extensive efforts the 3D arrangement and molecular interactions between TERT and TER have not been previously defined. Although divergent in size and sequence, TERs contain a t/PK domain and almost without exception a separate activating domain (SL4 in *Tetrahymena*), each with a TERT binding site[33,42]. Here we have unambiguously located two elements of *Tetrahymena* TER that constitute known binding sites for TERT and modelled a path of the entire TER. The functional equivalent of *Tetrahymena* TER distal SL4 in vertebrate TER is P6/P6.1, which ultraviolet crosslinks to the same region of the TRBD where L4 is located in our model[43]. Our model structure thus provides insight into human telomerase TERT–TER interactions and explains the separable interactions of the TERT binding elements on the t/PK and activating domains of TER.

Using classification and/or 3D reconstruction of 16 differently labelled telomerase samples (Supplementary Table), we were able to identify the subunit arrangement of the holoenzyme. The electron microscopy results together with reconstituted enzyme activity assays suggest a subdivision of holoenzyme functional units: the TERT–TER–p65 catalytic core, p50–Teb1, and 7-1-4. Both structure determination and activity assays of reconstituted holoenzyme subcomplexes establish a central role for p50, a subunit lacking any predicted domain folds. The electron microscopy data reveal that 7-1-4 is a structural unit with dynamic orientation relative to the rest of the holoenzyme. We suggest that the positional dynamics of 7-1-4 coordinate telomerase holoenzyme with additional telomere synthesis or processing activities.

In the model for holoenzyme subunit interactions, the TERT TEN domain, the lower region of p50 and Teb1C have a triangulated arrangement that suggests coordination by pairwise direct contacts. The TERT TEN domain is required for RAP and has been implicated in both ssDNA and TER binding[5,41,42]. Although Teb1 seems to contact TERT, subcomplex structures never have Teb1 in the absence of p50, and reconstituted enzyme activity assays do not show Teb1 function in the absence of p50. The assembly of p50 with the RNP catalytic core markedly increases processive repeat synthesis, indicating that p50 stabilizes enzyme association with ssDNA in potential functional analogy to yeast Est3 and vertebrate TPP1[44–48], favouring a productive TERT TEN domain conformation and/or providing additional ssDNA contact. Subsequent p50-dependent recruitment of Teb1 further enhances activity, which we speculate could occur through interaction of p50 and the Teb1C OB fold. The physical location of p50 determined by electron microscopy and its functional significance determined by reconstitution assays suggest that p50 could be a critical determinant of holoenzyme assembly *in vivo*. This first view of the architecture of a complete telomerase holoenzyme provides unprecedented opportunity to understand the biological mechanisms for coupling of telomerase to its telomere substrates.

METHODS SUMMARY

Tetrahymena strain constructions and steps of tag-based affinity purification were done as described[6] and as in Methods. To label the tagged subunit for electron microscopy, telomerase particles were first purified using anti-Flag M2 antibody resin then bound to rabbit-IgG resin. The telomerase-bound IgG resin was then incubated with Fab derived from anti-Flag M2 IgG, and elution was effected by protease cleavage. Negatively stained electron microscopy specimens were prepared with fresh telomerase samples, stained with 0.8% uranyl formate, and examined with an FEI Tecnai F20 electron microscope operated at 200 kV. Frozen hydrated specimens were prepared using Quantifoil grids and imaged with an FEI Titan Krios electron microscope operated at 120 kV. The image processing tasks, including image classification and RCT reconstruction, were performed as described in Methods.

Telomerase activity assays were performed at room temperature using purified telomerase complexes on Flag antibody resin with standard *Tetrahymena* holoenzyme reaction conditions using 0.3 μM ^{32}P-labelled dGTP. Holoenzyme reconstitution used synthetic genes encoding TERT–F, p75, p65, p50, p45 and p19 for

expression in RRL; TER purified following *in vitro* transcription by T7 RNA polymerase; and N-terminally His_6-tagged Teb1BC purified following bacterial expression[21].

Full Methods and any associated references are available in the online version of the paper.

Received 22 October 2012; accepted 8 March 2013.
Published online 3 April 2013.

1. Artandi, S. E. & DePinho, R. A. Telomeres and telomerase in cancer. *Carcinogenesis* **31,** 9–18 (2010).
2. Armanios, M. & Blackburn, E. H. The telomere syndromes. *Nature Rev. Genet.* **13,** 693–704 (2012).
3. Blackburn, E. H., Greider, C. W. & Szostak, J. W. Telomeres and telomerase: The path from maize, *Tetrahymena* and yeast to human cancer and aging. *Nature Med.* **12,** 1133–1138 (2006).
4. Egan, E. D. & Collins, K. Biogenesis of telomerase ribonucleoproteins. *RNA* **18,** 1747–1759 (2012).
5. Podlevsky, J. D. & Chen, J. J. L. It all comes together at the ends: Telomerase structure, function, and biogenesis. *Mutat. Res.* **730,** 3–11 (2012).
6. Min, B. & Collins, K. An RPA-related sequence-specific DNA-binding subunit of telomerase holoenzyme is required for elongation processivity and telomere maintenance. *Mol. Cell* **36,** 609–619 (2009).
7. Witkin, K. L. & Collins, K. Holoenzyme proteins required for the physiological assembly and activity of telomerase. *Genes Dev.* **18,** 1107–1118 (2004).
8. Singh, M. *et al.* Structural basis for telomerase RNA recognition and RNP assembly by the holoenzyme La family protein p65. *Mol. Cell* **47,** 16–26 (2012).
9. O'Connor, C. M. & Collins, K. A novel RNA binding domain in *Tetrahymena* telomerase p65 initiates hierarchical assembly of telomerase holoenzyme. *Mol. Cell. Biol.* **26,** 2029–2036 (2006).
10. Stone, M. D. *et al.* Stepwise protein-mediated RNA folding directs assembly of telomerase ribonucleoprotein. *Nature* **446,** 458–461 (2007).
11. Akiyama, B. M., Loper, J., Najarro, K. & Stone, M. D. The C-terminal domain of *Tetrahymena thermophila* telomerase holoenzyme protein p65 induces multiple structural changes in telomerase RNA. *RNA* **18,** 653–660 (2012).
12. Bryan, T. M., Goodrich, K. J. & Cech, T. R. Telomerase RNA bound by protein motifs specific to telomerase reverse transcriptase. *Mol. Cell* **6,** 493–499 (2000).
13. Lai, C. K., Mitchell, J. R. & Collins, K. RNA binding domain of telomerase reverse transcriptase. *Mol. Cell. Biol.* **21,** 990–1000 (2001).
14. Lai, C. K., Miller, M. C. & Collins, K. Template boundary definition in *Tetrahymena* telomerase. *Genes Dev.* **16,** 415–420 (2002).
15. Rouda, S. & Skordalakes, E. Structure of the RNA-binding domain of telomerase: Implications for RNA recognition and binding. *Structure* **15,** 1403–1412 (2007).
16. Jacobs, S. A., Podell, E. R. & Cech, T. R. Crystal structure of the essential N-terminal domain of telomerase reverse transcriptase. *Nature Struct. Mol. Biol.* **13,** 218–225 (2006).
17. Gillis, A. J., Schuller, A. P. & Skordalakes, E. Structure of the *Tribolium castaneum* telomerase catalytic subunit TERT. *Nature* **455,** 633–637 (2008).
18. Mitchell, M., Gillis, A., Futahashi, M., Fujiwara, H. & Skordalakes, E. Structural basis for telomerase catalytic subunit TERT binding to RNA template and telomeric DNA. *Nature Struct. Mol. Biol.* **17,** 513–518 (2010).
19. Robart, A. R. & Collins, K. Human telomerase domain interactions capture DNA for TEN domain-dependent processive elongation. *Mol. Cell* **42,** 308–318 (2011).
20. Zeng, Z. *et al.* Structural basis for *Tetrahymena* telomerase processivity factor Teb1 binding to single-stranded telomeric-repeat DNA. *Proc. Natl Acad. Sci. USA* **108,** 20357–20361 (2011).
21. Min, B. & Collins, K. Multiple mechanisms for elongation processivity within the reconstituted *Tetrahymena* telomerase holoenzyme. *J. Biol. Chem.* **285,** 16434–16443 (2010).
22. Radermacher, M., Wagenknecht, T., Verschoor, A. & Frank, J. Three-dimensional reconstruction from a single-exposure, random conical tilt series applied to the 50S ribosomal subunit of *Escherichia coli*. *J. Microsc.* **146,** 113–136 (1987).
23. Cunningham, D. D. & Collins, K. Biological and biochemical functions of RNA in the *Tetrahymena* telomerase holoenzyme. *Mol. Cell. Biol.* **25,** 4442–4454 (2005).
24. Chen, Y. *et al.* Structure of stem-loop IV of *Tetrahymena* telomerase RNA. *EMBO J.* **25,** 3156–3166 (2006).
25. Richards, R. J., Theimer, C. A., Finger, L. D. & Feigon, J. Structure of the *Tetrahymena thermophila* telomerase RNA helix II template boundary element. *Nucleic Acids Res.* **34,** 816–825 (2006).
26. Richards, R. J. *et al.* Structural study of elements of *Tetrahymena* telomerase RNA stem-loop IV domain important for function. *RNA* **12,** 1475–1485 (2006).
27. Arnold, K., Bordoli, L., Kopp, J. & Schwede, T. The SWISS-MODEL workspace: A web-based environment for protein structure homology modelling. *Bioinformatics* **22,** 195–201 (2006).
28. Steczkiewicz, K. *et al.* Human telomerase model shows the role of the TEN domain in advancing the double helix for the next polymerization step. *Proc. Natl Acad. Sci. USA* **108,** 9443–9448 (2011).
29. Friedman, K. L. & Cech, T. R. Essential functions of amino-terminal domains in the yeast telomerase catalytic subunit revealed by selection for viable mutants. *Genes Dev.* **13,** 2863–2874 (1999).
30. Armbruster, B. N., Banik, S. S. R., Guo, C., Smith, A. C. & Counter, C. M. N-terminal domains of the human telomerase catalytic subunit required for enzyme activity *in vivo*. *Mol. Cell. Biol.* **21,** 7775–7786 (2001).
31. Romi, E. *et al.* High-resolution physical and functional mapping of the template adjacent DNA binding site in catalytically active telomerase. *Proc. Natl Acad. Sci. USA* **104,** 8791–8796 (2007).
32. O'Connor, C. M., Lai, C. K. & Collins, K. Two purified domains of telomerase reverse transcriptase reconstitute sequence-specific interactions with RNA. *J. Biol. Chem.* **280,** 17533–17539 (2005).
33. Theimer, C. A. & Feigon, J. Structure and function of telomerase RNA. *Curr. Opin. Struct. Biol.* **16,** 307–318 (2006).
34. Cole, D. I. *et al.* New models of *Tetrahymena* telomerase RNA from experimentally derived constraints and modeling. *J. Am. Chem. Soc.* **134,** 20070–20080 (2012).
35. Lai, C. K., Miller, M. C. & Collins, K. Roles for RNA in telomerase nucleotide and repeat addition processivity. *Mol. Cell* **11,** 1673–1683 (2003).
36. Mason, D. X., Goneska, E. & Greider, C. W. Stem-loop IV of *Tetrahymena* telomerase RNA stimulates processivity in trans. *Mol. Cell. Biol.* **23,** 5606–5613 (2003).
37. Wu, J. Y., Stone, M. D. & Zhuang, X. A single-molecule assay for telomerase structure-function analysis. *Nucleic Acids Res.* **38,** e16 (2010).
38. Eckert, B. & Collins, K. Roles of telomerase reverse transcriptase N-terminal domain in assembly and activity of *Tetrahymena* telomerase holoenzyme. *J. Biol. Chem.* **287,** 12805–12814 (2012).
39. Fan, J. & Pavletich, N. P. Structure and conformational change of a replication protein A heterotrimer bound to ssDNA. *Genes Dev.* **26,** 2337–2347 (2012).
40. Rosenfeld, K. K., Ziv, T., Goldin, S., Glaser, F. & Manor, H. Mapping of DNA binding sites in the *Tetrahymena* telomerase holoenzyme proteins by UV cross-linking and mass spectrometry. *J. Mol. Biol.* **410,** 77–92 (2011).
41. Collins, K. Single-stranded DNA repeat synthesis by telomerase. *Curr. Opin. Chem. Biol.* **15,** 643–648 (2011).
42. Blackburn, E. H. & Collins, K. Telomerase: An RNP enzyme synthesizes DNA. *Cold Spring Harb. Perspect. Biol.* **3,** a003558 (2011).
43. Bley, C. J. *et al.* RNA–protein binding interface in the telomerase ribonucleoprotein. *Proc. Natl Acad. Sci. USA* **108,** 20333–20338 (2011).
44. Lee, J., Mandell, E. K., Rao, T., Wuttke, D. S. & Lundblad, V. Investigating the role of the Est3 protein in yeast telomere replication. *Nucleic Acids Res.* **38,** 2279–2290 (2010).
45. Yen, W. F., Chico, L., Lei, M. & Lue, N. F. Telomerase regulatory subunit Est3 in two *Candida* species physically interacts with the TEN domain of TERT and telomeric DNA. *Proc. Natl Acad. Sci. USA* **108,** 20370–20375 (2011).
46. Talley, J. M., DeZwaan, D. C., Maness, L. D., Freeman, B. C. & Friedman, K. L. Stimulation of yeast telomerase activity by the ever shorter telomere 3 (Est3) subunit is dependent on direct interaction with the catalytic protein Est2. *J. Biol. Chem.* **286,** 26431–26439 (2011).
47. Zaug, A. J., Podell, E. R., Nandakumar, J. & Cech, T. R. Functional interaction between telomere protein TPP1 and telomerase. *Genes Dev.* **24,** 613–622 (2010).
48. Sexton, A. N., Youmans, D. T. & Collins, K. Specificity requirements for human telomere protein interaction with telomerase holoenzyme. *J. Biol. Chem.* **287,** 34455–34464 (2012).

Supplementary Information is available in the online version of the paper.

Acknowledgements This work was supported by grants from NSF MCB1022379 and NIH GM48123 to J.F., NIH GM54198 to K.C., GM071940 and AI069015 to Z.H.Z., Ruth L. Kirschstein NRSA postdoctoral fellowship GM101874 to E.J.M., and Ruth L. Kirschstein NRSA pre-doctoral training grant GM007185 fellowship for H.C. and D.D.C. We acknowledge the use of instruments at the Electron Imaging Center for NanoMachines supported by NIH (1S10RR23057 to ZHZ) and CNSI at UCLA.

Author Contributions J.J. and E.J.M. purified and characterized electron microscopy samples, collected and analysed electron microscopy data, and wrote the paper; K.H., B.E. and B.M. designed and made strains, expression plasmids, initial purifications and reconstituted holoenzyme; H.C. purified telomerase; D.D.C. refined and modelled elements of TER; Z.H.Z., K.C. and J.F. supervised the research, analysed data and wrote the paper.

Author Information Reprints and permissions information is available at www.nature.com/reprints. The authors declare no competing financial interests. Readers are welcome to comment on the online version of the paper. Correspondence and requests for materials should be addressed to J.F. (feigon@mbi.ucla.edu), K.C. (kcollins@berkeley.edu) or Z.H.Z (hong.zhou@ucla.edu).

METHODS

Strain construction, growth and analysis. *Tetrahymena* strains TERT–FZZ, Teb1–FZZ, p75–FZZ, p65–FZZ, p50–FZZ, MS2hp, p45–FZZ and p19–FZZ were previously described[6,23]. New strains ZZF–p50, TERT–ZZ/F–Teb1C and TERT–ZZ/F–Teb1BC were selected for targeted replacement of the endogenous locus (ZZF–p50 or TERT–ZZ) and/or for *MTT1* promoter-driven transgene integration at *BTU1* (F–Teb1C, F–Teb1BC) using the *neo2* and *bsr2* cassettes[6,49]. Cells were grown to mid-log phase ($2–4 \times 10^5$ cells per ml) at 30 °C in modified Neff medium (0.25% proteose peptone (EMD Milipore Chemicals), 0.25% BD Bacto yeast extract (Becton Dickinson), 0.2% glucose, 30 μM $FeCl_3$). For large-scale purifications, transgene expression was induced by addition of 6 μM $CdCl_2$ 1 h before harvesting. Cell extract preparation and affinity purifications for subunit identification and activity assays were performed as described[6]. Genotypes were verified by Southern blots and western blots using rabbit IgG (Sigma) to detect the ZZ tag or anti-Flag M2 mouse monoclonal antibody (Sigma) to detect the Flag tag. Reconstituted enzyme activity assays were performed at room temperature using purified telomerase complexes on Flag antibody resin following standard *Tetrahymena* holoenzyme reaction conditions (50 mM Tris-acetate, pH 8.0, 10 mM spermidine, 5 mM 2-mercaptoethanol, 2 mM $MgCl_2$, 100 nM $d(GT_2G_3)_3$, 200 μM dTTP, and 0.3 μM ^{32}P-labelled dGTP) for 5 min or with 3.0 μM ^{32}P-labelled dGTP for 15 min[6]. Holoenzyme reconstitution used synthetic genes encoding TERT–FZZ, p75, p65, p50, p45 and p19 for expression in RRL; TER purified following *in vitro* transcription by T7 RNA polymerase; and N-terminally His_6-tagged Teb1BC purified following bacterial expression[21].

Cell extract preparation and affinity purification for electron microscopy. Cells were collected by centrifugation (5 min, 2,100*g*), washed in 20 mM HEPES NaOH, pH 8.0, and then resuspended in lysis buffer (30 ml per l of growth) containing H2EG50 (20 mM HEPES NaOH, pH 8.0, 50 mM NaCl, 1 mM EDTA TS, 1 mM TCEP HCl, and 10% glycerol) supplemented with 0.1% Triton X-100, 0.2% IGEPAL CA-630, 0.1 mM PMSF, 5 μM proteosome inhibitor MG-132, and 1,000-fold dilution of Sigma Protease Inhibitor Cocktail P8340. To effect cell lysis, resuspensions were rotated end-over-end for 20 min and cleared by ultracentrifugation (1 h, 145,000*g*).

To minimize proteolysis, all purification steps were carried out at 4 °C and additional washes were used in the early steps of purification as described below. Rabbit-IgG agarose slurry (Sigma) (3 μl per ml of cell extract) was washed 3× in lysis buffer, then added to cell extract for binding with end-over-end rotation overnight. Resin was collected by centrifugation (1 min, 3,200*g*) and washed 3× with no incubation and then 3× with end-over-end rotation (10 min) in wash buffer (20 mM HEPES NaOH, pH 8.0, 50 mM NaCl, 1 mM $MgCl_2$, 1 mM TCEP HCl, 10% glycerol, and 0.1% IGEPAL CA-630). Telomerase was eluted with tobacco etch virus (TEV) protease (30 nM) in wash buffer for 1 h. After elution, supernatant containing holoenzyme was incubated with washed anti-Flag M2 affinity gel (Sigma) for 1 h (4 μl slurry per g of pelleted cells). After binding, anti-Flag M2 affinity gel was washed as above. Elution was effected by addition of glycerol-free wash buffer containing 3×Flag peptide (Sigma, 200 ng μl^{-1}).

Fab labelling for subunit identification. Anti-Flag Fab was prepared by incubating monoclonal mouse anti-Flag M2 IgG (Sigma) with resin-immobilized papain (Thermo Scientific Pierce) and purified according to the manufacturer's protocol. To prevent masking of the 3×Flag epitope present on the target subunit by the 3×Flag peptide required for elution, the tandem purification was done in reverse order with anti-Flag M2 affinity gel purification followed by rabbit-IgG agarose purification. Washing and elution were done as described above. To effect Fab labelling, holoenzyme-enriched rabbit-IgG agarose was incubated (1 h, 4 °C) with wash buffer containing anti-Flag Fab (7.5 μg ml^{-1}). Excess Fab was removed by washing 5× with wash buffer. Labelled holoenzyme was eluted with wash buffer containing His_6-TEV protease (2 nM). After elution, His_6-TEV protease was removed from the elution by incubating with washed Ni-NTA agarose (30 min, 4 °C).

Holoenzyme purification by MS2cp. *Tetrahymena* expressing MS2hp TER were collected, lysed and clarified as described above. N-terminal His_6–ZZF–MS2cp bacterially expressed from pET28 was purified using Ni-NTA agarose. Rabbit-IgG agarose was incubated with His_6–ZZF–MS2cp in a 1:1 stoichiometry to anticipated holoenzyme yield based on previous preparations. The enriched rabbit-IgG agarose was then washed 3× and added to clarified extract for overnight incubation. Purification then proceeded as described above.

Electron microscopy specimen preparation and data collection. For negative staining electron microscopy, 2 μl of telomerase sample was applied to a glow-discharged grid coated with carbon film. The sample was left on the carbon film for 10 s, followed by negative staining with 0.8% uranyl formate. Negatively stained specimens were carefully examined by electron microscopy, and only the regions with particles fully embedded in stain were selected for imaging. Electron microscopy micrographs were recorded on a TIETZ F415MP 16-megapixel CCD camera at 68,027× magnification in an FEI Tecnai F20 electron microscope operated at 200 kV. The micrographs were saved by 2× binning and had a pixel size of 4.4 Å. To overcome the problems of preferred orientation and structural variability of the samples, 3D reconstructions were carried out using RCT method, which takes advantage of classification to differentiate different conformations and tilting to get lateral views for 3D reconstruction[22]. RCT images were collected with the grids tilted at two angles successively (65° and 0°) for each specimen area of interest with the assistance of Leginon automation software[50,51]. To minimize the potential smearing/stretching on 3D maps due to the missing cone problem in RCT data collection, a high tilt angle (65°) was used. For samples where only 2D image analysis was performed, micrographs were taken without tilting of the grids. Total numbers of micrographs and particles used for analysis are summarized in the Supplementary Table.

For cryo-electron microscopy, 2.5 μl of sample was applied to a glow-discharged Quantifoil R2/1 grid. The grid was then blotted with filter paper to remove excess sample, and flash-frozen in liquid ethane with an FEI Vitrobot Mark IV. The grid was loaded into an FEI Titan Krios electron microscope operated at 120 kV. Micrographs were acquired with a Gatan UltraScan4000 16-megapixel CCD camera at 65,162× magnification with defocus values ranging from −1.9 to −4.0 μm and an exposure dose of 20 $e^- Å^{-2}$, and without tilting of the grids. The micrographs with a pixel size of 2.3 Å were used for data processing without binning.

2D image reference-free classification. Particles from the untilted micrographs were automatically picked using DoGpicker[52]. All particles in the micrographs, including a small number of aggregated particles, were initially picked to avoid bias in selecting particles. Particles were boxed out in 96 × 96 pixels (or 144 × 144 pixels for cryo-electron microscopy images) using *batchboxer* in EMAN[53]. The defocus value of each micrograph was determined by CTFFIND[54] and the particles were corrected for contrast transfer function (CTF) by phase-flipping with the corresponding defocus and astigmatism values using bsoft[55]. The phase-corrected particles were then iteratively (normally 9 iterations) classified using the *refine2d.py* program in EMAN. The classification for each sample was done independently without using any model or reference. The aggregated particles clustered in the few classes showing poor structures were manually eliminated during the iterations of classification. For the samples at very low concentration (Fab-labelled p75–F, p19–F and p65–F telomerase, and MS2cp-labelled MS2hp telomerase), a looser criterion for DoGpicker was used to pick more particles and consequently some 'fake' particles from the stain background were also selected. The class averages were visually inspected at several different iterations of classification to remove the 'fake' particles that were clustered in a small set of class averages that show no structural features.

For the RCT 3D reconstructions (Supplementary Table), the screened particles from the above steps were re-classified using the Correspondence Analysis method in SPIDER[56].The class averages from the above EMAN classification step were used as references for multi-reference alignment in SPIDER. Each new class from this analysis was used for an RCT 3D reconstruction.

RCT 3D reconstruction and refinement. Corresponding particles from tilt pairs (65° and 0°) were picked using *ApTiltPicker.py* in Appion[52] modified to optimize automatic particle picking and verified by visual inspection. The 0° tilt particles were classified as described above. Next, 3D RCT maps were reconstructed from 65° tilt particles. Particles within each class of the 0° tilt data set all have the same conformation and the same orientation except in-plane rotation. Their corresponding 65° tilt particles have different orientations due to in-plane rotation and were combined to reconstruct one 3D map. Each 3D map was iteratively refined with SPIDER followed by FREALIGN[57] by refinement of the centre of 65° tilt particles in the corresponding class. A representative refinement procedure is shown in Supplementary Fig. 3b. The orientations of 65° tilt particles were calculated from the in-plane rotation of the corresponding 0° tilt particles and the geometric relationship between the 65° and 0° tilt micrographs, and kept fixed during structure refinement. Multiple 3D maps were generated from RCT 3D reconstruction because particles in different conformations were classified into different classes each of which generated an individual 3D map. Representative 3D maps are shown in Supplementary Fig. 3c. Each 3D map was refined using only the 65° tilt particles in its corresponding class. The defocus value of each 65° tilt particle was calculated by CTFTILT program[54] and then applied to 3D reconstructions with FREALIGN for proper correction of phase and amplitude in CTF.

To estimate the resolution of the representative 3D map of Teb1–F telomerase in the 'stable' conformation, the 2,220 65° tilt particles used to reconstruct that 3D map were split into odd- and even-numbered halves and the halves of data were used to reconstruct two 3D maps with FREALIGN using the determined orientations and image centres, respectively, to calculate Fourier shell correlation (FSC). The resolution is 25 Å at FSC = 0.5 (Supplementary Fig. 4b). For comparison, the FSC was also calculated using the recently introduced 'gold standard' FSC

method[58], in which the halves of data (both 65° and 0° tilt) were split at the beginning for independent orientation determination, 3D reconstruction, and refinement to generate two independent 3D maps. The 'gold standard' FSC suggests resolutions of 29 Å at FSC = 0.5 and 24 Å at FSC = 0.143 (Supplementary Fig. 4b). Since a high tilt angle (65°) was used for RCT 3D reconstructions, the missing cone was minimized and did not have notable impact on the structural interpretation of the 3D maps at the present resolution.

Evaluation of sample integrity by size-exclusion chromatography (SEC). To confirm that the affinity-purified telomerase holoenzymes were intact after purification and that negative staining did not induce significant aggregation, we obtained an SEC profile of a sample of affinity purified TERT–F telomerase and electron microscopy images from the peak fractions (Supplementary Fig. 1c, d). The sample (50 µl) was run at 50 µl min^{-1} on a Superdex 200 column in the same buffer used for the electron microscopy samples except IGEPAL CA-630 was replaced by Tween-80. The SEC profile shows that the telomerase holoenzyme runs as a single peak with a constant $A_{260\,nm}/A_{280\,nm}$ ratio indicative of a largely intact RNA–protein complex. The class averages of particles from the peak fraction are identical to those for the affinity-purified sample (data not shown). There are no later eluting peaks from dissociated subunits (which would have different $A_{260\,nm}/A_{280\,nm}$ ratios).

Localization of Fab-labelled subunits. Each protein was assigned by identifying the characteristic Fab density in the class averages and 3D reconstructions. The 3×Flag tag allows up to three Fabs to bind simultaneously. Fab was observed attached to all tagged telomerase particles except for p45–F. For p45–F telomerase, Fabs were observed bound to free p45–F protein, while the p45–F telomerase holoenzyme particles appeared unchanged. The location of p45 in the holoenzyme was therefore assigned based on the density remaining after assignment of TERT–F, Teb1–F, p75–F, p65–F, F–p50 and p19–F.

Fitting of atomic models into the 3D electron microscopy maps. The homology model of *Tetrahymena* TERT RT-CTE domains was built using amino acids 520–1117 and the *Tribolium* TERT crystal structure (PDB ID: 3KYL) as a template with SWISS-MODEL[27]. The model of *Tetrahymena* TERT (TRBD, RT, and CTE domains) was built by joining the crystal structure of *Tetrahymena* TRBD (PDB ID: 2R4G) and the homology model of RT-CTE domains using the *Tribolium* TERT crystal structure as reference for structural alignment. The model of *Tetrahymena* TERT was then manually placed in an approximate position in the electron microscopy density map, followed by docking into the electron microscopy density map accurately using the "Fit in Map" function in UCSF Chimera[59]. The location of the TEN domain, absent in *Tribolium* TERT[17], was supported by definition of the subunit boundaries of the adjacent Teb1C and p50. The crystal structure of *Tetrahymena* TERT TEN domain (PDB ID: 2B2A) was manually placed into the electron microscopy density map. Its position was iteratively adjusted to fit the empty density adjacent to the boundaries of Teb1 and p50 and the rest of TERT. Because the orientation of the TEN domain could not be determined based on the electron microscopy density due to the limit of resolution, we oriented it to be consistent with the homology model of human TERT[28]. For fitting of p65 xRRM2:SL4, the putative electron microscopy density of p65–TER cut from the full electron microscopy density map was used in order to avoid interference from unrelated structures. The model of p65 xRRM2:SL4[8] was manually placed in the electron microscopy density map based on the location of the C terminus determined by Fab labelling and then docked using the "Fit in Map" function in UCSF Chimera. Its position was further manually adjusted to avoid clashing with the model of TERT. To confirm the fittings of TERT and p65 xRRM2:SL4, these two structures were also fit into the electron microscopy density map using the *colores* program in Situs[60]. The fitting with *colores* was automated by 6D-space search and contour-based matching, and did not require manual placing of high-resolution structures to approximate positions in electron microscopy density maps. The crystal structure of Teb1C (PDB ID: 3U50) was manually placed into the electron microscopy density map and its orientation was adjusted so that the position of its C terminus was consistent with the result from the Fab labelling experiment. The homology model of p65 La-RRM1:AUUUU-3′[8,61] was manually placed into the electron microscopy density map, and its orientation was adjusted to match the shape of the electron microscopy density map. Cross-correlation for the fittings were: TERT TRBD-RT-CTE, 0.91; TERT TEN, 0.84; p65 xRRM2:SL4, 0.80; p65 La-RRM1:AUUUU-3′, 0.86; and Teb1C, 0.82. Although the position and orientation of p65 xRRM2:SL4 are well determined, the cross-correlation coefficient reflects the absence of the β2–β3 loop and amino acids linking xRRM2 to RRM1 in the crystal structure[8].

Structures of SL2, distal SL4 and the PK. Previously reported NMR structures of SL2 and distal SL4[25,26] were re-refined using a new nuclear Overhauser enhancement (NOE) restraint list derived from re-analysis of all previously obtained 2D nuclear Overhauser enhancement spectroscopy (NOESY) and 3D NOESY-heteronuclear multiple quantum correlation (HMQC) spectra and a new set of residual dipolar couplings (RDC) restraints (63 for SL2 and 48 for distal SL4) collected using pf1 bacteriophage for the alignment media. The new PDB accession numbers for SL2 and distal SL4 are 2M22 and 2M21, respectively, and BMRB accession numbers are 18892 and 18891, respectively. A grid search produced optimal values for the magnitude and asymmetry of the RDC alignment tensor of $D_a = -22.3$ Hz, $R = 0.38$ for SL2, and $D_a = -17.5$ Hz, $R = 0.40$ for SL4. The structures were calculated from an extended, unfolded RNA conformation using XPLOR-NIH v.2.9.8[62,63] following standard XPLOR protocols. A model structure of the PK was generated based on the secondary structure and two U-A-U triples predicted by sequence analysis[64]. XPLOR-NIH was used to calculate the structure from an extended RNA conformation as previously described[62,63]. A mock NMR restraint list was derived based on the solution structure of the human telomerase PK[65]. For the two stems, A-form RNA restraints were used for the dihedral angles and NOEs. NOEs for residues in the stems include H6/H8 (Py/Pu) to its own sugar protons and to the sugar protons (H1′, H2′, H3′, H4′) of the $n-1$ residue, H6/H8 to H6/H8 sequential, and imino sequential NOEs. For the PK loop 1, base-triple hydrogen bond restraints, planarity restraints with PK stem 2 residues, and sequential stacking NOEs were used to form the structured triple helix. PK loop 2 was given H6/H8 sequential NOEs and H6/H8–H1′ NOEs within the minor groove of PK stem 1 to place it in the expected conformation.

Modelling of TER. First, the position of the template in TER was determined by matching the crystal structure of *Tribolium* TERT–nucleic acid complex (PDB ID: 3KYL) with the docked model of *Tetrahymena* TERT. Second, the position of SL4 was determined by the docking of the atomic model of p65 xRRM2:SL4 complex into the electron microscopy density map. Third, the atomic model of SL2 was manually placed into the electron microscopy density map and its position was iteratively adjusted to match the result from MS2cp labelling experiment. S1 (modelled as A-form RNA) and the PK were placed into the electron microscopy density map based on physical constraints with the rest of TER. S1 is connected to S4 by 4 nucleotides and to S2 by 10 nucleotides. The model of the 31 nucleotide PK, which is connected to S1 by 3 nucleotides and to the template by the TRE, was fit into the only region of unoccupied density, between the TRBD and TEN domains, remaining after all the other major elements of TERT and TER were localized. Although the modelled positions of the TRE 3′ to the template (Fig. 1a) and the top of the pseudoknot could potentially be swapped with the TEN domain, they would still be on the same side (right side or behind in Fig. 2a or 2b, respectively) of the TERT TRBD-RT-CTE ring that has the active site and bound template. In either case, the TRE appears to be close to the TEN domain. The single-stranded regions of TER (except the template) were initially modelled as ideal A-form single-stranded RNA and their structures were modified using the "Minimize structure" function in UCSF Chimera to connect with their respective folded RNA fragments. The electron microscopy density maps and the modelled protein and RNA structures were visualized with UCSF Chimera.

49. Couvillion, M. T. & Collins, K. Biochemical approaches including the design and use of strains expressing epitope-tagged proteins. *Methods Cell Biol.* **109,** 347–355 (2012).
50. Suloway, C. *et al.* Automated molecular microscopy: The new Leginon system. *J. Struct. Biol.* **151,** 41–60 (2005).
51. Suloway, C. *et al.* Fully automated, sequential tilt-series acquisition with Leginon. *J. Struct. Biol.* **167,** 11–18 (2009).
52. Voss, N. R., Yoshioka, C. K., Radermacher, M., Potter, C. S. & Carragher, B. DoG Picker and TiltPicker: Software tools to facilitate particle selection in single particle electron microscopy. *J. Struct. Biol.* **166,** 205–213 (2009).
53. Ludtke, S. J., Baldwin, P. R. & Chiu, W. EMAN: Semiautomated software for high-resolution single-particle reconstructions. *J. Struct. Biol.* **128,** 82–97 (1999).
54. Mindell, J. A. & Grigorieff, N. Accurate determination of local defocus and specimen tilt in electron microscopy. *J. Struct. Biol.* **142,** 334–347 (2003).
55. Heymann, J. B. Bsoft: Image and molecular processing in electron microscopy. *J. Struct. Biol.* **133,** 156–169 (2001).
56. Frank, J. *et al.* SPIDER and WEB: Processing and visualization of images in 3D electron microscopy and related fields. *J. Struct. Biol.* **116,** 190–199 (1996).
57. Grigorieff, N. FREALIGN: High-resolution refinement of single particle structures. *J. Struct. Biol.* **157,** 117–125 (2007).
58. Scheres, S. H. & Chen, S. Prevention of overfitting in cryo-EM structure determination. *Nature Methods* **9,** 853–854 (2012).
59. Pettersen, E. F. *et al.* UCSF Chimera—A visualization system for exploratory research and analysis. *J. Comput. Chem.* **25,** 1605–1612 (2004).
60. Chacón, P. & Wriggers, W. Multi-resolution contour-based fitting of macromolecular structures. *J. Mol. Biol.* **317,** 375–384 (2002).
61. Jacks, A. *et al.* Structure of the C-terminal domain of human La protein reveals a novel RNA recognition motif coupled to a helical nuclear retention element. *Structure* **11,** 833–843 (2003).
62. Schwieters, C. D., Kuszewski, J. J. & Marius Clore, G. Using Xplor–NIH for NMR molecular structure determination. *Prog. Nucl. Magn. Reson. Spectrosc.* **48,** 47–62 (2006).
63. Schwieters, C. D., Kuszewski, J. J., Tjandra, N. & Marius Clore, G. The Xplor–NIH NMR molecular structure determination package. *J. Magn. Reson.* **160,** 65–73 (2003).

64. Ulyanov, N. B., Shefer, K., James, T. L. & Tzfati, Y. Pseudoknot structures with conserved base triples in telomerase RNAs of ciliates. *Nucleic Acids Res.* **35,** 6150–6160 (2007).

65. Theimer, C. A., Blois, C. A. & Feigon, J. Structure of the human telomerase RNA pseudoknot reveals conserved tertiary interactions essential for function. *Mol. Cell* **17,** 671–682 (2005).

CONTRIBUTION TO:

THE ARCHITECTURE OF *TETRAHYMENA* TELOMERASE HOLOENZYME

Introduction

In Jiang & Miracco et al. 2013 Nature [1], the negative stain electron microscopy structure of *Tetrahymena* telomerase is reported at 25 Å resolution. In this work the authors were able to determine the relative locations of six out of seven of the known protein subunits through fab labelling of an engineered 3x FLAG tag on the C-termini of TERT, p65, Teb1, p75 and p19, and on the N-terminus of p50 [2]. The C-terminus of p45 was also labelled but 2D class averages failed to identify a convergent position for the fab. To localize the RNA subunit, an optimized hairpin that binds to the bacteriophage MS2 coat protein [3, 4] was introduced, via replacement at the endogenous locus, to the end of Stem-loop II (SL2) on TER (**Figure 2.6**) by our collaborators in the Collins lab. This mutation was previously shown to not interfere with telomerase activity *in vivo* and *in vitro* [5].

The MS2 coat protein binds the MS2 hairpin (MS2-hp) as a 30 kDa dimer that is distinguishable by negative stain EM. By comparing the negative stain 2D class averages of the MS2 bound telomerase with that of free telomerase, the relative location of the MS2 hairpin and thus SL2 can be determined. To obtain a homogenous and MS2 labelled sample, the purification was performed using ZZtag-TEVsite-FLAGtag-MS2 coat protein to pull down telomerase. The V75E, A81G MS2 coat protein mutant which allows dimerization but suppresses capsid formation was used [6].

Results

The purification of MS2-telomerase was ~1/2 - 1/4 of a normal yield and much less pure (**Figure 2.7**). However, the negative stain EM images of the sample yielded 2D class averages of sufficient quality to identify and locate the MS2 coat protein dimer bound to the telomerase RNA (**Figure 2.8**) relative to the holoenzyme. Interestingly, in many of the class averages, p75, p45 and p19 appear to be sterically hindered by the MS2 coat protein and cause the p75-p45-p19 subcomplex to adopt an

alternative conformation relative to the holoenzyme or be completely displaced. The results and implications are discussed in detail in Jiang & Miracco et al. 2013 Nature [1].

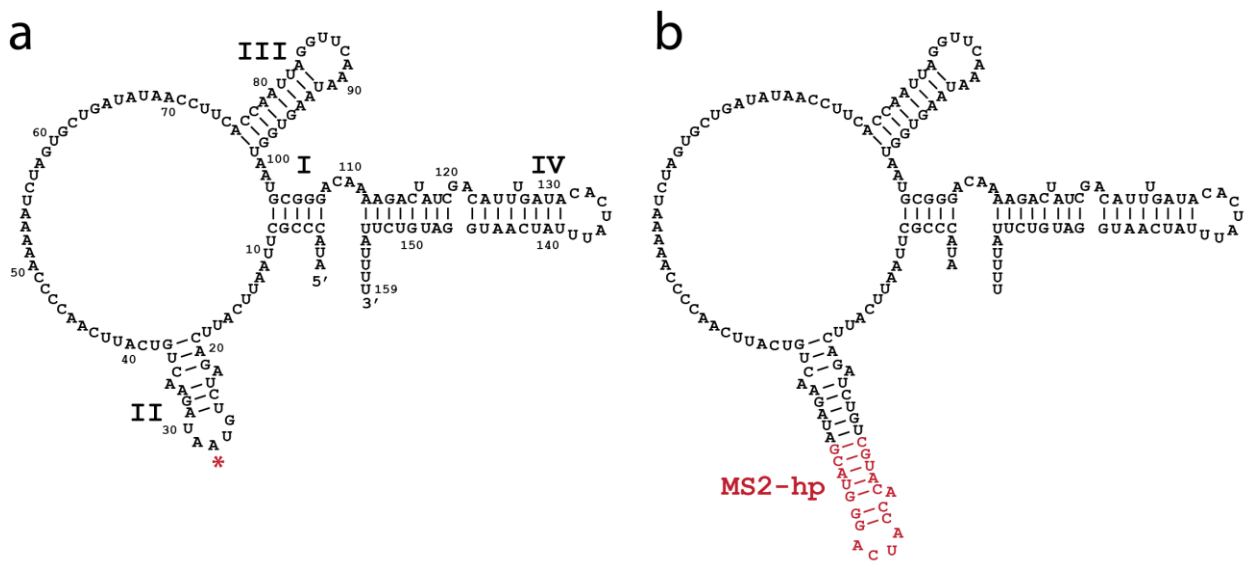

Figure 2.6. MS2-hp addition to *Tetrahymena* TR stem-loop II. (*a*) Wild-type *Tetrahymena* telomerase RNA. (*b*) *Tetrahymena* telomerase RNA with residue A28 (*) replaced by a 19 residue hairpin (red) optimized for MS2 coat protein binding.

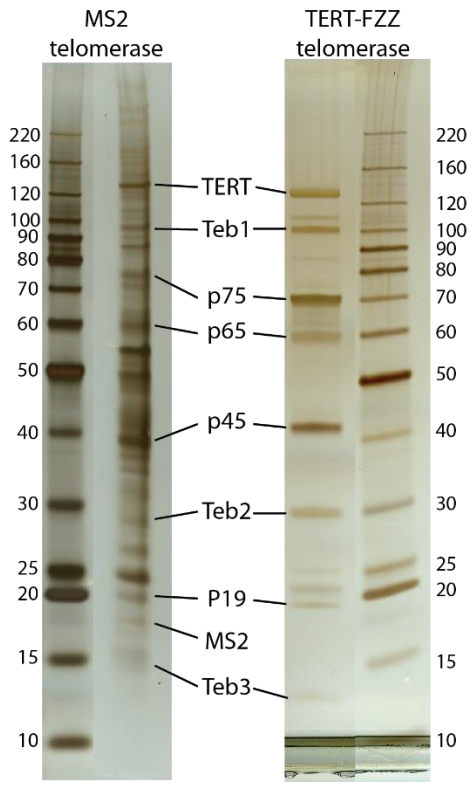

Figure 2.7. Silver stained 4-12% SDS PAGE gels of MS2 purified telomerase. MS2 purified (left) compared to TERT-FZZ purified (right) telomerase. The molecular weight standard used is the Benchmark unstained ladder from Invitrogen.

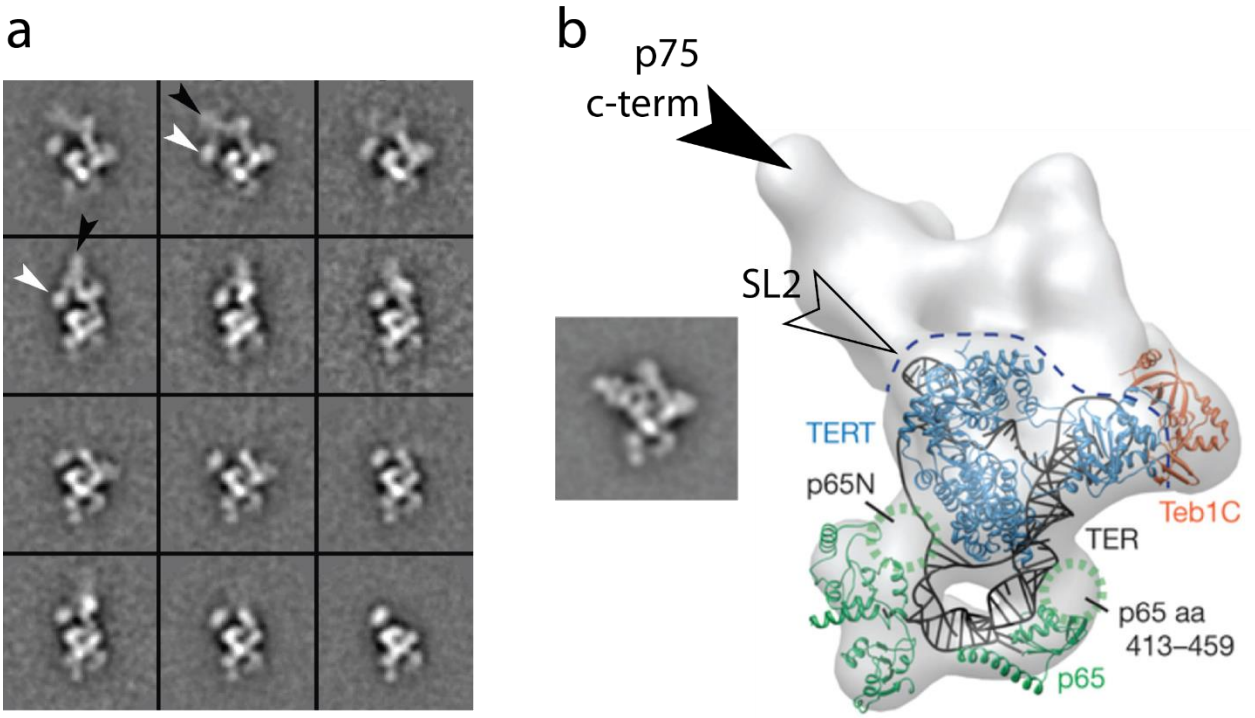

Figure 2.8. Localization of stem-loop II of *Tetrahymena* telomerase TR. (*a*) Representative negative stain EM class averages of purified MS2 bound telomerase. C-terminus of p75 is denoted with a black arrow and the MS2 coat protein dimer is indicated with a white arrow. (*b*) Typical 2D class average of telomerase with no MS2 or fab labelling and final 25Å 3D reconstruction with TERT (blue), TR (black), p65 (green), and Teb1C (orange) modelled in. SL2 is located 'behind' TERT.

Methods

12 liters of *Tetrahymena* culture at ~400,000 cells/ml (~75g pellet) were harvested by centrifugation (4,000 g), lysed by detergent, and clarified by ultracentrifugation (150,000 g) to generate ~300 mls of soluble lysate. MS2-hp telomerase was pulled down from the lysate by overnight end over end incubation of 300 ul of "MS2 resin" (ZZtag-tevsite-FLAGtag-MS2 bound IgG resin). Resin was collected and washed 3 times "fast" and 3 times "slow" (10 minute incubations in wash buffer rotating end over end). FLAGtag-MS2 bound telomerase was "eluted" from the resin using 500 ul of wash buffer with 10 ug of TEV protease with end over end rotation for 1 hour. The cleavage eluate is further purified by binding to 50 ul of FLAG resin, 3 fast and 3 slow washes, and elution with 50 ul of 1mg/ml FLAG-peptide.

To generate "MS2 resin," Histag-ZZtag-TEVsite-FLAGtag-MS2 was first purified by nickel affinity and size exclusion chromatography from recombinant expression in *E. coli*. 10 ug of purified Histag-ZZtag-TEVsite-FLAGtag-MS2 which represents ~5x stoichiometric excess of theoretical telomerase yield (~10 ug) was bound to 300 ul of IgG resin. This amount and method was chosen to optimize pulldown of MS2-hp telomerase while preventing oversaturation of the IgG with free MS2 which could compete with MS2-telomerase in the final FLAG purification step.

REFERENCES

1. Jiang, J., et al., *The architecture of Tetrahymena telomerase holoenzyme.* Nature, 2013. **496**(7444): p. 187-92.

2. Min, B. and K. Collins, *An RPA-related sequence-specific DNA-binding subunit of telomerase holoenzyme is required for elongation processivity and telomere maintenance.* Mol Cell, 2009. **36**(4): p. 609-19.

3. Grahn, E., et al., *Crystallographic studies of RNA hairpins in complexes with recombinant MS2 capsids: implications for binding requirements.* RNA, 1999. **5**(1): p. 131-8.

4. van den Worm, S.H., et al., *Crystal structures of MS2 coat protein mutants in complex with wild-type RNA operator fragments.* Nucleic Acids Res, 1998. **26**(5): p. 1345-51.

5. Cunningham, D.D. and K. Collins, *Biological and biochemical functions of RNA in the Tetrahymena telomerase holoenzyme.* Mol Cell Biol, 2005. **25**(11): p. 4442-54.

6. Lecuyer, K.A., L.S. Behlen, and O.C. Uhlenbeck, *Mutants of the Bacteriophage-Ms2 Coat Protein That Alter Its Cooperative Binding to Rna.* Biochemistry, 1995. **34**(33): p. 10600-10606.

CHAPTER THREE

Structure of *Tetrahymena* telomerase reveals previously unknown subunits, functions, and interactions

RESEARCH ARTICLE

STRUCTURAL BIOLOGY

Structure of *Tetrahymena* telomerase reveals previously unknown subunits, functions, and interactions

Jiansen Jiang,[1,2,3]* Henry Chan,[1]* Darian D. Cash,[1] Edward J. Miracco,[1]† Rachel R. Ogorzalek Loo,[4] Heather E. Upton,[5] Duilio Cascio,[1,6] Reid O'Brien Johnson,[1] Kathleen Collins,[5] Joseph A. Loo,[1,4,6] Z. Hong Zhou,[2,3] Juli Feigon[1,3,6]‡

Telomerase helps maintain telomeres by processive synthesis of telomere repeat DNA at their 3′-ends, using an integral telomerase RNA (TER) and telomerase reverse transcriptase (TERT). We report the cryo–electron microscopy structure of *Tetrahymena* telomerase at ~9 angstrom resolution. In addition to seven known holoenzyme proteins, we identify two additional proteins that form a complex (TEB) with single-stranded telomere DNA-binding protein Teb1, paralogous to heterotrimeric replication protein A (RPA). The p75-p45-p19 subcomplex is identified as another RPA-related complex, CST (CTC1-STN1-TEN1). This study reveals the paths of TER in the TERT-TER-p65 catalytic core and single-stranded DNA exit; extensive subunit interactions of the TERT essential N-terminal domain, p50, and TEB; and other subunit identities and structures, including p19 and p45C crystal structures. Our findings provide structural and mechanistic insights into telomerase holoenzyme function.

Telomerase is a ribonucleoprotein (RNP) complex that extends the telomere DNA at the 3′ ends of linear chromosomes, thereby counteracting the loss of DNA from replication and nucleolytic processing (*1*, *2*). Although telomerase is largely inactive in somatic cells, it is active in stem cells and highly active in most cancer cell lines, where its activity is necessary for their immortal phenotype (*3*–*5*). Thus, telomerase is an important regulator of aging, tumorigenesis, and stem cell renewal. Telomerase uses a template contained within the integral telomerase RNA (TER) and a telomerase reverse transcriptase (TERT) to synthesize multiple copies of the G-strand telomere repeat (TTGGGG in ciliates and TTAGGG in vertebrates). Telomerase recruitment to telomeres is regulated by the cell cycle, where its activity requires interplay between telomere end-protection and telomerase proteins (*6*). Telomere end-maintenance also requires coordinated recruitment of telomerase and DNA polymerase α for synthesis of the G and C strands, respectively (*7*, *8*). In humans, telomerase is recruited to telomeres by components of shelterin (*6*). Specifically, the TERT essential N-terminal (TEN) domain interacts with TPP1 (*9*–*11*), which, in complex with protection of telomeres 1 (POT1), is a processivity factor (*6*, *12*, *13*). The budding yeast telomerase holoenzyme subunit Est3 is a structural homolog of the oligosaccharide/oligonucleotide-binding (OB) fold of TPP1 (*14*) and, like TPP1, interacts with the TEN domain (*15*). In addition to recruiting telomerase, the human TPP1-POT1 complex recruits the replication protein A (RPA)–like CST (CTC1-STN1-TEN1) complex. RPA binds sequence-nonspecifically to single-stranded DNA (ssDNA) and plays a central role in DNA replication and repair through protein recruitment (*16*); CST complexes have been proposed as telomere-specific RPAs (*17*). CST stimulates DNA polymerase α for C-strand synthesis and has other diverse functions in different organisms (*8*, *18*–*20*). Mammalian CST acts as an inhibitor of telomerase action, determines telomeric 3′ overhang structure, and plays broader roles in telomere duplex replication and genome-wide replication restart (*8*, *18*, *20*, *21*). Budding yeast CST (Cdc13-Stn1-Ten1) subunit Cdc13 recruits the telomerase holoenzyme to telomeres via interaction of Cdc13 with telomerase subunit Est1, associated with Est3 (*22*–*24*).

Telomerase can synthesize telomere repeats in vitro with only TERT and TER, but physiological function requires a variety of other proteins (*25*, *26*). Unlike yeast and mammalian telomerase, *Tetrahymena* telomerase is constitutively assembled (*27*, *28*), making it possible to purify and study all holoenzyme components in a stable complex (*29*). In addition to TERT and TER, the *Tetrahymena* telomerase holoenzyme contains six other known proteins: p65, p75, p45, p19, p50, and Teb1 (*28*). TER contains a template/pseudoknot (t/PK) domain, which encloses a template with sequence complementarity to ~1.5 telomere repeats, and a separate activating domain (*30*). Although TER is essential for activity, the physical arrangement of TER on TERT has remained largely unknown. TERT comprises a telomerase RNA binding domain (TRBD), reverse transcriptase (RT), and C-terminal extension (CTE) that form a TERT "ring" (*31*), and a separate TEN domain (*32*) that is important for DNA handling and telomere repeat addition processivity (RAP) (*6*, *26*). p65 binds the TER activating domain [stem-loop 4 (SL4)], inducing a large bend in the RNA that facilitates assembly of TERT with TER to form the RNP catalytic core (*33*, *34*). Teb1 is a paralog of human RPA70, the large subunit of RPA (*16*, *28*). Direct single-stranded telomere DNA binding by Teb1 is necessary for telomerase recruitment to telomeres (*27*), where it may compete for binding with the *Tetrahymena* telomere end-binding Pot1a (*35*). p75, p45, and p19 form a ternary complex whose structure and function remain largely unknown (*28*). The 25 Å resolution negative-stain electron microscopy (EM) structure and individual subunit affinity labeling revealed the overall architecture of *Tetrahymena* telomerase, where TERT occupies the center of the holoenzyme with p65 bound to SL4 below (*29*). p50, which forms a central hub linking the TERT-TER-p65 catalytic core, p75-p45-p19, and Teb1, can greatly increase RAP and, with Teb1, can dramatically enhance the rate and processivity of long-product synthesis (*29*, *36*). A detailed mechanistic description of telomerase and its interaction at telomeres has been hampered by a lack of structural models, due to difficulties in obtaining samples of sufficient quantity and quality, as well as subunit complexity and flexibility and low sequence identity among subunits from different organisms. Here we report 9.4 and 8.9 Å cryo–electron microscopy (cryo-EM) structures of *Tetrahymena* telomerase holoenzyme. Combining the cryo-EM structures with data from x-ray crystallography, nuclear magnetic resonance (NMR) spectroscopy, negative-stain EM, and mass spectrometry, we discovered two RPA-related complexes: an RPA paralog TEB, comprising Teb1 and previously undetected proteins Teb2 and Teb3, and a CST complex comprising the previously structurally uncharacterized p75-p45-p19. Both are tethered to p50, a potential structural and functional homolog of TPP1, which in turn binds TERT. A pseudoatomic model of the TERT-TER-p65 catalytic core reveals the path of TER on TERT and the location of the TEN domain, and an exit path for the telomeric repeat DNA is proposed, together providing insights into the enzyme mechanism.

Cryo-EM reconstruction and overall structure

Telomerase holoenzyme endogenously assembled in *Tetrahymena thermophila* was affinity-purified

[1]Department of Chemistry and Biochemistry, University of California, Los Angeles (UCLA), Los Angeles, CA 90095, USA. [2]Department of Microbiology, Immunology, and Molecular Genetics, UCLA, Los Angeles, CA 90095, USA. [3]California Nanosystems Institute, UCLA, Los Angeles, CA 90095, USA. [4]Department of Biological Chemistry, UCLA, Los Angeles, CA 90095, USA. [5]Department of Molecular and Cell Biology, University of California, Berkeley, Berkeley, CA 94720, USA. [6]UCLA–U.S. Department of Energy (DOE) Institute of Genomics and Proteomics, UCLA, Los Angeles, CA 90095, USA.
*These authors contributed equally to this work. †Present address: Moderna Therapeutics, Cambridge, MA 02141, USA.
‡Corresponding author. E-mail: feigon@mbi.ucla.edu

from a strain bearing a C-terminal 3×Flag (F) and tandem protein A (ZZ) tag on TERT (TERT-FZZ) (*29*). Cryo-EM specimens of *Tetrahymena* telomerase holoenzyme were prepared using "holey" carbon grids and imaged using a Gatan K2 Summit direct electron detection camera with drift correction (fig. S1). In addition to the preferred front view, particles showed various orientations, which are required for three-dimensional (3D) reconstructions (fig. S2 and methods). Using 40,754 particles, we obtained the intact structure of the *Tetrahymena* telomerase holoenzyme at an overall resolution of 9.4 Å (Fig. 1, A to C, and fig. S1). The negative-stain EM study revealed that the p75-p45-p19 subcomplex is conformationally dynamic (*29*), which is also apparent in the cryo-EM images (fig. S1, C and D). Therefore, to improve the resolution of the less flexible region, we used a soft mask to exclude the p75-p45-p19 subcomplex from the cryo-EM structure refinement. The resulting reconstruction has an overall resolution of 8.9 Å, with distinguishable secondary structure elements of proteins and RNA (Fig. 1, D to F, and figs. S1 and S3).

Using the features of the secondary structure elements, we were able to rigid-body fit the available atomic-resolution and homology models of protein domains and RNA helical elements (table S1) unambiguously into the 8.9 Å cryo-EM map, except for p75-p45-p19 homologs that were fit into the 9.4 Å cryo-EM map (Fig. 1 and fig. S3). All helical elements of TER—i.e., stem 1 (S1), stem-loop 2 (SL2), SL4, and the pseudoknot (PK)—are clearly visible with distinct grooves (Fig. 1F), and the path of the single-stranded regions can be approximately traced, although bases cannot be discerned. This allowed us to build a pseudoatomic model of the TERT-TER-p65 catalytic core and Teb1C. The locations of these subunit domains are the same as modeled in the negative-stain EM map within experimental resolution (*29*), with two exceptions: Teb1C [whose C terminus was correctly localized by Fab labeling (*29*)] is behind the TEN domain where the PK had been placed, whereas the PK is on the opposite side of TERT by the CTE. In addition, as discussed below, Teb1 forms a heterotrimer with two newly identified proteins, whose location was previously assigned to Teb1C. The p75-p45-p19 ternary complex, whose subunit boundaries could not be determined in the negative-stain EM map (*29*), is revealed to contain an RPA-like heterotrimer of OB-fold proteins with the domain structure of a CST complex. Overall the pseudoatomic models of the TERT-TER-p65 catalytic core, Teb1-Teb2-Teb3, and p75-p45-p19, which are all linked to p50 in the cryo-EM maps, reveal an intricate network of interactions between the subunits.

The TER t/PK domain encircles the TERT ring

Tetrahymena TERT TRBD-RT-CTE forms a ring-shaped structure and was modeled using the crystal structure of a partial *Tetrahymena* TRBD (residues 259 to 265 and 277 to 519) (*37*) and a homology model based on the RT-CTE in the *Tribolium* (flour beetle) TERT crystal structure (Fig. 2A) (*31*, *38*). *Tribolium* TERT lacks the TEN domain, and therefore the position of TEN relative to the TERT ring has remained uncertain. Fitting of the *Tetrahymena* TEN domain crystal structure (*32*) into the cryo-EM map (Fig. 1F) revealed its location on the active-site side of the TERT ring, stacked over the CTE (Fig. 2A and fig. S4A). Residues 640 to 740 of the insertion in fingers domain (IFD) in the RT [which are not modeled, as the *Tribolium* TERT IFD is much shorter than in *Tetrahymena* and other organisms (*39*, *40*)] appear to be near the TEN domain (Figs. 1B and 2A). The evolutionarily nonconserved sequence (residues 178 to 258) that connects TEN to the TERT ring has no available atomic structure and appears undefined in the cryo-EM maps. Consistent with this lack of a fixed conformation, the TEN domain can be assembled in trans with TER and the TERT ring to form an active catalytic core without linker residues 196 to 215 (*41*, *42*).

Tetrahymena TER comprises a circular t/PK domain, closed by a short S1, that contains the template, the 3′-flanking template recognition element (TRE), the template boundary element (TBE; also called the TERT binding element), SL2, and PK; and an activating domain (SL4), which is connected to S1 by a short single-stranded linker (Fig. 2B) (*30*). TER was modeled by fitting previously determined (SL2, p65xRRM:S4, L4) and newly determined (PK) (table S4) NMR structures into the cryo-EM density (see methods). The core t/PK domain encircles the TERT ring approximately perpendicularly, such that the template extends across the bottom of the RT domain on one side of the TERT ring, whereas the PK is on the other side next to the CTE (Fig. 2, C to E, and fig. S4). The bottom of S2 is adjacent to the TRBD CP motif, and the 3′ end of the TBE is also near the T motif (Fig. 2C and fig. S4), as predicted (*29*, *37*).

The PK, a conserved element of TER that has been proposed to contribute directly to catalysis (*43*), is on the opposite side of the TERT ring and far from the active site (~20 Å away) (Fig. 2, C and E, and fig. S4A). The PKs of human and yeast TERs contain conserved interactions that stabilize the PK fold through formation of base triples between loops and stems that are important for activity (*43*–*45*). The smaller *Tetrahymena* telomerase PK has two base triples in the NMR structure at 10°C and is not stably folded at higher temperatures in the absence of TERT (*46*). Based on the position of the PK on TERT, we conclude that, rather than contributing directly to catalysis, the correct PK fold is important for proper positioning of TER on TERT. It is plausible that the PK acts like a watchband ratchet clasp during catalytic core assembly, partially or completely unfolding to allow the TER t/PK domain to fit around the TERT ring and then locking onto the TERT ring by folding of the PK. An indirect effect on assembly may explain why mutations that either stabilize or destabilize the PK, at least for human TER, affect telomerase activity in vitro (*45*).

Outside of the TER t/PK domain, only L4 in S1/SL4 comes into contact with TERT (Fig. 2, C, E, and F;

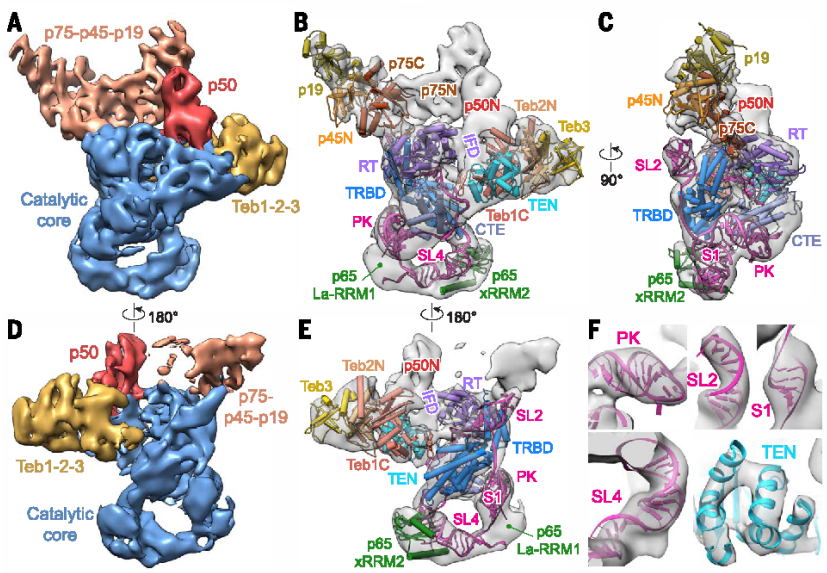

Fig. 1. Cryo-EM reconstructions of *Tetrahymena* telomerase holoenzyme. (**A**) Front view of the 9.4 Å cryo-EM map, with the catalytic core, Teb1C-Teb2N-Teb3 (TEB), p75C-p45N-p19 (CST), and p50N colored in blue, gold, copper, and red, respectively. (**B**) Front view of the 9.4 Å cryo-EM map (gray surface) with pseudoatomic models of the TERT-TER-p65 catalytic core, Teb1C-Teb2N-Teb3, and p75C-p45N-p19. (**C**) Side view of the cryo-EM map and pseudoatomic models shown in (B). (**D**) Back view of the 8.9 Å cryo-EM map colored as in (A). (**E**) Back view of the 8.9 Å cryo-EM map, showing pseudoatomic models of TERT-TER-p65 and Teb1C-Teb2N-Teb3. (**F**) Close-up views of fitting of TER helical domains PK, SL2, S1, and SL4 and TEN domain into the 8.9 Å cryo-EM map. TERT domains are TEN (cyan), TRBD (dark blue), RT (violet, with IFD labeled in violet), and CTE (light blue). Other proteins and TER are colored individually.

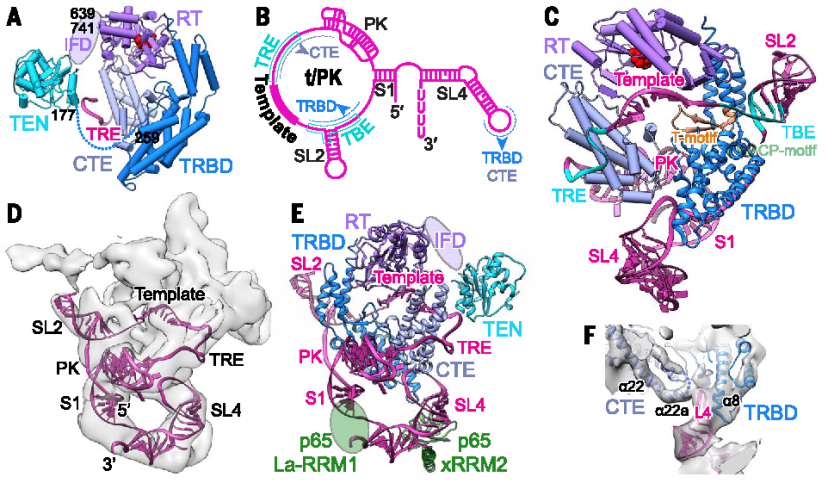

Fig. 2. Structure of the TERT-TER-p65 catalytic core. (**A**) Model structure of TERT, showing the putative IFD (light violet), active-site catalytic triad residues (red), linker (dotted blue line), and TER TRE. (**B**) Secondary structure of TER. Locations of CTE and TRBD on TER are indicated with dotted lines. (**C**) Pseudoatomic model of TERT ring-TER, showing TBE-template-TRE and L4 on TERT, viewed from the active-site side of TERT. (**D**) Front view of the 8.9 Å cryo-EM map, showing a pseudoatomic model of TER. (**E**) Front view of the pseudoatomic model TERT-TER-p65 catalytic core. The putative location of IFD is shown as violet oval. (**F**) A region of the 8.9 Å cryo-EM map and pseudoatomic model showing L4 at the interface of TRBD (helix α8) and CTE (helix α22a, residues 975 to 983). The numbering of *Tetrahymena* TERT secondary structure elements follows that of the *Tribolium* TERT structure.

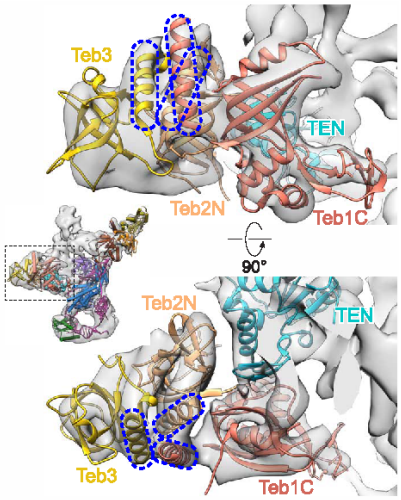

Fig. 3. Identification of two previously unknown holoenzyme proteins, Teb2 and Teb3. Shown are two views of the knob and Teb1C region of the 8.9 Å cryo-EM map with a model of Teb1C-Teb2N-Teb3 based on fitting of RPA70C-RPA32N-RPA14 into the cryo-EM map, followed by replacement of RPA70C with Teb1C, except for the RPA70C C-terminal α helix. The TEN domain is shown in cyan. The three-helix bundle between the C-terminal residues of Teb1C, Teb2N, and Teb3 (modeled from RPA) is highlighted with dashed lines. The inset shows the corresponding back view of the holoenzyme for reference.

and fig. S4A). The p65 La-RRM1 binds the 3′ polyU tail (*33*, *47*). La-RRM1 has low resolution in the cryo-EM map, probably due to flexibility or partial disassociation (fig. S1), but appears to be associated with both the 3′ tail and the 5′ end of S1, thereby possibly linking the 3′ and 5′ ends of TER (Fig. 2E). p65 C-terminal xRRM2 (*33*) binds to and bends S4, inserting L4 between the end of TRBD helix α8 and a short helix from the CTE (α22a) that does not exist in *Tribolium* TERT but has well-defined density in the 8.9 Å cryo-EM map (Fig. 2F). In complex with p65, SL4 stimulates activity, hierarchal assembly, and holoenzyme stability (*33*, *34*, *47*, *48*). L4 binds with high affinity to the TRBD, but its specificity for the CTE remains unknown. A hypothesis consistent with the above, as well as the location of L4 far from the active site and PK, proposes that L4 stabilizes a closed conformation of the TERT ring via specific interactions with TRBD and CTE.

The TER single-stranded region containing TRE, the template, and 3′TBE spans the active-site side of the TERT ring between the CTE and the TEN domain, across the RT, and over the TRBD T/CP pocket, respectively (Fig. 2C). The cryo-EM structure is of telomerase in the apo state before binding telomeric ssDNA. The TRE nucleotides, on the 3′ side of the template, pass between the CTE and the TEN domain and could contact the TEN domain. There is clear cryo-EM density for the 3′ half of the template only (fig. S3E), suggesting flexible positioning of the 5′ residues close to the TBE. Based on the distance from TER S2, the template appears to be positioned near where it would be at the end of telomere repeat synthesis—i.e., the 5′ end of the template is closest to the active site. The template also appears to be displaced by ~7 Å from its position at the active site in the crystal structure of *Tribolium* TERT in complex with an RNA-DNA hybrid helix (*38*), as proposed for the strand-separation step (*49*). The position of S2/TBE on TERT relative to the 5′ end of the template suggests a structural mechanism for template boundary definition. The single-stranded residues of the TBE, which flank S2, wrap on either side of the TERT ring (Fig. 2C and fig. S4B). At the end of telomere repeat synthesis, the S2 and TBE-TRBD interactions could act as an anchor to prevent residues beyond the template from being pulled into the active site (Fig. 2C and fig. S4B).

Teb1 forms an RPA-like complex with two newly identified proteins

Although Teb1 has four OB-fold domains (N, A, B, and C) (*50*), only the Teb1C domain and, in some cases, very weak density for Teb1B were apparently visible in the negative-stain EM class averages of *Tetrahymena* telomerase (*29*). Fitting of Teb1C into the cryo-EM map revealed density of unknown origin in the "knob" next to Teb1C (Fig. 3 and fig. S5A). An exhaustive analysis of the potential positions and fittings of other holoenzyme proteins revealed no known candidates for the knob density (fig. S5A). Because Teb1 is an RPA70 paralog, we investigated whether this part of the cryo-EM map might contain paralogs of the other two RPA subunits (RPA32 and RPA14). We found that the crystal structure of the RPA heterotrimeric core complex (RPA70C-RPA32N-RPA14) (*51*) fit particularly well into the cryo-EM map, with RPA70C positioned in the cryo-EM density for Teb1C and the RPA32N and RPA14 OB folds in the knob (Fig. 3). RPA trimerization requires the formation of a three–α-helix bundle from the C-termini of RPA70, RPA14, and RPA32N. The predicted C-terminal α helix of Teb1C is disordered in the crystal structure (*50*). However, in the cryo-EM map there is clear density of three α helices involved in the trimerization, with one of them near the C terminus of Teb1C, which we modeled in from the RPA70 structure (Fig. 3 and fig. S3H).

To confirm the presence of putative Teb1 heterotrimer proteins in the holoenzyme, we used liquid chromatography–tandem mass spectrometry (LC-MS/MS) to analyze telomerase purified from the TERT-FZZ strain. All seven of the known *Tetrahymena* telomerase proteins, plus two additional hypothetical proteins (TTHERM_001113129 and TTHERM_00439320) (www.ciliate.org), were detected with high confidence (table S2A). PSI-BLAST (Position-Specific Iterated Basic Local Alignment Search Tool) (*52*) searches of corrected cDNA sequences of these 31- and 14-kD proteins showed homology with predicted RPA32 and RPA14 homologs, respectively. Secondary structure predictions by Jpred4 (*53*) are consistent with an OB fold for the 14-kD protein and an N-terminal OB fold and C-terminal winged-helix (WH) domain for the 31-kD protein. Multiple sequence alignments of these domains with RPA32 and RPA14 orthologs show high similarity (fig. S6). We previously observed that telomerase purified from

a *Tetrahymena* strain containing N-terminally ZZF-tagged p50 (F-p50 telomerase) lacks the knob (fig. S5B) and has low RAP, which was attributed to the loss of Teb1 induced by the ZZF-tag on p50 (*29*). We analyzed F-p50 telomerase by LC-MS/MS and found that the two newly identified proteins and Teb1 are absent (table S2B), which confirms that these two additional proteins are located at the knob in the cryo-EM map and form a complex with Teb1. We conclude that there are two previously undetected proteins in the *Tetrahymena* telomerase holoenzyme that form a heterotrimer with Teb1, here named TEB, paralogous to the ssDNA binding RPA, except specific for telomeric G-strand DNA. In *Tetrahymena*, only the large subunit of RPA, Rfa1, has been identified (*54*). Transcript expression levels of the two newly discovered Teb1-binding proteins, here named Teb2 and Teb3, are much higher than other telomerase proteins and more similar to the level of Rfa1, as judged by expressed sequence tag abundance (*55*). These observations suggest that these two subunits may be shared between *Tetrahymena* RPA and TEB.

Multiple interactions between TEN, TEB, and p50 regulate telomerase activity

The TEN domain has been identified as a major determinant of telomerase activity (*6*, *42*). In addition to its potential TRE interaction (Fig. 2), the cryo-EM map reveals that TEN is adjacent to p50, Teb1C, Teb2N, and the IFD (Fig. 4, A and B). TEN, Teb1C, and p50 contact each other in a triangular arrangement. The Teb1C-TEN interaction is clearly defined in the pseudoatomic models (Fig. 4C). A Teb1 Phe^{590}→Ala^{590} (F590A)/F648A double mutant was previously shown to ablate purification of telomerase by Teb1-FZZ expressed in cells (*27*). These two residues of Teb1 are on the Teb1C-TEN interface (Fig. 4C), accounting for the loss of function. In the cryo-EM map, the density of TEN is also in contact with that of Teb2. TEN residues 77 to 87, which are missing in the crystal structure due to disorder (*32*), might form a structured interface with Teb2N in the holoenzyme (Fig. 4D). In vitro telomerase reconstitution activity assays, which lacked Teb2 and Teb3, showed that deletion of the Teb1C putative C-terminal α helix (ΔCTαH) had little effect on activity (*27*, *54*). However, purification of Teb1(ΔCTαH)-FZZ expressed in vivo did not recover any telomerase activity or holoenzyme subunits, indicating no in vivo telomerase assembly with Teb1(ΔCTαH) (*27*). Thus, Teb2 and Teb3, which interact with the Teb1 C-terminal α helix, likely stabilize association of Teb1 with telomerase.

To provide biochemical evidence for these interactions, we used in vitro reconstitution of complexes with individual TEB subunits expressed in rabbit reticulocyte lysate (RRL) to investigate whether Teb2-Teb3 had any effect on telomerase activity (Fig. 4E). Our activity assays were designed to be sensitive to improved holoenzyme assembly of Teb1 by the use of a very low level of Teb1 expressed in RRL, rather than a saturating concentration of purified bacterially expressed protein, and by purification of RNP from unbound Teb1 before the activity assay. Addition of Teb1 to the catalytic core plus p50 greatly increases RAP, as expected from previous studies (*29*, *36*). Coexpression of Teb2-Teb3 with Teb1 further increased overall activity, consistent with additional stabilization from synergistic interaction of Teb2 with the TEN domain and Teb1C. Addition of Teb2-Teb3 alone, without Teb1, provided no activity enhancement. Together, the cryo-EM structure, activity assays, and in vivo functional studies (*27*) discussed above support the notion that the TEN-TEB protein interaction network has crucial physiological importance.

The cryo-EM density of p50N appears to contact the TEN domain, as well as Teb1C, the IFD, and p75-p45-p19 (Figs. 1, B and E, and 4A). p50, which has no known sequence or structural homology to other proteins, has a 30-kD N-terminal domain (p50N) that is required for the high level of processive repeat synthesis conferred by p50 binding to the catalytic core (*36*). Only p50N is apparently visible in the class averages and 3D reconstructions of negative-stain EM images (*36*) and also in the cryo-EM maps. Like TPP1, p50 contacts the TEN domain (Fig. 4, A and B), and like TPP1-POT1 (*13*), p50-Teb1 greatly increases RAP (*36*). These data suggest that p50 could be a structural and functional ortholog to vertebrate TPP1. Although TPP1 was initially identified as a telomere binding protein complex with POT1 bound to the G-strand overhang to block telomerase access, it has emerged as also being the direct mediator of telomerase recruitment, activation, and homeostasis set-point regulation (*6*, *7*, *56*, *57*). We fit the structure of the TPP1 OB fold into the 8.9 Å cryo-EM map, but only the characteristic OB-fold β barrel matches well to the cryo-EM density (fig. S3, M to O). This is not surprising, due to the expected cofolding of p50 loops and helices with its interaction partners. Though the fitting does not provide definitive structural homology to TPP1, it does provide evidence that p50N is an OB fold.

The TEN domain has an extensive interface with p50 that apparently includes residues 122 to 127, which are missing in the crystal structure due to disorder (*32*) (Fig. 4B) and may cofold with p50. We tested whether other TEN domain interactions with p50 inferred from the pseudoatomic model and cryo-EM map were important

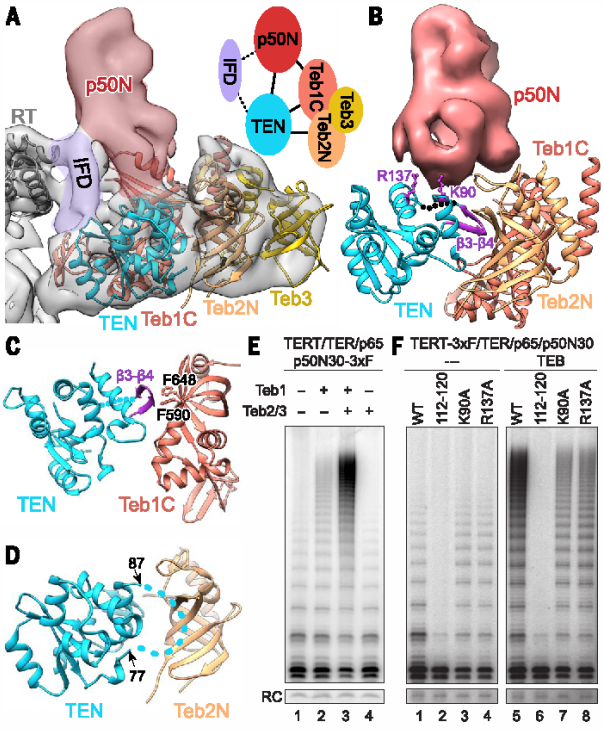

Fig. 4. Subunit interactions between p50, TEN, IFD, Teb1C, Teb2N, and Teb3. (**A**) Region of the 8.9 Å cryo-EM map showing density linking p50N, TEN, IFD, and TEB. The inset shows a schematic of the interactions. Dotted lines represent inferred interactions from the cryo-EM density and atomic models fitted to the cryo-EM map. (**B**) Interactions between p50N (red, cryo-EM density), TEN, Teb1C, and Teb2N. The TEN residue K90 side chain corresponding to the human TEN domain residue K78 that interacts with TPP1, R137, and the β3-β4 hairpin (residues 112 to 120) is highlighted in violet. (**C**) Interactions between TEN and Teb1C. Teb1C F590/F648 residues (orange stick) that together abrogate the Teb1C-TEN interaction and the TEN β3-β4 hairpin (violet) are indicated. TEN residues 122 to 127, disordered in the crystal structure, are represented by dotted lines in (B) and (C). (**D**) Interactions between TEN and Teb2N. TEN residues 77 to 87, disordered in the crystal structure, are shown as a dashed line. Pseudoatomic models of TEN, Teb1C, and Teb2N interactions are based on crystal structures of TEN, Teb1C, and RPA32N-RPA14 fit into the 8.9 Å cryo-EM map. (**E** and **F**) In vitro reconstitution telomerase activity assays for the effect of (E) TEB proteins and (F) TEN domain mutations on the catalytic core assembled with p50N30. TEN domain mutations were tested without (lanes 1 to 4) and with (lanes 5 to 8) TEB. WT, wild type; RC, recovery control.

for RNP activity stimulation by p50, in a manner similar to TEN interactions with TPP1 and Est3. A cluster of residues on human TPP1 (and Est3), called the TEL patch, has been identified as the surface of interaction with TEN (*9*–*11*, *14*, *56*, *57*). This interaction is essential for human telomerase recruitment to telomeres. Human TEN residues whose substitution disrupts the interaction of telomerase with TPP1 without greatly affecting catalytic activity have been identified; among these, a direct interaction between Lys^{78} (K78) and TPP1 has been demonstrated (*57*). The equivalent *Tetrahymena* TEN residue based on homology modeling of human TEN with the crystal structure of *Tetrahymena* TEN is K90, which is located near the density for p50 in the cryo-EM map (Fig. 4B). We used our in vitro telomerase reconstitution activity assay to investigate whether K90A at the putative TEN-p50 TEL patch interface imposes a defect in p50 stimulation of telomerase activity (Fig. 4F). K90A had a modest but notable effect on overall activity. The same results were obtained for TEN R137A (R, Arg), which is also located at the TEN-p50 interface in the cryo-EM map. These results support similar interactions between *Tetrahymena* TEN-p50 and human TEN-TPP1. TEN K90A and R137A did not abrogate TEB stimulation of high RAP (Fig. 4F), consistent with direct TEN domain interactions with TEB and p50-bridged TERT-TEB association. TEN residues 112 to 120 form a β hairpin, exclusive to *Tetrahymena* TEN, that inserts at the interface between p50, Teb1C, and Teb2N (Fig. 4B). An adjacent block sequence substitution $TEN_{(108\text{-}113}$NAAIRS) (N, Asn; I, Ile; S, Ser) abolishes p50 binding (*42*). In our experiment, we replaced the β hairpin with GSSG (G, Gly). This substitution abolished p50 activity stimulation, even with added TEB, which is consistent with disruption of both p50 and TEB interactions, but did not affect catalytic core activity. Taken together, these results validate the network of TEN-p50-Teb1C-Teb2N interactions proposed based on the cryo-EM structure (Fig. 4, A to D) and provide supporting evidence that p50 is a structural and functional paralog of TPP1.

The cryo-EM density that we attribute to the IFD appears to independently contact p50 and the TEN domain N terminus, which is disordered in the crystal structure (*32*) (Figs. 1B and 4A). The IFD is exclusive to TERTs and is important for the translocation step required for RAP (*39*, *40*). We suggest that the human TERT IFD may have parallel, as yet undetected, interactions with the TPP1 OB fold and TEN domains.

p75-p45-p19 is a CST complex

We determined a 2.3 Å x-ray crystal structure of p19 (table S3), which revealed an OB fold most structurally homologous to human Ten1 (Fig. 5A and fig. S7), suggesting the possibility that p75-p45-p19 might be a CST- or second RPA-like complex. We found that human RPA70C-RPA32N-RPA14, which fit the cryo-EM density of TEB as described above, also fit equally well in the density at the "tip" of the p75-p45-p19 subcomplex in the 9.4 Å cryo-EM map (Fig. 5B). For our model, RPA14 was then replaced with the p19 crystal structure, except for its unstructured C terminus, which forms an α helix in a three-helix bundle with the other two proteins in the RPA complex (Fig. 5B). p19 α2 and α3, which are lacking in RPA14, fit well into the cryo-EM density at the very end of the tip.

The positions of the C-terminal α helices of RPA70C and RPA14 correspond to the locations of the C termini of p75 and p19 determined by Fab labeling in negative-stain EM (Fig. 5B) (*29*). We used copurification and limited proteolysis to establish that p45 is composed of an N-terminal domain (p45N) that binds p19 and an independently folded C-terminal domain (p45C) (see methods). These results are consistent with the hypothesis that p45 is a Stn1 or RPA32 homolog. Previous attempts to locate the position of p45 in the holoenzyme by Fab labeling of its C terminus were unsuccessful, as Fab was apparently not visible in negative-stain EM class averages of telomerase holoenzyme (*29*). Based on the above, we hypothesized that p45C might be connected to p45N in the p75-p45-p19 subcomplex via a flexible linker, and thus Fab-bound p45C was not visible in holoenzyme class averages due to positional flexibility relative to the holoenzyme. We screened >2000 negative-stain EM particles of Fab-labeled p45-F telomerase. The majority had a cluster of three Fab (the 3×FLAG tag can bind up to three Fab) located in various positions ~100 Å from the location of p45N (Fig. 5D and fig. S8). The C-terminal domains of RPA32 and Stn1 are composed of WH and tandem WH (WH1-WH2) domains, respectively (*17*, *19*, *58*, *59*). We determined a 2.4 Å crystal structure of p45C (table S3) and found that it comprises the WH1-WH2 domains (Fig. 5C). The OB fold followed by two WH domains suggests that p45 is a Stn1 homolog (*17*, *19*, *58*, *59*). Structural alignments (fig. S7), sequence alignments (fig. S6), and phylogenetic cluster analysis (fig. S9) of p19 and p45 domains also support their identification as Ten1 and Stn1 orthologs, despite low sequence homology of CST proteins between kingdoms. In the 9.4 Å cryo-EM map, the remaining unmodeled density in the p75-p45-p19 complex, which appears to contain at least two additional OB folds and contacts p50, can only be attributed to p75 (Fig. 5B). Consistent with this observation, among p75-p45-p19, p75 is necessary and sufficient to bind p50 in vitro (*36*). There are distinct differences between p75 and Teb1 in terms of their interaction with p50 and their effect on telomerase activity. The cryo-EM maps show that p75 contacts p50 with a domain near its N terminus; in contrast, Teb1 binds p50 and the TEN domain with its C-terminal OB fold. How the potential p75 ortholog CTC1 interacts with telomerase is unknown, but it is interesting to note that the functionally divergent Cdc13 binds yeast telomerase holoenzyme protein Est1 through a recruitment domain adjacent to its N-terminal OB fold (*8*, *17*, *24*). In vitro reconstitution assays show that the addition of p75 (or p75-p45-p19) to the catalytic core plus p50 stimulates activity slightly but without an increase in

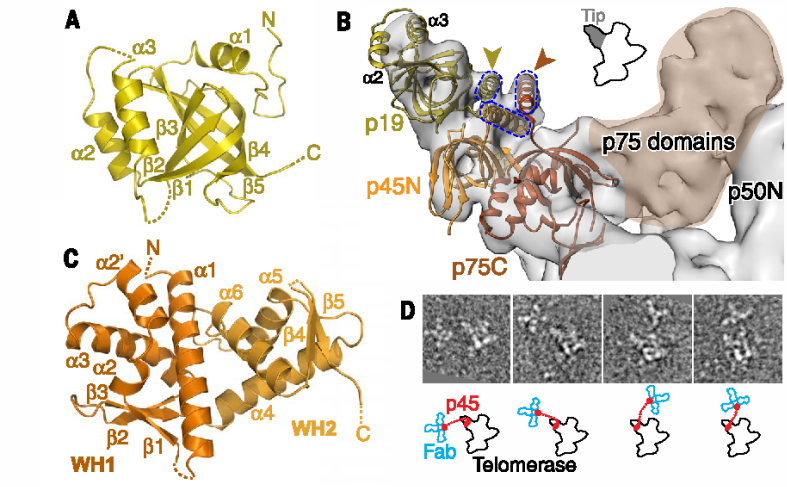

Fig. 5. Identification of p75-p45-p19 as a *Tetrahymena* CST complex. (**A**) Crystal structure of p19, an OB fold. (**B**) Model of p75C-p45N-p19 based on fitting of RPA70C-RPA32N-RPA14 into the 9.4 Å cryo-EM map, followed by replacement of RPA14 by p19, except for the RPA14 C-terminal helix. p19 α2 and α3 account for the density at the end of the tip. Gold and orange arrowheads point to the locations of the p19 and p75 C termini, respectively, previously determined by Fab labeling in negative-stain EM (*29*). The three-helix bundle between the C-terminal residues of p75, p45N, and p19 (modeled from RPA) is illustrated with dashed lines. (**C**) Crystal structure of p45C, a WH-WH domain. β5 is domain-swapped from a neighboring protein in the crystal lattice. (**D**) (Top) Negative-stain EM images of four typical p45-Fab–labeled telomerase holoenzyme particles, showing a cluster of 3 Fab bound to the C terminus of p45 at various locations near the holoenzyme. The side length of each image box is 44 nm. (Bottom) Corresponding outlines of telomerase and Fabs are shown in black and blue, respectively. Red dots indicate the p45C (attached to 3 Fab) and p45N (on telomerase) domains; dotted lines represent the linker.

RAP; in contrast, Teb1-p50 interaction stimulates high RAP (*29*, *36*). We conclude that p75-p45-p19 is structurally and functionally distinct from TEB and is most similar to a CST complex. CST has been identified in yeasts, plants, and mammals (*8*, *19*); this is the first evidence for the presence of CST in ciliates.

The telomeric DNA exits the template toward Teb1C

To obtain information on the path of telomere DNA on telomerase, we prepared a holoenzyme bound to a short telomeric DNA, biotin-5′-d $(GTTGGG)_2GT_LT_LG_LG_LG$, where T_L and G_L are locked nucleic acid (LNA) nucleotides (*60*). For this DNA, six nucleotides (nts) should bind the template and 13 nts should extend out from its 3′ end. We then bound biotin with streptavidin, linking two telomerase holoenzymes together via the biotin binding sites in each streptavidin tetramer. Visualization of these dimers of the telomerase holoenzyme by negative-stain EM confirms that the telomere DNA is bound (Fig. 6, A to C). The class averages and 3D reconstructions show clearly visible density of streptavidin located near Teb1C-Teb2N and the putative location of Teb1B (*29*) on the backside of the telomerase holoenzyme (Fig. 6, B to D). These results reveal that telomeric DNA exits the template from the backside of telomerase and toward Teb1C (Fig. 6D). Furthermore, within the resolution (~30 Å) of negative-stain EM, there is no large-scale structural rearrangement of TERT between the apo structure without DNA and the structure with telomeric DNA bound to the template, consistent with the crystal structure of *Tribolium* TERT without TER (*31*) versus with an RNA-DNA hairpin mimicking a template-DNA hybrid (*38*).

Implications for telomerase catalytic activity and association with telomeres

The cryo-EM structures, p45C and p19 crystal structures, PK NMR structure, domain modeling, and mass spectrometry data presented here reveal a complex RNP composed of three ternary complexes tethered by p50: a TERT-TER-p65 catalytic core; an RPA paralog TEB, comprising Teb1-Teb2-Teb3; and a *Tetrahymena* CST complex comprising p75-p45-p19. TER wraps around the TERT ring and interacts with all four domains of TERT. The TEN domain is close to TER, the TERT ring IFD, p50, Teb1, and Teb2, signaling its importance in the catalytic cycle of telomerase. In addition to the protein domains visible in the cryo-EM map, there are several domains that are not observed due to flexible positioning or intrinsic disorder in the absence of binding partners; these are Teb1 N, A, and B; putative Teb2C, p45C, p50C, p65N; and possibly p75N (schematized in Fig. 7A). Teb1A and Teb1B bind telomere DNA (*54*), whereas the others (except for p65N) may recruit proteins involved in C-strand synthesis, nucleolytic end-processing, unwinding of G quadruplexes, telomere end-binding, and DNA repair, thereby coordinating telomere maintenance.

In the catalytic core, the TER interactions with TERT are exclusively from the t/PK domain and

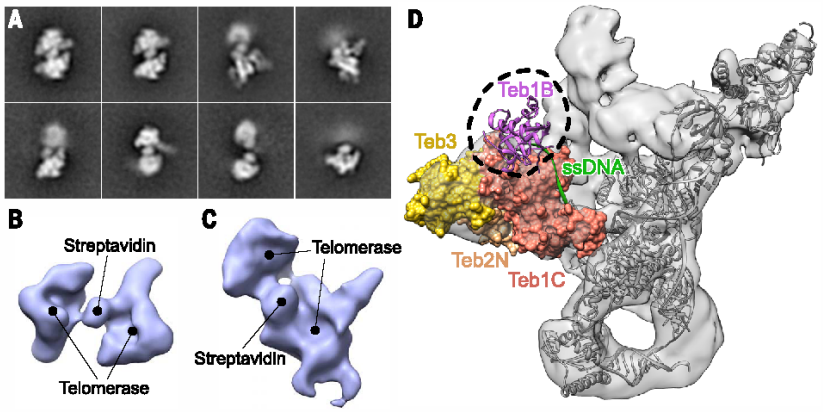

Fig. 6. Telomere ssDNA exits from the backside of the *Tetrahymena* telomerase holoenzyme. (**A**) Negative-stain EM class averages of the telomerase holoenzyme dimerized by primer-biotin-streptavidin-biotin-primer. The side length of each image box is 42 nm. (**B** and **C**) Random conical tilt (RCT) reconstruction of dimeric telomerase holoenzymes. One of two telomerase holoenzymes in (C) shows uninterpretable features due to flexible positioning of the two holoenzymes relative to each other. (**D**) A 9.4 Å cryo-EM map of the telomerase holoenzyme (gray surface) and the position of primer-attached streptavidin (black dashed circle), as identified by negative-stain EM RCT reconstruction in (B) and (C). Teb1B (purple) and ssDNA (green) exiting through Teb1C are modeled by fitting the crystal structure of the RPA:ssDNA complex (PDB ID 4GNX).

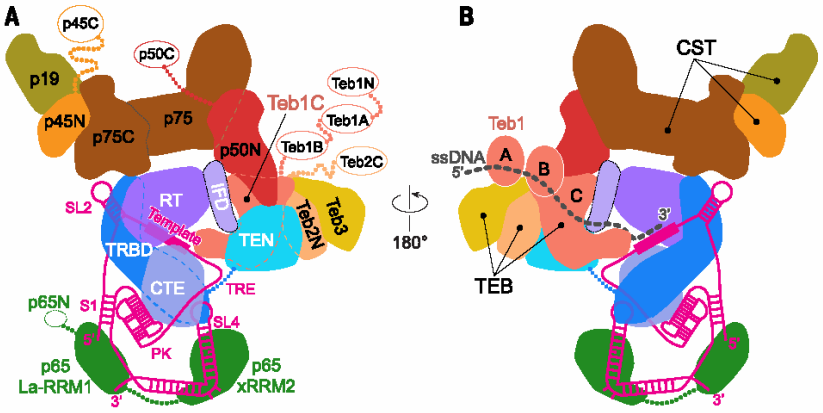

Fig. 7. Schematics of the complete *Tetrahymena* telomerase holoenzyme and DNA exit path. (**A**) Arrangement of the subunits and domains of the *Tetrahymena* telomerase catalytic core, TEB, and CST complexes tethered to p50, shown as front view. Domains connected by flexible linkers and not seen in the cryo-EM map are shown with oval outlines. (**B**) Arrangement of the holoenzyme with proposed path of telomere ssDNA, shown as back view. Teb1AB domains are presumed to be ordered when DNA-bound.

L4. Because a t/PK and a stem terminus element like L4 are almost universally found in other organisms (*2*, *30*) and TERT is highly conserved, *Tetrahymena* telomerase provides general insights into TER-TERT interactions and assembly. Human TER has a much larger pseudoknot, but the region containing the tertiary stem-loop interactions is comparable in size and probably interacts with TERT at the same location near the CTE, and the human TER t/PK could similarly encircle the TERT ring. This would place the other end of the pseudoknot close to the TEN domain, as implicated biochemically (*41*). Vertebrate telomerase contains a conserved three-way junction, the CR4-CR5 domain, that binds the TRBD (*61*) and has a stem-loop (P6.1) that is critical for activity (*62*). The P6.1 loop probably inserts at the TRBD-CTE interface (*61*, *63*), similarly to *Tetrahymena* TER L4.

In the cryo-EM structure of apo telomerase presented here, the template is apparently positioned with the 5′ end near the active site. This places the 3′ end of the template close to Teb1C, where the telomeric DNA binds as it exits the holoenzyme. We suggest that this would facilitate (re)binding of the primer to the template 3′ end before translocation. Based on homology with the crystal structures of the RPA-ssDNA complex (*51*), a model of Teb1AB bound to ssDNA based on the Pot1AB-ssDNA complex (*50*), and the position

of the 5′ end of telomeric DNA on telomerase revealed by streptavidin labeling, we can model a possible path of the telomere DNA on telomerase (Fig. 7B). Although the DNA is shown going straight from the template to Teb1, it is possible that during the catalytic cycle the DNA strand may interact with TEN, TRBD, and/or CTE. Within the catalytic core, the TEN domain has been implicated to play a role in ssDNA handling and act as an anchor site (*32*, *64*) and/or in active-site use of the DNA–template RNA hybrid (*41*). The TEN domain is positioned so that the exiting end of the short DNA–template helix could contact its (unmodeled) N and C termini at the end of a complete telomere repeat synthesis, where this interaction could facilitate template DNA strand separation and help direct the DNA toward Teb1 (fig. S10).

The identification of two RPA related complexes in the *Tetrahymena* telomerase holoenzyme and their constitutive rather than cell-cycle–regulated association allows us to use studies of the *Tetrahymena* telomerase holoenzyme to inform models for interaction and function of human TPP1-POT1 and CST. Like p50-TEN, the interaction between human TPP1 and TEN is essential for bridging telomerase to telomeres (*9*, *11*, *56*, *57*). Although Teb1C is homologous to RPA70C, Teb1AB is more similar to POT1 (*50*), which suggests that TEB functions to temporarily prevent rebinding of the telomere-bound Tpt1-Pot1a complex (*65*). Consistent with the conformational flexibility of p75-p45-p19 around p50 (*29*), this CST complex could bind the telomeric DNA as it exits Teb1 to recruit DNA polymerase α for coordinated C-strand synthesis. In summary, the structure of the *Tetrahymena* telomerase catalytic core and identification of telomerase holoenzyme subcomplexes homologous to those found at mammalian, plant, and yeast telomeres provide new mechanistic insights and suggest commonalities of telomerase interaction, action, and regulation at telomeres.

Materials and methods

EM specimen preparation and data collection

Tetrahymena telomerase holoenzyme was purified following the previously described protocol (*29*), with some modifications. Briefly, 12 liters of cell culture of TERT-FZZ strain was used for tandem affinity purification following the established procedures (*29*). The final Flag elution was effected by incubating the telomerase-bound anti-Flag M2 affinity gel with 1.5 ml of elution buffer (20 mM HEPES·NaOH at pH 8.0, 50 mM NaCl, 1 mM $MgCl_2$, 1 mM TCEP·HCl, 0.025% IGEPAL CA-630, and 200 ng/μl of 3×Flag peptide) at 4°C. The eluate was incubated with 30 mg of Bio-Beads SM-2 absorbent (Bio-Rad) at 4°C for 2 hours by end-over-end rotation. The supernatant was then concentrated to 30 μl using a Microcon YM-10 centrifugal filter (Millipore).

For cryo-EM, 2.5 μl of the sample was applied to a glow-discharged Quantifoil R2/1 grid. The grid was blotted with filter paper to remove excess sample and was flash-frozen in liquid ethane with FEI Vitrobot Mark IV. The frozen-hydrated grids were loaded into an FEI Titan Krios electron microscope operated at 300 kV for automated image acquisition with Leginon (*66*). Micrographs were acquired with a Gatan K2 Summit direct electron detection camera operated in the electron-counting mode at a calibrated magnification of 36,764× (pixel size of 1.36 Å on the sample level) and defocus values ranging from −2.0 to −7.0 μm. A GIF Quantum LS Imaging Filter (Gatan) was installed between the electron microscope and the K2 camera, but the energy filter (slit) was not used. The dose rate on the camera was set to ~8 electrons (e^-) per pixel per second, and the total exposure time was 12 s fractionated into 48 frames of images with a 0.25-s exposure time for each frame. Frame images were aligned and averaged for correction of beam-induced drift using the graphics processing unit–accelerated motion correction program (*67*). The average images from all frames were used for defocus determination and particle picking, and those from the first 28 frames (corresponding to ~30 $e^-/Å^2$ of total dose on sample) were used for further data processing, including image classification and 3D structure refinement. A total of 4210 micrographs were used in the data processing.

Image processing

The defocus value of each cryo-EM micrograph was determined by CTFFIND (*68*), and the micrographs were corrected for contrast transfer function (CTF) by phase-flipping with the corresponding defocus and astigmatism values using Bsoft (*69*). A total of 478,698 particles were automatically picked using DoGpicker (*70*) and windowed out in dimensions of 256 pixels by 256 pixels using batchboxer in EMAN (*71*). The particles were binned to dimensions of 128 pixels by 128 pixels (pixel size of 2.72 Å) before the following processing. The binned particles were subjected to 2D and 3D classifications by RELION (*72*), following the recommended procedure (www2.mrc-lmb.cam.ac.uk/relion/). We performed two consecutive rounds of 2D classifications; in each round, the particles were classified into 100 classes for 25 iterations. After each round of 2D classification, class averages were visually inspected, and particles in the "bad" classes (i.e., those with fuzzy or uninterpretable features or fuzzy density of the p75-p45-p19 subcomplex) (fig. S1B) were removed. About 20% of the class averages were kept after each round of 2D classification, and 47,251 particles were selected for the following 3D classification. The previously obtained negative-stain EM reconstruction at 25 Å resolution (*29*) was low-pass filtered to 60 Å to serve as the initial model for 3D classification. The 3D classification generated five classes (fig. S1D), four of which showed an intact holoenzyme structure and were combined into a data set of 40,754 particles for 3D autorefinements by RELION as follows: First, a 3D autorefinement was performed using a spherical mask. The resolution was estimated to be 9.4 Å by the relion_postprocess program using the "gold-standard" Fourier shell correlation at a 0.143 criterion, with a soft mask for which the masking effect was corrected by phase randomization. Second, the density corresponding to the flexible p75-p45-p19 subcomplex was removed from the 9.4 Å cryo-EM map using the "Volume Erase" tool in UCSF Chimera (*73*), and the resulting map was used to generate a soft-edge mask by the relion_mask_create program. This soft-edge mask was then used in the other 3D autorefinement, in which the p75-p45-p19 subcomplex was excluded during the structure refinement and only included in the final reconstruction. The resolution of this focused refinement was 8.9 Å, estimated as described above. The cryo-EM maps were sharpened with B-factor and low-pass filtered to the stated resolution using the relion_postprocess program. The local resolution was calculated with ResMap (*74*), using two cryo-EM maps independently refined from halves of data.

Tetrahymena telomerase holoenzyme particles adopted a preferred front view in negative-stain EM grids (*29*) or in cryo-EM Quantifoil grids with holey carbon or coated with continuous carbon film, probably due to its irregular and flattened shape. We tried numerous sample and cryo-EM grid conditions to overcome this preferred orientation problem. The current protocol involving Bio-Beads had the most improved effect on the orientation distribution. However, ~60% of the particles were still in the front view configuration in the cryo-EM images. To assess the effect of preferred orientation on reconstruction resolution, the particles were divided into halves ("uniform" and "preferred") that showed more uniform or more preferred orientation distribution, respectively (fig. S2). Briefly, the particle orientation file (the "data.star" file generated by RELION 3D autorefinement) of 40,754 particles was analyzed to group particles with the same orientation (same AngleRot and AngleTilt). A threshold of particle count was set so that the particles above the threshold in each orientation group (where the particle count in that group was larger than the threshold) were sent to the preferred half, and the rest were kept in the uniform half. Separation of particles within an orientation group was random. These two halves of the data set were then subjected to 3D autorefinement, using the same parameters as those for the 8.9 Å reconstruction. Comparisons of orientation distributions and 3D reconstructions show that the uniform half had sufficient orientations to obtain a high-quality 3D reconstruction at an overall resolution better than 9.3 Å, and addition of the preferred half only improved the resolution modestly (fig. S2).

Fitting of atomic models into the cryo-EM maps

For the pseudoatomic model of TERT-TER-p65 and Teb1C, the x-ray crystal and NMR structures of *Tetrahymena* TERT TRBD [Protein Data Bank identification code (PDB ID) 2R4G] (*37*), TERT TEN (PDB ID 2B2A) (*32*), Teb1C (PDB ID 3U50) (*50*), TER SL2 (PDB ID 2FRL) (*29*), the model of p65 xRRM2:SL4 (*33*), and the homology model of *Tetrahymena* TERT RT-CTE domains based on *Tribolium* TERT (PDB IDs 3DU6 and 3KYL; TERT CTE residues 1058 to 1117 were not modeled due to low sequence homology to *Tribolium* TERT) (*29*, *31*, *38*)—which were previously assembled

together by fitting into the negative-stain EM 3D reconstruction (*29*)—were placed as a whole in an approximate position in the cryo-EM maps, followed by fitting the individual domain structures into the cryo-EM map using the "Fit in Map" function in UCSF Chimera (*73*). These domain structures or models fit into the cryo-EM map with subtle rotations and translocations, except for Teb1C, which was moved to the cryo-EM density behind TEN and next to TRBD and matched this with high consistency. The PK structure (PDB ID 2N6Q) was manually placed into the cryo-EM density matching its size and shape, as identified by exhaustive visual inspection of the cryo-EM map, and then fit into the density using UCSF Chimera. S1 was modeled as an ideal A-form helix and fit into cryo-EM density that matched its shape near the PK and SL4. The template was located by fitting the crystal structure of *Tribolium* TERT in complex with an RNA-DNA hybrid helix (PDB ID 3KYL) (*38*) into the cryo-EM map and finding unmodeled density near the RNA strand. The density assigned for the template is displaced by ~7 Å relative to that in the fitted *Tribolium* TERT. The remaining single-stranded regions of TER connecting the above fitted structure elements were modeled into the cryo-EM densities using Coot (*75*) as follows: First, ideal A-form single-stranded RNA fragments were approximately placed between the flanking high-resolution RNA structures. The bond angles of the RNA backbone were then manually adjusted until the backbone fit into the cryo-EM density that was assigned to the RNA after the protein subunits were fit into the cryo-EM map. Last, standard bond angles and lengths of the backbone of the single-stranded RNA fragments were achieved with the use of the "Regularize Zone" tool in Coot. Because the RNA bases were not distinguishable in the 8.9 Å cryo-EM map, only the backbone of the single-stranded regions was modeled. For the pseudoatomic model of Teb1-Teb2-Teb3, RPA70C: RPA32N:RPA14 from the crystal structure of RPA (PDB ID 1L1O) (*51*) was fit into the cryo-EM maps by the colores program of Situs, using the exhaustive 6D search algorithm (*76*). The structure of the RPA trimer fit with high consistency into the cryo-EM map in the density assigned for Teb1C and the adjacent knob. For the final model, RPA70C was replaced by Teb1C, which fits in the same density, except for the C-terminal helix that is disordered in the Teb1C crystal structure but is apparently well ordered in the cryo-EM maps. RPA32N and RPA14 in the model are paralogs of Teb2 and Teb3, respectively. During the Situs fitting of RPA70C:RPA32N:RPA14 to the 9.4 Å cryo-EM map, a second location, corresponding to the tip of the density assigned to the p75-p45-p19 subcomplex, was identified with high confidence, which suggests that it was also an RPA homolog. For the pseudoatomic model of p75C-p45N-p19, RPA14 was manually replaced by p19 (PDB ID 5DFM), except for its C-terminal helix that is disordered in the p19 crystal structure. The crystal structure of the TPP1 OB fold (PDB ID 2I46) (*13*) was placed in the cryo-EM density assigned to p50N and then fit using UCSF Chimera. The cryo-EM maps and the modeled protein and RNA structures were visualized with UCSF Chimera and PyMOL (*77*).

Structure determination of p19, p45C, and TER PK

Full-length p19 (*28*) was fused via a triple alanine linker to the wild-type maltose binding protein (MBP) vector as described in (*78*), expressed in *Escherichia coli*, and purified by amylose affinity and size exclusion chromatography (SEC). To obtain diffracting native crystals, a 2:1 mixture of 12 mg/ml of MBP-p19 and the reservoir solution (0.1 M sodium acetate at pH 4.6 and 2.0 M ammonium sulfate) was set up in a 24-well hanging drop format. Full-length p45 (*79*) was fused to His-tagged MBP via a tobacco etch virus (TEV) protease cleavage site, expressed in *E. coli*, and copurified with cells expressing 6×His-tagged p19 using Ni–nitrilotriacetic acid (NTA) affinity and SEC. p45C (residues 162 to 373) was identified via limited chymotrypsin proteolysis of full-length p45 bound to p19. p45C was fused to His-tagged MBP via the TEV protease cleavage site, expressed in *E. coli*, and purified by Ni-NTA affinity and SEC. To obtain diffracting native crystals, a 1:1 mixture of 14 mg/ml of p45C and the reservoir solution [0.1 M Na·HEPES at pH 7.5, 5% (v/v) MPD, and 10% (w/v) polyethylene glycol 6000) was set up in a 24-well hanging drop format. Data were collected at 100 K at Advanced Photon Source–Northeastern Collaborative Access Team (APS-NECAT) beamline 24-ID-C on a DECTRIS-PILATUS 6 M pixel detector. Data were indexed, integrated, and scaled using XDS/XSCALE (*80*). Structures were solved with the molecular replacement program PHASER (*81*), using initial models from SeMet data sets. Final models were iteratively built and refined in Coot (*75*) and PHENIX (*82*). In the crystal structure of p45C, β5 in WH2 is domain-swapped from a neighboring protein in the crystal lattice. This domain-swapped β5 was used to build a biological unit model of p45C (Fig. 5C). NMR assignments were obtained, and solution structure of the TER pseudoknot (nucleotides 68 to 100) was determined following established protocols for human and yeast TER pseudoknots (*44*, *45*, *83*). Sample conditions were ~1 mM RNA in 10 mM $NaPO_4$ at pH 6.3 and 50 mM KCl at 10°C. The structures were calculated with a total of 414 nuclear Overhauser effect distance, 171 dihedral angle, 82 H bond, and 79 residual dipolar coupling restraints using standard protocols in Xplor-NIH 2.9.8. Pairwise root mean square deviation for the 10 lowest-energy structures (out of 100) was 0.83 Å for all heavy atoms (table S4).

Mass spectrometry

Telomerase was purified from *Tetrahymena* TERT-FZZ and ZZF-p50 strains as described in (*29*), up to the final anti-FLAG resin wash step before elution. Telomerase was batch-washed on the resin three times by incubation in 1 ml of IGEPAL-free wash buffer at 4°C, rotating end-over-end for 10 min, and was eluted twice by incubation at room temperature with 50 µl of 0.1% trifluoroacetic acid for 30 min each time. For enzymatic digestion of the samples, 70 µl of deoxycholic acid (0.1% w/v) in 1 M NH_4HCO_3 was added to the elution. Cysteines were alkylated by adding iodoacetamide to 4 mM and incubating at room temperature. After 30 min, excess dithiothreitol was added to quench residual iodoacetamide, and trypsin (300 ng) was added to initiate digestion. The solution was incubated at 37°C overnight, after which it was acidified to pH 2 with trifluoroacetic acid, to precipitate the deoxycholic acid. The deoxycholic acid was extracted from the aqueous layer with three 200-µl aliquots of water-saturated ethyl acetate (*84*). The digested peptides were dried and resuspended in 1% formic acid. The resulting tryptic peptides were measured by LC-MS/MS, using an EASY-nLC 1000 (Thermo Scientific, Waltham, MA) coupled to a Q-Exactive Orbitrap mass spectrometer (Thermo Scientific) and an EASY-Spray nano–electrospray ionization source. Peptides were injected onto a 75 µm by 15 cm, 3 µm, 100 Å PepMap C18 reversed-phase LC column and separated using a linear gradient from 5% solvent B (0.1% formic acid in acetonitrile) and 95% solvent A (0.1% formic acid in water) to 50% solvent B in 2 hours at a constant flow rate of 300 nl/min. Eluted peptides were analyzed with a top-ten data-dependent acquisition method and identified using Proteome Discoverer (version 1.4; Thermo Scientific) coupled to MASCOT (version 2.4.1; Matrix Science, London). Orbitrap MS resolving power was set to 70,000 at a mass/charge ratio (m/z) of 200 for MS1 and 17,500 at a m/z of 200 for MS2. Tryptic peptides with up to two missed cleavages were searched against a *T. thermophila* protein database (www.ciliate.org) supplemented with common protein contaminant and enzyme sequences (27,046 sequences), with dynamic modifications for carbamidomethyl (C), oxidation (M), deamidation (N, Q), and peptide *N*-terminal cyclization to eliminate NH_3 (Q, carbamidomethyl-cys) or H_2O (E) (C, Cys; M, Met; Q, Gln; E, Glu). Precursor- and product-ion mass tolerances were set to 10 parts per million (or less) and 0.01 daltons, respectively.

Telomerase reconstitution and activity assays

Telomerase subcomplexes were assembled separately and then combined. The RNP catalytic core was assembled by TERT expression in RRL in the presence of purified bacterially expressed p65 and in vitro transcribed TER. Additional RRL synthesis reactions generated p50N30, Teb1, or coexpressed TEB complex subunits. One subunit was tagged with 3×FLAG (p50N30-F for TEB subunit function studies or TERT-F for TERT TEN domain mutational analysis). Subcomplexes were combined, bound to FLAG antibody resin, and assayed by primer extension as described previously (*29*), using radiolabeled deoxyguanosine triphosphate (dGTP) and primer $(GTTGGG)_3$ at a final concentration of 200 nM. Elongation time was 10 min unless otherwise indicated. Products were resolved by denaturing gel electrophoresis, including an end-labeled oligonucleotide added before product precipitation as a recovery control.

Preparation of DNA-LNA–bound telomerase linked by streptavidin and negative-stain EM

Three-repeat biotinylated LNA/DNA primer was purchased from Exiqon as biotin-5′-GTTGGGG-TTGGGGT$_L$T$_L$G$_L$G$_L$G. Telomerase was purified as described (*29*) from TERT-FZZ strain up to the TEV protease cleavage step, during which 5 μM three-repeat primer and 50 μM dGTP were added to the immunoglobulin G resin. Immediately before the 10-min wash steps of the telomerase-bound flag resin, the resin was split, and one-half was incubated in 50 μl of wash buffer, whereas the other was incubated in 50 μl of wash buffer with 5 μM streptavidin, rotating end-over-end at 4°C for 30 min. Three wash steps were then performed as usual, after which the two resins were recombined and batch-eluted with 3×FLAG peptide, according to the original protocol. Negative-stain EM samples were prepared, imaged, and processed as previously described (*29*).

REFERENCES AND NOTES

1. E. H. Blackburn, C. W. Greider, J. W. Szostak, Telomeres and telomerase: The path from maize, *Tetrahymena* and yeast to human cancer and aging. *Nat. Med.* **12**, 1133–1138 (2006). doi: 10.1038/nm1006-1133; pmid: 17024208
2. E. H. Blackburn, K. Collins, Telomerase: An RNP enzyme synthesizes DNA. *Cold Spring Harbor Perspect. Biol.* **3**, a003558 (2011). doi: 10.1101/cshperspect.a003558; pmid: 20660025
3. M. Armanios, E. H. Blackburn, The telomere syndromes. *Nat. Rev. Genet.* **13**, 693–704 (2012). doi: 10.1038/nrg3246; pmid: 22965356
4. B. Bernardes de Jesus, M. A. Blasco, Telomerase at the intersection of cancer and aging. *Trends Genet.* **29**, 513–520 (2013). doi: 10.1016/j.tig.2013.06.007; pmid: 23876621
5. S. E. Artandi, R. A. DePinho, Telomeres and telomerase in cancer. *Carcinogenesis* **31**, 9–18 (2010). doi: 10.1093/carcin/bgp268; pmid: 19887512
6. J. Nandakumar, T. R. Cech, Finding the end: Recruitment of telomerase to telomeres. *Nat. Rev. Mol. Cell Biol.* **14**, 69–82 (2013). doi: 10.1038/nrm3505; pmid: 23299958
7. J. A. Stewart, M. F. Chaiken, F. Wang, C. M. Price, Maintaining the end: Roles of telomere proteins in end-protection, telomere replication and length regulation. *Mutat. Res.* **730**, 12–19 (2012). doi: 10.1016/j.mrfmmm.2011.08.011; pmid: 21945241
8. L. Y. Chen, J. Lingner, CST for the grand finale of telomere replication. *Nucleus* **4**, 277–282 (2013). doi: 10.4161/nucl.25701; pmid: 23851344
9. F. L. Zhong *et al.*, TPP1 OB-fold domain controls telomere maintenance by recruiting telomerase to chromosome ends. *Cell* **150**, 481–494 (2012). doi: 10.1016/j.cell.2012.07.012; pmid: 22863003
10. A. N. Sexton, D. T. Youmans, K. Collins, Specificity requirements for human telomere protein interaction with telomerase holoenzyme. *J. Biol. Chem.* **287**, 34455–34464 (2012). doi: 10.1074/jbc.M112.394767; pmid: 22893708
11. J. Nandakumar *et al.*, The TEL patch of telomere protein TPP1 mediates telomerase recruitment and processivity. *Nature* **492**, 285–289 (2012). doi: 10.1038/nature11648; pmid: 23103865
12. H. Xin *et al.*, TPP1 is a homologue of ciliate TEBP-β and interacts with POT1 to recruit telomerase. *Nature* **445**, 559–562 (2007). doi: 10.1038/nature05469; pmid: 17237767
13. F. Wang *et al.*, The POT1-TPP1 telomere complex is a telomerase processivity factor. *Nature* **445**, 506–510 (2007). doi: 10.1038/nature05454; pmid: 17237768
14. T. Rao *et al.*, Structure of Est3 reveals a bimodal surface with differential roles in telomere replication. *Proc. Natl. Acad. Sci. U.S.A.* **111**, 214–218 (2014). doi: 10.1073/pnas.1316453111; pmid: 24344315
15. J. M. Talley, D. C. DeZwaan, L. D. Maness, B. C. Freeman, K. L. Friedman, Stimulation of yeast telomerase activity by the ever shorter telomere 3 (Est3) subunit is dependent on direct interaction with the catalytic protein Est2. *J. Biol. Chem.* **286**, 26431–26439 (2011). doi: 10.1074/jbc.M111.228635; pmid: 21659533
16. A. Prakash, G. E. Borgstahl, The structure and function of replication protein A in DNA replication. *Subcell. Biochem.* **62**, 171–196 (2012). doi: 10.1007/978-94-007-4572-8_10; pmid: 22918586
17. K. A. Lewis, D. S. Wuttke, Telomerase and telomere-associated proteins: Structural insights into mechanism and evolution. *Structure* **20**, 28–39 (2012). doi: 10.1016/j.str.2011.10.017; pmid: 22244753
18. L. Y. Chen, S. Redon, J. Lingner, The human CST complex is a terminator of telomerase activity. *Nature* **488**, 540–544 (2012). doi: 10.1038/nature11269; pmid: 22763445
19. C. M. Price *et al.*, Evolution of CST function in telomere maintenance. *Cell Cycle* **9**, 3157–3165 (2010). doi: 10.4161/cc.9.16.12547; pmid: 20697207
20. P. Wu, H. Takai, T. de Lange, Telomeric 3′ overhangs derive from resection by Exo1 and Apollo and fill-in by POT1b-associated CST. *Cell* **150**, 39–52 (2012). doi: 10.1016/j.cell.2012.05.026; pmid: 22748632
21. F. Wang *et al.*, Human CST has independent functions during telomere duplex replication and C-strand fill-in. *Cell Reports* **2**, 1096–1103 (2012). doi: 10.1016/j.celrep.2012.10.007; pmid: 23142664
22. N. F. Lue, E. Y. Yu, M. Lei, A popular engagement at the ends. *Nat. Struct. Mol. Biol.* **20**, 10–12 (2013). doi: 10.1038/nsmb.2483; pmid: 23288360
23. T. M. Tucey, V. Lundblad, Regulated assembly and disassembly of the yeast telomerase quaternary complex. *Genes Dev.* **28**, 2077–2089 (2014). doi: 10.1101/gad.246256.114; pmid: 25240060
24. R. J. Wellinger, V. A. Zakian, Everything you ever wanted to know about *Saccharomyces cerevisiae* telomeres: Beginning to end. *Genetics* **191**, 1073–1105 (2012). doi: 10.1534/genetics.111.137851; pmid: 22879408
25. E. D. Egan, K. Collins, Biogenesis of telomerase ribonucleoproteins. *RNA* **18**, 1747–1759 (2012). doi: 10.1261/rna.034629.112; pmid: 22875809
26. J. D. Podlevsky, J. J. Chen, It all comes together at the ends: Telomerase structure, function, and biogenesis. *Mutat. Res.* **730**, 3–11 (2012). doi: 10.1016/j.mrfmmm.2011.11.002; pmid: 22093366
27. H. E. Upton, K. Hong, K. Collins, Direct single-stranded DNA binding by Teb1 mediates the recruitment of *Tetrahymena thermophila* telomerase to telomeres. *Mol. Cell. Biol.* **34**, 4200–4212 (2014). doi: 10.1128/MCB.01030-14; pmid: 25225329
28. B. Min, K. Collins, An RPA-related sequence-specific DNA-binding subunit of telomerase holoenzyme is required for elongation processivity and telomere maintenance. *Mol. Cell* **36**, 609–619 (2009). doi: 10.1016/j.molcel.2009.09.041; pmid: 19941821
29. J. Jiang *et al.*, The architecture of *Tetrahymena* telomerase holoenzyme. *Nature* **496**, 187–192 (2013). doi: 10.1038/nature12062; pmid: 23552895
30. C. A. Theimer, J. Feigon, Structure and function of telomerase RNA. *Curr. Opin. Struct. Biol.* **16**, 307–318 (2006). doi: 10.1016/j.sbi.2006.05.005; pmid: 16713250
31. A. J. Gillis, A. P. Schuller, E. Skordalakes, Structure of the *Tribolium castaneum* telomerase catalytic subunit TERT. *Nature* **455**, 633–637 (2008). doi: 10.1038/nature07283; pmid: 18758444
32. S. A. Jacobs, E. R. Podell, T. R. Cech, Crystal structure of the essential N-terminal domain of telomerase reverse transcriptase. *Nat. Struct. Mol. Biol.* **13**, 218–225 (2006). doi: 10.1038/nsmb1054; pmid: 16462747
33. M. Singh *et al.*, Structural basis for telomerase RNA recognition and RNP assembly by the holoenzyme La family protein p65. *Mol. Cell* **47**, 16–26 (2012). doi: 10.1016/j.molcel.2012.05.018; pmid: 22705372
34. M. D. Stone *et al.*, Stepwise protein-mediated RNA folding directs assembly of telomerase ribonucleoprotein. *Nature* **446**, 458–461 (2007). doi: 10.1038/nature05600; pmid: 17322903
35. N. K. Jacob, R. Lescasse, B. R. Linger, C. M. Price, *Tetrahymena* POT1a regulates telomere length and prevents activation of a cell cycle checkpoint. *Mol. Cell. Biol.* **27**, 1592–1601 (2007). doi: 10.1128/MCB.01975-06; pmid: 17158924
36. K. Hong *et al.*, *Tetrahymena* telomerase holoenzyme assembly, activation, and inhibition by domains of the p50 central hub. *Mol. Cell. Biol.* **33**, 3962–3971 (2013). doi: 10.1128/MCB.00792-13; pmid: 23918804
37. S. Rouda, E. Skordalakes, Structure of the RNA-binding domain of telomerase: Implications for RNA recognition and binding. *Structure* **15**, 1403–1412 (2007). doi: 10.1016/j.str.2007.09.007; pmid: 17997966
38. M. Mitchell, A. Gillis, M. Futahashi, H. Fujiwara, E. Skordalakes, Structural basis for telomerase catalytic subunit TERT binding to RNA template and telomeric DNA. *Nat. Struct. Mol. Biol.* **17**, 513–518 (2010). doi: 10.1038/nsmb.1777; pmid: 20357774
39. N. F. Lue, Y. C. Lin, I. S. Mian, A conserved telomerase motif within the catalytic domain of telomerase reverse transcriptase is specifically required for repeat addition processivity. *Mol. Cell. Biol.* **23**, 8440–8449 (2003). doi: 10.1128/MCB.23.23.8440-8449.2003; pmid: 14612390
40. M. Xie, J. D. Podlevsky, X. Qi, C. J. Bley, J. J. Chen, A novel motif in telomerase reverse transcriptase regulates telomere repeat addition rate and processivity. *Nucleic Acids Res.* **38**, 1982–1996 (2010). doi: 10.1093/nar/gkp1198; pmid: 20044353
41. R. A. Wu, K. Collins, Human telomerase specialization for repeat synthesis by unique handling of primer-template duplex. *EMBO J.* **33**, 921–935 (2014). doi: 10.1002/embj.201387205; pmid: 24619002
42. B. Eckert, K. Collins, Roles of telomerase reverse transcriptase N-terminal domain in assembly and activity of *Tetrahymena* telomerase holoenzyme. *J. Biol. Chem.* **287**, 12805–12814 (2012). doi: 10.1074/jbc.M112.339853; pmid: 22367200
43. F. Qiao, T. R. Cech, Triple-helix structure in telomerase RNA contributes to catalysis. *Nat. Struct. Mol. Biol.* **15**, 634–640 (2008). doi: 10.1038/nsmb.1420; pmid: 18500353
44. D. D. Cash *et al.*, Pyrimidine motif triple helix in the *Kluyveromyces lactis* telomerase RNA pseudoknot is essential for function in vivo. *Proc. Natl. Acad. Sci. U.S.A.* **110**, 10970–10975 (2013). doi: 10.1073/pnas.1309590110; pmid: 23776224
45. C. A. Theimer, C. A. Blois, J. Feigon, Structure of the human telomerase RNA pseudoknot reveals conserved tertiary interactions essential for function. *Mol. Cell* **17**, 671–682 (2005). doi: 10.1016/j.molcel.2005.01.017; pmid: 15749017
46. M. Mihalusova, J. Y. Wu, X. Zhuang, Functional importance of telomerase pseudoknot revealed by single-molecule analysis. *Proc. Natl. Acad. Sci. U.S.A.* **108**, 20339–20344 (2011). doi: 10.1073/pnas.1017686108; pmid: 21571642
47. C. M. O'Connor, K. Collins, A novel RNA binding domain in *Tetrahymena* telomerase p65 initiates hierarchical assembly of telomerase holoenzyme. *Mol. Cell. Biol.* **26**, 2029–2036 (2006). doi: 10.1128/MCB.26.6.2029-2036.2006; pmid: 16507983
48. A. J. Berman, A. R. Gooding, T. R. Cech, *Tetrahymena* telomerase protein p65 induces conformational changes throughout telomerase RNA (TER) and rescues telomerase reverse transcriptase and TER assembly mutants. *Mol. Cell. Biol.* **30**, 4965–4976 (2010). doi: 10.1128/MCB.00827-10; pmid: 20713447
49. X. Qi *et al.*, RNA/DNA hybrid binding affinity determines telomerase template-translocation efficiency. *EMBO J.* **31**, 150–161 (2012). doi: 10.1038/emboj.2011.363; pmid: 21989387
50. Z. Zeng *et al.*, Structural basis for *Tetrahymena* telomerase processivity factor Teb1 binding to single-stranded telomeric-repeat DNA. *Proc. Natl. Acad. Sci. U.S.A.* **108**, 20357–20361 (2011). doi: 10.1073/pnas.1113624108; pmid: 22143754
51. E. Bochkareva, S. Korolev, S. P. Lees-Miller, A. Bochkarev, Structure of the RPA trimerization core and its role in the multistep DNA-binding mechanism of RPA. *EMBO J.* **21**, 1855–1863 (2002). doi: 10.1093/emboj/21.7.1855; pmid: 11927569
52. S. F. Altschul *et al.*, Gapped BLAST and PSI-BLAST: A new generation of protein database search programs. *Nucleic Acids Res.* **25**, 3389–3402 (1997). doi: 10.1093/nar/25.17.3389; pmid: 9254694
53. C. Cole, J. D. Barber, G. J. Barton, The Jpred 3 secondary structure prediction server. *Nucleic Acids Res.* **36** (suppl. 2), W197–W201 (2008). doi: 10.1093/nar/gkn238; pmid: 18463136
54. B. Min, K. Collins, Multiple mechanisms for elongation processivity within the reconstituted *Tetrahymena* telomerase holoenzyme. *J. Biol. Chem.* **285**, 16434–16443 (2010). doi: 10.1074/jbc.M110.119172; pmid: 20363756
55. J. Xiong *et al.*, Transcriptome analysis of the model protozoan, *Tetrahymena thermophila*, using deep RNA sequencing. *PLOS ONE* **7**, e30630 (2012). doi: 10.1371/journal.pone.0030630; pmid: 22347391
56. A. N. Sexton *et al.*, Genetic and molecular identification of three human TPP1 functions in telomerase action: Recruitment, activation, and homeostasis set point regulation. *Genes Dev.* **28**, 1885–1899 (2014). pmid: 25128433

57. J. C. Schmidt, A. B. Dalby, T. R. Cech, Identification of human TERT elements necessary for telomerase recruitment to telomeres. *eLife* **3**, e03563 (2014). doi: 10.7554/eLife.03563
58. J. Sun *et al.*, Stn1-Ten1 is an Rpa2-Rpa3-like complex at telomeres. *Genes Dev.* **23**, 2900–2914 (2009). doi: 10.1101/gad.1851909; pmid: 20008938
59. C. Bryan, C. Rice, M. Harkisheimer, D. C. Schultz, E. Skordalakes, Structure of the human telomeric Stn1-Ten1 capping complex. *PLOS ONE* **8**, e66756 (2013). doi: 10.1371/journal.pone.0066756; pmid: 23826127
60. B. Vester, J. Wengel, LNA (locked nucleic acid): High-affinity targeting of complementary RNA and DNA. *Biochemistry* **43**, 13233–13241 (2004). doi: 10.1021/bi0485732; pmid: 15491130
61. J. Huang *et al.*, Structural basis for protein-RNA recognition in telomerase. *Nat. Struct. Mol. Biol.* **21**, 507–512 (2014). doi: 10.1038/nsmb.2819; pmid: 24793650
62. J. L. Chen, K. K. Opperman, C. W. Greider, A critical stem-loop structure in the CR4-CR5 domain of mammalian telomerase RNA. *Nucleic Acids Res.* **30**, 592–597 (2002). doi: 10.1093/nar/30.2.592; pmid: 11788723
63. C. J. Bley *et al.*, RNA-protein binding interface in the telomerase ribonucleoprotein. *Proc. Natl. Acad. Sci. U.S.A.* **108**, 20333–20338 (2011). doi: 10.1073/pnas.1100270108; pmid: 22123986
64. A. J. Zaug, E. R. Podell, T. R. Cech, Mutation in TERT separates processivity from anchor-site function. *Nat. Struct. Mol. Biol.* **15**, 870–872 (2008). doi: 10.1038/nsmb.1462; pmid: 18641663
65. B. R. Linger, G. B. Morin, C. M. Price, The Pot1a-associated proteins Tpt1 and Pat1 coordinate telomere protection and length regulation in *Tetrahymena*. *Mol. Biol. Cell* **22**, 4161–4170 (2011). doi: 10.1091/mbc.E11-06-0551; pmid: 21900503
66. C. Suloway *et al.*, Automated molecular microscopy: The new Leginon system. *J. Struct. Biol.* **151**, 41–60 (2005). doi: 10.1016/j.jsb.2005.03.010; pmid: 15890530
67. X. Li *et al.*, Electron counting and beam-induced motion correction enable near-atomic-resolution single-particle cryo-EM. *Nat. Methods* **10**, 584–590 (2013). doi: 10.1038/nmeth.2472; pmid: 23644547
68. J. A. Mindell, N. Grigorieff, Accurate determination of local defocus and specimen tilt in electron microscopy. *J. Struct. Biol.* **142**, 334–347 (2003). doi: 10.1016/S1047-8477(03)00069-8; pmid: 12781660
69. J. B. Heymann, D. M. Belnap, Bsoft: Image processing and molecular modeling for electron microscopy. *J. Struct. Biol.* **157**, 3–18 (2007). doi: 10.1016/j.jsb.2006.06.006; pmid: 17011211
70. N. R. Voss, C. K. Yoshioka, M. Radermacher, C. S. Potter, B. Carragher, DoG Picker and TiltPicker: Software tools to facilitate particle selection in single particle electron microscopy. *J. Struct. Biol.* **166**, 205–213 (2009). doi: 10.1016/j.jsb.2009.01.004; pmid: 19374019
71. S. J. Ludtke, P. R. Baldwin, W. Chiu, EMAN: Semiautomated software for high-resolution single-particle reconstructions. *J. Struct. Biol.* **128**, 82–97 (1999). doi: 10.1006/jsbi.1999.4174; pmid: 10600563
72. S. H. Scheres, RELION: Implementation of a Bayesian approach to cryo-EM structure determination. *J. Struct. Biol.* **180**, 519–530 (2012). doi: 10.1016/j.jsb.2012.09.006; pmid: 23000701
73. E. F. Pettersen *et al.*, UCSF Chimera—A visualization system for exploratory research and analysis. *J. Comput. Chem.* **25**, 1605–1612 (2004). doi: 10.1002/jcc.20084; pmid: 15264254
74. A. Kucukelbir, F. J. Sigworth, H. D. Tagare, Quantifying the local resolution of cryo-EM density maps. *Nat. Methods* **11**, 63–65 (2014). doi: 10.1038/nmeth.2727; pmid: 24213166
75. P. Emsley, K. Cowtan, *Coot*: Model-building tools for molecular graphics. *Acta Crystallogr. D* **60**, 2126–2132 (2004). doi: 10.1107/S0907444904019158; pmid: 15572765
76. P. Chacón, W. Wriggers, Multi-resolution contour-based fitting of macromolecular structures. *J. Mol. Biol.* **317**, 375–384 (2002). doi: 10.1006/jmbi.2002.5438; pmid: 11922671
77. The PyMOL Molecular Graphics System, Version 1.7.4, Schrödinger, LLC.
78. A. F. Moon, G. A. Mueller, X. Zhong, L. C. Pedersen, A synergistic approach to protein crystallization: Combination of a fixed-arm carrier with surface entropy reduction. *Protein Sci.* **19**, 901–913 (2010). pmid: 20196072
79. K. L. Witkin, K. Collins, Holoenzyme proteins required for the physiological assembly and activity of telomerase. *Genes Dev.* **18**, 1107–1118 (2004). doi: 10.1101/gad.1201704; pmid: 15131081
80. W. Kabsch, Integration, scaling, space-group assignment and post-refinement. *Acta Crystallogr. D* **66**, 133–144 (2010). doi: 10.1107/S0907444909047374; pmid: 20124693
81. A. J. McCoy *et al.*, *Phaser* crystallographic software. *J. Appl. Cryst.* **40**, 658–674 (2007). doi: 10.1107/S0021889807021206; pmid: 19461840
82. P. V. Afonine *et al.*, Towards automated crystallographic structure refinement with *phenix.refine*. *Acta Crystallogr. D* **68**, 352–367 (2012). doi: 10.1107/S0907444912001308; pmid: 22505256
83. N. K. Kim *et al.*, Solution structure and dynamics of the wild-type pseudoknot of human telomerase RNA. *J. Mol. Biol.* **384**, 1249–1261 (2008). doi: 10.1016/j.jmb.2008.10.005; pmid: 18950640
84. J. Erde, R. R. Loo, J. A. Loo, Enhanced FASP (eFASP) to increase proteome coverage and sample recovery for quantitative proteomic experiments. *J. Proteome Res.* **13**, 1885–1895 (2014). doi: 10.1021/pr4010019; pmid: 24552128

ACKNOWLEDGMENTS

This work was supported in part by grants from the NIH (GM048123) and NSF (MCB1022379) to J.F., NIH grant GM071940 to Z.H.Z., NIH grant GM103479 to J.A.L., NIH grant R01GM054198 to K.C., American Heart Association postdoctoral fellowship 14POST18870059 to J.J., NIH Ruth L. Kirschstein National Research Service Award (NRSA) postdoctoral fellowship GM101874 to E.J.M., NIH Ruth L. Kirschstein NRSA predoctoral training grant fellowship under GM007185 to H.C. and R.O.J., and NSF Graduate Research Fellowship under DGE-1106400 to H.E.U. We acknowledge support for the NMR core, crystallization core, and x-ray core facilities by DOE grant DE-FC0302ER63421 and the Electron Imaging Center for NanoMachines by NIH grants S10RR23057 and S10OD018111 and NSF DBI-133813. The APS of Argonne National Laboratory is supported by NIH grants P41 RR015301 and P41 GM103403. Use of the APS is supported by DOE under contract DE-AC02-06CH11357. Additional support for EM time was provided to J.F. by National Center for Advancing Translational Sciences UCLA Clinical and Translational Science Institute grant UL1TR000124. We thank M. Sawaya and M. Collazo for help with crystallography and M. Capel, K. Rajashankar, N. Sukumar, F. Murphy, and I. Kourinov of NECAT. The 9.4 and 8.9 Å cryo-EM density maps of *Tetrahymena* telomerase holoenzyme have been deposited in the Electron Microscopy Data Bank under accession numbers EMD-6442 and EMD-6443, respectively. Coordinates and structure factors for the x-ray crystal structures of p19 and p45C have been deposited in the PDB with accession codes 5DFM and 5DFN, respectively. Coordinates and restraints for the solution NMR structure of the TER PK and chemical shifts have been deposited in the PDB (accession code 2N6Q) and Biological Magnetic Resonance Bank (accession code 25777), respectively. Nucleotide sequence data are available in the third-party annotation (TPA) section of the DNA Data Bank of Japan, European Molecular Biology Laboratory, and GenBank databases under the accession numbers TPA: BK009378 and BK009379.

SUPPLEMENTARY MATERIALS

www.sciencemag.org/content/350/6260/aab4070/suppl/DC1
Figs. S1 to S10
Tables S1 to S4
References (*85*–*88*)

23 April 2015; accepted 1 September 2015
Published online 15 October 2015
10.1126/science.aab4070

www.sciencemag.org/cgi/content/full/science.aab4070/DC1

Supplementary Materials for

Structure of *Tetrahymena* telomerase reveals previously unknown subunits, functions, and interactions

Jiansen Jiang, Henry Chan, Darian D. Cash, Edward J. Miracco, Rachel R. Ogorzalek Loo, Heather E. Upton, Duilio Cascio, Reid O'Brien Johnson, Kathleen Collins, Joseph A. Loo, Z. Hong Zhou, Juli Feigon*

*Corresponding author. E-mail: feigon@mbi.ucla.edu

Published 15 October 2015 on *Science* Express
DOI: 10.1126/science.aab4070

This PDF file includes:

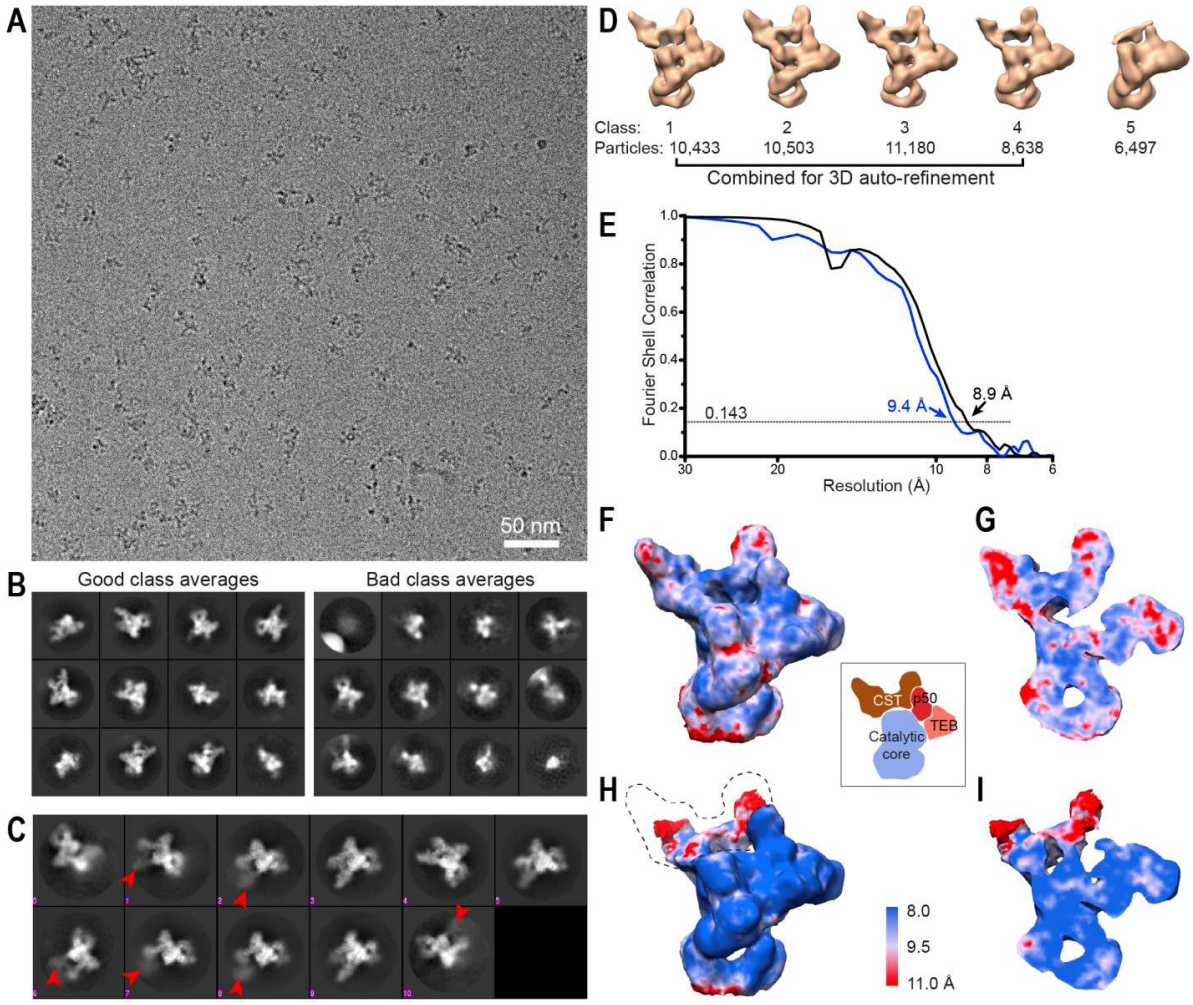

Fig. S1. Cryo-EM of *Tetrahymena* telomerase holoenzyme and resolution estimation. (**A**) A full-size (3710 × 3710 pixels) drift-corrected cryo-EM micrograph of *Tetrahymena* telomerase holoenzyme acquired at -4.9 µm defocus. (**B**) Representative cryo-EM 2D class averages of particles that are assessed as 'good' (left) or 'bad' (right) classes by visual inspection during data processing. (**C**) Cryo-EM 2D class averages of front-view particles. Red arrowheads depict the missing or fuzzy density of the flexible p75-p45-p19 subcomplex. The side length of each image box in (B) and (C) is 35 nm. (**D**) Cryo-EM 3D reconstructions generated by 3D classification. The density for p75-p45-p19 is missing in class 5 due to its flexibility. The particles sorted to the classes (1-4) that show an intact holoenzyme structure were combined together for the 3D auto-refinement. (**E**) 'Gold standard' FSC curves between two independently refined maps from the 3D auto-refinement that were carried out with a spherical mask including all subunits (blue) or with a soft-edge mask excluding p75-p45-p19 subcomplex (black). Each FSC curve was calculated with an auto-mask that was corrected by phase randomization. The resolutions were estimated at the 0.143 criterion. (**F-I**) Surface views (F, H) and cut-through views (G, I) of the unsharpened cryo-EM maps refined with a spherical mask (F, G) and with a soft-edge mask excluding the p75-p45-p19 subcomplex (H, I). The cryo-EM maps are colored by local

resolution estimated by ResMap using two cryo-EM maps independently refined from halves of data. The region corresponding to the masked p75-p45-p19 is depicted by the dashed line in (H). The inset is the schematic of the subcomplex organization shown in the same view as the local resolution maps.

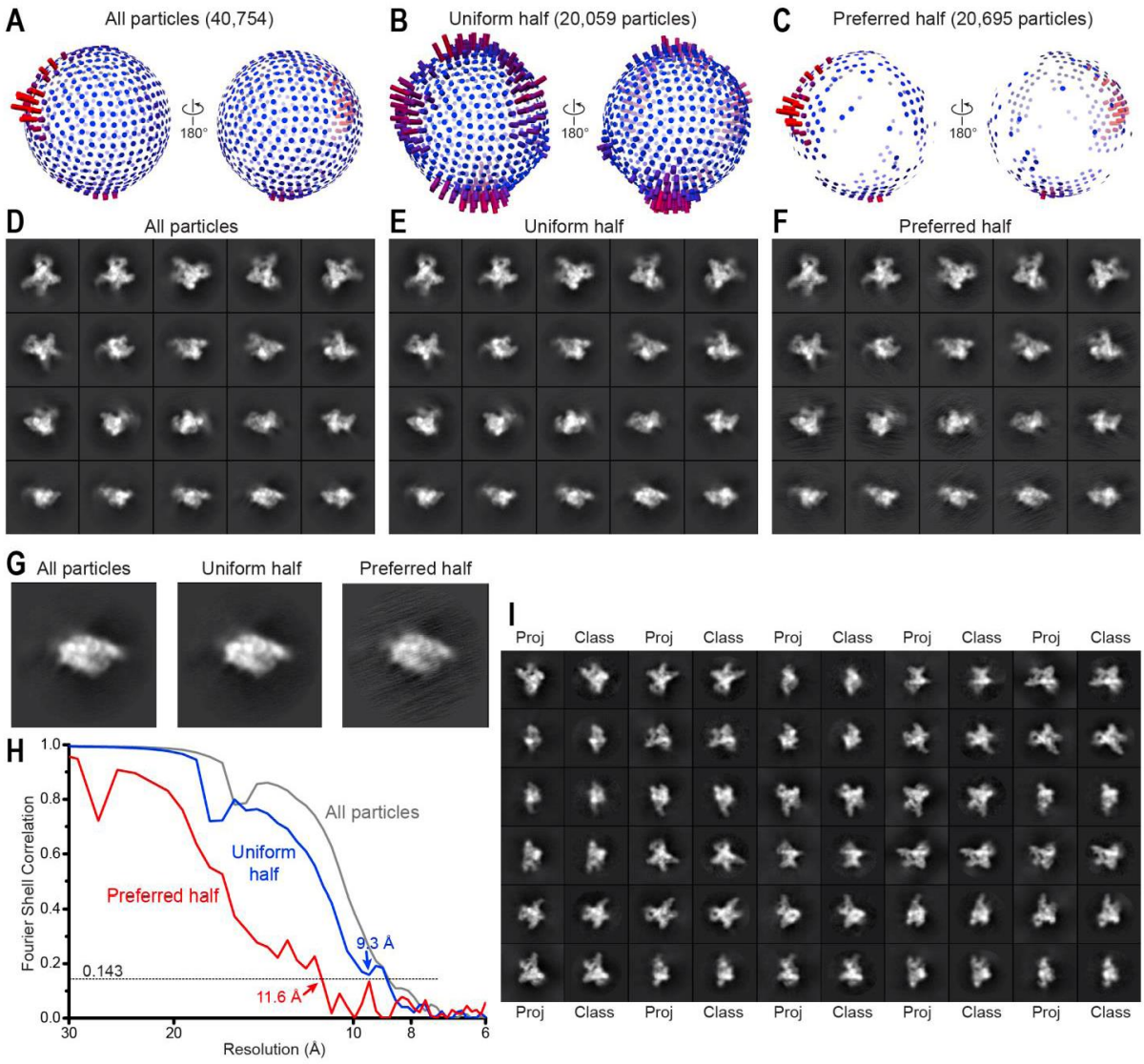

Fig. S2. Assessment of orientation distribution of *Tetrahymena* telomerase holoenzyme particles and its impact on reconstruction resolution. (**A-C**) Euler angle distributions, generated by RELION 3D auto-refinement, of all particles (**A**) used in the 8.9-Å reconstruction, the half of all particles that are more uniformly distributed ('uniform half') (**B**), and the other half that show strongly preferred orientation ('preferred half') (**C**). Note the histograms show relative particle counts at different orientations within each data set and are not comparable across data sets for absolute particle counts. The 3D auto-refinements of three data sets were all carried out with a soft-edge mask excluding p75-p45-p19 subcomplex using the same parameters in RELION. (**D-F**) Projections (30° interval) of the unfiltered 3D reconstructions from all particles, the 'uniform half', and the 'preferred half'. Some projections from the 'preferred half' (F) show striped artifacts resulting from missing information; the projections from all particles (D) and the 'uniform half' (E) are isotropic without the artifacts, indicating that the quality of reconstruction from all particles or the 'uniform half' was not degraded by the problem of preferred orientation existing in the 'preferred half'. (**G**) Close-up view of representative

projections that show striped artifacts from the 'preferred half' but not from all particles or the 'uniform half'. (**H**) 'Gold standard' FSC curves of the refinements using all particles (grey), the 'uniform half' (blue), and the 'preferred half' (red). (**I**) Comparison of representative projections ('Proj') from the 9.4-Å cryo-EM map and the corresponding class averages ('Class'). The side length of each image box in (D-G and I) is 35 nm.

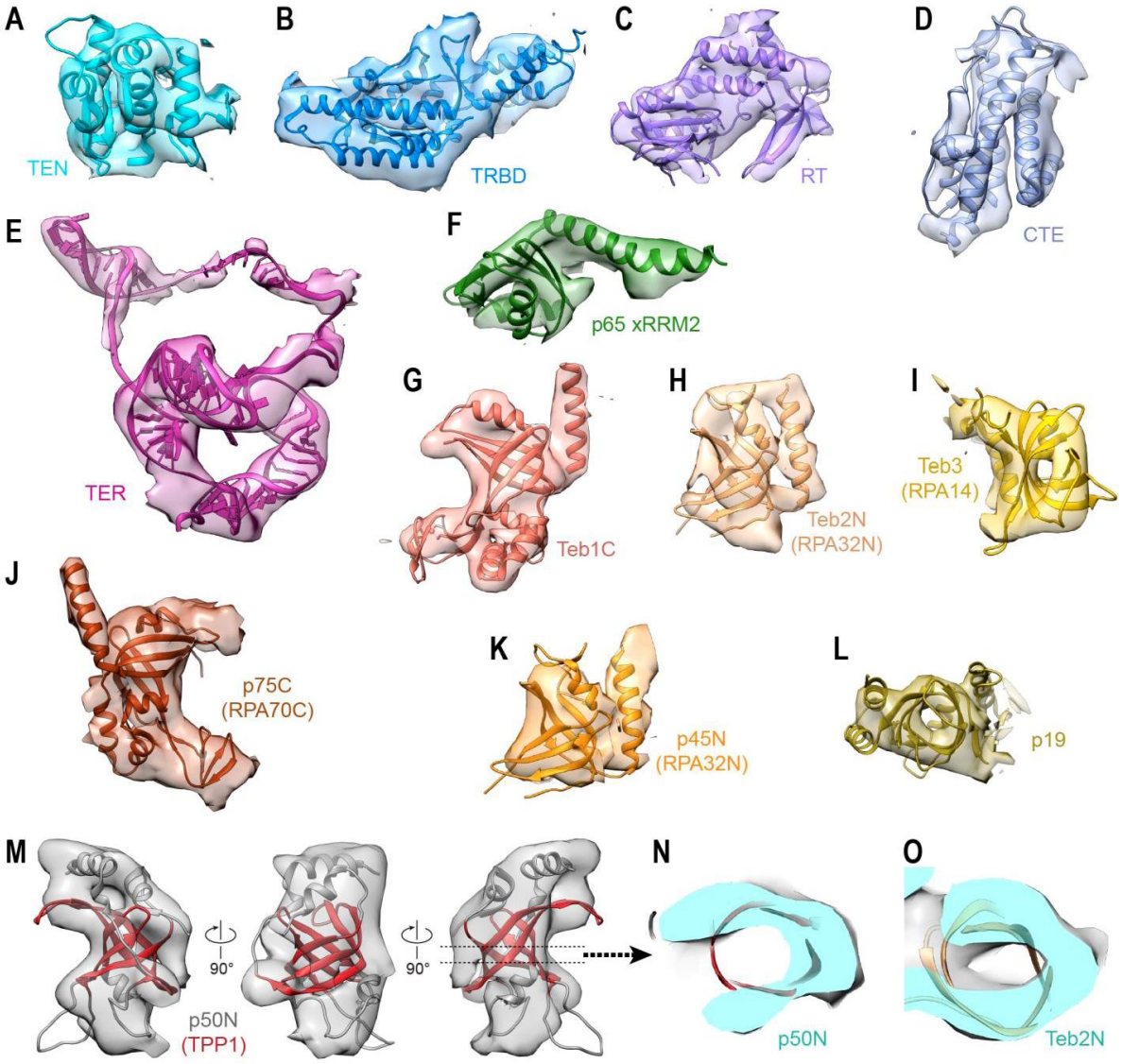

Fig. S3. Fitting of atomic structures or homology models in the cryo-EM maps. (**A-M**) Fitting of TERT (**A**) TEN, (**B**) TRBD, (**C**) homology model of RT and (**D**) homology model of CTE, (**E**) TER, (**F**) p65 xRRM2, (**G**) Teb1C, (**H**) RPA32N for Teb2N, (**I**) RPA14 for Teb3, (**J**) RPA70C for p75C, (**K**) RPA32N for p45N, and (**L**) p19, (**M**) TPP1 for p50N. Three views are shown to illustrate good fit of OB-fold β-barrel (red); loops and helices are in gray. (**N, O**) Horizontal cross section through density of (**N**) p50N and (**O**) Teb2N to show the hole in the density corresponding to the center of the OB-fold β-barrel. The atomic or homology models used in the fitting are summarized in table S1. Atomic or homology models are shown as ribbons and cryo-EM maps are show as transparent surfaces. 8.9-Å and 9.4-Å cryo-EM maps are used in (A-I, M-O) and (J-L), respectively.

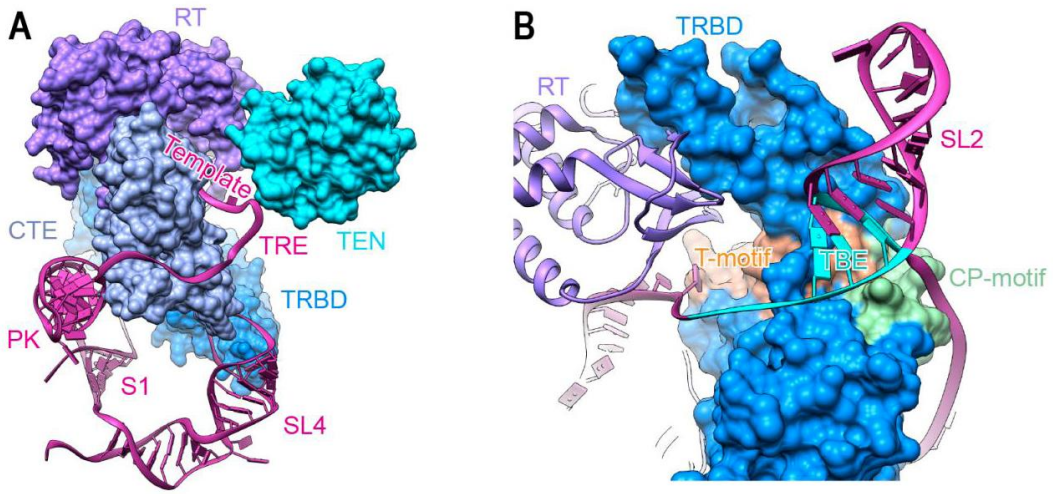

Fig. S4. Model of the TERT-TER complex. (**A**) Front view of TERT-TER complex illustrating the positions of the PK and template on opposite sides of TERT ring, the TEN domain, and the TRE between the TERT ring and TEN domain, with possible contact to TEN. (**B**) Close-up view of the interaction between TER SL2/TBE and TERT TRBD illustrating the location of TBE single-strand nts on either side of TERT ring near CP motif. The T and CP motif of TRBD and TER TBE are colored in brown, green, and cyan, respectively.

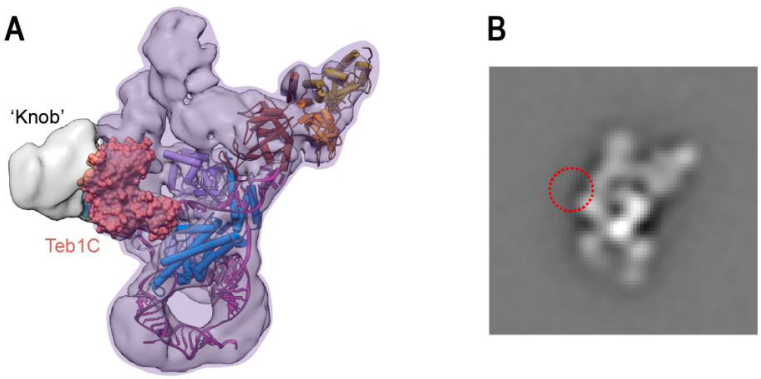

Fig. S5. The cryo-EM density of the newly discovered proteins Teb2 and Teb3. (**A**) "Back view" of the 9.4-Å cryo-EM map fit with known structures (ribbons and space-fill model). The cryo-EM density assigned to previously known subunits is superimposed with a shade of purple. Based on exhaustive fitting of available atomic models and visual inspection, the "knob" density does not correspond to any previously identified subunits. (**B**) Negative-stain EM class average of p50-F telomerase. Sample preparation, data acquisition, and processing have been described previously (*29*). Red dashed circle marks the location of the missing "knob" density. The side length of the image box is 35 nm.

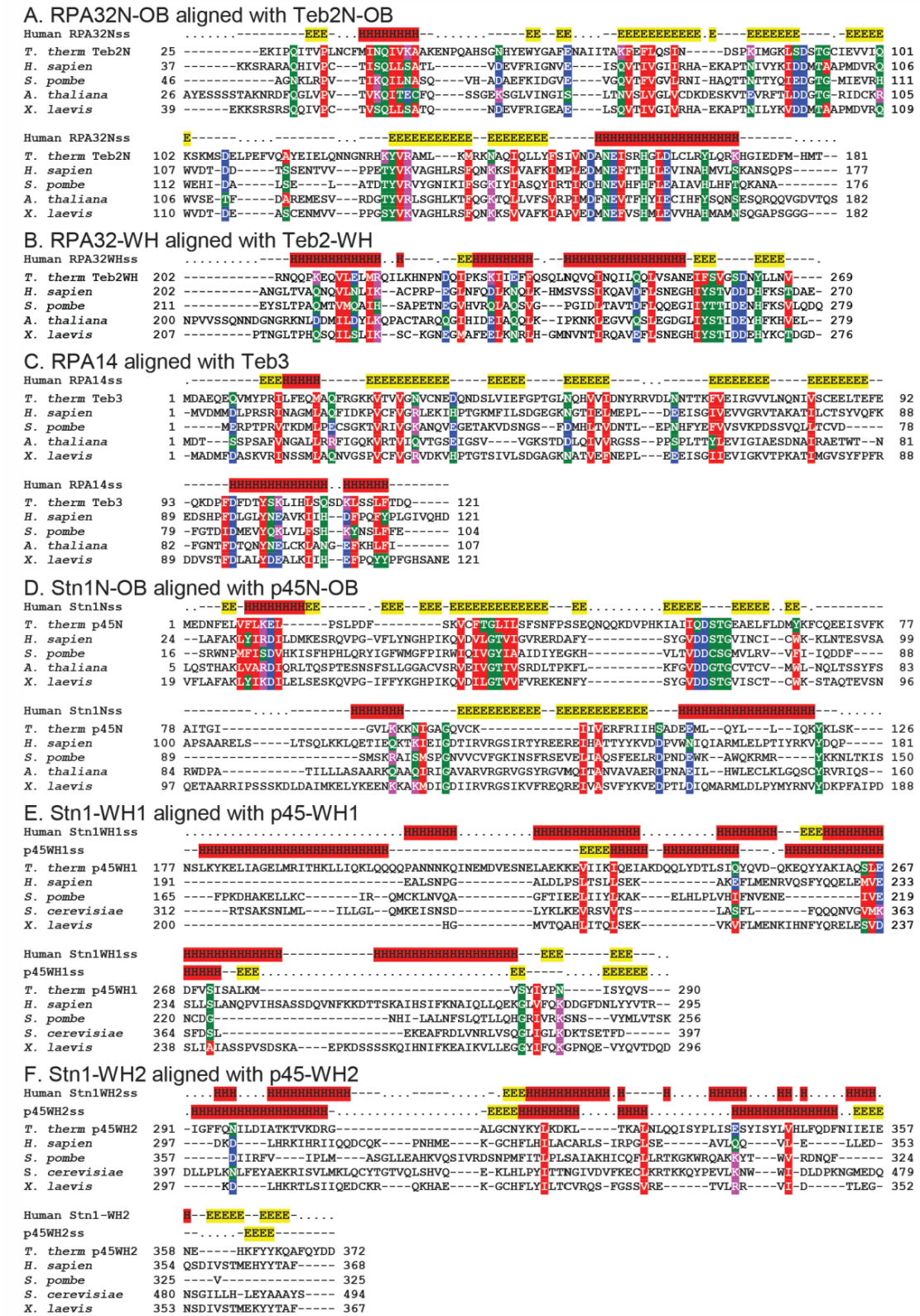
A. RPA32N-OB aligned with Teb2N-OB
B. RPA32-WH aligned with Teb2-WH
C. RPA14 aligned with Teb3
D. Stn1N-OB aligned with p45N-OB
E. Stn1-WH1 aligned with p45-WH1
F. Stn1-WH2 aligned with p45-WH2

Fig. S6. Multiple sequence alignments of TEB2/3, RPA2/3, Stn1, Ten1, p45 and p19. Secondary structures from the previously reported crystal structures of human proteins and crystal structures of *Tetrahymena* proteins reported here (p45C WH1/WH2 and p19) are shown as "." for gaps, "-" for loops, "E" for beta-sheet, and "H" for alpha-helix. Conserved or similar residues are highlighted according to their chemical characteristics: hydrophobic, polar, negatively charged, positively charged. (**A**) RPA32N OB-fold aligned with Teb2N OB-fold. (**B**) RPA32 WH domain aligned with Teb2 WH domain. (**C**) RPA14 aligned with Teb3. (**D**) Stn1N OB-fold aligned with p45N OB-fold. (**E**) Stn1 WH1 domain aligned with p45 WH1 domain. (**F**) Stn1 WH2 domain aligned with p45 WH2 domain. (**G**) Ten1 aligned with p19. Alignments reveal close homology of Teb2/3 with RPA2/3. Consistent with previous observations of low sequence homology of Stn1 and Ten1 across kingdoms, p45 and p19 show lower sequence homology with Stn1 and Ten1 proteins. Multiple sequence alignments were performed using CLUSTAL.

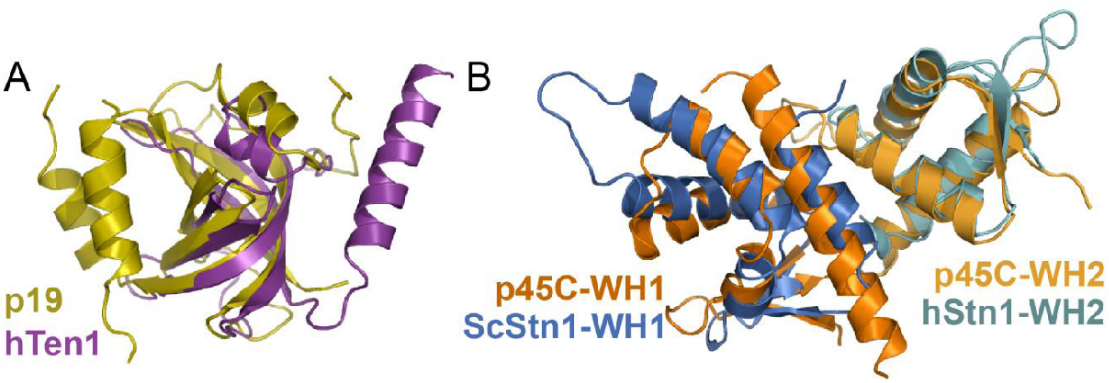

Fig. S7. p19 and p45C are structurally similar to Ten1 and Stn1C. (**A**) Structural alignment of p19 (yellow) with human Ten1 [PDB 4JOI] (purple). RMSD = 2.5Å. (**B**) Structural alignment of p45 WH1 (orange) and WH2 (yellow-orange) domains with *S. cerevisiae* Stn1C-WH1 [PDB 3KEY] (blue) and human Stn1C-WH2 [PDB 4JQF] (teal), respectively. RMSD = 2.8 and 1.9, respectively. Structural alignments were made using the Dali server (http://ekhidna.biocenter.helsinki.fi/dali_server).

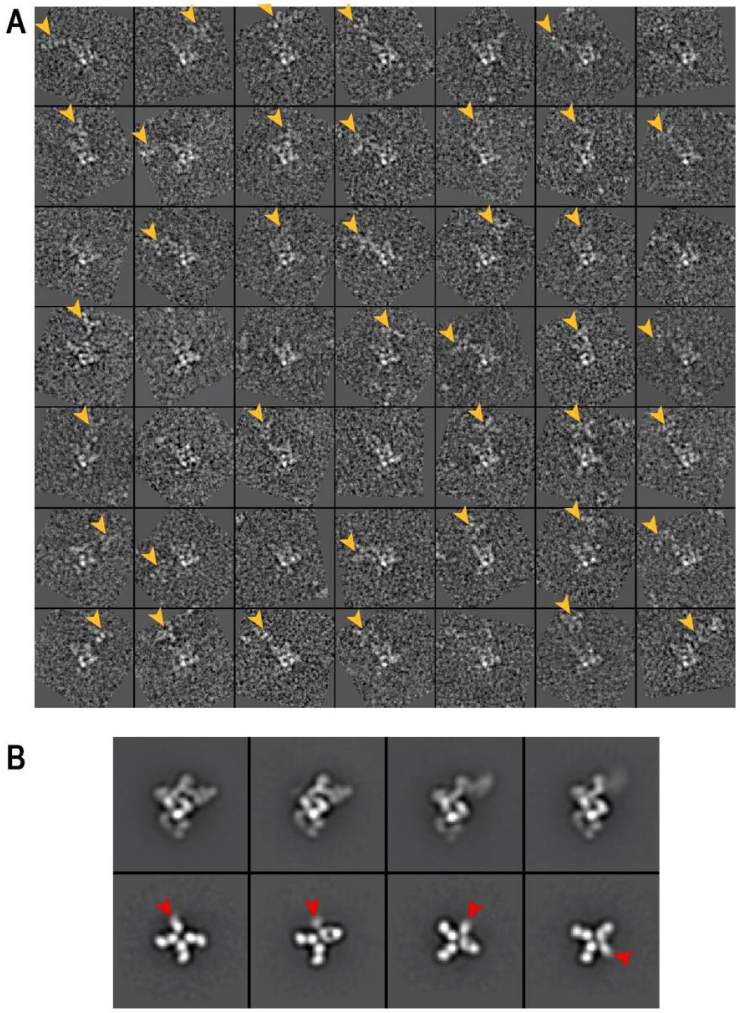

Fig. S8. Fab-labeled p45-F telomerase holoenzyme. (**A**) Randomly selected negative-stain EM particle images of telomerase homoenzyme with the C-terminus of p45-F labeled with anti-FLAG Fab. Distinguishable densities of Fab are marked with yellow arrowheads. Particles are rotated to match the orientation of telomerase holoenzyme among them for the ease of visualization. The Fab density mostly appears in the top-left corner of the image that is near the position of p45N. (**B**) Negative-stain EM class averages of Fab-labeled p45-F telomerase holoenzyme particles. Two families of class averages are observed: telomerase holoenzyme (first row) and 3 Fab attached to the C-terminus of p45 (second row). Red arrowheads mark the density of the C-terminal domain of p45. No class averages show these two structures together due to the flexible positioning between them, attributed to unstructured linker residues. The side length of each image box in (A) and (B) is 56 nm and 42 nm, respectively. Sample preparation, data acquisition, and processing have been described previously (*29*).

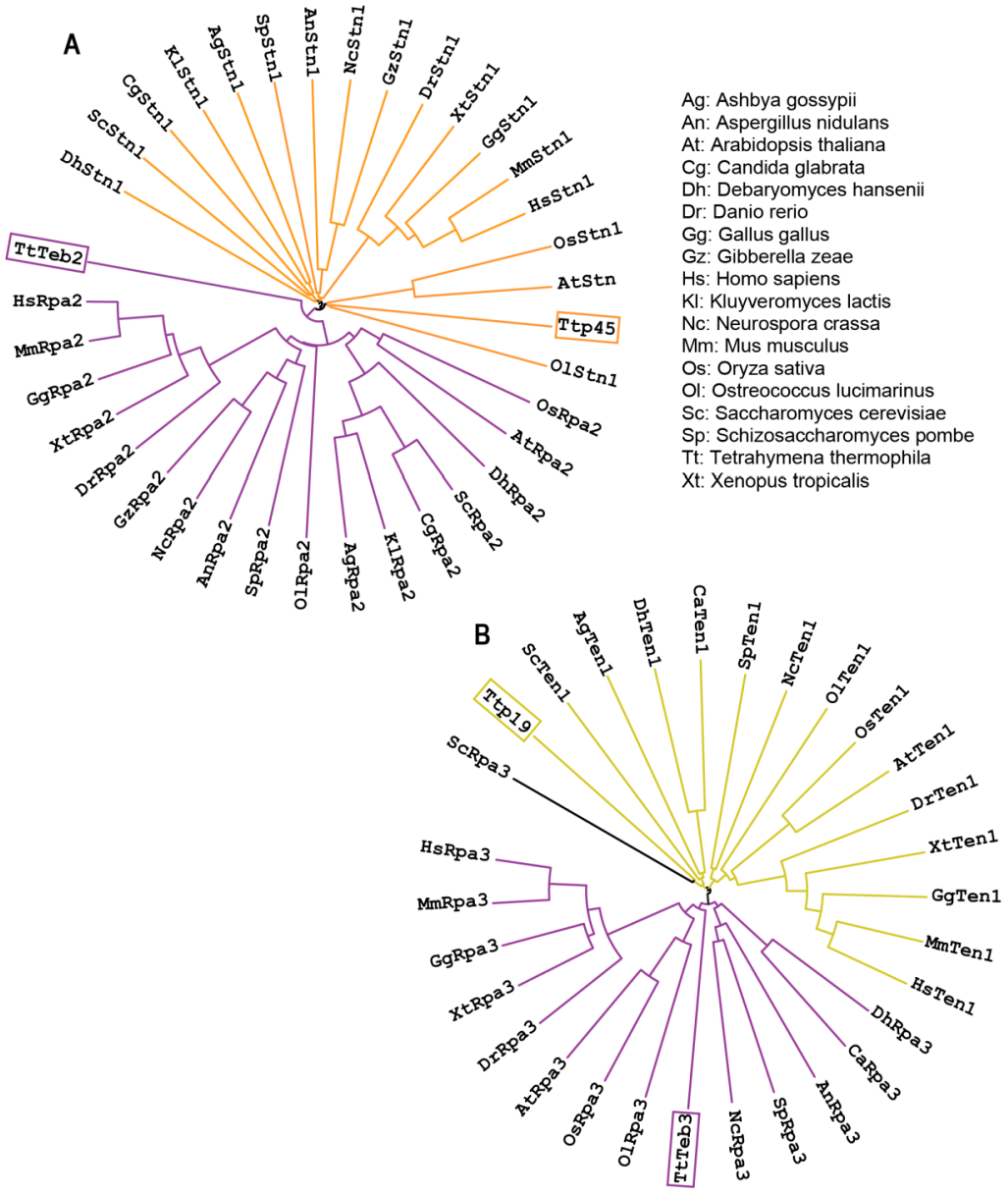

Fig. S9. Phylogenetic cluster analysis of Stn1/Rpa2 and Ten1/Rpa3. (**A**) Stn1 and Rpa2 and (**B**) Ten1 and Rpa3 cluster in distinct monophyletic groups. Shown is a rooted maximum likelihood phylogeny of Stn1 and Rpa2 (A) and Ten1 and Rpa3 (B) inferred using the WAG amino-acid transition model in RAxML [A. Stamatakis: "RAxML Version 8: A tool for Phylogenetic Analysis and Post-Analysis of Large Phylogenies" in *Bioinformatics*, **30**, 1312-1313, 2014] from sequence alignment generated with ClustalW2. Alignments of the two protein families were conducted simultaneously and the cluster analyses show that (A) p45 clusters with Stn1 while Teb2 clusters with Rpa2 and (B) p19 clusters with Ten1 while Teb3 clusters with Rpa3.

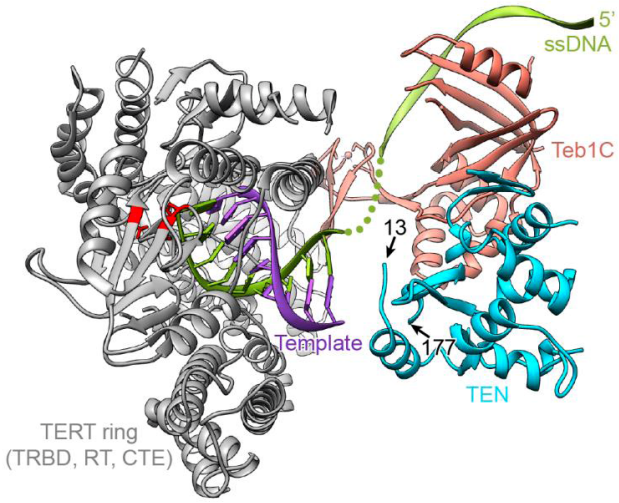

Fig. S10. Model of ssDNA exiting the template. Models of DNA (green) paired with the template (purple) and bound to Teb1C are based on the fitting of the crystal structures of *Tribolium* TERT (PDB ID: 3KYL) and RPA:ssDNA complex (PDB ID: 4GNX), respectively. The green dots indicate the region connecting the ssDNA from the two model structures. The N- and C-termini of the crystal structure of TEN are depicted by its amino acid numbers. TERT ring is in gray, active site catalytic triad residues are shown in red, and TEN is in cyan.

Table S1. X-ray crystal and NMR structures used in the fitting of the cryo-EM maps of *Tetrahymena* telomerase holoenzyme

Subunit	Domain	Structure fitted in the cryo-EM maps	Related PDB ID	Ref
TERT	TEN	*Tetrahymena* TERT TEN	2B2A	(*32*)
	TRBD	*Tetrahymena* TERT TRBD	2R4G	(*37*)
	RT	Homology model derived from *Tribolium* TERT	3DU6	(*31*)
	CTE	Homology model derived from *Tribolium* TERT	3DU6	(*31*)
TER	SL4	Model derived from *Tetrahymena* p65 xRRM2/TER S4 complex and L4	4ERD, 2M21	(*29, 33, 85*)
	SL2	*Tetrahymena* TER SL2	2M22	(*29, 86*)
	PK	*Tetrahymena* TER PK	2N6Q	this work
	Template	Homology model derived from *Tribolium* TERT/RNA-DNA hybrid complex	3KYL	(*38*)
	S1	Ideal A-form RNA helix	--	--
p65	xRRM2	p65 xRRM2/TER S4 complex	4ERD	(*33*)
p65	La+RRM1	hLa complex	2VOP	(*33, 87*)
Teb1	C	*Tetrahymena* Teb1C	3U50	(*50*)
Teb2	N	RPA32N in human RPA trimer	1L1O	(*51*)
Teb3		RPA14 in human RPA trimer	1L1O	(*51*)
p75	C	RPA70C in human RPA trimer	1L1O	(*51*)
p45	N	RPA32N in human RPA trimer	1L1O	(*51*)
p19		*Tetrahymena* p19	5DFM	this work
p50	N	Human TPP1	2I46	(*13*)
Telomere ssDNA		*Tribolium* TERT/RNA-DNA hybrid and fungal RPA/ssDNA complexes	3KYL, 4GNX	(*38, 88*)

Table S2A. Telomerase proteins identified from TERT-FZZ telomerase preparations by LC-MS/MS

			Replicate 1				Replicate 2				Replicate 3			
TTHERM ID	Protein	MW (kDa)	Uni. Pep[a]	Sig. Pep[b]	% Cov[c]	Score[d]	Uni. Pep[a]	Sig. Pep[b]	% Cov[c]	Score[d]	Uni. Pep[a]	Sig. Pep[b]	% Cov[c]	Score[d]
00112560	TERT	134.1	30	22	22	393	84	70	53	2440	37	22	30	370
000318539	p65	64.6	22	17	41	300	49	42	62	1447	36	20	50	358
01049190	p50	50.3	14	8	29	276	27	26	45	2539	11	7	29	147
0059040	p75	74.3	21	10	24	150	42	31	50	955	28	15	40	437
0083360	p45	43.8	17	11	34	201	30	27	59	1475	14	7	33	198
00658760	p19	19.5	7	3	38	88	9	8	50	223	1	1	8	39
00218760	Teb1	82.6	12	7	15	148	18	15	21	1479	5	2	8	251
00113129	Teb2	31.1	9	7	42	414	15	13	49	858	8	5	35	334
00439320	Teb3	14.0	8	7	44	406	9	8	51	507	5	3	40	409

Table S2B. Telomerase proteins identified from ZZF-p50 telomerase preparations by LC-MS/MS

			Replicate 1				Replicate 2			
TTHERM ID	Protein	MW (kDa)	Uni. Pep[a]	Sig. Pep[b]	% Cov[c]	Score[d]	Uni. Pep[a]	Sig. Pep[b]	% Cov[c]	Score[d]
00112560	TERT	134.1	15	3	12	40	40	33	31	616
000318539	p65	64.6	7	3	12	74	36	29	47	828
01049190	p50	50.3	16	8	38	118	30	24	60	1218
0059040	p75	74.3	24	15	33	256	25	19	37	334
0083360	p45	43.8	12	6	27	128	20	15	50	746
00658760	p19	19.5	7	4	33	79	9	7	44	241
00218760	Teb1	82.6	0	0	-	-	0	0	-	-
00113129	Teb2	31.1	0	0	-	-	1	1	-	-
00439320	Teb3	14.0	0	0	-	-	0	0	-	-

[a]Number of unique peptide sequences identified at ≤ 10 ppm mass accuracy
[b]Number of unique peptide sequences identified with E-value < 0.05 (>95% confidence that the match was not random)
[c]Percentage of theoretical sequence covered by identified peptides
[d]Mascot score employing all peptides with E-value < 0.05

Table S3. X-Ray Data Collection and Refinement Statistics

	MBP-p19	P45C
Data Collection		
Space group	$P2_13$	F222
Unit cell dimensions		
a, b, c (Å)	150.60, 150.60, 150.60	88.03, 124.62, 173.77
α, β, γ (˚)	90.00, 90.00, 90.00	90.00, 90.00, 90.00
Reflections observed	993,498	101,012
Unique reflections	50,601	18,884
Multiplicity	19.6	5.3
Wavelength (Å)	0.9795	0.9791
Resolution (Å)	2.30	2.38
Highest Resolution Shell (Å)	2.30 – 2.36	2.38 – 2.45
R_{sym} (%)[a]	11.9 (103.3)	6.4 (72.8)
$R_{p.i.m}$ (%)[b]	3.9 (30.4)	3.3 (30.7)
CC(1/2)	99.9 (90.0)	99.9 (86.7)
I/σ	19.4 (3.4)	14.1 (2.5)
Completeness (%)	99.9 (98.7)	97.8 (78.6)
Wilson B value (Å^2)	40.16	53.10
Refinement		
Resolution (Å)	86.89 – 2.30	86.89 – 2.38
Resolution (Å) (last shell)	2.30 – 2.33	2.38 – 2.45
Reflections used	50,569	18,334
R_{work}(%) / R_{free}(%)[c]	17.5 / 22.6; (22.7 / 31.4)	20.7 / 26.4; (32.9 / 41.5)
Protein molecules in Asymmetric Unit	2	2
Number of non-H atoms		
Protein	7784	2730
Non-protein	207	6
RMS Deviations		
Bond lengths (Å)	0.008	0.008
Bond angles (˚)	1.14	1.01
Average B-factor (Å^2)		
Protein atoms	45.2	62.8
Non-protein atoms	56.8	50.4
Ramachandran plot regions[c]		
Favored	97.2	98.19
Allowed	2.8	1.81
Outliers	0.00	0.00

Highest resolution shell shown in parenthesis

[a] $R_{sym} = 100 \times \Sigma(I\text{-}I(mean))^2 / \Sigma(I)^2$

[b] $R_{p.i.m.} = 100 \times \Sigma\sqrt{(1/(N-1))}\Sigma\ (I\text{-}I(mean)) / \Sigma(I)^2$

where I is the observed intensity of the reflection HKL and the sum is taken over all reflections HKL and N is the redundancy

[c] $R_{factor} = 100 \times \Sigma||F_{obs}| - |F_{calc}|| / \Sigma|F_{obs}|$

F_{calc} and F_{obs} are the calculated and observed structure factor amplitudes, respectively. R_{work} refers to the R_{factor} for the data utilized in the refinement and R_{free} refers to the R_{factor} for 5% of the reflections randomly chosen that were excluded from the refinement

[c] Percentage of residues in Ramachandran plot regions were determined using Molprobity (Chen et.al 2010).

Table S4. NMR restraints and structure statistics for *Tetrahymena* TER pseudoknot

Parameter	Value
NMR distance and dihedral restraints	
Distance restraints	
Total NOEs	414
Intraresidue NOEs	103
Interresidue NOEs	311
Sequential (|i-j|) = 1	176
Long range (|i-j|) > 1	135
Hydrogen bond restraints*	82
Total dihedral angle restraints	171
Sugar pucker	140
χ	31
RDCs	79
Structure statistics	
Violations (mean ± SD)	
Distance constraints (Å)	0.054 ± .001
Dihedral angle constraints (°)	0.020 ± .002
Maximum dihedral angle violation (°)	2.03
Maximum distance violation (°)	0.29
Deviations from idealized geometry	
Bond lengths (Å)	0.0057 ± .0001
Bond angles (°)	0.95 ± .02
Impropers (°)	0.61 ± .04
Average pairwise rmsd (Å) **	
Heavy	0.83 ± 0.23
Backbone	0.84 ± 0.24

* Two hydrogen bond restraints were used for each hydrogen bond.

** Pairwise RMSD was calculated for the lowest 10 energy structures.

References and Notes

1. E. H. Blackburn, C. W. Greider, J. W. Szostak, Telomeres and telomerase: The path from maize, *Tetrahymena* and yeast to human cancer and aging. *Nat. Med.* **12**, 1133–1138 (2006). Medline doi:10.1038/nm1006-1133

2. E. H. Blackburn, K. Collins, Telomerase: An RNP enzyme synthesizes DNA. *Cold Spring Harbor Perspect. Biol.* **3**, a003558 (2011). Medline doi:10.1101/cshperspect.a003558

3. M. Armanios, E. H. Blackburn, The telomere syndromes. *Nat. Rev. Genet.* **13**, 693–704 (2012). Medline doi:10.1038/nrg3246

4. B. Bernardes de Jesus, M. A. Blasco, Telomerase at the intersection of cancer and aging. *Trends Genet.* **29**, 513–520 (2013). Medline doi:10.1016/j.tig.2013.06.007

5. S. E. Artandi, R. A. DePinho, Telomeres and telomerase in cancer. *Carcinogenesis* **31**, 9–18 (2010). Medline doi:10.1093/carcin/bgp268

6. J. Nandakumar, T. R. Cech, Finding the end: Recruitment of telomerase to telomeres. *Nat. Rev. Mol. Cell Biol.* **14**, 69–82 (2013). Medline doi:10.1038/nrm3505

7. J. A. Stewart, M. F. Chaiken, F. Wang, C. M. Price, Maintaining the end: Roles of telomere proteins in end-protection, telomere replication and length regulation. *Mutat. Res.* **730**, 12–19 (2012). Medline doi:10.1016/j.mrfmmm.2011.08.011

8. L. Y. Chen, J. Lingner, CST for the grand finale of telomere replication. *Nucleus* **4**, 277–282 (2013). Medline doi:10.4161/nucl.25701

9. F. L. Zhong, L. F. Batista, A. Freund, M. F. Pech, A. S. Venteicher, S. E. Artandi, TPP1 OB-fold domain controls telomere maintenance by recruiting telomerase to chromosome ends. *Cell* **150**, 481–494 (2012). Medline doi:10.1016/j.cell.2012.07.012

10. A. N. Sexton, D. T. Youmans, K. Collins, Specificity requirements for human telomere protein interaction with telomerase holoenzyme. *J. Biol. Chem.* **287**, 34455–34464 (2012). Medline doi:10.1074/jbc.M112.394767

11. J. Nandakumar, C. F. Bell, I. Weidenfeld, A. J. Zaug, L. A. Leinwand, T. R. Cech, The TEL patch of telomere protein TPP1 mediates telomerase recruitment and processivity. *Nature* **492**, 285–289 (2012). Medline doi:10.1038/nature11648

12. H. Xin, D. Liu, M. Wan, A. Safari, H. Kim, W. Sun, M. S. O'Connor, Z. Songyang, TPP1 is a homologue of ciliate TEBP-β and interacts with POT1 to recruit telomerase. *Nature* **445**, 559–562 (2007). Medline doi:10.1038/nature05469

13. F. Wang, E. R. Podell, A. J. Zaug, Y. Yang, P. Baciu, T. R. Cech, M. Lei, The POT1-TPP1 telomere complex is a telomerase processivity factor. *Nature* **445**, 506–510 (2007). Medline doi:10.1038/nature05454

14. T. Rao, J. W. Lubin, G. S. Armstrong, T. M. Tucey, V. Lundblad, D. S. Wuttke, Structure of Est3 reveals a bimodal surface with differential roles in telomere replication. *Proc. Natl. Acad. Sci. U.S.A.* **111**, 214–218 (2014). Medline doi:10.1073/pnas.1316453111

15. J. M. Talley, D. C. DeZwaan, L. D. Maness, B. C. Freeman, K. L. Friedman, Stimulation of yeast telomerase activity by the ever shorter telomere 3 (Est3) subunit is dependent on

direct interaction with the catalytic protein Est2. *J. Biol. Chem.* **286**, 26431–26439 (2011). Medline doi:10.1074/jbc.M111.228635

16. A. Prakash, G. E. Borgstahl, The structure and function of replication protein A in DNA replication. *Subcell. Biochem.* **62**, 171–196 (2012). Medline doi:10.1007/978-94-007-4572-8_10

17. K. A. Lewis, D. S. Wuttke, Telomerase and telomere-associated proteins: Structural insights into mechanism and evolution. *Structure* **20**, 28–39 (2012). Medline doi:10.1016/j.str.2011.10.017

18. L. Y. Chen, S. Redon, J. Lingner, The human CST complex is a terminator of telomerase activity. *Nature* **488**, 540–544 (2012). Medline doi:10.1038/nature11269

19. C. M. Price, K. A. Boltz, M. F. Chaiken, J. A. Stewart, M. A. Beilstein, D. E. Shippen, Evolution of CST function in telomere maintenance. *Cell Cycle* **9**, 3157–3165 (2010). Medline doi:10.4161/cc.9.16.12547

20. P. Wu, H. Takai, T. de Lange, Telomeric 3′ overhangs derive from resection by Exo1 and Apollo and fill-in by POT1b-associated CST. *Cell* **150**, 39–52 (2012). Medline doi:10.1016/j.cell.2012.05.026

21. F. Wang, J. A. Stewart, C. Kasbek, Y. Zhao, W. E. Wright, C. M. Price, Human CST has independent functions during telomere duplex replication and C-strand fill-in. *Cell Reports* **2**, 1096–1103 (2012). Medline doi:10.1016/j.celrep.2012.10.007

22. N. F. Lue, E. Y. Yu, M. Lei, A popular engagement at the ends. *Nat. Struct. Mol. Biol.* **20**, 10–12 (2013). Medline doi:10.1038/nsmb.2483

23. T. M. Tucey, V. Lundblad, Regulated assembly and disassembly of the yeast telomerase quaternary complex. *Genes Dev.* **28**, 2077–2089 (2014). Medline doi:10.1101/gad.246256.114

24. R. J. Wellinger, V. A. Zakian, Everything you ever wanted to know about *Saccharomyces cerevisiae* telomeres: Beginning to end. *Genetics* **191**, 1073–1105 (2012). Medline doi:10.1534/genetics.111.137851

25. E. D. Egan, K. Collins, Biogenesis of telomerase ribonucleoproteins. *RNA* **18**, 1747–1759 (2012). Medline doi:10.1261/rna.034629.112

26. J. D. Podlevsky, J. J. Chen, It all comes together at the ends: Telomerase structure, function, and biogenesis. *Mutat. Res.* **730**, 3–11 (2012). Medline doi:10.1016/j.mrfmmm.2011.11.002

27. H. E. Upton, K. Hong, K. Collins, Direct single-stranded DNA binding by Teb1 mediates the recruitment of *Tetrahymena thermophila* telomerase to telomeres. *Mol. Cell. Biol.* **34**, 4200–4212 (2014). Medline doi:10.1128/MCB.01030-14

28. B. Min, K. Collins, An RPA-related sequence-specific DNA-binding subunit of telomerase holoenzyme is required for elongation processivity and telomere maintenance. *Mol. Cell* **36**, 609–619 (2009). Medline doi:10.1016/j.molcel.2009.09.041

29. J. Jiang, E. J. Miracco, K. Hong, B. Eckert, H. Chan, D. D. Cash, B. Min, Z. H. Zhou, K. Collins, J. Feigon, The architecture of *Tetrahymena* telomerase holoenzyme. *Nature* **496**, 187–192 (2013). Medline doi:10.1038/nature12062

30. C. A. Theimer, J. Feigon, Structure and function of telomerase RNA. *Curr. Opin. Struct. Biol.* **16**, 307–318 (2006). Medline doi:10.1016/j.sbi.2006.05.005

31. A. J. Gillis, A. P. Schuller, E. Skordalakes, Structure of the *Tribolium castaneum* telomerase catalytic subunit TERT. *Nature* **455**, 633–637 (2008). Medline doi:10.1038/nature07283

32. S. A. Jacobs, E. R. Podell, T. R. Cech, Crystal structure of the essential N-terminal domain of telomerase reverse transcriptase. *Nat. Struct. Mol. Biol.* **13**, 218–225 (2006). Medline doi:10.1038/nsmb1054

33. M. Singh, Z. Wang, B. K. Koo, A. Patel, D. Cascio, K. Collins, J. Feigon, Structural basis for telomerase RNA recognition and RNP assembly by the holoenzyme La family protein p65. *Mol. Cell* **47**, 16–26 (2012). Medline doi:10.1016/j.molcel.2012.05.018

34. M. D. Stone, M. Mihalusova, C. M. O'connor, R. Prathapam, K. Collins, X. Zhuang, Stepwise protein-mediated RNA folding directs assembly of telomerase ribonucleoprotein. *Nature* **446**, 458–461 (2007). Medline doi:10.1038/nature05600

35. N. K. Jacob, R. Lescasse, B. R. Linger, C. M. Price, *Tetrahymena* POT1a regulates telomere length and prevents activation of a cell cycle checkpoint. *Mol. Cell. Biol.* **27**, 1592–1601 (2007). Medline doi:10.1128/MCB.01975-06

36. K. Hong, H. Upton, E. J. Miracco, J. Jiang, Z. H. Zhou, J. Feigon, K. Collins, *Tetrahymena* telomerase holoenzyme assembly, activation, and inhibition by domains of the p50 central hub. *Mol. Cell. Biol.* **33**, 3962–3971 (2013). Medline doi:10.1128/MCB.00792-13

37. S. Rouda, E. Skordalakes, Structure of the RNA-binding domain of telomerase: Implications for RNA recognition and binding. *Structure* **15**, 1403–1412 (2007). Medline doi:10.1016/j.str.2007.09.007

38. M. Mitchell, A. Gillis, M. Futahashi, H. Fujiwara, E. Skordalakes, Structural basis for telomerase catalytic subunit TERT binding to RNA template and telomeric DNA. *Nat. Struct. Mol. Biol.* **17**, 513–518 (2010). Medline doi:10.1038/nsmb.1777

39. N. F. Lue, Y. C. Lin, I. S. Mian, A conserved telomerase motif within the catalytic domain of telomerase reverse transcriptase is specifically required for repeat addition processivity. *Mol. Cell. Biol.* **23**, 8440–8449 (2003). Medline doi:10.1128/MCB.23.23.8440-8449.2003

40. M. Xie, J. D. Podlevsky, X. Qi, C. J. Bley, J. J. Chen, A novel motif in telomerase reverse transcriptase regulates telomere repeat addition rate and processivity. *Nucleic Acids Res.* **38**, 1982–1996 (2010). Medline doi:10.1093/nar/gkp1198

41. R. A. Wu, K. Collins, Human telomerase specialization for repeat synthesis by unique handling of primer-template duplex. *EMBO J.* **33**, 921–935 (2014). Medline doi:10.1002/embj.201387205

42. B. Eckert, K. Collins, Roles of telomerase reverse transcriptase N-terminal domain in assembly and activity of *Tetrahymena* telomerase holoenzyme. *J. Biol. Chem.* **287**, 12805–12814 (2012). Medline doi:10.1074/jbc.M112.339853

43. F. Qiao, T. R. Cech, Triple-helix structure in telomerase RNA contributes to catalysis. *Nat. Struct. Mol. Biol.* **15**, 634–640 (2008). Medline doi:10.1038/nsmb.1420

44. D. D. Cash, O. Cohen-Zontag, N. K. Kim, K. Shefer, Y. Brown, N. B. Ulyanov, Y. Tzfati, J. Feigon, Pyrimidine motif triple helix in the *Kluyveromyces lactis* telomerase RNA pseudoknot is essential for function in vivo. *Proc. Natl. Acad. Sci. U.S.A.* **110**, 10970–10975 (2013). Medline doi:10.1073/pnas.1309590110

45. C. A. Theimer, C. A. Blois, J. Feigon, Structure of the human telomerase RNA pseudoknot reveals conserved tertiary interactions essential for function. *Mol. Cell* **17**, 671–682 (2005). Medline doi:10.1016/j.molcel.2005.01.017

46. M. Mihalusova, J. Y. Wu, X. Zhuang, Functional importance of telomerase pseudoknot revealed by single-molecule analysis. *Proc. Natl. Acad. Sci. U.S.A.* **108**, 20339–20344 (2011). Medline doi:10.1073/pnas.1017686108

47. C. M. O'Connor, K. Collins, A novel RNA binding domain in *Tetrahymena* telomerase p65 initiates hierarchical assembly of telomerase holoenzyme. *Mol. Cell. Biol.* **26**, 2029–2036 (2006). Medline doi:10.1128/MCB.26.6.2029-2036.2006

48. A. J. Berman, A. R. Gooding, T. R. Cech, *Tetrahymena* telomerase protein p65 induces conformational changes throughout telomerase RNA (TER) and rescues telomerase reverse transcriptase and TER assembly mutants. *Mol. Cell. Biol.* **30**, 4965–4976 (2010). Medline doi:10.1128/MCB.00827-10

49. X. Qi, M. Xie, A. F. Brown, C. J. Bley, J. D. Podlevsky, J. J. Chen, RNA/DNA hybrid binding affinity determines telomerase template-translocation efficiency. *EMBO J.* **31**, 150–161 (2012). Medline doi:10.1038/emboj.2011.363

50. Z. Zeng, B. Min, J. Huang, K. Hong, Y. Yang, K. Collins, M. Lei, Structural basis for *Tetrahymena* telomerase processivity factor Teb1 binding to single-stranded telomeric-repeat DNA. *Proc. Natl. Acad. Sci. U.S.A.* **108**, 20357–20361 (2011). Medline doi:10.1073/pnas.1113624108

51. E. Bochkareva, S. Korolev, S. P. Lees-Miller, A. Bochkarev, Structure of the RPA trimerization core and its role in the multistep DNA-binding mechanism of RPA. *EMBO J.* **21**, 1855–1863 (2002). Medline doi:10.1093/emboj/21.7.1855

52. S. F. Altschul, T. L. Madden, A. A. Schäffer, J. Zhang, Z. Zhang, W. Miller, D. J. Lipman, Gapped BLAST and PSI-BLAST: A new generation of protein database search programs. *Nucleic Acids Res.* **25**, 3389–3402 (1997). Medline doi:10.1093/nar/25.17.3389

53. C. Cole, J. D. Barber, G. J. Barton, The Jpred 3 secondary structure prediction server. *Nucleic Acids Res.* **36** (suppl. 2), W197–W201 (2008). Medline doi:10.1093/nar/gkn238

54. B. Min, K. Collins, Multiple mechanisms for elongation processivity within the reconstituted *Tetrahymena* telomerase holoenzyme. *J. Biol. Chem.* **285**, 16434–16443 (2010). Medline doi:10.1074/jbc.M110.119172

55. J. Xiong, X. Lu, Z. Zhou, Y. Chang, D. Yuan, M. Tian, Z. Zhou, L. Wang, C. Fu, E. Orias, W. Miao, Transcriptome analysis of the model protozoan, *Tetrahymena thermophila*, using deep RNA sequencing. *PLOS ONE* **7**, e30630 (2012). Medline doi:10.1371/journal.pone.0030630

56. A. N. Sexton, S. G. Regalado, C. S. Lai, G. J. Cost, C. M. O'Neil, F. D. Urnov, P. D. Gregory, R. Jaenisch, K. Collins, D. Hockemeyer, Genetic and molecular identification of three human TPP1 functions in telomerase action: Recruitment, activation, and homeostasis set point regulation. *Genes Dev.* **28**, 1885–1899 (2014). Medline

57. J. C. Schmidt, A. B. Dalby, T. R. Cech, Identification of human TERT elements necessary for telomerase recruitment to telomeres. *eLife* **3**, e03563 (2014). doi:10.7554/eLife.03563

58. J. Sun, E. Y. Yu, Y. Yang, L. A. Confer, S. H. Sun, K. Wan, N. F. Lue, M. Lei, Stn1-Ten1 is an Rpa2-Rpa3-like complex at telomeres. *Genes Dev.* **23**, 2900–2914 (2009). Medline doi:10.1101/gad.1851909

59. C. Bryan, C. Rice, M. Harkisheimer, D. C. Schultz, E. Skordalakes, Structure of the human telomeric Stn1-Ten1 capping complex. *PLOS ONE* **8**, e66756 (2013). Medline doi:10.1371/journal.pone.0066756

60. B. Vester, J. Wengel, LNA (locked nucleic acid): High-affinity targeting of complementary RNA and DNA. *Biochemistry* **43**, 13233–13241 (2004). Medline doi:10.1021/bi0485732

61. J. Huang, A. F. Brown, J. Wu, J. Xue, C. J. Bley, D. P. Rand, L. Wu, R. Zhang, J. J. Chen, M. Lei, Structural basis for protein-RNA recognition in telomerase. *Nat. Struct. Mol. Biol.* **21**, 507–512 (2014). Medline doi:10.1038/nsmb.2819

62. J. L. Chen, K. K. Opperman, C. W. Greider, A critical stem-loop structure in the CR4-CR5 domain of mammalian telomerase RNA. *Nucleic Acids Res.* **30**, 592–597 (2002). Medline doi:10.1093/nar/30.2.592

63. C. J. Bley, X. Qi, D. P. Rand, C. R. Borges, R. W. Nelson, J. J. Chen, RNA-protein binding interface in the telomerase ribonucleoprotein. *Proc. Natl. Acad. Sci. U.S.A.* **108**, 20333–20338 (2011). Medline doi:10.1073/pnas.1100270108

64. A. J. Zaug, E. R. Podell, T. R. Cech, Mutation in TERT separates processivity from anchor-site function. *Nat. Struct. Mol. Biol.* **15**, 870–872 (2008). Medline doi:10.1038/nsmb.1462

65. B. R. Linger, G. B. Morin, C. M. Price, The Pot1a-associated proteins Tpt1 and Pat1 coordinate telomere protection and length regulation in *Tetrahymena*. *Mol. Biol. Cell* **22**, 4161–4170 (2011). Medline doi:10.1091/mbc.E11-06-0551

66. C. Suloway, J. Pulokas, D. Fellmann, A. Cheng, F. Guerra, J. Quispe, S. Stagg, C. S. Potter, B. Carragher, Automated molecular microscopy: The new Leginon system. *J. Struct. Biol.* **151**, 41–60 (2005). Medline doi:10.1016/j.jsb.2005.03.010

67. X. Li, P. Mooney, S. Zheng, C. R. Booth, M. B. Braunfeld, S. Gubbens, D. A. Agard, Y. Cheng, Electron counting and beam-induced motion correction enable near-atomic-resolution single-particle cryo-EM. *Nat. Methods* **10**, 584–590 (2013). Medline doi:10.1038/nmeth.2472

68. J. A. Mindell, N. Grigorieff, Accurate determination of local defocus and specimen tilt in electron microscopy. *J. Struct. Biol.* **142**, 334–347 (2003). Medline doi:10.1016/S1047-8477(03)00069-8

69. J. B. Heymann, D. M. Belnap, Bsoft: Image processing and molecular modeling for electron microscopy. *J. Struct. Biol.* **157**, 3–18 (2007). Medline doi:10.1016/j.jsb.2006.06.006

70. N. R. Voss, C. K. Yoshioka, M. Radermacher, C. S. Potter, B. Carragher, DoG Picker and TiltPicker: Software tools to facilitate particle selection in single particle electron microscopy. *J. Struct. Biol.* **166**, 205–213 (2009). Medline doi:10.1016/j.jsb.2009.01.004

71. S. J. Ludtke, P. R. Baldwin, W. Chiu, EMAN: Semiautomated software for high-resolution single-particle reconstructions. *J. Struct. Biol.* **128**, 82–97 (1999). Medline doi:10.1006/jsbi.1999.4174

72. S. H. Scheres, RELION: Implementation of a Bayesian approach to cryo-EM structure determination. *J. Struct. Biol.* **180**, 519–530 (2012). Medline doi:10.1016/j.jsb.2012.09.006

73. E. F. Pettersen, T. D. Goddard, C. C. Huang, G. S. Couch, D. M. Greenblatt, E. C. Meng, T. E. Ferrin, UCSF Chimera—A visualization system for exploratory research and analysis. *J. Comput. Chem.* **25**, 1605–1612 (2004). Medline doi:10.1002/jcc.20084

74. A. Kucukelbir, F. J. Sigworth, H. D. Tagare, Quantifying the local resolution of cryo-EM density maps. *Nat. Methods* **11**, 63–65 (2014). Medline doi:10.1038/nmeth.2727

75. P. Emsley, K. Cowtan, *Coot*: Model-building tools for molecular graphics. *Acta Crystallogr. D* **60**, 2126–2132 (2004). Medline doi:10.1107/S0907444904019158

76. P. Chacón, W. Wriggers, Multi-resolution contour-based fitting of macromolecular structures. *J. Mol. Biol.* **317**, 375–384 (2002). Medline doi:10.1006/jmbi.2002.5438

77. The PyMOL Molecular Graphics System, Version 1.7.4, Schrödinger, LLC.

78. A. F. Moon, G. A. Mueller, X. Zhong, L. C. Pedersen, A synergistic approach to protein crystallization: Combination of a fixed-arm carrier with surface entropy reduction. *Protein Sci.* **19**, 901–913 (2010). Medline

79. K. L. Witkin, K. Collins, Holoenzyme proteins required for the physiological assembly and activity of telomerase. *Genes Dev.* **18**, 1107–1118 (2004). Medline doi:10.1101/gad.1201704

80. W. Kabsch, Integration, scaling, space-group assignment and post-refinement. *Acta Crystallogr. D* **66**, 133–144 (2010). Medline doi:10.1107/S0907444909047374

81. A. J. McCoy, R. W. Grosse-Kunstleve, P. D. Adams, M. D. Winn, L. C. Storoni, R. J. Read, *Phaser* crystallographic software. *J. Appl. Cryst.* **40**, 658–674 (2007). Medline doi:10.1107/S0021889807021206

82. P. V. Afonine, R. W. Grosse-Kunstleve, N. Echols, J. J. Headd, N. W. Moriarty, M. Mustyakimov, T. C. Terwilliger, A. Urzhumtsev, P. H. Zwart, P. D. Adams, Towards automated crystallographic structure refinement with *phenix.refine*. *Acta Crystallogr. D* **68**, 352–367 (2012). Medline doi:10.1107/S0907444912001308

83. N. K. Kim, Q. Zhang, J. Zhou, C. A. Theimer, R. D. Peterson, J. Feigon, Solution structure and dynamics of the wild-type pseudoknot of human telomerase RNA. *J. Mol. Biol.* **384**, 1249–1261 (2008). Medline doi:10.1016/j.jmb.2008.10.005

84. J. Erde, R. R. Loo, J. A. Loo, Enhanced FASP (eFASP) to increase proteome coverage and sample recovery for quantitative proteomic experiments. *J. Proteome Res.* **13**, 1885–1895 (2014). Medline doi:10.1021/pr4010019

85. R. J. Richards, H. Wu, L. Trantirek, C. M. O'Connor, K. Collins, J. Feigon, Structural study of elements of *Tetrahymena* telomerase RNA stem-loop IV domain important for function. *RNA* **12**, 1475–1485 (2006). Medline doi:10.1261/rna.112306

86. R. J. Richards, C. A. Theimer, L. D. Finger, J. Feigon, Structure of the *Tetrahymena thermophila* telomerase RNA helix II template boundary element. *Nucleic Acids Res.* **34**, 816–825 (2006). Medline doi:10.1093/nar/gkj481

87. O. Kotik-Kogan, E. R. Valentine, D. Sanfelice, M. R. Conte, S. Curry, Structural analysis reveals conformational plasticity in the recognition of RNA 3′ ends by the human La protein. *Structure* **16**, 852–862 (2008). Medline doi:10.1016/j.str.2008.02.021

88. J. Fan, N. P. Pavletich, Structure and conformational change of a replication protein A heterotrimer bound to ssDNA. *Genes Dev.* **26**, 2337–2347 (2012). Medline doi:10.1101/gad.194787.112

CHAPTER FOUR

Structural characterization of *Tetrahymena* p75 (Ctc1 of CST)

Introduction

The realization that the p75-p45-p19 subcomplex in *Tetrahymena* telomerase is a CST complex was insightful albeit somewhat surprising [1, 2]. This chapter will discuss the discovery and characterization of p75-p45-p19 as a CST complex along with ongoing work and unpublished data on the characterization of p75 and its interaction with p50.

CST is a telomere associated protein complex that was first identified in *Saccharomyces cerevisiae* as the heterotrimeric complex comprising Cdc13-Stn1-Ten1 [3-5]. In *S. cerevisiae*, CST plays many roles in telomere maintenance including the recruitment and inhibition of telomerase for G-strand synthesis as well as the recruitment of DNA polymerase-alpha (pol-α) primase complex for C-strand synthesis [6, 7]. It is also the major single stranded telomeric DNA (sstDNA) capping complex in *S. cerevisiae*, taking the role of POT1-TPP1 in humans [8]. Due to the low sequence homology of the CST proteins, these proteins were initially thought to be unique to yeast. However, more recent biochemical, genetic, and structural data have identified this protein complex in vertebrates and plants [9-11]. In humans, CST (Ctc1-Stn1-Ten1) has also been shown to be recruitment factors for DNA pol-α primase for C-strand synthesis and to inhibit telomerase recruitment by blocking the interaction of the TERT-TEN domain with TPP1 [3, 5, 12-15].

Despite a lack of sequence homology for these proteins between different phyla, CST proteins are conserved structurally. A breakthrough in understanding the structural biology of these proteins was the realization that the trimeric CST is structurally similar and possesses similar domain organization to the trimeric replication protein A (RPA) complex [16] (**Figure 4.1**). Particularly the Stn1 and Ten1 proteins appear to be the most well conserved and crystal structures of domains of human and yeast Stn1 & Ten1 confirmed their structural homology to RPA32 & RPA14 respectively, and to each other [17-19] (**Figure 4.2**). The largest subunit (Ctc1 in humans, Cdc13 in yeast, p75 in *Tetrahymena*) is the most divergent and to date, only individual domain structures of Cdc13 have been solved to atomic resolution [20-24].

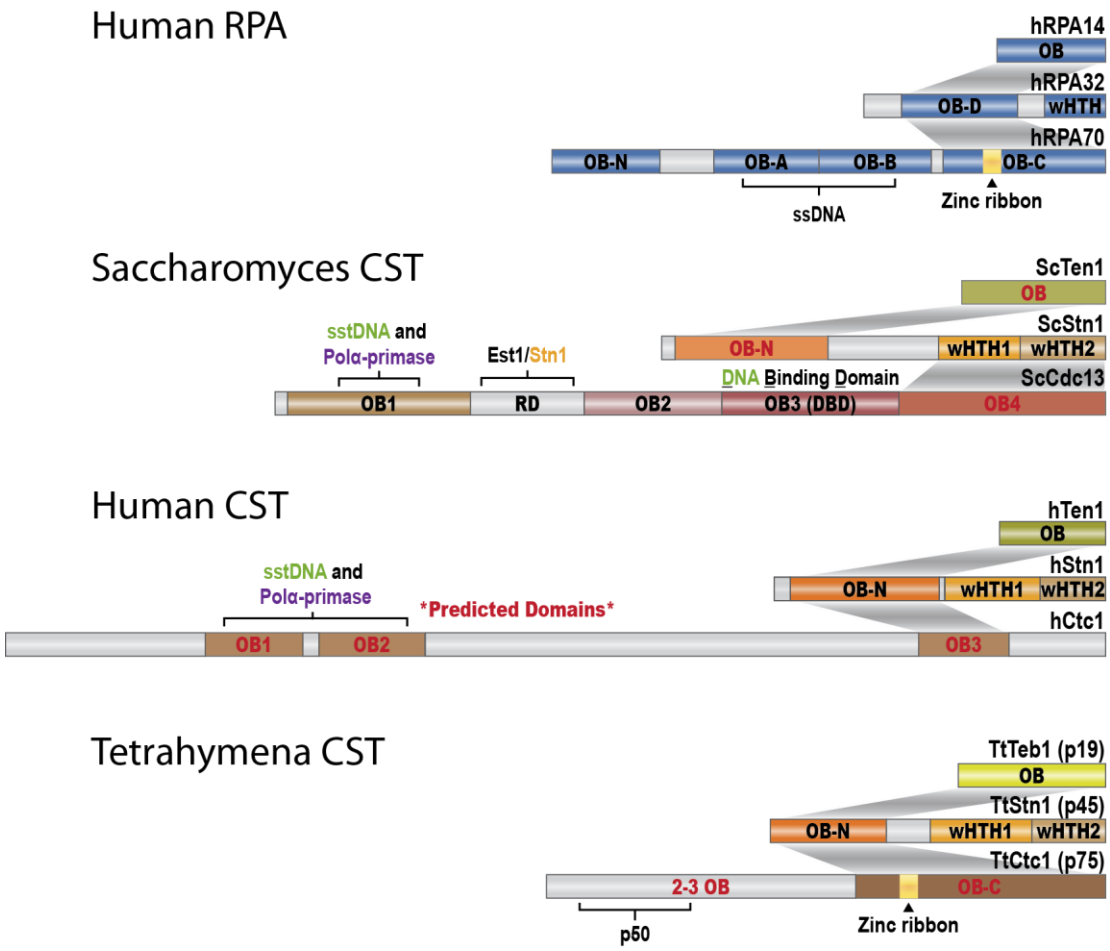

Figure 4.1. Domain organizations of trimeric human RPA and trimeric CST proteins. *S. cerevisiae*, human, and *T. thermophila* CST proteins are compared. Well studied interactions are indicated and domains without solved structures are labelled with red text.

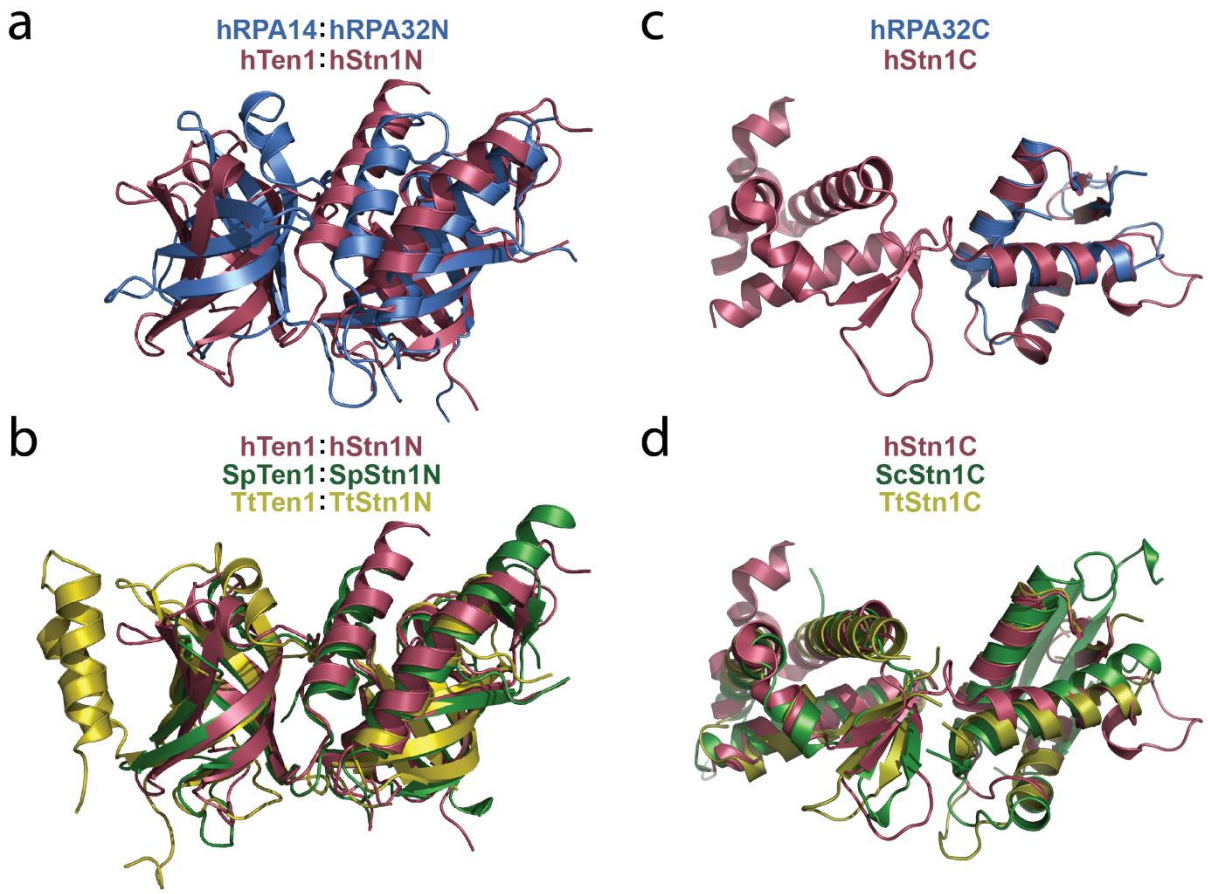

Figure 4.2. Structural superposition of RPA and CST proteins. (*a*) human RPA32N:RPA14 with human Stn1N:Ten1; (*b*) human Stn1N:Ten1 with *Schizzosaccharomyces pombe* Stn1N:Ten1 and *Tetrahymena* Stn1N:Ten1; (*c*) human RPA32C terminal WH superposed onto the C-terminal WH domain of the Stn1C tandem WH domain; (*d*) human Stn1C WH-WH domain with the separated N and C terminal WH domains from S. cerevisiae and *Tetrahymena*.

Results

The crystal structures of p19 and of p45 C-terminal domain are structurally homologous to human and yeast Ten1 and Stn1 C-terminal, indicating that p19 and p45 are the *Tetrahymena* equivalents of Ten1 and Stn1 [1]. A co-crystal structure of the p19:p45 N-terminal domain (p45N) complex has also been reported, further confirming the homology [2]. As p75-p45-p19 were known to form a trimeric complex [25, 26], it follows that p75 is the large subunit of *Tetrahymena* CST. This was supported by fitting a model of the p75C-p45N-p19 trimeric core, based on the RPA trimeric core structure and the crystal structures of p19 and p45N, into the 9 Å cryo-EM map (**Figure 4.3**) [1, 2, 27]. As no structure of a trimeric CST has ever been solved, the data and fitting provided in this 9 Å structure provided the first glimpse of a trimeric CST [28, 29]. Interestingly, these fittings and the EM map suggested the presence of only 3 OB folds in p75, though its proposed homology to the largest subunit of RPA suggests it should contain four. It is possible that the most N-terminal domain is flexible with respect to the core and therefore is invisible in the 3D cryo-EM reconstruction.

P75 N-terminal domain expression and purification

Full length p75 remains recalcitrant to soluble recombinant expression in E. coli so we attempted to produce the N-terminal domain of p75 (p75N). A range of domain limits were proposed based on a secondary structure prediction of p75 [30] and the minimum secondary structure requirement for OB-folds (5 beta strands and 1-2 alpha helices) [31] (**Figure 4.4a**). These were cloned into an MBP-p75N-GFP construct for the purpose of expression testing and based on a qualitative assessment of the fluorescence of the soluble fraction of a small scale expression, the p75N(1-203) and p75N(33-203) constructs were chosen for initial expression (**Figure 4.4b**). Both constructs were expressed in *E. coli* and were purified at scale for NMR; however, p75N(33-203) precipitated after TEV cleavage from the MBP and GFP solubility tags, indicating that the N-terminal motif of p75N is necessary for solubility of the free domain. ^{15}N-labelled p75N(1-203) was purified

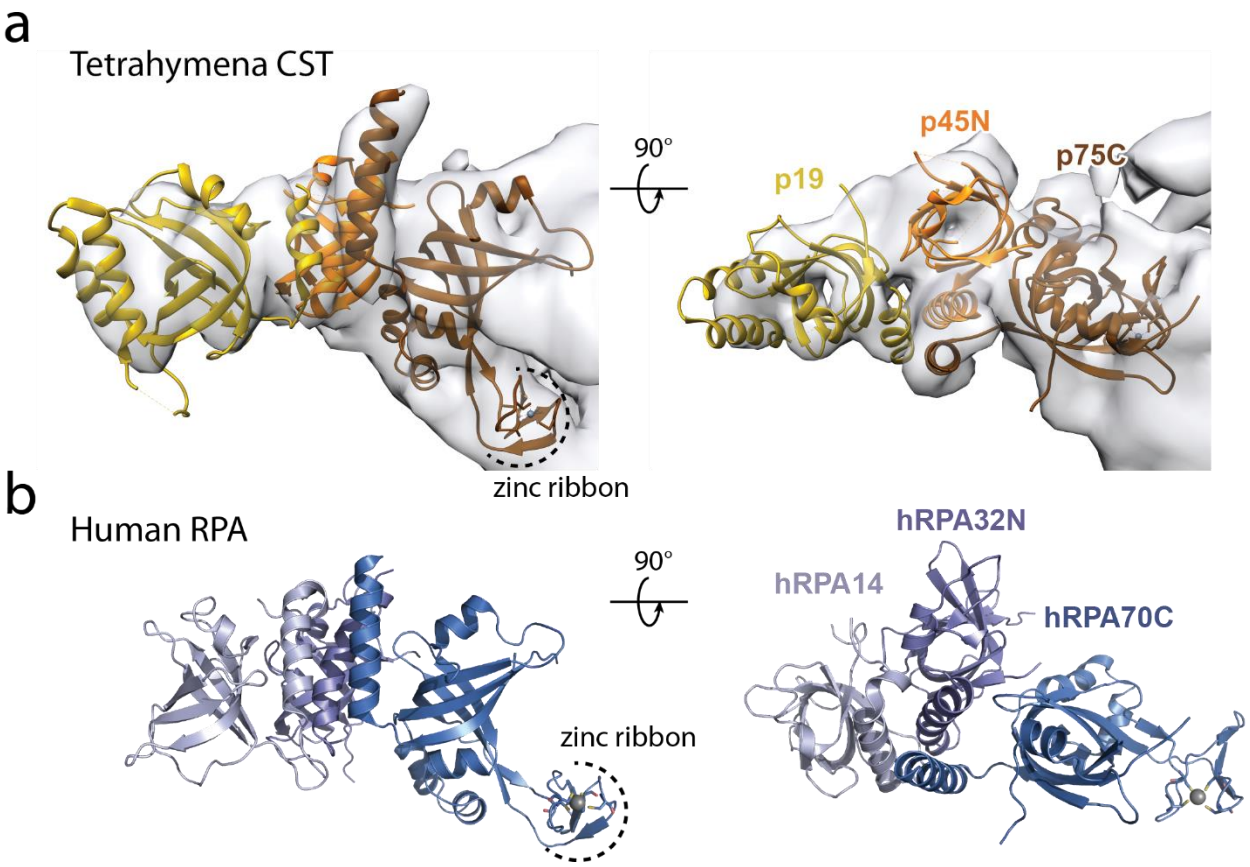

Figure 4.3. Docking model of p75-p45-p19 trimeric core. (*a*) Region of *Tetrahymena* telomerase 9A cryo-EM map comprising the CST (p75C, p45N, p19) trimeric core with a model of the CST trimeric core modeled in. Model is based on the p19-p45N crystal structure [5DOI] and the (*b*) human RPA trimeric core crystal structure [1L1O].

a

b

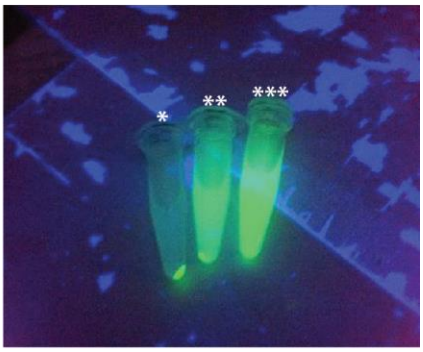

	N-term	
C-term	1	33
163	**	***
183	**	**
190	***	***
203	***	***
230	**	**
245	**	**
260	**	**
273	**	**
321	*	*

Figure 4.4. Construct determination of p75 N-terminal OB. (*a*) Construct design for expression testing of p75N based on secondary structure prediction by JPRED. (*b*) Results of expression testing based on GFP fluorescence of clarified soluble fraction under long-wave UV light. Example of representative qualitative assessment for fluorescence is shown in top panel and indicated with *, ** or ***.

to high purity and concentration (30mg/ml) by nickel affinity and size exclusion chromatography. A 2D [^{15}N, ^{1}H]-HSQC with relatively strong and dispersed peaks was obtained, indicating this construct was well folded (**Figure 4.5a**). However, only 162 out of a possible 197 (82%) amide peaks were counted, suggesting that the construct could possess an excess flexible tail. p75N constructs (1-163, 183, 190, 230) were purified and 2D [^{15}N, ^{1}H]-HSQC spectra were collected (**Figure 4.5**). Based on these data, construct p75N(1-183) (hereto referred as p75N) was used for further structure determination.

NMR assignments of free p75N domain

Conventional triple resonance backbone assignment experiments (HNCACB, CBCA(CO)NH, HNCA, HN(CO)CA) on ^{15}N^{13}C labelled p75N failed to yield spectra with sufficient signal to noise to interpret, despite the quality of the 2D [^{15}N, ^{1}H]-HSQC spectra. This could be due to intrinsic conformational flexibility of the protein occurring at a timescale that can cause the signal to relax and decay too quickly. This issue appears to be common for telomeric OB-fold proteins as it was previously experienced with *Tetrahymena* p19 as well as with the Est3 protein from *S. cerevisiae*, whose structure revealed homology to the human TPP1 OB-fold [32]. To compensate, backbone assignments were determined using the trHNCACB, trHN(co)CACB, trHNCA, trHN(co)CA, trHNCO, and trHN(ca)CO spectra collected on an 800 MHz Bruker instrument with 'triply labelled' ^{2}H^{13}C ^{15}N-p75N [33, 34](**Figure 4.6**). Conventional sidechain assignment experiments (HCCH-TOCSY, HCCH-COSY) on ^{1}H^{13}C^{15}N-p75N failed to yield spectra of sufficient quality to obtain interpretable spectra. Thus a strategy to assign the protein by starting with assigning the protonated methyls in a 'triple labelled' sample (based on Otten 2010 [35]) is currently being pursued.

Interaction of p75N with p50

Based on the p75-p45-p19 modeling and analysis of the cryo-EM density data, the C-terminal domain of p75 possesses a zinc ribbon (**Figure 4.3a**). Analysis of the primary sequence of p75

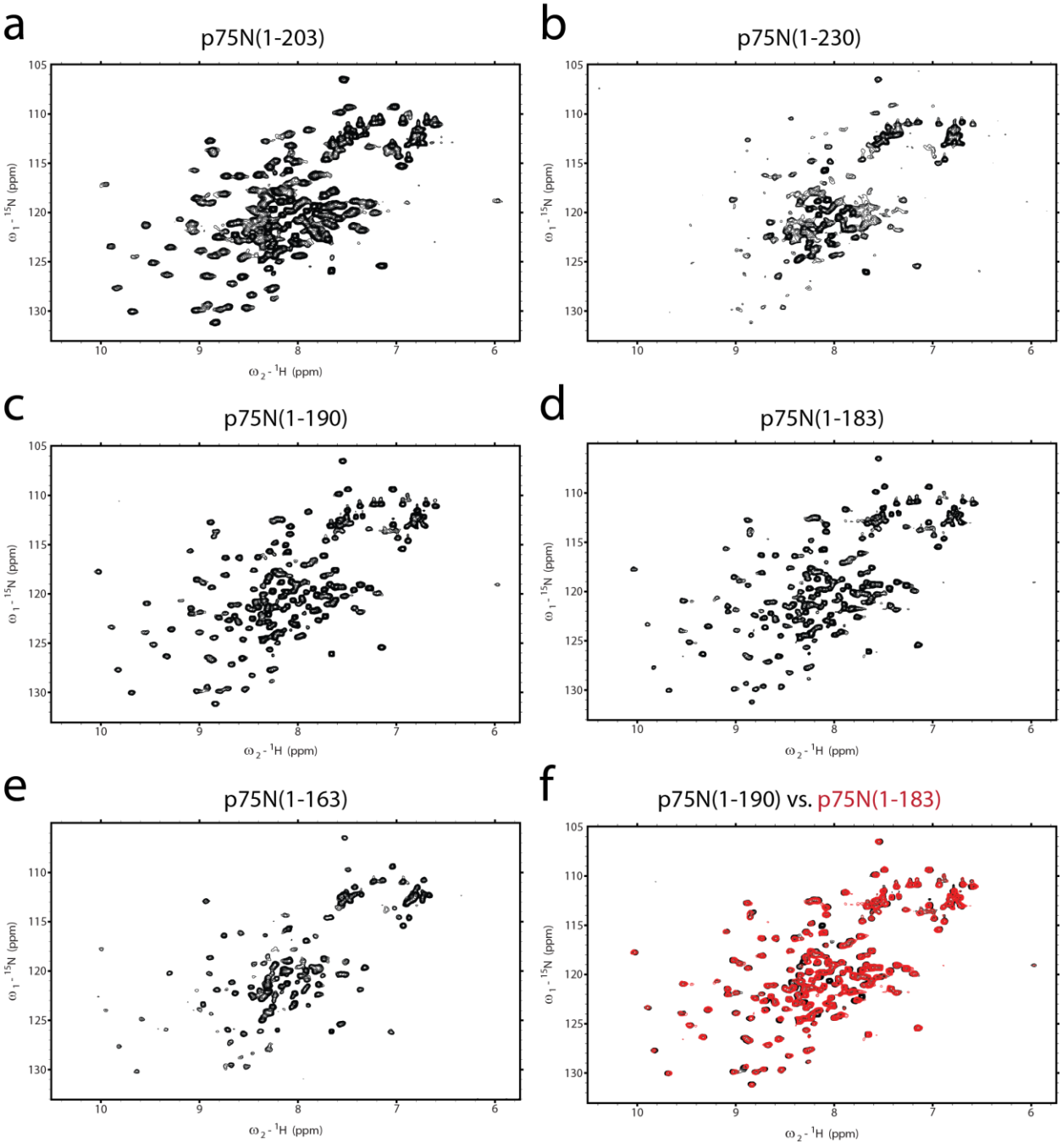

Figure 4.5. 2D [^{15}N, ^{1}H]-HSQC spectra of p75N constructs (*a*) 1-203, (*b*) 1-230, (*c*) 1-190, (*d*) 1-183, and (*e*) 1-163. (*f*) Overlay comparison of 2D [^{15}N, ^{1}H]-HSQC of p75N(1-190) vs p75N(1-183).

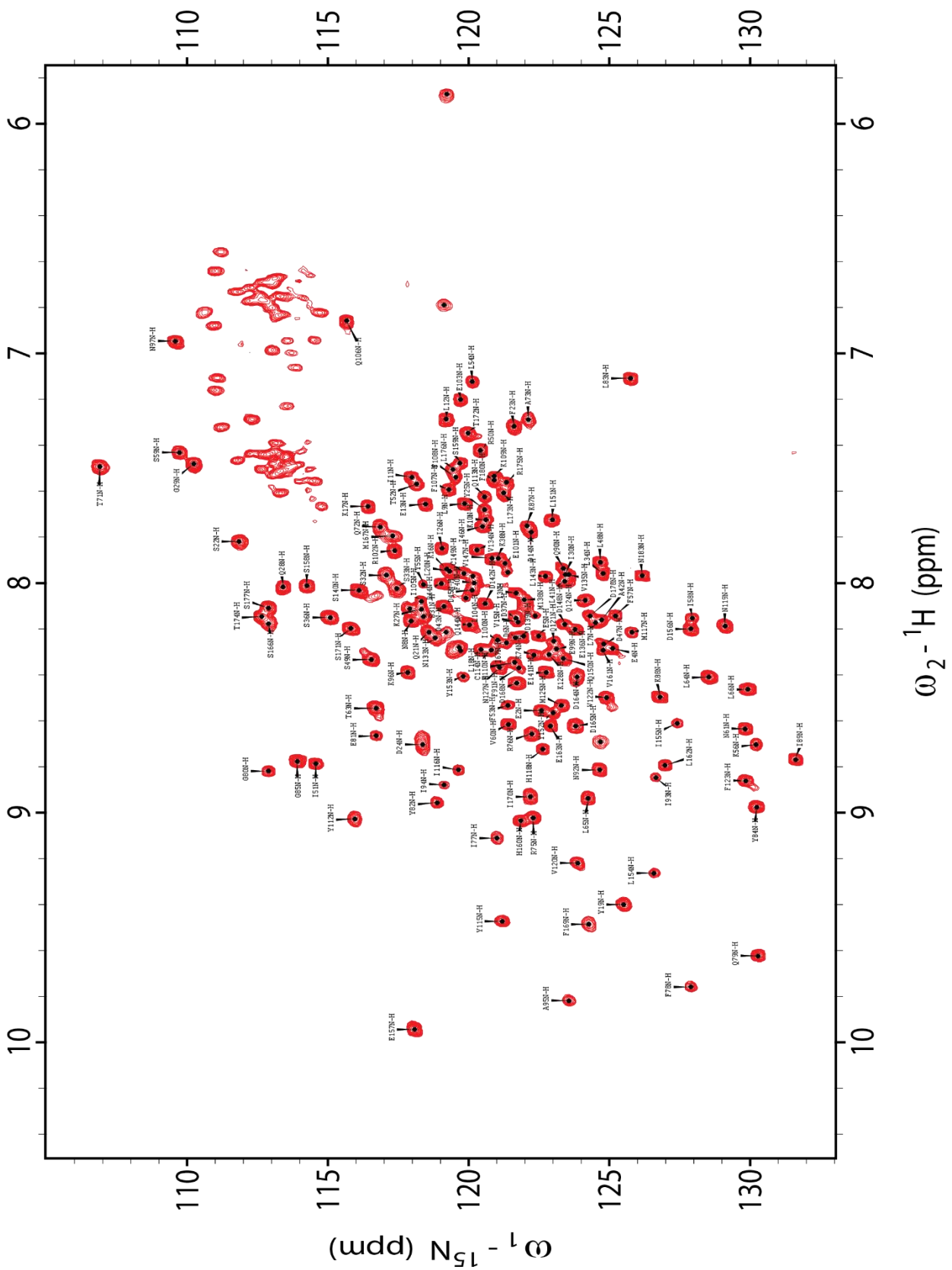

Figure 4.6. Assigned 2D [^{15}N, ^{1}H]-TROSY of triply labelled p75N(1-183).

suggests that this zinc ribbon motif resides in residues 396-418, placing the N-terminus of p75 C-terminal OB near residue 350 based on the domain limits of other RPA70C homologs relative to the zinc ribbon [27, 36]. As OB-folds are generally 100-200 residues in size, this strongly suggests that p75 possesses only 3 OB-folds and furthermore that p75N interacts with p50, bridging the entire CST complex to the RNP core (**Figure 4.7a**). To study this interaction, a peptide consisting of residues 213-265 of the p50 protein was cloned onto the C-terminus of MBP (**Figure 4.7b**). These residues of p50 were chosen based on a previous study with negative stain EM fab labelling and radioactive pulldown data [26, 37] and the 9 Å cryo-EM structure [1] that suggested residue 252 of p50 could be found near the N-terminal region of p75 (**Figure 4.7c**). To investigate the potential interaction between p50(213-265) and p75N, 2D [^{15}N, ^{1}H]-HSQC spectra of titrations of unlabeled MBP-p50(213-265) with ^{15}N-p75N were obtained. The MBP tag on p50(213-265) was retained because long stretches of unstructured peptide are likely to aggregate when purified and concentrated (**Figure 4.8**). The titration data showed an initial broadening and disappearance of many peaks at sub-stoichiometric ratios of p50(213-265) to p75N and re-appearance of peaks (at new chemical shifts) at 1:1 and above, although with broader linewidths. This suggested an interaction with the MBP-p50(213-265) that was saturating at 1:1. The general line broadening of the p75N (21.7 kDa) signals is likely due to the higher molecular weight of the complex (49.1 kDa of MBP-p50(213-265)). Therefore, TEV protease was added directly to the samples in the NMR tube to remove the MBP. This gave improved 2D [^{15}N, ^{1}H]-HSQC spectra of p75N in complex with p50(213-265) (27.7 kDa) with narrower linewidths due to release of the MBP (43 kDa) (**Figure 4.9**). These spectra indicate that the interaction occurs at approximately a 1:1 stoichiometry and is in the slow exchange regime on the NMR timescale. The reverse labelling scheme (^{15}N-p50(213-265) with unlabeled p75N) was employed and 2D [^{15}N, ^{1}H]-HSQC spectra were measured which are consistent with the above data (data not shown).

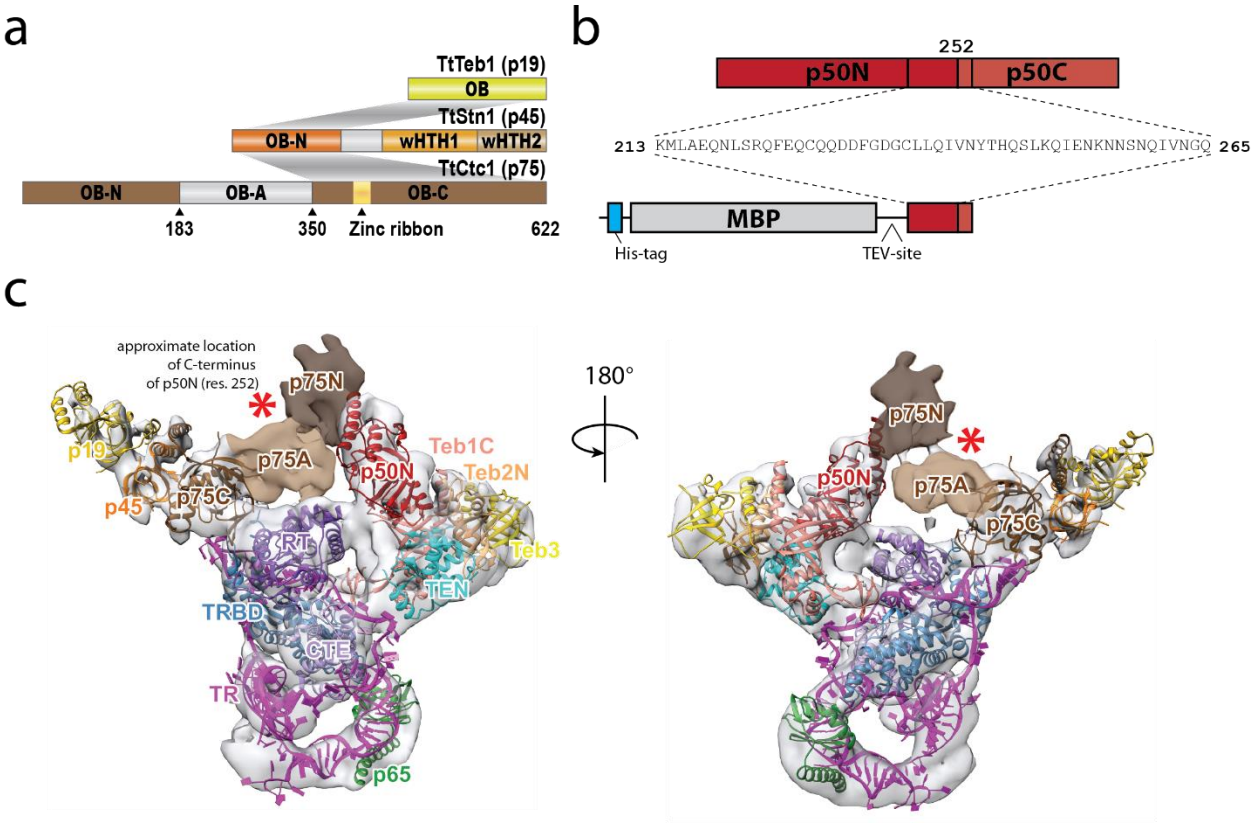

Figure 4.7. p50 interaction with p75N. (*a*) Schematic representation of *Tetrahymena* CST with proposed domain limits and motifs on p75. (*b*) Construct design for p50(213-265) based on (*c*) approximate location of p50 residue 252 (*) relative to the proposed subunit docking model of the holoenzyme.

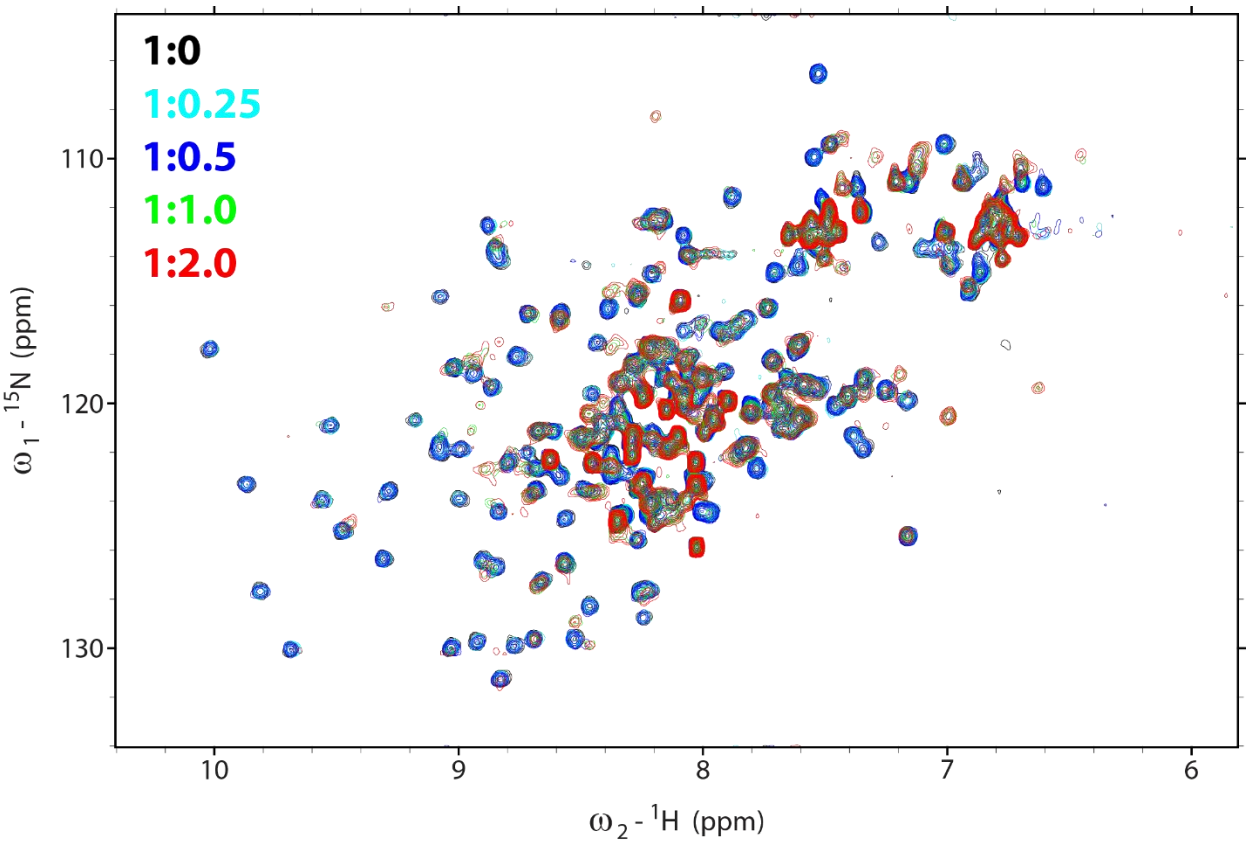

Figure 4.8. Titration series of unlabeled MBPp50(213-265) into 100uM 15N-p75N as measured by 2D [^{15}N, ^{1}H]-HSQC.

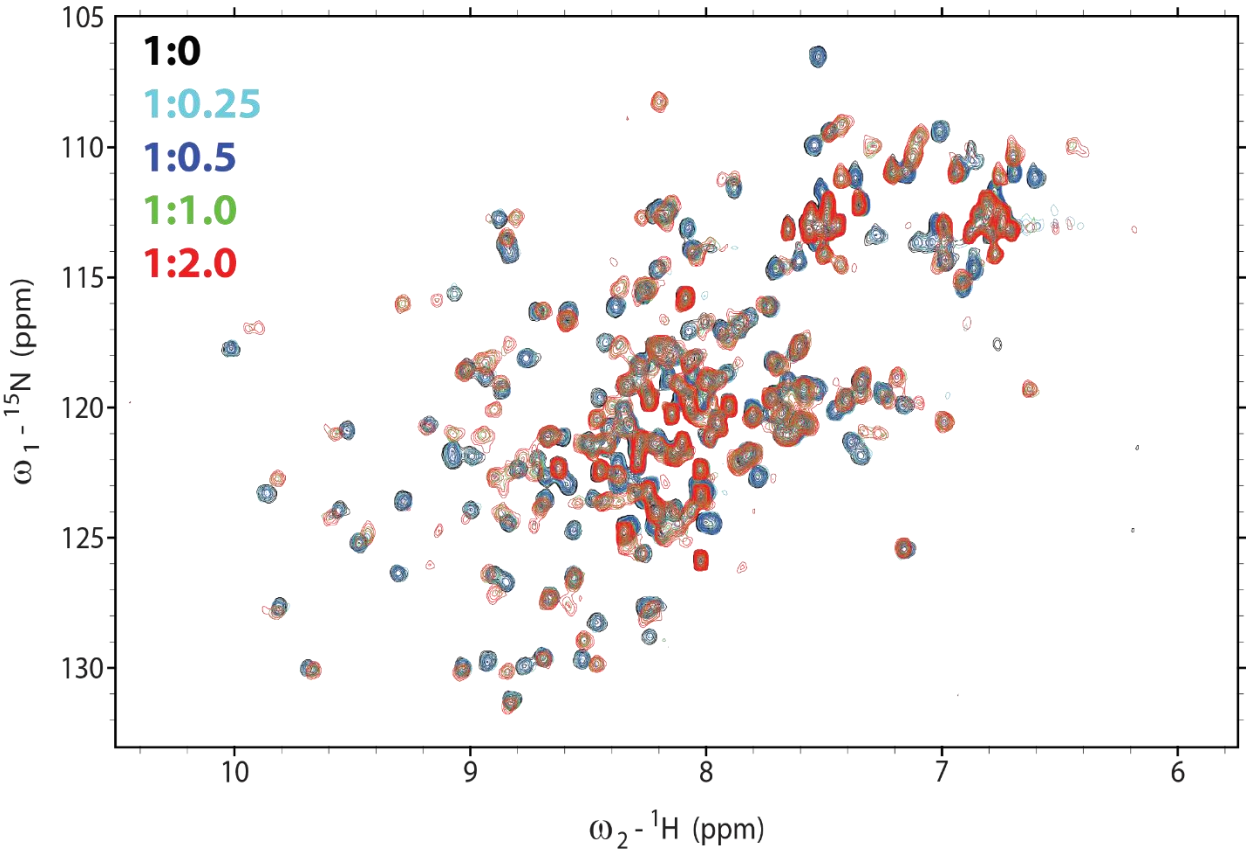

Figure 4.9. Titration series of unlabeled p50(213-265) cleaved from MBP by TEV protease into 100uM 15N-p75N as measured by 2D [^{15}N, ^{1}H]-HSQC.

Attempts to measure the affinity of MBP-p50(213-265) to p75N by ITC failed to produce results with sufficient signal to noise, suggesting that the interaction could be mediated primarily by hydrophobic contacts and is thermodynamically driven by entropic/entropy changes. There could also be a competition between MBP-p50(213-265) interacting with p75N vs. other p50 peptides. These explanations are consistent with the observation that when cleaved and purified from MBP, free p50(213-265) will aggregate in a concentration and temperature dependent manner. Notably, this aggregation is markedly suppressed in the presence of stoichiometric amounts of p75N.

To determine the minimal p50 peptide that can still fully bind to p75N, a series of truncation mutants were made to p50(213-265) and binding by 2D [^{15}N, ^{1}H]-HSQC p75N chemical shift perturbation was determined (**Figure 4.10**). Based on these data, p50(228-250) was determined to be the minimal binding core of p50 to p75N, confirmed by NMR titration spectra which show all major chemical shifts observed from p50(213-265) and binding in the slow exchange regime at 1:1 stoichiometry (**Figure 4.11**). As expected, reducing the size of the p50 peptide improved the quality of the spectra of ^{15}N-p75N:p50 complex; however, the spectral quality was increased even when compared with the apo ^{15}Np75N spectra, as evidenced by a more uniform distribution of peak intensity and greater peak dispersion. As a result, several previously unassigned backbone residues from the apo ^{2}H^{13}C ^{15}N-p75N protein could be assigned in the ^{2}H^{13}C ^{15}N-p75N:p50(228-250) complex, despite the increase in molecular weight from the 2.7 kDa peptide. This is possibly due to the peptide contributing to the conformational stability of p75N, versus the apo p75N which is suspected to be conformationally heterogeneous at a timescale unfavorable for NMR.

The reverse labelling scheme for the minimal peptide (^{13}C^{15}Np50(228-250) with unlabeled p75N) was also employed for the purpose of assignment and structure determination of the peptide. Comparison of the 2D [^{15}N, ^{1}H]-HSQC of the minimal p50 peptide with and without unlabeled p75N reveal dramatic chemical shifts for nearly every residue of p50(228-250) with the exception of the two most C-terminal residues (**Figure 4.12a**). In addition, despite the line

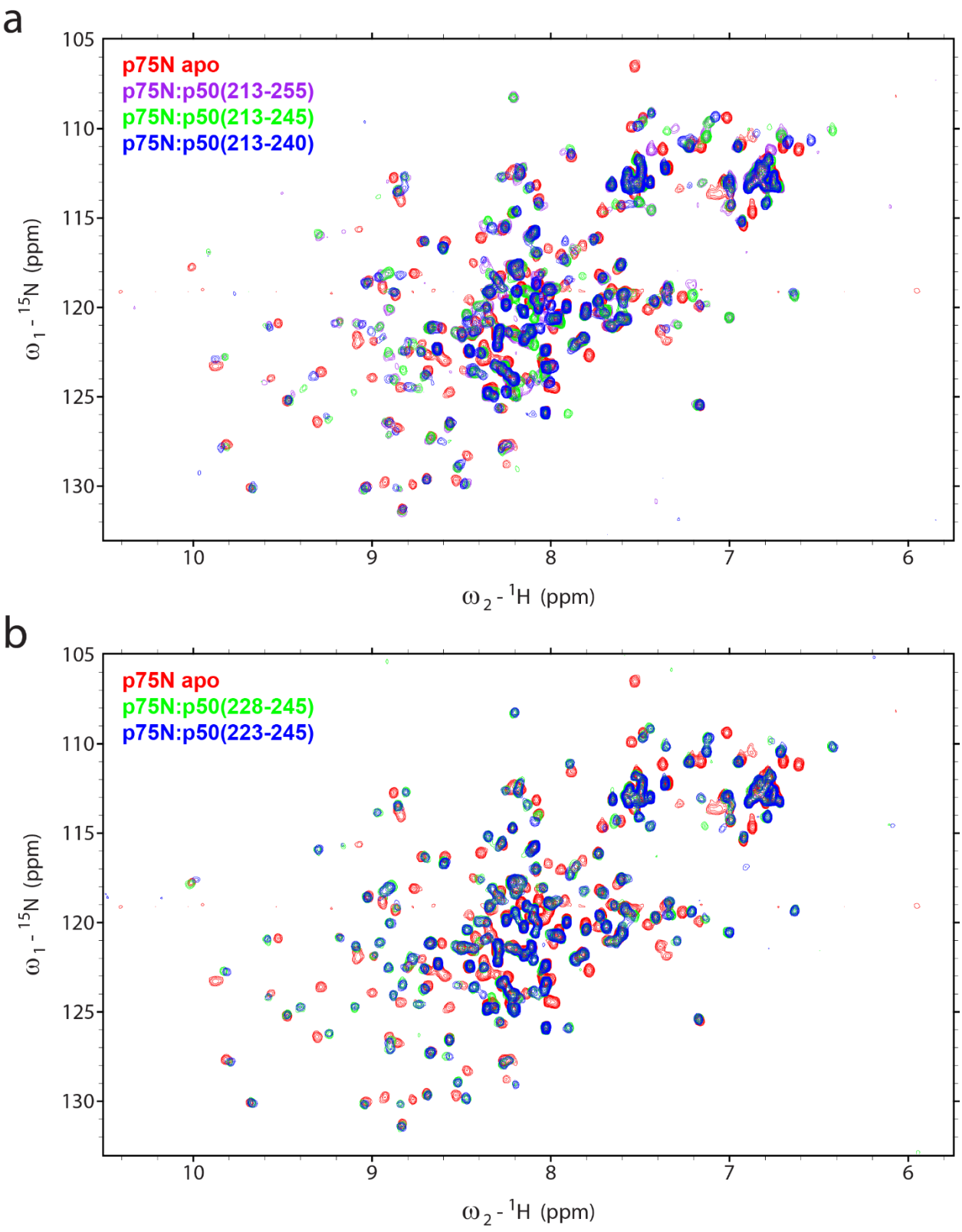

Figure 4.10. Overlay of 2D [^{15}N, ^{1}H]-HSQC spectra of N15p75N bound to different p50 constructs at 1 to 1 stoichiometry at 100uM.

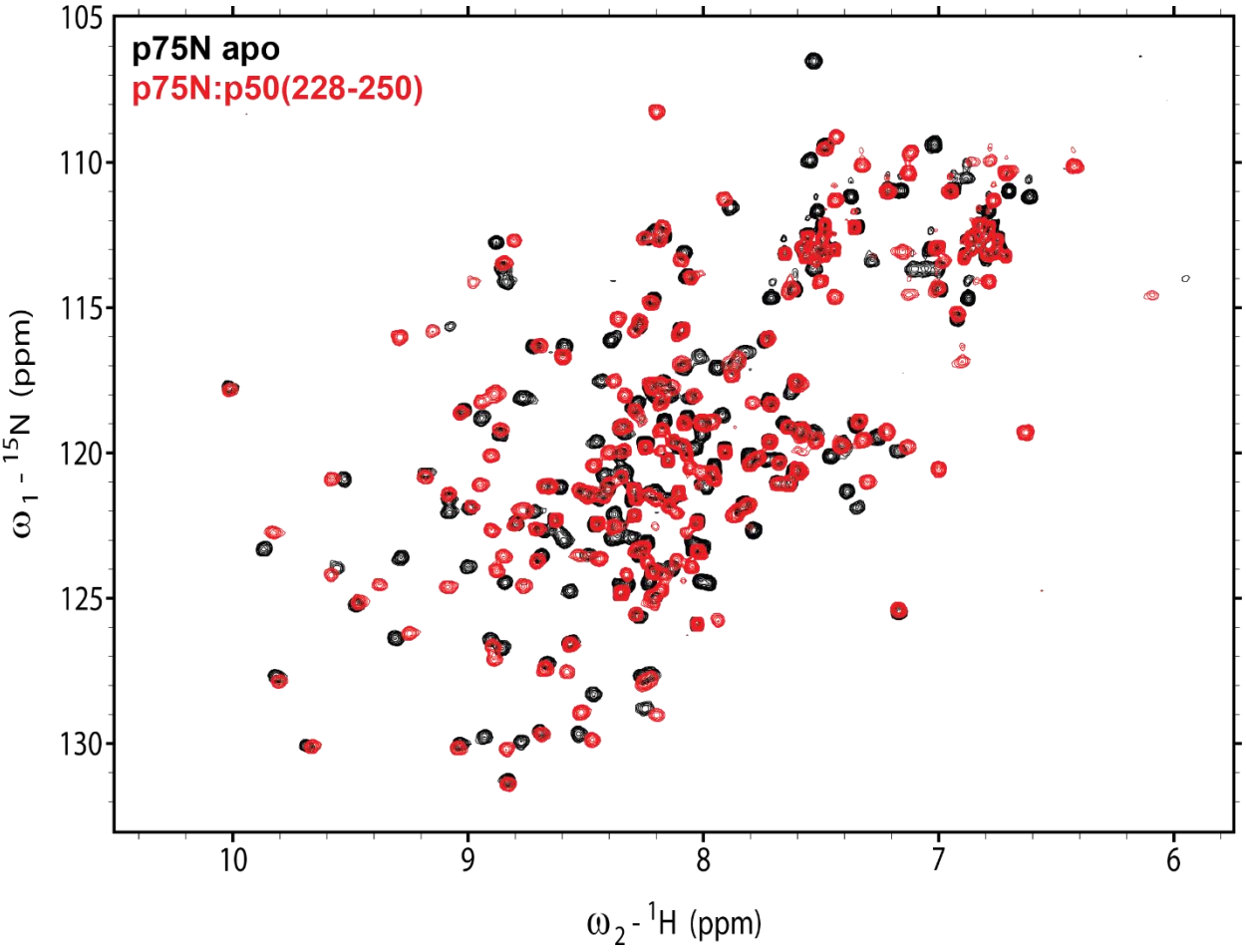

Figure 4.11. Overlay of 2D [^{15}N, ^{1}H]-HSQC spectra of ^{15}N-p75N free vs ^{15}N-p75N bound to p50(228-250) at 1 to 1 stoichiometry at 100uM.

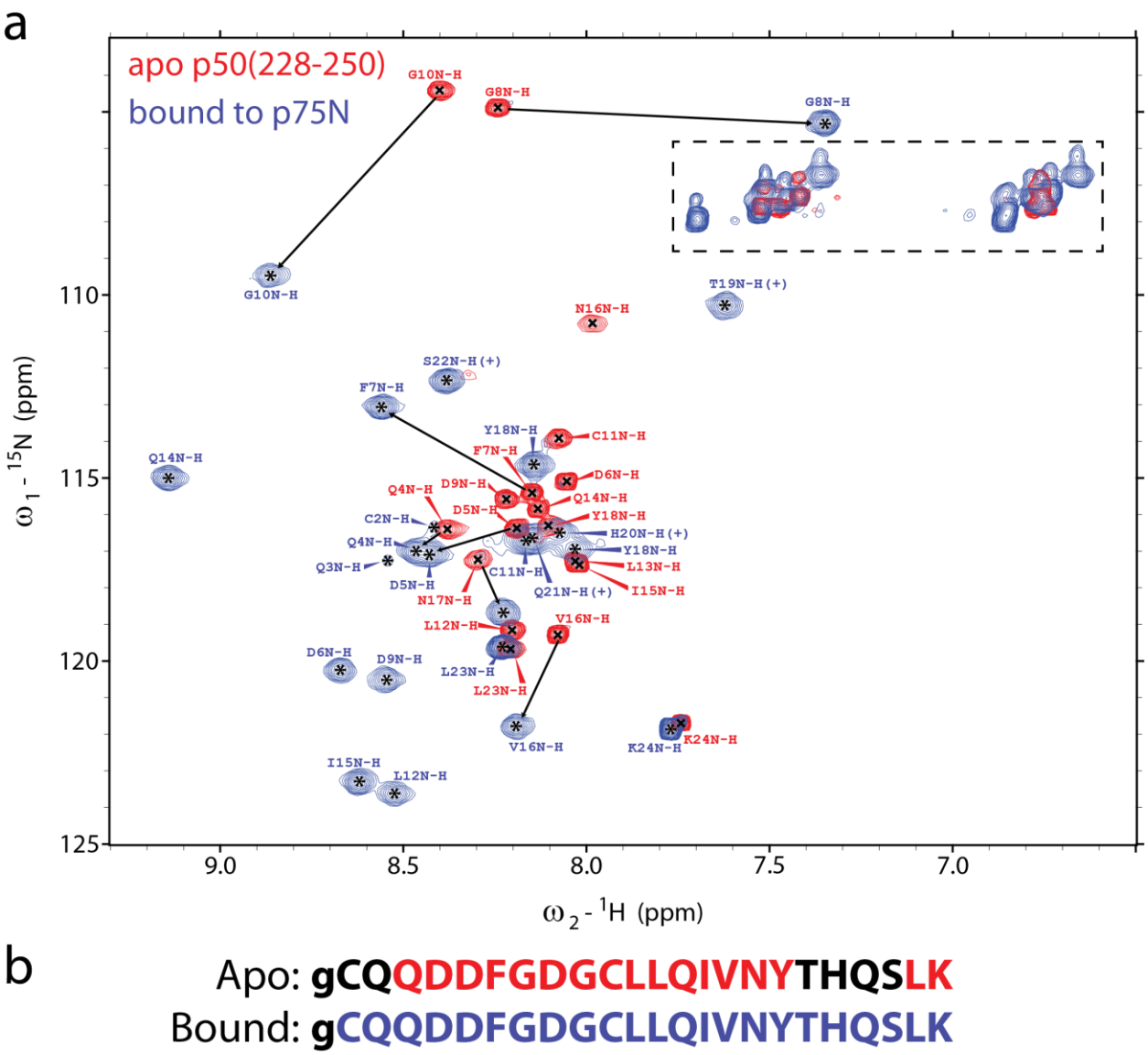

Figure 4.12. Interaction of p75N with p50(228-250). (*a*) Overlay of 2D [^{15}N, ^{1}H]-HSQC spectra of ^{13}C^{15}N-p50(228-250) free vs ^{13}C^{15}N-p50(228-250) bound to unlabeled p75N at 1 to 1 stoichiometry at 500 uM. Chemical shifts from the sidechain amides are indicated by a dashed box. (*b*) Backbone assignment coverage of p50(228-250) apo (red) vs. bound to p75N (blue).

broadening that occurred from association with the 21.7 kDa p75N domain, six missing and unassigned peaks from the free peptide were visible and assignable in the complex. The amount and size of the chemical shift perturbations of the free peptide vs. the p75N bound peptide support the validity and specificity of this interaction. This is further supported by obvious chemical shift changes in the amide side chain region of the spectra (**Figure 4.12b**).

DNA Pol-α primase interaction with p75N

One of the proposed functions of CST is the recruitment of DNA pol-α primase for complementary strand synthesis after telomeric extension of the 3' end by telomerase [12-14]. In *S. cerevisiae*, structural evidence for this is given by a co-crystal structure of Cdc13 N-terminal domain with a 35 aa peptide from the N-terminal regulatory region of Pol1, the catalytic subunit of the pol-α complex [21]. To determine if an analogous interaction in *Tetrahymena* exists, fragments of from the N-terminal region *Tetrahymena* Pol1 were tested for binding to p75N by NMR (**Figure 4.13**). These preliminary data suggest that residues 85-125 of *Tetrahymena* Pol1 participate in an interaction with p75N for recruitment of pol-α primase. However, the NMR data does not suggest that the binding of the Pol1 peptide is tight as even a 1:6 titration of the peptide does not result in line-broadened peaks returning in the HSQC. It remains possible that this peptide is interacting non-specifically with p75N. It should be noted however that the shifted peaks from this interaction do not overlap with the majority of the shifted peaks in the interaction with p50(228-250), described above.

Conclusions/Future directions

The identification of p75, p45, and p19 as *Tetrahymena* CST greatly enhanced our understanding of the *Tetrahymena* telomerase holoenzyme structure. Thus far, high resolution crystal or NMR structures have proved invaluable in generating docking models for the 'intermediate' resolution cryo-EM structure of *Tetrahymena* telomerase. However, the largest and most divergent subunit of CST (p75 and Ctc1) remains the most uncharacterized structurally

a

Residue range	Binding by NMR
105 - 265	No
105 - 225	No
85 - 225	Yes
85 - 205	Yes
85 - 185	Yes
85 - 165	Yes
85 - 145	Yes
85 - 125	Impure expression
65 - 125	Yes
65 - 205	Yes
65 - 185	Yes
65 - 165	Yes
65 - 145	Yes
65 - 125	Yes

b

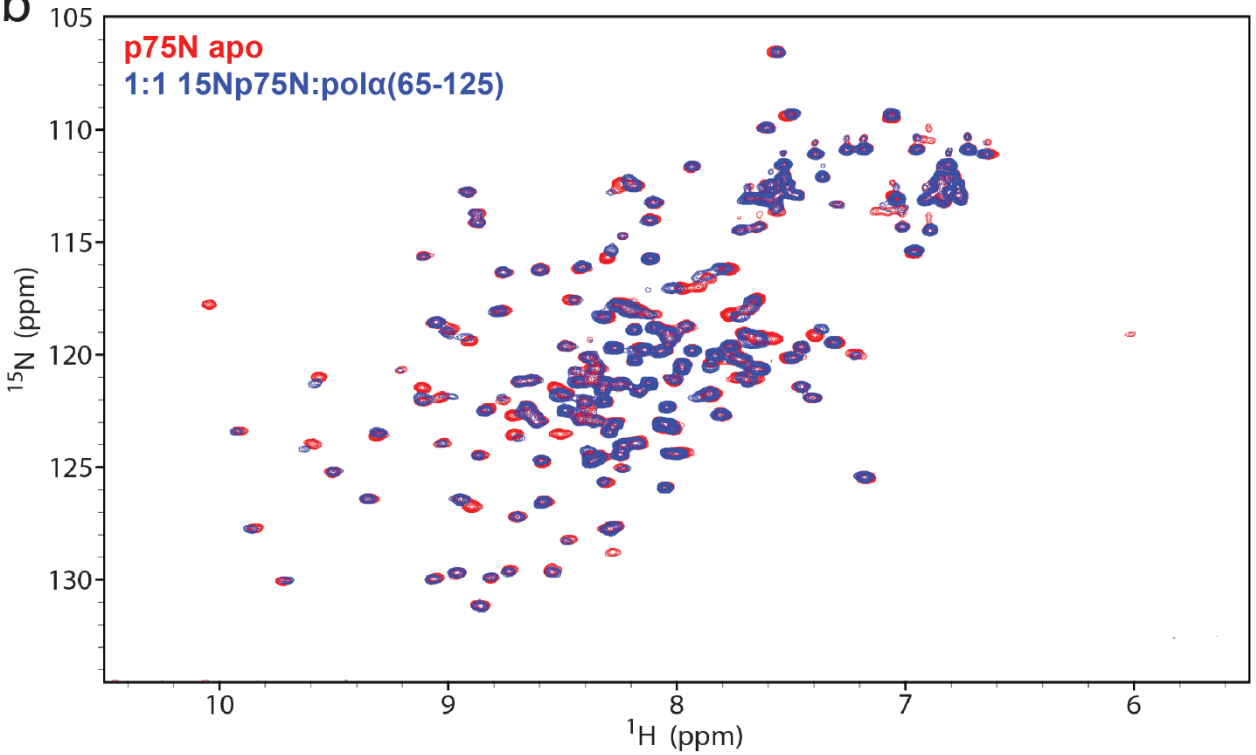

Figure 4.13. Interaction of p75N with DNA Pol1. (*a*) *Tetrahymena* DNA Pol1 constructs tested for binding to 15N-p75N by 15N-HSQC. (*b*) Representative binding of Pol1 peptide (65-125) to 15N-p75N at 1 to 1 stoichiometry at 100uM.

[29, 38]. In addition, how CST interacts with p50 (TPP1 in humans) remains a subject of extreme interest.

Here, we have determined domain limits for the N-terminal domain of p75, the largest subunit of *Tetrahymena* CST and the minimal binding core from p50 that interacts with this construct. An atomic resolution structure of p75 and its complex with p50 is simultaneously being pursued by cryo-EM studies of the telomerase holoenzyme and NMR and crystallography studies of p75N with the p50 peptide binding core.

Crystallography of P75N

A multitude of constructs for the crystallization of the p75N domain were attempted but all failed to yield hits. These are listed in **Table 4.1**.

Methods

Unless otherwise stated, all protein samples were expressed in ½ liters of M9 minimal media expression. Protein was purified using a 5 ml IMAC nickel affinity column followed by TEV protease cleavage in dialysis. Reverse IMAC was employed to remove HisMBP and TEV protease. Size exclusion chromatography was performed on a 330 mL S75 column. 'Triple labelled' ($^{2}H^{15}N^{13}C$) p75N was produced from ½ liters of D2O, 2g of 13C glucose, 0.5g of 15N NH4 and the standard M9 minimal media protocol with standard reagents (not perdeuterated). For size exclusion chromatography and data collection the following buffer conditions were determined to be optimal by micro dialysis button test: 20 mM Tris pH 7.5, 50 mM $NaCl_2$, 1 mM TCEP, 3 mM NaN_3. 8% D2O was used for all NMR samples. For 3D backbone assignment spectra, protein samples were prepared to 0.5 – 0.8 mM. For titration and binding studies protein samples were prepared to 0.1 mM.

Construct	Label	Rationale
p75N(1-183)	--	minimal p75N construct as determined by NMR
p75N(1-183)	Se-met	p75N is very soluble, seleno-methionine labelling can decrease solubility which can facilitate crystallization
p75N(1-183)Δ10,13,17L	--	Changing these three residues on alpha helix of p75N caused it to dimerize which can facilitate crystallization
MBP-3xAla-p75N(1-183)	--	same MBP fusion construct that yielded crystals for p19
MBP-3xAla-p75N(3-183)	--	changing the linker could alter crystal packing
MBP-3xAla-p75N(5-183)	--	""
MBP-3xAla-p75N(7-183)	--	""
MBP(LLLL)-3xAla-p75N(1-183)	--	MBP(LLLL) variant dimerizes and was shown to crystallize more readily than WT MBP

Table 4.1. p75 N-terminal domain constructs attempted for crystal trials.

REFERENCES

1. Jiang J, Chan H, Cash DD, Miracco EJ, Ogorzalek Loo RR, Upton HE, Cascio D, O'Brien Johnson R, Collins K, Loo JA *et al*: Structure of *Tetrahymena* telomerase reveals previously unknown subunits, functions, and interactions. *Science* 2015, 350(6260):aab4070.

2. Wan B, Tang T, Upton H, Shuai J, Zhou Y, Li S, Chen J, Brunzelle JS, Zeng Z, Collins K *et al*: The *Tetrahymena* telomerase p75-p45-p19 subcomplex is a unique CST complex. *Nat Struct Mol Biol* 2015, 22(12):1023-1026.

3. Grandin N, Reed SI, Charbonneau M: Stn1, a new Saccharomyces cerevisiae protein, is implicated in telomere size regulation in association with Cdc13. *Gene Dev* 1997, 11(4):512-527.

4. Grandin N, Damon C, Charbonneau M: Ten1 functions in telomere end protection and length regulation in association with Stn1 and Cdc13. *EMBO J* 2001, 20(5):1173-1183.

5. Nugent CI, Hughes TR, Lue NF, Lundblad V: Cdc13p: a single-strand telomeric DNA-binding protein with a dual role in yeast telomere maintenance. *Science* 1996, 274(5285):249-252.

6. Churikov D, Corda Y, Luciano P, Geli V: Cdc13 at a crossroads of telomerase action. *Front Oncol* 2013, 3:39.

7. Lin J, Zakian VA: The Saccharomyces CDC13 protein is a single-strand TG1-3 telomeric DNA-binding protein in vitro that affects telomere behavior in vivo. *Proc Natl Acad Sci U S A* 1996, 93(24):6.

8. Evans SK, Lundblad V: Est1 and Cdc13 as comediators of telomerase access. *Science* 1999, 286(5437):117-120.

9. Miyake Y, Nakamura M, Nabetani A, Shimamura S, Tamura M, Yonehara S, Saito M, Ishikawa F: RPA-like mammalian Ctc1-Stn1-Ten1 complex binds to single-stranded DNA and protects telomeres independently of the Pot1 pathway. *Mol Cell* 2009, 36(2):193-206.

10. Price CM, Boltz KA, Chaiken MF, Stewart JA, Beilstein MA, Shippen DE: Evolution of CST function in telomere maintenance. *Cell Cycle* 2010, 9(16):3157-3165.

11. Surovtseva YV, Churikov D, Boltz KA, Song X, Lamb JC, Warrington R, Leehy K, Heacock M, Price CM, Shippen DE: Conserved telomere maintenance component 1 interacts with STN1 and maintains chromosome ends in higher eukaryotes. *Mol Cell* 2009, 36(2):207-218.

12. Casteel DE, Zhuang S, Zeng Y, Perrino FW, Boss GR, Goulian M, Pilz RB: A DNA polymerase-{alpha}{middle dot}primase cofactor with homology to replication protein A-32 regulates DNA replication in mammalian cells. *J Biol Chem* 2009, 284(9):5807-5818.

13. Chen LY, Redon S, Lingner J: The human CST complex is a terminator of telomerase activity. *Nature* 2012, 488(7412):540-544.

14. Qi HY, Zakian VA: The Saccharomyces telomere-binding protein Cdc13p interacts with both the catalytic subunit of DNA polymerase alpha and the telomerase-associated Est1 protein. *Gene Dev* 2000, 14(14):1777-1788.

15. Leehy KA, Lee JR, Song X, Renfrew KB, Shippen DE: MERISTEM DISORGANIZATION1 encodes TEN1, an essential telomere protein that modulates telomerase processivity in Arabidopsis. *Plant Cell* 2013, 25(4):1343-1354.

16. Gao H, Cervantes RB, Mandell EK, Otero JH, Lundblad V: RPA-like proteins mediate yeast telomere function. *Nat Struct Mol Biol* 2007, 14(3):208-214.

17. Gelinas AD, Paschini M, Reyes FE, Heroux A, Batey RT, Lundblad V, Wuttke DS: Telomere capping proteins are structurally related to RPA with an additional telomere-specific domain. *Proc Natl Acad Sci U S A* 2009, 106(46):19298-19303.

18. Sun J, Yu EY, Yang YT, Confer LA, Sun SH, Wan K, Lue NF, Lei M: Stn1-Ten1 is an Rpa2-Rpa3-like complex at telomeres. *Gene Dev* 2009, 23(24):2900-2914.

19. Bryan C, Rice C, Harkisheimer M, Schultz DC, Skordalakes E: Structure of the human telomeric Stn1-Ten1 capping complex. *PLoS One* 2013, 8(6):e66756.

20. Mitchell MT, Smith JS, Mason M, Harper S, Speicher DW, Johnson FB, Skordalakes E: Cdc13 N-terminal dimerization, DNA binding, and telomere length regulation. *Mol Cell Biol* 2010, 30(22):5325-5334.

21. Sun J, Yang Y, Wan K, Mao N, Yu TY, Lin YC, DeZwaan DC, Freeman BC, Lin JJ, Lue NF *et al*: Structural bases of dimerization of yeast telomere protein Cdc13 and its interaction with the catalytic subunit of DNA polymerase alpha. *Cell Res* 2011, 21(2):258-274.

22. Mason M, Wanat JJ, Harper S, Schultz DC, Speicher DW, Johnson FB, Skordalakes E: Cdc13 OB2 dimerization required for productive Stn1 binding and efficient telomere maintenance. *Structure* 2013, 21(1):109-120.

23. Mitton-Fry RM, Anderson EM, Theobald DL, Glustrom LW, Wuttke DS: Structural basis for telomeric single-stranded DNA recognition by yeast Cdc13. *J Mol Biol* 2004, 338(2):241-255.

24. Yu EY, Sun J, Lei M, Lue NF: Analyses of Candida Cdc13 Orthologues Revealed a Novel OB Fold Dimer Arrangement, Dimerization-Assisted DNA Binding, and Substantial Structural Differences between Cdc13 and RPA70. *Molecular and Cellular Biology* 2012, 32(1):186-198.

25. Min B, Collins K: An RPA-related sequence-specific DNA-binding subunit of telomerase holoenzyme is required for elongation processivity and telomere maintenance. *Mol Cell* 2009, 36(4):609-619.

26. Jiang J, Miracco EJ, Hong K, Eckert B, Chan H, Cash DD, Min B, Zhou ZH, Collins K, Feigon J: The architecture of *Tetrahymena* telomerase holoenzyme. *Nature* 2013, 496(7444):187-192.

27. Bochkareva E, Korolev S, Lees-Miller SP, Bochkarev A: Structure of the RPA trimerization core and its role in the multistep DNA-binding mechanism of RPA. *EMBO J* 2002, 21(7):1855-1863.

28. Feigon J, Chan H, Jiang J: Integrative structural biology of *Tetrahymena* telomerase - insights into catalytic mechanism and interaction at telomeres. *FEBS J* 2016, 283(11):2044-2050.

29. Chan H, Wang Y, Feigon J: Progress in Human and *Tetrahymena* Telomerase Structure. *Annu Rev Biophys* 2017, 46:199-225.

30. Drozdetskiy A, Cole C, Procter J, Barton GJ: JPred4: a protein secondary structure prediction server. *Nucleic Acids Res* 2015, 43(W1):W389-394.

31. Horvath MP: Structural anatomy of telomere OB proteins. *Crit Rev Biochem Mol Biol* 2011, 46(5):409-435.

32. Rao T, Lubin JW, Armstrong GS, Tucey TM, Lundblad V, Wuttke DS: Structure of Est3 reveals a bimodal surface with differential roles in telomere replication. *Proc Natl Acad Sci U S A* 2014, 111(1):214-218.

33. Salzmann M, Pervushin K, Wider G, Senn H, Wuthrich K: TROSY in triple-resonance experiments: new perspectives for sequential NMR assignment of large proteins. *Proc Natl Acad Sci U S A* 1998, 95(23):13585-13590.

34. Pervushin K, Riek R, Wider G, Wuthrich K: Attenuated T2 relaxation by mutual cancellation of dipole-dipole coupling and chemical shift anisotropy indicates an avenue to NMR structures of very large biological macromolecules in solution. *Proc Natl Acad Sci U S A* 1997, 94(23):12366-12371.

35. Otten R, Chu B, Krewulak KD, Vogel HJ, Mulder FA: Comprehensive and cost-effective NMR spectroscopy of methyl groups in large proteins. *J Am Chem Soc* 2010, 132(9):2952-2960.

36. Zeng Z, Min B, Huang J, Hong K, Yang Y, Collins K, Lei M: Structural basis for *Tetrahymena* telomerase processivity factor Teb1 binding to single-stranded telomeric-repeat DNA. *Proceedings of the National Academy of Sciences of the United States of America* 2011, 108(51):20357-20361.

37. Hong K, Upton H, Miracco EJ, Jiang J, Zhou ZH, Feigon J, Collins K: *Tetrahymena* telomerase holoenzyme assembly, activation, and inhibition by domains of the p50 central hub. *Molecular and Cellular Biology* 2013, 33(19):3962-3971.

38. Rice C, Skordalakes E: Structure and function of the telomeric CST complex. *Comput Struct Biotechnol J* 2016, 14:161-167.

CHAPTER FIVE

Identification and characterization of Tetrahymena Rlp2

Introduction

The discovery of two new RPA related proteins, Teb2 and Teb3, and the trimeric RPA related complex, TEB, in *Tetrahymena* telomerase led to several insights [1]. One is that POT1, the human equivalent to Teb1, is more closely related to RPA70 than previously thought; a hypothesis which is discussed at length in Chan et al. 2017 [2] (Chapter 6) and supported by recent crystal structures of POT1 [3, 4]. Another, was that Teb2 and Teb3 were actually shared subunits between *Tetrahymena* RPA and *Tetrahymena* telomerase TEB (**Figure 5.1**), a hypothesis confirmed by our recent publication in collaboration with the Collins lab [5]. In the work leading up to that publication, a new RPA32-like protein in *Tetrahymena* was discovered and briefly studied for the purpose of future structural determination. This chapter will present the preliminary unpublished data on this new protein, now called Rlp2, and discuss potential future directions.

Results

In previous work performed by the Collins lab, two RPA70 homologs were identified in *Tetrahymena* and characterized [6]. However, the corresponding RPA32 and RPA14 subunits that would complete the orthologous heterotrimer were not found. Thus, when Teb2 and Teb3 were discovered, in our previous cryo-EM and mass spec studies [1], to be RPA32 and RPA14 homologs it was thought that these could be the missing RPA32/RPA14 homologs and that they were shared between the three RPA70 homologs, Teb1, Rlp1, and Rfa1, to form three distinct RPA-like heterotrimers. Though existing expression profiling and microarray data supported this proposal [7, 8], it is surprising given that the sequence similarity between these proteins, Teb1, Rlp1, and Rfa1, is relatively low and they are all expected to interact with Teb2-Teb3 similarly, as predicted by the RPA heterotrimer.

Thus a psi-BLAST was performed on the *Tetrahymena* proteome querying Teb2 and Teb3 in an effort to identify any other possible RPA homologs. Surprisingly, the Teb3 search did not yield any significant hits, further supporting the hypothesis that it is the RPA14 homolog. We note that the

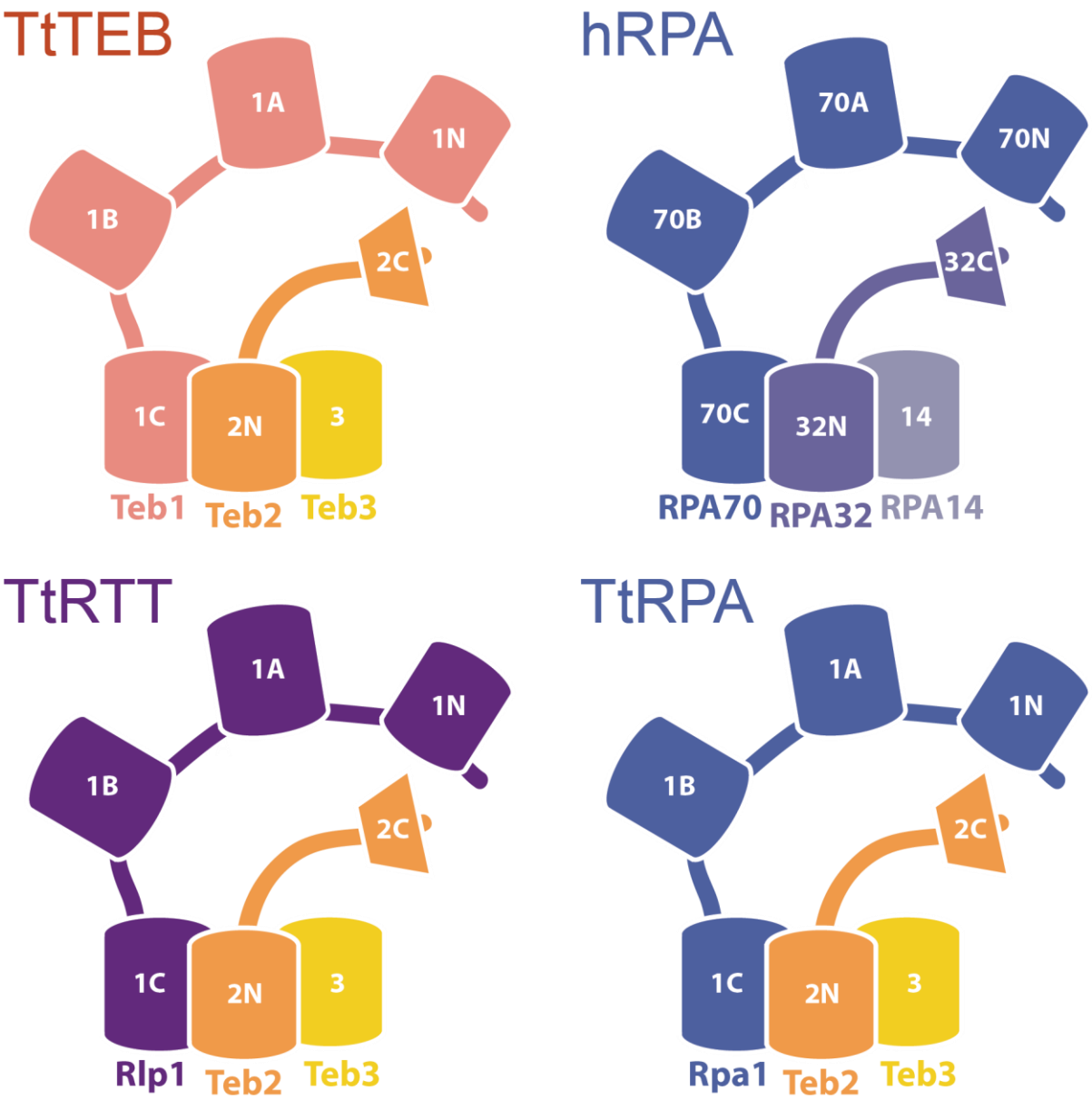

Figure 5.1. Schematic of RPA trimeric complexes in *Tetrahymena*. Teb2 and Teb3 subunits are shared between *Tetrahymena* TEB, RTT, and RPA with different large subunits. The homologous human RPA comprising RPA70, RPA32, and RPA14 is shown for comparison.

RPA14-like p19 was not identified as a hit. This was expected due to the high sequence divergence of CST proteins. However, RPA proteins are well conserved and are readily identifiable based on sequence similarity across species (Teb2 and Teb3 possess significant sequence similarity to RPA32 and RPA14 respectively). However, psi-BLAST of Teb2 identified a single protein with sequence similarity and the appropriate size and predicted secondary structure elements consistent with an RPA32, which will heretofore be referred to as Rlp2 (RPA like protein 2).

When expressed in *E. coli* and co-lysed with pellets expressing Teb1C and Teb3, Rlp2 could be purified via nickel affinity chromatography. The size exclusion profile and resultant SDS-PAGE suggested it forms a well-folded dimer of Rlp2-Teb3 that does not bind to Teb1C.

Domain limits of Rlp2

RPA32-like proteins generally possess two domains. An N-terminal OB-fold that interacts with an RPA70C-like OB-fold and an RPA14-like OB-fold to form a RPA heterotrimeric core; and a C-terminal winged-helix (WH) motif. Based on the secondary structure prediction of Rlp2, domain limits for the Rlp2 C-terminal WH were proposed (**Figure 5.2ab**) with 229-283 representing the minimal construct. Attempts to express and purify the C-terminal WH were successful but neither Rlp2(229-283) nor the larger construct of Rlp2(209-283) yielded a well folded-domain, as determined by NMR (**Figure 5.2cd**).

A range of domain limits for the Rlp2 N-terminal OB-fold was expressed and purified (**Figure 5.3a**) and co-lysed with Teb3. Out of the tested constructs only Rlp2(18-228) and Rlp2(53-228) expressed and purified as a monodispersed peak on SEC bound to Teb3. The expression tests of these proposed domain limits are consistent with a multiple alignment of Rlp2, hRPA32, and Teb2, suggesting that the C-terminus of the Rlp2 N-OB was determined but the N-terminus could potentially be further trimmed (**Figure 5.3b**). Interestingly, these constructs did not appear to form a dimer of dimers based on the SEC profile suggesting that the dimerization of Rlp2-Teb3 is facilitated by the C-terminal domain of Rlp2.

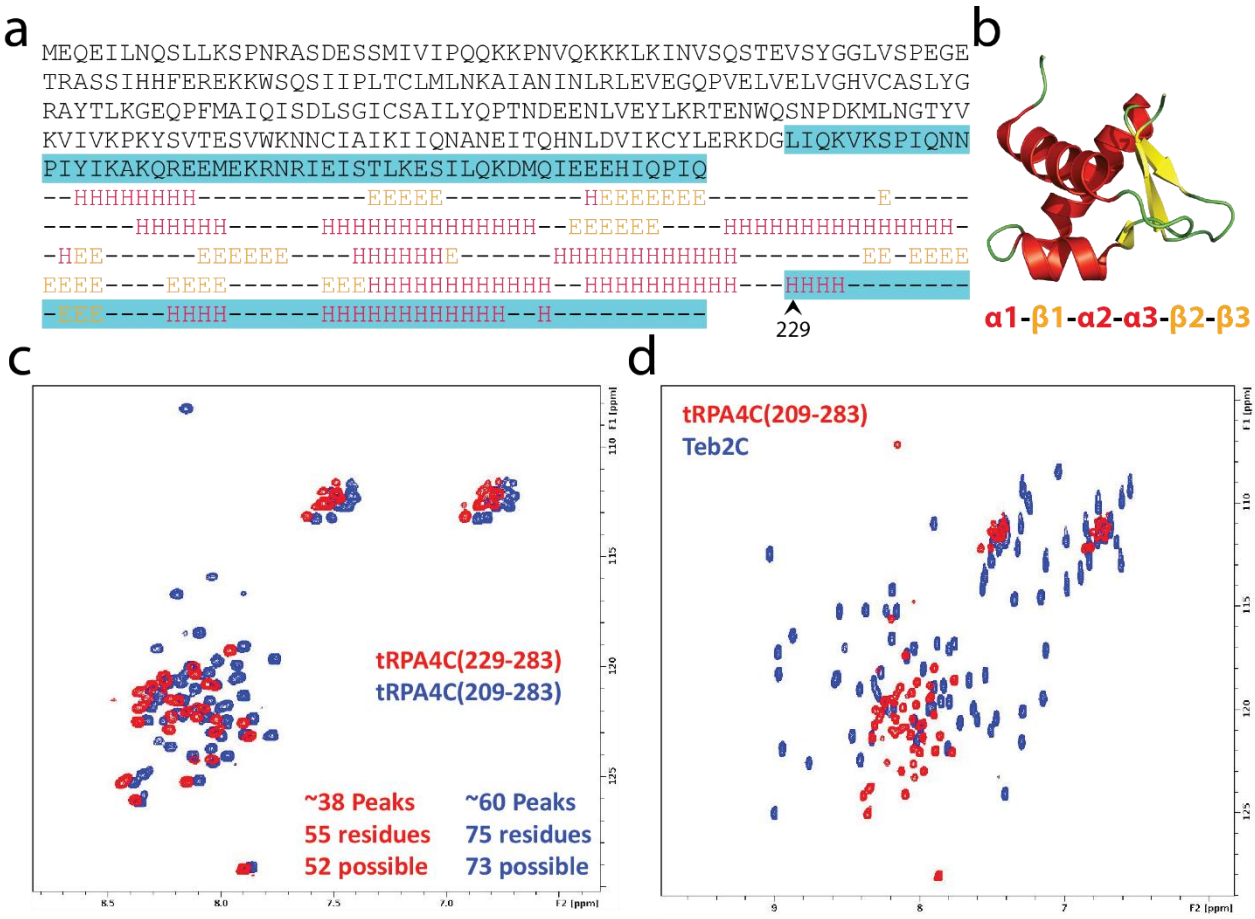

Figure 5.2. Structural characterization of C-terminal domain of Rlp2. (*a*) Sequence and secondary structure prediction of Rlp2. Highlighted in blue is the putative winged-helix (WH) domain which has the minimum secondary structure requirements illustrated in (*b*) the structure of the human RPA32 C-terminal (WH). (*c*) Overlay of the 15N-HSQCs of the putative minimal 229-293 Rlp2 WH and an extended 209-293 construct. (*d*) Comparison of 15N-HSQC Rlp2(209-293) with that of Teb2 C-terminal WH. These spectra strongly suggest that the recombinantly expressed Rlp2 C-terminal domain does not form a well-folded WH domain.

a

RPA4 Construct	Results
RPA4 (53-170)	Eliminated during expression testing- did not express well
RPA4 (53-185)	RPA4 in insoluble fraction, only one band in elution
RPA4 (53-197)	Only one band in elution fraction, aggregated in dialysis
RPA4 (53-215)	RPA4 in insoluble fraction, only one band in elution, one peak on SEC
RPA4 (53-228)	Successful purification of complex, two peaks in SEC
RPA4 (18-170)	RPA4 in insoluble fraction, only one band in elution, one peak on SEC
RPA4 (18-185)	RPA4 in insoluble fraction, only one band in elution, one peak on SEC
RPA4 (18-197)	RPA4 in insoluble fraction, only one band in elution, one peak on SEC
RPA4 (18-215)	RPA4 in insoluble fraction, only one band in elution, one peak on SEC
RPA4 (18-228)	Successful purification of complex, two peaks in SEC

b

```
hRPA32      ------------------------------------MWNSGFESYGSSSYGGAGGYTQS
TtTeb2      ----------------------------------------------MSNRVQG---GFDNN
TtRlp2      MEQEILNQSLLKSPNRASDESSMIVIPQQKKPNVQKKKLKINVSQSTEVSYG---GLVSP
                              18                                      53

hRPA32      PGGFGSPAPSQAEKKSRARAQHIVPCTISQL---LSAT---------LVDEVFRIGNVEI
TtTeb2      SGNNQSA----QKQQAEKIPQITVPLNCFMINQIVKAAKENPQAH--SGNHYEWYGAFEN
TtRlp2      EGETRASSI-HHFEREKKWSQSIIPLTCLMLNKAIANINLRLEVEGQPVELVELVGHVCA

hRPA32      SQV--------------TIVGIIRHAEKAPTNIVYKIDDMTAAP----MDVRQWVDTDDT
TtTeb2      AIITAKFEFLQSINDSPKIMGKLSDSTG-CIEVVIQKSKMSDELPEFVQAYEIELQNN--
TtRlp2      SLYGRAYTL---KGEQPFMAIQISDLSGICSAILYQPTNDEENLVEYLKRTENWQSNPDK
                                                                    170

hRPA32      SSENTVVPPETYVKVAGHLRSF----QNKKSLVAFKIMPLEDMNEFTTHILEVINAHMVL
TtTeb2      ------GNRHKYVRAMLKMRKN-----AQIQLLYFSI--VNDANEISRHGLDLCLRYLQR
TtRlp2      ------MLNGTYVKVIVKPKYSVTESVWKNNCIAIKI--IQNANEITQHNLDVIKCYLER
                           185         197                 215

hRPA32      SKANSQPSAGRAPISNPG-MSEAGNFGGNSFMPANGLTVAQNQVLNLIKACP-------R
TtTeb2      KHGIED--FMHMTNDKAHNNHNASAQKVHYQIDRN--QQPKEQVLELMRQILKHNPNDQI
TtRlp2      KDGLIQ--KVKSPIQNNPIYIKA---KQREEMEK----RNRIEISTLKESILQKDM--QI
               228

hRPA32      PEGLNFQDLKNQLKHMSVSSIKQAVDFLSNEGHIYSTVDDDHFKSTDAE
TtTeb2      PKSKIIEFFQSQLNQVQI---NQILQQLVSANEIFSVGSDNYLLNV---
TtRlp2      EEEH--------IQPIQ--------------------------------
```

Figure 5.3. Rlp2 N-terminal domain construct design. (*a*) Table of Rlp2 N-terminal constructs tested for soluble expression and Teb3 binding. (*b*) Multiple alignment of hRPA32, TtTeb2, and TtRlp2 performed by Clustal Omega [9].

Conclusions and future directions

The data presented in this chapter contributed to analysis of the pull down LC/MS/MS data presented in Upton et al. 2017 [5]. Briefly, Teb3 was tagged at the endogenous locus and purified from cell extract. Rlp2 was identified as one of the components bound to Teb3. However, it remains to be determined if Rlp2 exists in the cell as a dimer with Teb3 or if it forms a heterotrimeric complex with Rlp1 which was also pulled down with Teb3.

That these OB-folds are apparently interchangeable in the formation of these RPA-like complexes is a subject of extreme interest to structural biology and the understanding of protein-protein interactions. It will be interesting to note the differences between the interaction interfaces between Teb3-Teb2 vs. Teb3-Rlp2. Optimal crystal constructs will likely require trimming the N-terminus of the N-terminal OB fold of Rlp2 to generate the minimum OB fold that can still bind to Teb3. Removal of the putative C-terminal dimerization domain may or may not be necessary as dimerization can often facilitate crystal packing. It also remains to be determined if Teb3-Rlp2 can interact with *Tetrahymena* Rlp1 or Rpa1 to form the trimeric complex and whether or not the excess C-terminal or N-terminal domains are required or inhibit formation of the heterotrimer. These complexes, if they form, also warrant structural investigation for reasons stated above as well as for general understanding of RPA complexes.

REFERENCES

1. Jiang J, Chan H, Cash DD, Miracco EJ, Ogorzalek Loo RR, Upton HE, Cascio D, O'Brien Johnson R, Collins K, Loo JA *et al*: Structure of Tetrahymena telomerase reveals previously unknown subunits, functions, and interactions. *Science* 2015, 350(6260):aab4070.

2. Chan H, Wang Y, Feigon J: Progress in Human and Tetrahymena Telomerase Structure. *Annu Rev Biophys* 2017, 46:199-225.

3. Rice C, Shastrula PK, Kossenkov AV, Hills R, Baird DM, Showe LC, Doukov T, Janicki S, Skordalakes E: Structural and functional analysis of the human POT1-TPP1 telomeric complex. *Nat Commun* 2017, 8:14928.

4. Chen C, Gu P, Wu J, Chen X, Niu S, Sun H, Wu L, Li N, Peng J, Shi S *et al*: Structural insights into POT1-TPP1 interaction and POT1 C-terminal mutations in human cancer. *Nat Commun* 2017, 8:14929.

5. Upton HE, Chan H, Feigon J, Collins K: Shared Subunits of Tetrahymena Telomerase Holoenzyme and Replication Protein A Have Different Functions in Different Cellular Complexes. *J Biol Chem* 2017, 292(1):217-228.

6. Min BS, Collins K: Multiple Mechanisms for Elongation Processivity within the Reconstituted Tetrahymena Telomerase Holoenzyme. *Journal of Biological Chemistry* 2010, 285(22):16434-16443.

7. Miao W, Xiong J, Bowen J, Wang W, Liu Y, Braguinets O, Grigull J, Pearlman RE, Orias E, Gorovsky MA: Microarray analyses of gene expression during the Tetrahymena thermophila life cycle. *PLoS One* 2009, 4(2):e4429.

8. Xiong J, Yuan D, Fillingham JS, Garg J, Lu X, Chang Y, Liu Y, Fu C, Pearlman RE, Miao W: Gene network landscape of the ciliate Tetrahymena thermophila. *PLoS One* 2011, 6(5):e20124.

9. Sievers F, Wilm A, Dineen D, Gibson TJ, Karplus K, Li WZ, Lopez R, McWilliam H, Remmert M, Soding J *et al*: Fast, scalable generation of high-quality protein multiple sequence alignments using Clustal Omega. *Mol Syst Biol* 2011, 7.

CHAPTER SIX

Progress in Human and *Tetrahymena*

Telomerase Structure Determination

Progress in Human and *Tetrahymena* Telomerase Structure Determination

Henry Chan,* Yaqiang Wang,* and Juli Feigon

Department of Chemistry and Biochemistry, University of California, Los Angeles, California 90095-1569; email: feigon@mbi.ucla.edu, henrychan106@ucla.edu, yaqiang@mbi.ucla.edu

Annu. Rev. Biophys. 2017. 46:199–225

First published online as a Review in Advance on March 15, 2017

The *Annual Review of Biophysics* is online at biophys.annualreviews.org

https://doi.org/10.1146/annurev-biophys-062215-011140

*These authors contributed equally to this manuscript.

Keywords

telomerase RNA, electron microscopy, telomerase reverse transcriptase, CST, replication protein A, H/ACA RNP

Abstract

Telomerase is an RNA–protein complex that extends the 3′ ends of linear chromosomes, using a unique telomerase reverse transcriptase (TERT) and template in the telomerase RNA (TR), thereby helping to maintain genome integrity. TR assembles with TERT and species-specific proteins, and telomerase function in vivo requires interaction with telomere-associated proteins. Over the past two decades, structures of domains of TR and TERT as well as other telomerase- and telomere-interacting proteins have provided insights into telomerase function. A recently reported 9-Å cryo–electron microscopy map of the *Tetrahymena* telomerase holoenzyme has provided a framework for understanding how TR, TERT, and other proteins from ciliate as well as vertebrate telomerase fit and function together as well as unexpected insight into telomerase interaction at telomeres. Here we review progress in understanding the structural basis of human and *Tetrahymena* telomerase activity, assembly, and interactions.

Contents

INTRODUCTION AND OVERVIEW

Telomeres and telomerase are the nucleoprotein complexes that together protect the ends of linear chromosomes and provide a solution to the end replication problem (10, 11). First detected ~30 years ago in the ciliated protozoan *Tetrahymena thermophila* as a terminal transferase activity (52, 53), telomerase was subsequently found to extend the 3′ ends of linear chromosomes by reverse transcription of telomeric repeats (TTAGGG in vertebrates and TTGGGG in *Tetrahymena*) through the use of an integral RNA template (10) (**Figure 1*a***). Since its discovery, telomerase has emerged as a major player in tumorigenesis, stem cell renewal, and cellular aging. Shortened telomeres can lead to cellular senescence, and a majority of cancers require upregulated telomerase activity to maintain immortal cell replication (4, 5, 9, 44, 100, 146). Additionally, telomerase insufficiency or dysregulation due to mutations in telomerase proteins, telomerase RNA, and telomere-associated proteins are linked to a wide variety of inherited diseases (4, 42, 68, 112, 137, 139, 146, 160). The catalytic core of telomerase comprises an integral telomerase RNA [TR; also called hTR or TERC (human), TER (ciliate), and TLC1 (yeast)], identified in 1989 (54), and the telomerase reverse transcriptase (TERT), identified in 1997 (92). Since then, a host of additional proteins that aid in assembly, recruitment, regulation, activity, and nucleic acid handling have been identified (38, 112, 140, 150).

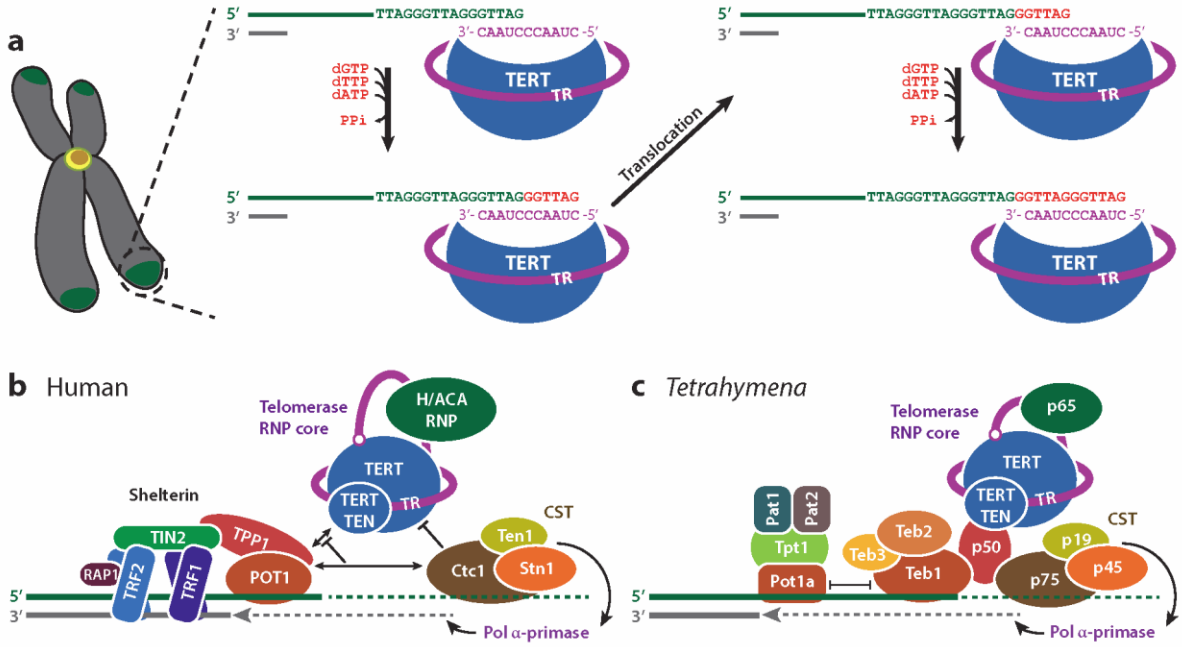

Figure 1

Schematics of telomere extension by telomerase and of human and *Tetrahymena* telomerase and telomerase-associated proteins at the telomeres. (*a*) Telomerase uses its integral RNA template for the reverse transcription of telomeric repeats onto the 3′ ends of chromosomes. The 3′ end of the DNA aligns with the 3′ end of the template in register to allow synthesis of the telomere repeat. After synthesis of a repeat (GGTTAG in humans), the telomerase template must shift register (translocate) by one repeat before nucleotide addition can reinitiate. (*b*) The human telomerase RNP core (TERT, TR, H/ACA scaRNP proteins) is recruited to telomeres by the shelterin complex. CST interaction with TPP1–POT1 inhibits telomerase activity. (*c*) *Tetrahymena* telomerase RNP core (TERT, TR, p65) is constitutively assembled with the p50, TEB, and CST accessory proteins. Abbreviations: RNP, ribonucleoprotein; scaRNP, small Cajal body ribonucleoprotein; TERT, telomerase reverse transcriptase; TR, telomerase RNA.

The protein components beyond TERT that constitute the telomerase holoenzyme have historically been difficult to define. Many associate with the telomere and catalytic core transiently as a function of cell cycle and lack obvious homology among different organisms (89, 91, 140). In addition, TRs are divergent between species in sequence and size, ranging from 147 to 205 nucleotides (nt) in ciliates, 312 to 559 nt in vertebrates, and 928 to >2,425 nt in yeasts (121, 122), and interact with apparently species-specific proteins. However, biochemical, genetic, and recent structural studies of TR, TERT, and other telomere- and telomerase-associated proteins have enhanced our understanding of their functions and revealed that these components often share commonalities of structure, function, and evolutionary themes (91, 112, 122).

These commonalities were highlighted in the recent 9-Å cryo–electron microscopy (EM) structure of *Tetrahymena* telomerase; nearly 30 years after the discovery, there is now a near complete model of the *Tetrahymena* telomerase holoenzyme (69). An unexpected finding was that components of the constitutively assembled *Tetrahymena* telomerase holoenzyme share homologies with human, yeast, and plant protein complexes that interact with telomerase at telomeres. This study has allowed three decades of data on telomerase function and interaction at telomeres from diverse organisms to be placed in a structural context (41, 69). Here we review structural advances in the

field for ciliate (primarily *Tetrahymena*) and vertebrate (primarily human) telomerase with respect to TERT and TR domains, other proteins that bind to TR, and the proteins involved in G-strand single-stranded telomere repeat DNA (sstDNA) handling.

Overview of Human and *Tetrahymena* Telomerase and Interaction at Telomeres

The minimal components for telomerase catalytic activity in vitro are TERT and TR. Early studies established the basic mechanism for telomerase activity whereby TERT processively synthesizes multiple repeats of the G-strand telomeric sequence using the template, contained within the larger TR and comprising ~1.5–1.8 repeats of a sequence complementary to the telomeric repeat (53, 122). The 3′ end of the template aligns and base pairs with the 3′ end of the G-strand overhang, leaving template bases complementary to a single telomere repeat unpaired, and nucleotides are processively added until the 5′ end of the template is reached (**Figure 1*a***). Upon completion of one telomere repeat, the template has to realign with the newly formed end of the telomere, a process known as translocation, so that subsequent telomere repeats can be added. The complete steps in the enzymatic cycle have been the subject of intense investigations that are beyond the scope of this review (14, 119, 175), but many details, especially for the translocation step, remain to be defined. At some point, the synthesis of the G-strand stops, and DNA-polymerase α-primase is recruited to synthesize the complementary C-strand (**Figure 1*b*,*c***).

Telomerase contains multiple proteins in addition to TERT that bind directly or indirectly to the single TR. Here we define the telomerase ribonucleoprotein (RNP) core as TR, TERT, and additional proteins that bind directly to the TR and stay associated at least temporarily after assembly (**Figures 1** and **2**). Depending on the organism, the telomerase ribonucleoprotein (RNP) core can be constitutively associated or transiently associated via cell cycle regulation with other accessory proteins. In humans, the telomerase core RNP includes, in addition to TERT, the H/ACA small Cajal body RNP (scaRNP) complex proteins: dyskerin, NOP10, NHP2, and likely GAR1 [although it contacts dyskerin and not TR (84, 130)], as well as TCAB1 (166) [also called WDR79 (161)]—the gene product of WRAP53 (97), which directs the telomerase RNP to Cajal bodies (**Figure 2*a***) (39, 140). Human telomeric DNA is protected by the six-component shelterin protein complex composed of the following: RAP1; the double-stranded telomeric DNA-binding TRF1 and TRF2; the sstDNA-binding POT1; and TIN2 and TPP1, which serve as mediators for shelterin assembly and telomerase recruitment (**Figure 1*b***) (34, 60, 150, 169, 180, 189). Telomerase is recruited to telomeres primarily by a direct TPP1 interaction with TERT (111, 145, 189), and telomerase activity requires a switch in TPP1–POT1 function from telomere end protection to telomerase processivity factor (144, 169). Association of human telomerase to shelterin is mutually exclusive with and inhibited by a TPP1–POT1 interaction with the Ctc1–Stn1–Ten (CST) complex (24). In humans, the sstDNA-binding CST inhibits telomerase activity and recruits the DNA-polymerase α-primase complex (Pol α-primase) for C-strand synthesis (**Figure 1*b***) (22, 24). CST is related to the trimeric replication protein A (RPA) complex, the major single-stranded DNA–binding protein that plays numerous roles in DNA replication and repair (123, 153).

In contrast to human telomerase, *Tetrahymena* telomerase is constitutively assembled (104, 165). TERT, TR, and the La-related protein p65 comprise the *Tetrahymena* telomerase RNP core (**Figures 1*c*** and **2*b***), as revealed by the cryo-EM structure (69). p50 links TERT to the two recently structurally characterized RPA-like sstDNA-binding complexes TEB (which comprises Teb1, Teb2, and Teb3) and CST (61, 69, 70). TEB is important for proper recruitment of telomerase to telomeres (69, 165), whereas *Tetrahymena* CST, comprising p75, p45, and p19 (69), is linked to C-strand synthesis (**Figure 1*c***) (168). The G-overhang is capped by a four-protein

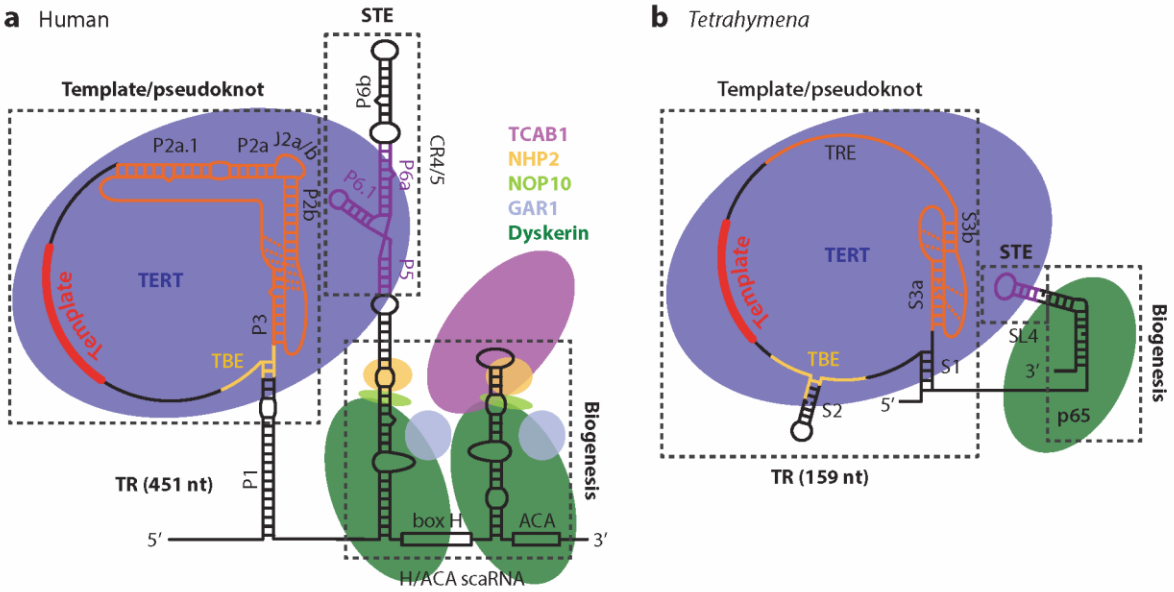

Figure 2

Schematics of human and *Tetrahymena* telomerase RNP cores illustrating TR secondary structure and known protein components. TR contains three major structural and functional domains: template/pseudoknot (t/PK), stem terminus element (STE), and biogenesis. (*a*) Human telomerase core RNP includes TERT, TR, and the H/ACA proteins. Human TERT (*blue*) interacts with the t/PK and the STE [conserved regions 4 and 5 (CR4/5)] (*violet*). In the t/PK, the template, pseudoknot, and template boundary element (TBE) are highlighted in red, orange, and yellow, respectively. Helical regions are labeled as P (20). The biogenesis domain comprises an H/ACA scaRNA motif that interacts with the H/ACA proteins dyskerin (*dark green*), NOP10 (*light green*), NHP2 (*gold*), GAR1 (*pale blue*), and TCAB1 (*light purple*). (*b*) *Tetrahymena* telomerase RNP core includes TR, TERT (*blue*), and p65 (*dark green*). Domains of the t/PK and STE are colored as in panel *a*, with the addition of the single-stranded template recognition element (TRE) in orange. The biogenesis domain at the 3′ end of TR is bound by p65; its N-terminal La module binds the TR polyU tail for biogenesis, and the C-terminal xRRM binds stem 4 around the GA bulge for assembly. Abbreviations: nt, nucleotide; RNP, ribonucleoprotein; scaRNA, small Cajal body ribonucleoprotein; TR, telomerase RNA.

complex—Pat1, Pat2, Tpt1, and Pot1a—and Pot1a is proposed to be mutually exclusive with TEB/telomerase binding to the G-overhang (**Figure 1*c***) (124).

Although there are many seminal structural studies of telomere- and telomerase-associated proteins from yeast, specifically the Pot1 and CST proteins (48, 81, 108, 155), there are few structures from yeast TRs (17) and yeast telomerase RNP cores. For this reason and also space limitations, this review focuses on human and ciliate *Tetrahymena* telomerase. We refer the interested reader to excellent reviews on yeast and plant telomerase (28, 77, 89, 94, 98, 120, 172, 173). Advances in single molecule and fluorescence resonance energy transfer studies of telomerase are covered in this volume by Parks & Stone.

TELOMERASE RNA DOMAIN STRUCTURES

The TR secondary structure and associated proteins of the human and *Tetrahymena* telomerase RNP core are illustrated in **Figure 2**. TR variability in size, sequence, and domains can be explained by its identification as a rapidly evolving long noncoding RNA, with regions of structural homology attributed to its roles in TERT interaction and function (113, 122). Two nearly

universally present structural elements that are required together for TERT binding and catalysis in vitro have been identified: a template/pseudoknot (t/PK) (also called core or pseudoknot) domain and a stem terminus element (STE) [also called activating domain and, in vertebrates, conserved regions 4 and 5 (CR4/5)] (122, 158, 187). In addition, TRs from diverse organisms contain a 3′ species-specific RNA stability/biogenesis element (**Figure 2**). Differences between organisms in the requirements for 3′-end processing, stabilization, and nuclear compartment localization account for much of the diversity in TR and TR binding proteins (**Figure 2**) (39, 122, 167).

Template/Pseudoknot Domain

The t/PK includes the template, a 5′ template-adjacent template boundary element (TBE) (21, 78, 162), and a pseudoknot connected to the 3′ end of the template by a single-stranded region, usually enclosed in a circle by a stem (**Figure 2**). Ciliates have the smallest and simplest H-type pseudoknots, with ~30 nt, whereas vertebrates and yeasts have pseudoknots with additional subdomain(s) in their longer stem 1 (P2 in humans). In vertebrate telomerase, the full-length pseudoknot includes a minimal pseudoknot (P2b–P3), essentially equivalent to the complete ciliate pseudoknot, containing most of the conserved bases (**Figures 2** and **3*a***); an adjacent helical region that includes a 5–6-nt bulge conserved in location but not sequence (P2a–J2a/b–P2b); and, at least in mammals, a helical extension (P2a.1) (**Figures 2*a*** and **3*b***) (121). The structure of the human telomerase minimal pseudoknot (**Figure 3*a***) (74, 157) established that the pseudoknot is stabilized by tertiary interactions between the loops and stems and, in particular, a run of U · A · U base triples that has become known as the triple helix (127, 147). A direct correlation between pseudoknot stability and telomerase activity was demonstrated by thermodynamic analysis, through the use of nucleotide substitutions and compensatory mutations (157). Biochemical, mutational, and structural studies of yeast and medaka fish pseudoknots have revealed a conserved structure and confirmed the importance of the base triples for pseudoknot stability and telomerase function (**Figure 3*a***) (17, 127, 147, 163, 171). A recent structure of the *Tetrahymena* pseudoknot revealed a more limited set of base triples, explaining in part its lower stability (**Figure 3*a***) (18, 69).

Figure 3

Structures of TR domains. (*a*) Solution structures of minimal (P2b–P3) pseudoknots from human (*Homo sapiens*) (PDB ID 2K95), yeast (*Kluyveromyces lactis*) (PDB ID 2M8K), and *Tetrahymena* (*Tetrahymena thermophila*) (PDB ID 2N6Q). Secondary structure schematic of the human P2b–P3 pseudoknot is shown on far left (18, 74). (*b*) Sequence and secondary structure of the human TR t/PK domain. Subdomains for which NMR structures have been determined are boxed with dashed lines: P2a–J2a.1–P2a.1 (*purple–black–orange*), P2a–J2a/b–P2b (PDB ID 2L3E) (*orange–green–red*), P2b–P3 pseudoknot (*red–blue–gold*). P1b (*tan*) is the closing helix of the TBE (187). (*c*) Model structure of the human t/PK. For the model, the subdomain structures were computationally combined to make the P2–P3 pseudoknot (188). The single-stranded region (*gray*) containing the template (*black*) is shown with a DNA primer (*cyan*) bound. (*d*) Sequence and secondary structures of medaka (*Oryzias latipes*) STE (CR4/5), NMR structure (PDB ID 2MHI), and crystal structure of the complex with medaka TERT TRBD (PDB ID 4O26). Nucleotides proposed to interact with TRBD are colored green. (*e*) Sequence and secondary structures of *Tetrahymena* STE (stem-loop 4), NMR structure (PDB ID 2FEY), and structure of the complex with *Tetrahymena* p65 and TERT TRBD [modeled from crystal structure of p65 xRRM-stem 4 (PDB ID 4ERD), NMR structure of loop 4 (PDB ID 2M21) (149)], and TRBD from the cryo–electron microscopy model (69). The GA bulge nucleotides involved in p65 binding are colored cyan. (*f*) Sequence and secondary structure of human TR biogenesis domain (H/ACA) and secondary structure and solution NMR structure of the 3′ apical stem-loop (CR7) containing the CAB and BIO boxes. Open boxes within the CR7 indicate the location of the CAB box (*magenta*) and BIO box (*green*). Nucleotides important for TCAB1 and putative NHP2 binding are highlighted in magenta and green, respectively, in the secondary structure schematic and are colored by residue type on the surface of the NMR solution structure of the CR7 hairpin (PDB ID 2QH2): A (*orange*), U (*green*), G (*blue*), C (*red*). Human TR domains are named P for paired regions and J for junction regions (20, 159). Abbreviations: CR4/5; conserved regions 4 and 5; NMR, nuclear magnetic resonance; STE, stem terminus element; TBE, template boundary element; TERT, telomerase reverse transcriptase; t/PK, template/pseudoknot; TR, telomerase RNA; TRBD, telomerase RNA binding domain.

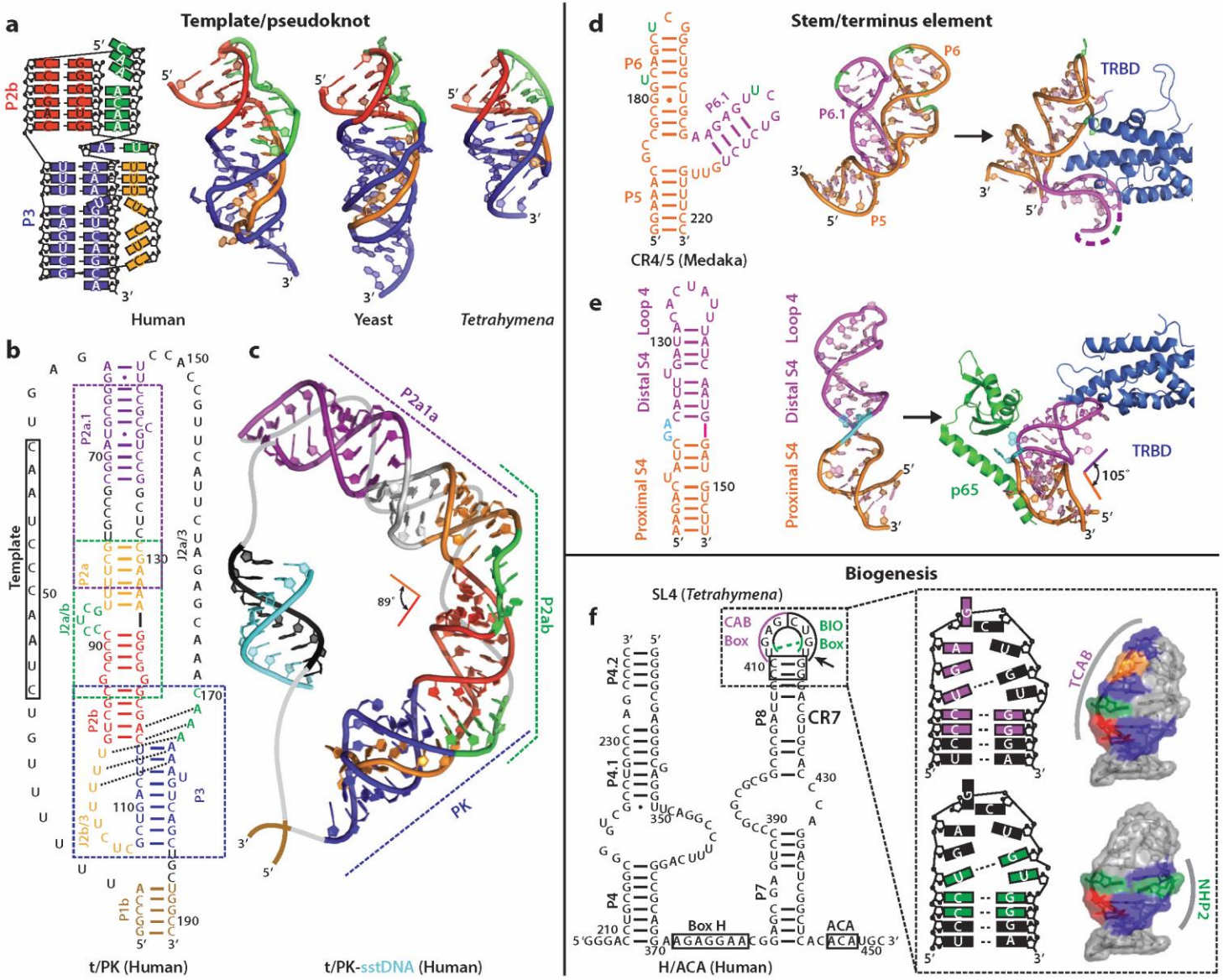
a
Template/pseudoknot
P2b
P3
Human
Yeast
Tetrahymena
b
Template
P2a.1
P2a
J2a/b
J2a/3
P2b
J2b/3
P3
P1b
t/PK (Human)
c
P2a1a
P2ab
PK
89°
t/PK-sstDNA (Human)
d
Stem/terminus element
P6
P6.1
P5
CR4/5 (Medaka)
TRBD
e
Loop 4
Distal S4
Proximal S4
p65
105°
TRBD
Biogenesis
f
SL4 (Tetrahymena)
CAB Box
BIO Box
CR7
P8
P4.2
P4.1
P4
P7
Box H
ACA
H/ACA (Human)
TCAB
NHP2

Structures and dynamics of the additional subdomains of the pseudoknots of human and of medaka, the latter of which contains the smallest known vertebrate TR (312 nt) (178), have also been studied by nuclear magnetic resonance (NMR) (73, 171, 188). The structure of the human P2a–J2a/b–P2b subdomain [P2ab] showed that the 5-nt J2a/b bulge induces a large (89°) and somewhat flexible bend between P2a and P2b (**Figure 3*b*,*c***) that defines the overall topology of the full-length pseudoknot (188). In mammals, P2a.1 is connected to P2a by an internal loop that forms a series of mismatched base pairs, so P2a and P2a.1 [P2a1a] essentially form a single helix as shown for human TR. In medaka, this region was predicted to be single stranded but appears to form a small hairpin stacked on P2a, extending the similarity between mammalian and nonmammalian vertebrate TR full-length pseudoknots (171). The subdomain structures of the full-length pseudoknot were computationally combined, and the single-stranded template and adjacent nucleotides were included to make models of the t/PK for human TR (**Figure 3*c***) and medaka TR (171, 188). These models approximate the structure of the t/PK when bound to TERT; t/PK may form alternate structures when not bound to TERT (30, 47, 59, 114).

The t/PK also contains the TBE, a short helix flanked by single-stranded DNA. In human TR, this helix also closes the t/PK into a circle, whereas in *Tetrahymena*, it is a hairpin located a few nucleotides 5′ of the template (**Figure 2**) (21, 67, 78, 133, 187). The TBE binds with high affinity to the TERT TRBD (telomerase RNA binding domain) (117), providing an anchor point that prevents TR nucleotides beyond the 5′ end of the template from being pulled into the active site (discussed below) (67, 69).

Stem Terminus Element

In vertebrate TR, the STE is the CR4/5, which is a helical region extending from the 5′ hairpin of the H/ACA scaRNA domain (**Figures 2** and **3*d***). This region of TR forms a three-way junction (P5, P6, and P6.1 emanating from an internal loop); the P6.1 hairpin has a 3-nt loop and is highly conserved in vertebrates (135). The binding site was mapped to TRBD by cross-linking (**Figure 3*d***) (12). The structure of medaka STE (CR4/5) has been solved both free from (73) and bound to TERT TRBD (**Figure 3*d***) (63). Binding to the TRBD induces a large conformational change in the position of P6.1 relative to P6 and a rearrangement of base interactions in the three-way junction. P6.1 is almost parallel to P6 in the free RNA, but in complex with TRBD, it is approximately perpendicular to and on the opposite side of P6. TRBD helices between the QFP and T motifs insert deep into the cleft between the two stems, forming an extensive interface (**Figure 3*d***). Although the nucleotides of the P6.1 hairpin loop are not visible in the medaka TRBD–CR4/5 crystal structure, the P6.1 apical loop is proposed to insert at the interface between the TRBD and the C-terminal extension (CTE) (12, 63, 69). Two potential pseudouridine (ψ) modification sites were identified in human P6.1 by *N*-cyclohexyl-*N*′-*β*-(4-methylmorpholinium) ethylcarbodiimide *p*-tosylate probing at the highly conserved U307 and the loop closing U306, and structural studies indicated that these ψ affected the loop conformation (72). More recent genome-wide mapping by ψ-seq has confirmed the U307 modification site (143), and it will be interesting to see if it is important in the P6.1–CTE interaction.

In ciliates, the STE is simply a stem-loop, equivalent to P6.1. The structures of *Tetrahymena* stem-loop 4 (25), loop 4 (134), and stem 4 bound to the C-terminal xRRM of p65 have been solved (**Figure 3*e***) (149). Binding of p65 xRRM at a conserved GA bulge in stem-loop 4 induces a large conformational change that is important for hierarchical assembly of p65–TR with TERT (**Figure 3*e***) (116, 149, 152). Comparing the medaka CR4/5–TRBD structure with the pseudoatomic cryo-EM model of stem-loop 4–TRBD explains why the interaction of loop 4 with the TRBD is much weaker than CR4/5 with the TRBD, because the single stem would not have the

additional contacts afforded by P6 in vertebrates, and explains why p65 is required to help position loop 4 interact with TERT.

Telomerase RNA Biogenesis Element and Protein Interactions

The biogenesis element in vertebrate telomerase is an H/ACA scaRNA domain and is located at the 3′ end of the mature TR (**Figure 2**). Like other eukaryotic H/ACA RNAs, it contains two hairpins with large internal loops, a 5′ and 3′ hairpin followed, respectively, by an H box and ACA box (**Figure 3*f***). These hairpins each bind a set of H/ACA RNP proteins (dyskerin, NOP10, NHP2, GAR1) (**Figure 2*a***) (37). However, unlike classical H/ACA scaRNAs, the internal loops do not serve as guide sequences for site-specific pseudouridylation of snRNAs; rather, the TR H/ACA RNP is important for TR stability, localization to Cajal bodies, and possibly assembly (31, 39, 167). The 3′ hairpin apical loop contains the CAB box sequence (132) that binds TCAB1 (161, 166), which targets telomerase to Cajal bodies (159, 166). Structures of single hairpin archaeal H/ACA proteins, complexes, and H/ACA RNPs with bound substrates (56, 87, 99) and yeast H/ACA dyskerin/Cbf5-NOP10-L7Ae-GAR1 complexes (35, 85, 86) as well as NHP2 alone (76) have been reported and provide insight into how these proteins might assemble with TR (reviewed in 57, 75, 183). Archaeal H/ACA RNPs have the protein L7Ae, which specifically binds a kink-turn, in place of NHP2.

The 5′ hairpin of the vertebrate TR H/ACA domain is extended by the STE, the CR4/5 element that contains the three-way junction discussed above. The 3′ hairpin apical loop contains both the CAB box on the 5′ side and a region referred to as the BIO box on the 3′ side (**Figure 3*f***) (38). Structural and functional studies of wild-type and mutant hairpins established the sequence and structural elements important for targeting to Cajal bodies and RNP biogenesis, respectively (38, 159). The upper stem and conserved bulge U in the BIO box correspond to the predicted binding site for NHP2 (**Figure 3*f***) (76, 159). It is interesting to note that an equivalent site with a bulge U does not appear to be present in the 5′ hairpin. The BIO box has been shown to contribute to the enhanced assembly of the dyskerin–NOP10–NHP2–NAF1 complex with the H/ACA domain that is required for biological accumulation of TR (38). Association of the dyskerin complex has also been shown to protect the 3′ end from exonucleolytic digestion (39, 148). Thus, the 3′ H/ACA RNP contributes to biogenesis, stabilization, and localization. The H/ACA RNP may also contribute to positioning of the STE, but this remains to be determined.

In *Tetrahymena* TR, stem 4 and its 3′ UUUU single-stranded end, in complex with p65, function as the biogenesis element (**Figure 2*b***). In contrast to the vertebrate TR transcribed by RNAP II, ciliate TR is transcribed by RNAP III (39, 54). The polyU tail at the 3′ end of RNAP III transcripts are cotranscriptionally bound and protected by the La module (composed of La and RRM domains) of La protein. The N-terminal La module of p65, a LARP7 (La-related protein group 7), replaces that of La on the 3′ end of stem-loop 4, while its C-terminal xRRM domain binds and bends stem 4 (**Figure 3*e***) (149). Thus, p65 plays a dual role in TR stability and RNP assembly.

TELOMERASE REVERSE TRANSCRIPTASE DOMAIN STRUCTURES

The Telomerase Reverse Transcriptase Ring

TERT contains four evolutionarily conserved functional domains: TERT-essential N-terminal (TEN) domain, TRBD, reverse transcriptase (RT) domain, and CTE (**Figure 4*a***) (6, 71, 102,

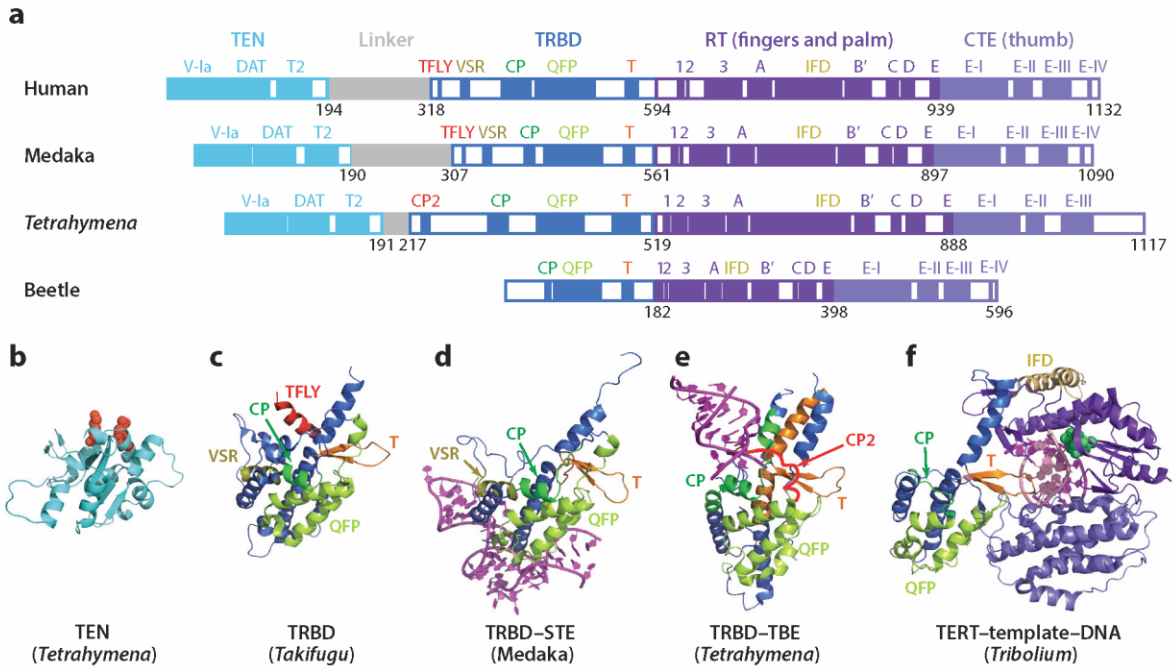

Figure 4

Domains and structures of TERT. (*a*) Domains and conserved motifs of human, medaka, *Tetrahymena*, and beetle TERTs, aligned at the RT domains. Crystal structures of (*b*) *Tetrahymena* TEN (PDB ID 2B2A) (*c*) *Takifugu* TRBD (PDB ID 4LMO), (*d*) medaka TRBD–STE complex (PDB ID 4O26), (*e*) *Tetrahymena* TRBD–TBE complex (PDB ID 5C9H), and (*f*) flour beetle TERT–template–DNA complex (PDB ID 3KYL). In panel *b*, residues that are proposed to be involved in interaction of the TEN domain with p50 (and TPP1 in human) are red spacefill. RNA and DNA are magenta and pink, respectively. The active site in panel *f* is green spacefill. Abbreviations: CTE, C-terminal extension; RT, reverse transcriptase; STE, stem terminus element; TEN, TERT-essential N-terminal; TERT, telomerase reverse transcriptase; TRBD, telomerase RNA binding domain.

121, 122, 177). Crystal structures of *Tribolium castaneum* TERT without and with an RNA DNA hybrid hairpin that mimics the template–DNA complex revealed that TRBD, RT, and CTE form a ring (**Figure 4*f***) (49, 106). Because *Tribolium* TERT lacks the TEN domain and the TR has not yet been found, questions have been raised about whether it might be another type of RT (83); regardless, its ring shape is clearly consistent with the EM maps for both human and *Tetrahymena* telomerase (69, 70, 105, 138). The RT includes the enzyme active site where the TR template is located, and the CTE promotes telomerase processivity; these two conserved domains correspond to the palm and fingers and the thumb domains, respectively, found in other polymerases (6, 177). The RT domain has two telomerase-specific regions—motif 3, which facilitates the realignment between DNA and RNA (179), and the insertions of fingers domain (IFD), which mediates telomerase processivity and facilitates telomerase recruitment to telomeres (26, 27, 49, 96). The *Tribolium* IFD is much smaller than that in human and *Tetrahymena*, and there is no good homology model in those organisms. The TRBD has specific binding sites for the TBE and the STE (1, 12, 58, 67, 79). *Tribolium* TRBD is also much smaller than that of *Tetrahymena* and vertebrates (**Figure 4*a***).

Telomerase Reverse Transcriptase Domain Structures and Telomerase RNA Interactions

Two *Tetrahymena* and two vertebrate TRBD structures have been determined (**Figure 4*c–e***) (58, 63, 67, 136). The recently reported crystal structure of the complete *Tetrahymena* TRBD with the TBE revealed the interface between TRBD CP2 (1) and the TBE (SL2 and its adjacent single strands) (**Figure 4*e***) (67). In vertebrates, the TFLY motif (equivalent to CP2 in ciliates) (**Figure 4*c***) within the N-terminus of the *Takifugu rubripes* TRBD has been shown to interact with P1 and adjacent single strands (vertebrate TBE) (58). The crystal structure of medaka TRBD with CR4/5 defined the TR interaction with this second TRBD high-affinity binding site (**Figure 4*d***), consistent with cross-linking results (12). The TEN domain, which is connected by a linker of variable length to the TRBD, is proposed to interact with DNA–template duplex and is essential for processivity (**Figure 4*b***) (66, 175, 184). The *Tetrahymena* TEN domain has a unique fold, with phylogenetically conserved residues that are important for activity and implicated in sstDNA binding (66). The location of the TEN domain relative to the TERT ring and TR was revealed in the cryo-EM model structure of *Tetrahymena* holoenzyme (**Figure 5**) (69).

ELECTRON MICROSCOPY STRUCTURES OF TELOMERASE

Negative Stain Electron Microscopy Structures

Negative stain EM structures at ~25-Å resolution of human (138) and *Tetrahymena* (70) telomerase were first reported in 2013. A dimeric human telomerase was affinity purified using a DNA primer from cells that had been transiently transfected with TR and TERT (32), and mass spectrometry indicated it contained TERT, TR, dyskerin, and NOP10 (138). The three-dimensional reconstruction of human telomerase showed a dumbbell shape with TERT fit into the density at each of the knobs; the connecting rod was attributed to a duplex region of TR.

There has been conflicting data on whether human telomerase is a monomer (3, 37, 39, 176) or obligate dimer (29, 138, 142, 174). A recent study established that in vitro human TERT–TR reconstitution yields active monomers or dimers depending on the purification method, and the dimerization can be suppressed both in vitro and in vivo by removing or modifying the linker between TRBD and TEN (176). *Tetrahymena* and yeast telomerase have been clearly shown to be monomers (7, 16).

In the negative stain EM study of *Tetrahymena* telomerase, samples with affinity tags on the subunits were used to identify the location of six of the seven then-known proteins and of TR domains (**Figure 5*a***) (70). A surprise of the negative stain EM map was the identification of p50 as a central hub that links the catalytic core, Teb1, and p75–p45–p19, and is essential for the processivity enhancement conferred by Teb1.

Cryo–Electron Microscopy Structure of *Tetrahymena* Telomerase

In the cryo-EM map at 9-Å resolution (69) protein α-helices, β-barrels, β-hairpins (but not β-sheets), and RNA helices can be readily identified when fit with known structures, but structures cannot be built de novo. Thus, the identification of subunit locations in the negative stain EM structure (70) and the NMR, crystal, and homology model structures of telomerase subunit domains (13, 49, 66, 69, 106, 136, 149, 169, 186) were crucial in constructing a pseudoatomic model of most of the holoenzyme (**Figure 5*a***) (41, 69). The pseudoatomic model of the telomerase RNP core was built starting from fitting TR, TERT, and p65 domain structures discussed above into

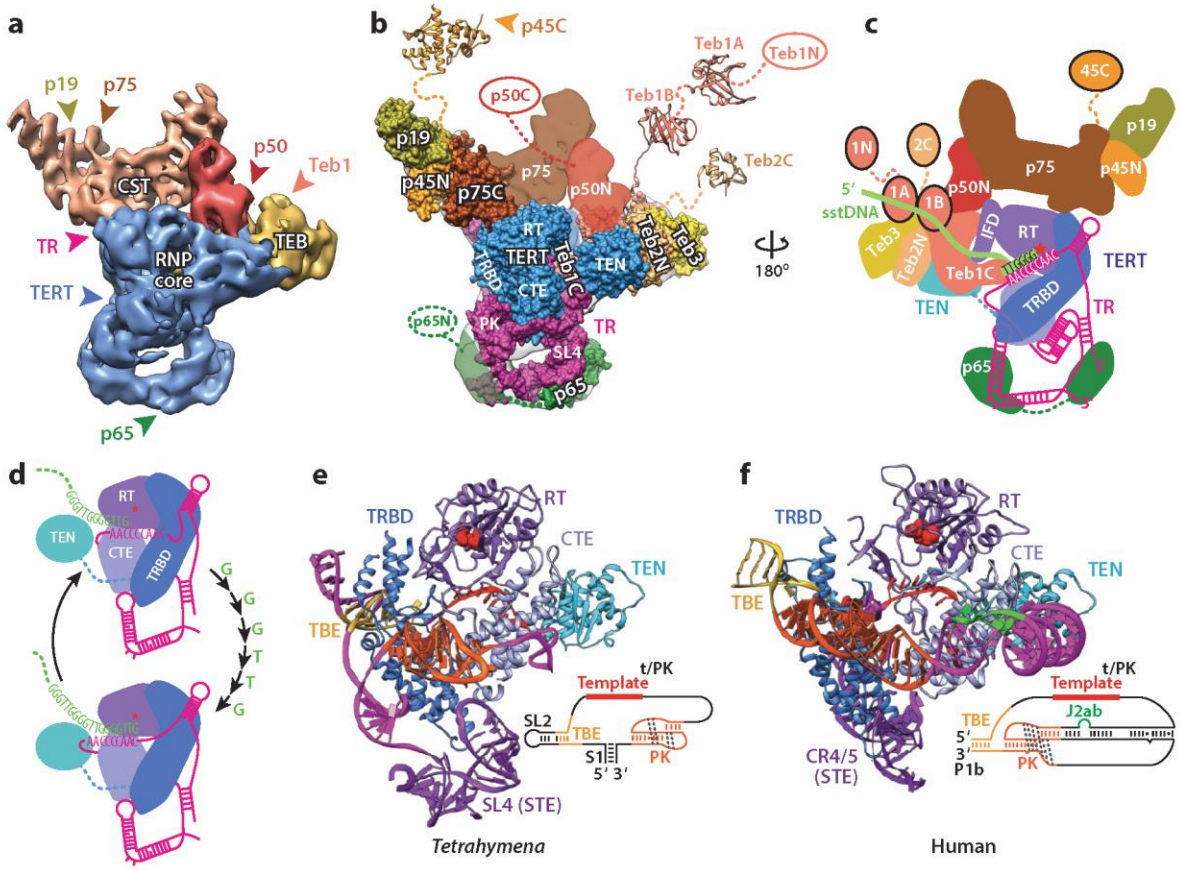

Figure 5

Cryo–electron microscopy (EM) structure of *Tetrahymena* telomerase and model of human TERT–t/PK. (*a*) Front view of the 9.4-Å cryo-EM map with the RNP core (*blue*), TEB (*gold*), CST (*tan*), and p50 (*red*). Arrows indicate location of protein C-terminus (or N-terminus for p50) and TR SL2 determined by Fab labeling and MS2 coat protein labeling, respectively, in negative stain EM (70). (*b*) Same color designation and labeling scheme as panel *a* but with pseudoatomic models of the RNP core, TEB trimer of OB folds, and CST trimer of OB folds. Additional domains of Teb1, Teb2, and p45, not visible in the cryo-EM map, are shown as crystal structures [Teb1A (PDB ID 3U4V), Teb1B (PDB ID 3U4Z), p45C (PDB ID 5DFN)], homology models (Teb2C based on PDB ID 1DPU), or ovals (70). (*c*) Schematic of *Tetrahymena* telomerase, 180° rotation from panel *b*, illustrating DNA bound to template and exit path. (*d*) Schematic illustrating movement of the template through the active site for one round of telomere repeat synthesis, and template boundary definition by the TBE. (*e*) Pseudoatomic model of *Tetrahymena* telomerase catalytic core, showing the path of TR on TERT. Inset shows schematic of the t/PK. TR elements in panels *e* and *f* are colored as in **Figure 2**. (*f*) Model of human telomerase catalytic core, based on the model of the human t/PK (171, 188), medaka CR4/5 with TRBD (PDB ID 4O26) (63), and the positions of homologous domains of *Tetrahymena* TR in the cryo-EM map. Inset shows schematic of the t/PK with TR elements colored as in the model. Abbreviations: CR4/5, conserved regions 4 and 5; CTE, C-terminal extension; OB, oligonucleotide/oligosaccharide binding; RNP, ribonucleoprotein; RT, reverse transcriptase; sstDNA, single-stranded telomere repeat DNA; STE, stem terminus element; TBE, template boundary element; TEN, TERT-essential N-terminal domain; TERT, telomerase reverse transcriptase; t/PK, template/pseudoknot; TR, telomerase RNA.

the EM map (**Figure 5*b***) (49, 66, 106, 136, 149). Of the TEB proteins, only Teb1 had been previously discovered (104); Teb2 and Teb3 were identified by mass spectrometry after discovering that the crystal structure of the three interacting oligosaccharide/oligonucleotide binding (OB) folds from the paralogous RPA complex (13) fit into a region of the EM map that could not be accounted for by the known proteins. Similarly, crystal structures of p19 and p45C that showed structural homology to Ten1 (OB fold) and Stn1C tandem winged-helix (WH) domains, respectively, suggested that the p75–p45–p19 complex is a CST, and the RPA complex also fit into a second site corresponding to the known locations of p75 and p19 (69). Despite its identification as a central hub, no homology or threading model of p50 could be identified that fit into the cryo-EM map, although it too appears to be a β-barrel, consistent with an OB fold. Of note, several protein domains are not visible in the cryo-EM map, specifically Teb1N, Teb1A, Teb1B, Teb2C, p50C, p65N, and p45C. These domains are apparently connected by flexible linkers and therefore are averaged out in the class averages because of flexible positioning. This explains why the location of p45 was not identified by Fab labeling in the negative stain EM (illustrated in **Figure 5*b***). In addition, the entire CST complex hinges as a unit around p50, as could be seen in the class averages (69, 70). The biological significance, if any, of this motion remains to be determined. The 9-Å resolution cryo-EM structure of the *Tetrahymena* telomerase holoenzyme provides a structural framework for understanding telomerase catalytic core assembly and TR interactions and interaction of telomerase with telomere-associated proteins. In the sections below, we compare and contrast *Tetrahymena* and human telomerase catalytic core and accessory protein complexes.

THE CATALYTIC CORE OF HUMAN AND *TETRAHYMENA* TELOMERASE

Pseudoatomic Model of *Tetrahymena* Telomerase Ribonucleoprotein Core

The cryo-EM structure of *Tetrahymena* telomerase provided the first view of the path of TR on TERT for the apo-enzyme and indicated specific locations of the TR elements important for function (**Figure 5*b–e***), thus providing a physical basis for interpreting and/or corroborating previous biochemical and mutational data on function. The TRBD-RT-CTE domains form the expected TERT ring structure, and the TEN domain is stacked over the CTE on the template side of the ring. The t/PK encircles the TERT ring approximately perpendicular to the plane of the ring, and loop 4 of the STE inserts between the TRBD and CTE. Of particular significance is the location of the conserved pseudoknot element on the opposite side of the TERT ring from the template, near the CTE, as there was little biochemical data on its location (**Figure 5*b*,*e***) (128). The location of the pseudoknot, far from the active site, suggests a role in assembly of TR on TERT, essentially locking the t/PK circle into place (18, 69), rather than a direct role in catalysis as previously suggested (127). The TRBD has high-affinity binding sites for the TBE and STE and threads through the t/PK circle to contact them (**Figure 5*d*,*e***). The location of the TBE relative to the template and TERT active site suggests that template boundary definition is determined by physical anchoring of the TBE to the TRBD, with the TR between the end of the template and the TBE maximally extended when the last DNA nucleotide is added to the template (**Figure 5*d***) (67, 69). This model is at least partially consistent with the TR accordion model for template positioning (8). However, how the 3′ end of the template is repositioned into the active site remains unknown. The single-stranded region on the 3′ side of the template wraps around the CTE (thumb domain), threading between the CTE and TEN domain but has no apparent anchor (**Figure 5*b*,*e***). The TEN domain is positioned such that the sstDNA–template

duplex could butt up against it at the end of a telomere repeat synthesis and play a role in strand separation (**Figure 5*c*,*d***) (2, 36). The STE of *Tetrahymena*, distal stem-loop 4, inserts between the TRBD and the CTE (**Figure 5*b*–*e***) (69, 70). A remarkable feature of the telomerase structure is the large hole at the so-called bottom, where stem 1–stem-loop 4 forms a U shape and only loop 4 interacts with TERT (**Figure 5*b***). Bending of stem 4 to ~105° by the C-terminal xRRM domain of p65 (**Figure 3*e***), apparently positions loop 4 to interact with TERT. In the absence of p65 xRRM, loop 4 would point away from TERT (**Figures 3*e*** and **5**).

Modeling the Vertebrate Telomerase Catalytic Core

Recently, model structures of vertebrate TERT–t/PK complexes have been proposed (**Figure 5*f***) (171) on the basis of the positions of TR (e.g., TBE, pseudoknot) and TERT domains in the cryo-EM model structure of *Tetrahymena* telomerase (69, 70) and the NMR model structures of medaka and human TR t/PK (171, 188). The vertebrate pseudoknot has an extended helical region where *Tetrahymena* has a single-stranded region (**Figure 2**). The bend at the human 5-nt bulge (J2ab) (**Figure 3*c***) allows the full-length pseudoknot to wrap around the TERT, with the end (P2a.1 helix) abutting the TEN domain (**Figure 5*f***). NMR dynamics studies of human P2a–J2a/b–P2b showed that the 5-nt bulge allows a limited range of motion of the two helices relative to each other, which may allow further bending at the J2a/b bulge in the complex and/or the RNA to flex during the telomere repeat cycle as the template moves through the active site (187, 188). The region of mismatched base pairs between P2a.1 and P2a (**Figure 2*b*,*c***) may provide a second hinge site for TR bending. For this review, we also modeled the human STE (CR4/5) (**Figure 2**), which is positioned on the TRBD based on the medaka TRBD–CR4/5 structure (**Figure 5*f***). P6.1 is predicted to insert to the TRBD–CTE interface (12, 63), similar to *Tetrahymena* loop 4 (69, 70). However, to avoid steric clash with the CTE, the position of the P6.1 loop would have to be changed. The vertebrate STE may be positioned for interaction with TERT by a bend induced in the RNA by binding of the H/ACA proteins (**Figure 2*a***) and/or by the conformational change in the CR4/5 three-way junction upon interaction with the TRBD (**Figure 3*b***).

PROTEINS INVOLVED IN sstDNA HANDLING AND TELOMERASE RECRUITMENT TO TELOMERES

Telomeric DNA ends in a 3′ single-stranded G-strand overhang that requires protection from exonuclease activity as well as DNA repair enzymes (118). Telomere end–protection proteins also play a dual role in the regulation of telomerase recruitment and activation. sstDNA-binding proteins can sequester the telomeric 3′ end, rendering the DNA inaccessible to telomerase and other DNA acting enzymes (101). However, some of these same proteins are required to recruit telomerase to telomeres and stimulate activity and processivity (112).

TPP1 and POT1

In humans, TPP1 is the major facilitator of telomerase activation and recruitment (112, 129, 180). It binds directly with the TERT TEN domain (111, 141, 144, 185, 189), TIN2, and the sstDNA-binding POT1, simultaneously bridging telomerase to shelterin components and the 3′ single-stranded G-overhang (**Figure 1*b***) (34, 93, 181, 185). TPP1 can also interact with the sstDNA-binding complex CST, which occludes telomerase recruitment and access to telomeres (24). Although the structural basis for how all of these factors cooperate to regulate telomerase

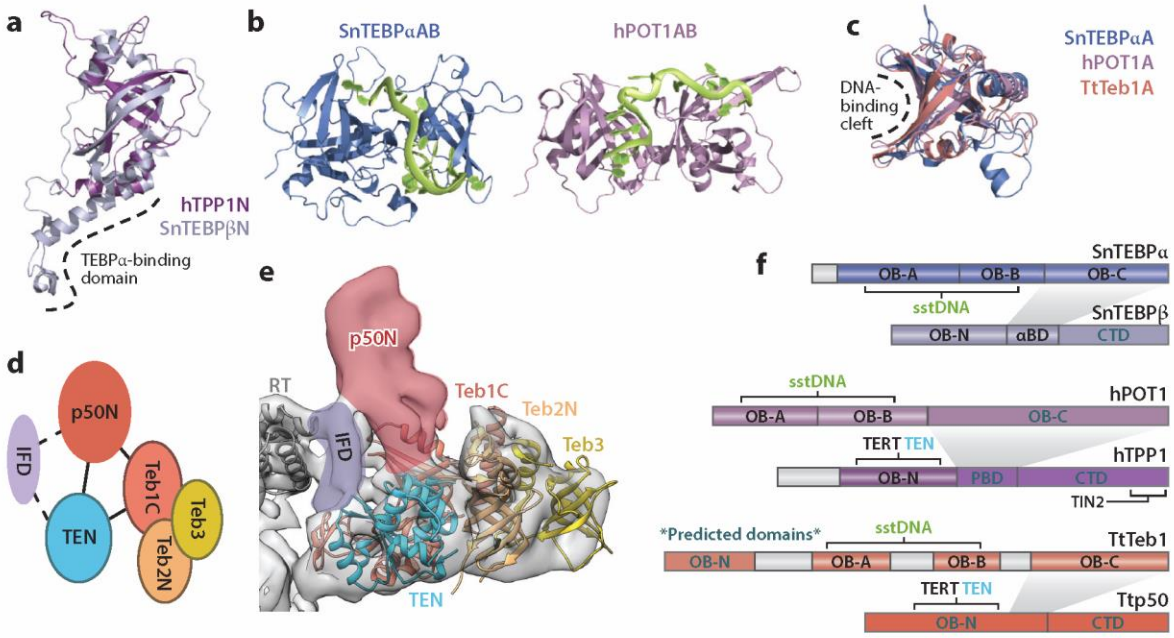

Figure 6

Domains, interactions, and structures of telomere G-strand binding and telomerase recruitment proteins. (*a*) Superposition of *Sterkiella* (*Sterkiella nova*) TEBPβ N-terminal OB (PDB ID 1OTC) with human TPP1 N-terminal OB (PDB ID 2I46). (*b*) Side-by-side comparison of the two N-terminal OB folds of *Sterkiella* TEBPα and human POT1, both bound to sstDNA. (*c*) Structural alignment of the most N-terminal sstDNA-binding OB fold from *Sterkiella* TEBPα (PDB ID 1OTC), human POT1 (PDB ID 1XJV), and *Tetrahymena* Teb1 (PDB ID 3U4V). (*d*) Schematic representation of interaction network between TERT, p50, and TEB proteins in *Tetrahymena* telomerase, based on the cryo-EM structure (69). (*e*) Region of 9-Å cryo-EM map with the p50 density and interactions with the TEN domain (PDB ID 2B2A), TEB [modeled from RPA heterotrimer (PDB ID 1L1O) with Teb1C (PDB ID 3U50) substituted for RPA70C], and the IFD. (*f*) Schematic of domains and interactions of *Sterkiella* TEBPα–TEBPβ, human POT1–TPP1, and *Tetrahymena* Teb1–p50. Abbreviations: EM, electron microscopy; IFD, insertions of fingers domain; OB, oligonucleotide/oligosaccharide binding; RPA, replication protein A; sstDNA, single-stranded telomere repeat DNA; TEN, TERT-essential N-terminal; TERT, telomerase reverse transcriptase.

activity is unknown, structures of individual domains and apparently homologous complexes have provided important insights.

Among the first studied telomere end–binding proteins were the *Sterkiella nova* (formerly *Oxytricha nova*) telomere end–binding proteins, TEBPα and TEBPβ. Seminal structures of the TEBPα–TEBPβ–sstDNA complex revealed that TEBPα consists of three OB folds, with the two N-terminal OB folds important for sstDNA binding, whereas the N-terminus of TEBPβ consists of a single OB fold with a C-terminal extension important for complex formation (**Figure 6*a*,*b*,*f***) (62). Structures of POT1AB OB folds bound to sstDNA and of the free TPP1 N-terminal OB fold revealed structural homologies to TEBPα and TEBPβ, respectively (**Figure 6*a–c***) (82, 169). The TPP1 N-terminal OB fold structurally aligns with the N-terminal domain of TEBPβ (**Figure 6*a***) whereas the two N-terminal POT1 OB folds bound to sstDNA are similar to the corresponding TEBPα N-terminal OB folds (**Figure 6*b*,*c*,*f***). Although not apparent in the crystal structure of TPP1, a C-terminal region of the OB fold in both TPP1 and TEBPβ is important for interaction with the C-terminal OB fold of POT1 (**Figure 6*a*,*f***) (62, 169, 180). These striking similarities

between the domain organizations suggest that POT1–TPP1 may structurally and functionally interact with each other in a similar manner to TEBPα–TEBPβ. However, consistent with data that TEBPα–TEBPβ inhibits in vitro telomerase activity (43), the TEBPα–TEBPβ–sstDNA complex structure is in a conformation that occludes the 3′ sstDNA end (62). This is in contrast to observations that TPP1–POT1 activates telomerase and increases processivity in vitro (169). It is possible that when bound to TERT, a distinct conformation of TPP1–POT1 exists that allows access to the 3′ sstDNA end.

Recruitment of telomerase to telomeres is primarily facilitated by the TPP1 OB fold, which binds to TERT at the TEN domain (144, 185, 189). A region of Glu- and Leu-rich residues have been identified as the so-called TEL patch on TPP1 and have been shown to interact directly with the TEN domain, and corresponding residues on the TEN domain have been shown to participate in this interaction (**Figure 4*b***) (111, 141, 185). Separation of function experiments support the notion that in addition to facilitating interaction with TERT, these TEL patch residues can exert a biochemical effect on telomerase that aids translocation independently of preventing primer dissociation (33, 111). A mechanistic explanation for these observations will likely require high-resolution structural understanding of translocation as well as of the TPP1–TEN interaction.

Tetrahymena Telomerase Recruitment and Telomere End Protection

In *Tetrahymena*, recruitment of telomerase to telomeres requires p50 and the sstDNA-binding protein Teb1 (165), which is part of the RPA-related TEB complex (69). Crystal structures of Teb1A and Teb1B showed that these domains and their mode of sstDNA binding are homologous to those of POT1A and POT1B (**Figure 6*c***) (186). Teb1C is structurally homologous to RPA70C, and Teb2 and Teb3 are RPA32 and RPA14 homologs, respectively. Intriguingly, a recent study establishes that Teb2 and Teb3 are actually shared subunits with *Tetrahymena* RPA (164). The domain topology of TEB is the same as that of RPA (**Figure 7*c***). Of the three TEB proteins, only Teb1 has been shown to bind directly to sstDNA (186), whereas Teb2 and Teb3 enhance telomerase activity likely by stabilizing association of Teb1 to telomerase (69, 164). Similar to POT1–TPP1, Teb1 can stimulate processivity of the catalytic core but only in the presence of p50 (61, 70). The recent cryo-EM structure of *Tetrahymena* telomerase provided the structural basis for this observation. p50 interacts directly with the TERT TEN domain and Teb1C, mediating the association of TEB with TERT (**Figure 6*d*,*e***) (69). Significantly, p50 interacts at the region on the TEN domain that corresponds with the human TEN–TPP1 interface (141). On the basis of this, p50–TEB is proposed to be functionally equivalent to TPP1–POT1, enhancing processivity and bridging telomerase to telomeres (69). Interestingly and consistent with recent studies implicating a TPP1–IFD interaction (26, 27), in the cryo-EM model the predicted IFD region of *Tetrahymena* TERT is next to p50 (69). Although there is no high-resolution structure of p50, the EM density shows that the region identified as p50N is a β-barrel similar in shape to the TPP1N OB fold (**Figure 6*e***) (69). If p50 is indeed a TPP1 homolog, then the cryo-EM structure provides a first glimpse of a TERT–TPP1–POT1 interaction (**Figure 6*e***).

The discovery that the POT1 homolog Teb1 is part of a heterotrimeric RPA–related complex TEB (**Figures 5*b*,*c*** and ***6d–f***) suggests a closer relationship between POT1 and RPA than previously appreciated. The POT1AB OB folds are structurally similar to the RPA70AB OB folds and bind DNA similarly. However, POT1C is not expected to be similar to RPA70C, nor is there evidence for the presence of POT1 binding RPA14/RPA32 homologs. Perhaps the smaller subunits of RPA were lost during evolution of POT1. The recurring presence of RPA as an evolutionary theme in telomerase (83) is also seen with the RPA-like CST complex (22), discussed in the next section.

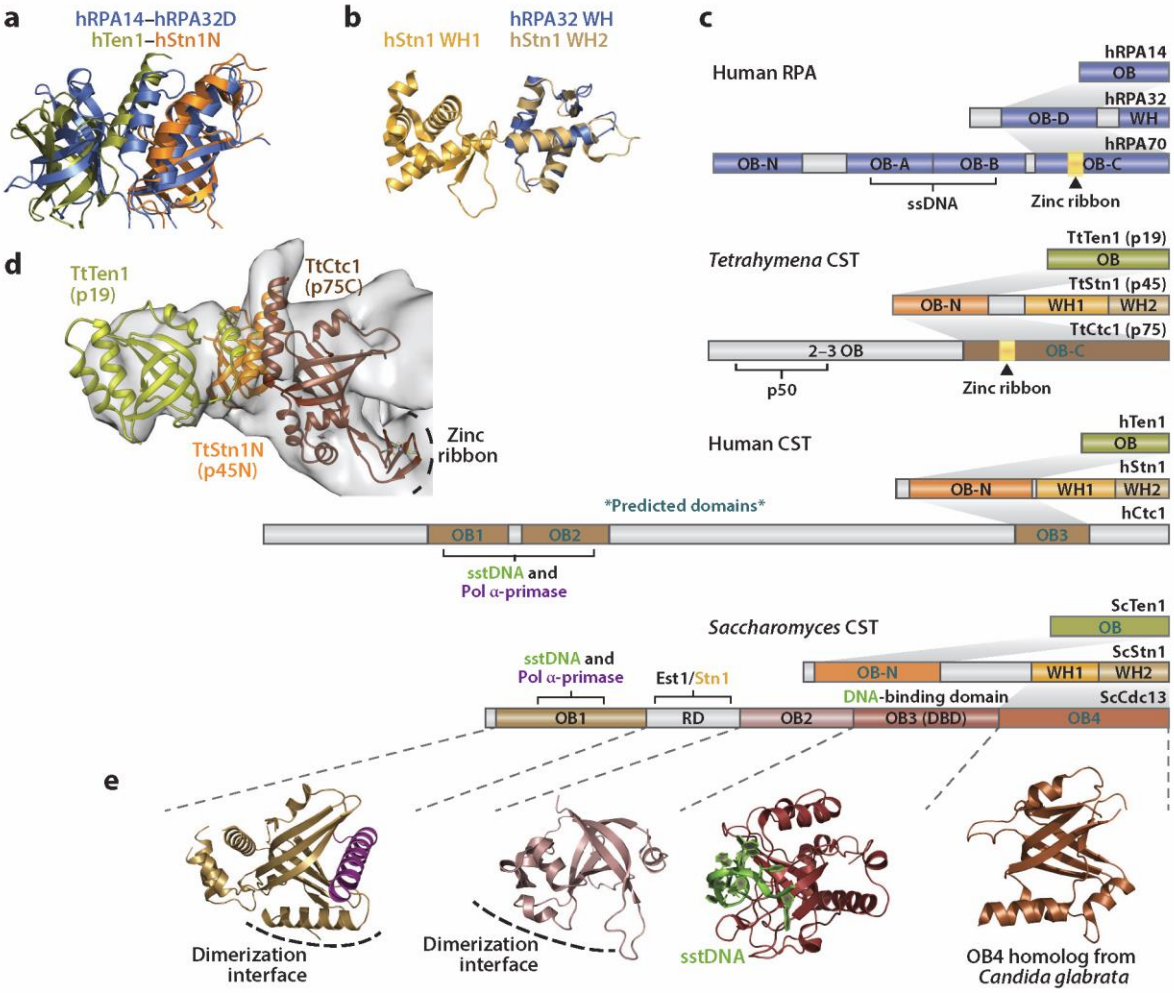

Figure 7

Domains, interactions, and structures of RPA and CST proteins. (*a*) Superpositions of structures of human RPA14–RPA32D (PDB ID 1QUQ) and Ten1–Stn1N complexes. (*b*) Structure of human Stn1 C-terminal tandem winged-helix domain (PDB ID 4JQF). Human RPA32 C-terminal winged-helix (PDB ID 1DPU) superpositions with Stn1 WH2. (*c*) Comparison of interactions and domain topologies of the human RPA, *Tetrahymena* CST, human CST, and *Saccharomyces* CST trimeric complexes. (*d*) Region of *Tetrahymena* telomerase cryo-EM density comprising the CST trimeric core with structures of Ten1–Stn1N (PDB ID 5DOI) and homology model of p75C [based on RPA70C (PDB ID 1L1O)] fit in (69). (*e*) Structures of *Saccharomyces* Cdc13 OB1 complexed to Pol α-peptide (PDB ID 3OIQ), OB2 (PDB ID 4HCE), and OB3–sstDNA complex (PDB ID 1S40) and *Candida* Cdc13 OB4 (PDB ID 3RMH). Abbreviations: EM, electron microscopy; OB, oligonucleotide/oligosaccharide binding; RPA, replication protein A; ssDNA, single-stranded DNA; sstDNA, single-stranded telomere repeat DNA; WH, winged helix.

It should be noted that POT1–TPP1 homologs (Pot1a–Tpt1) have previously been identified in *Tetrahymena* (**Figure 1***c*) (64, 90). The Pot1a–Tpt1 proteins are the single-stranded telomere capping proteins for these ciliates (90), although no evidence suggests that they are directly involved in the recruitment or stimulation of telomerase. Because the 3′ overhang in *Tetrahymena* is short (~2 to 3 telomeric repeats) (65), it is likely that the association of telomerase to telomeres via

p50–Teb1 is mutually exclusive with Tpt1–Pot1 bound to the 3′ sstDNA overhang (124). In humans, TPP1–POT1 switches from being inhibitory to activating upon telomerase recruitment (169, 180). In *Tetrahymena*, displacement of Tpt1–Pot1 by p50–TEB could be the first step in telomere extension.

CST PROTEINS INVOLVED IN C-STRAND SYNTHESIS AND TELOMERASE REGULATION

CST was originally identified in *S. cerevisiae* as the sstDNA-binding protein complex, comprising Cdc13, Stn1, and Ten1 (50, 51, 115). In *Saccharomyces*, it is the major capping mechanism for 3′ single-stranded telomere ends, and Cdc13 fulfills the roles of human POT1 in binding sstDNA and aiding recruitment of telomerase to telomeres (28, 88). Initially thought to be unique to yeast, because of the low sequence homology of these proteins, CST was subsequently identified in vertebrates and plants as Ctc1–Stn1–Ten1 (110, 125, 156). In plants, yeasts, and mammals, CST negatively regulates telomerase activity (24, 51, 80, 115), perhaps serving as a stop point for the subsequent recruitment of Pol α-primase by CST for C-strand synthesis (19, 24, 126). More recently, mammalian CST has been proposed to have extra telomeric roles in genome-wide replication restart as well as recovery from DNA damage and replication stress (151, 170).

A breakthrough in understanding the structural biology of CST was the prediction that these proteins have a domain organization akin to the trimeric RPA complex (45); this was later confirmed when the first structures of Stn1 and Ten1 from yeast were solved (48, 155). Most recently, the *Tetrahymena* telomerase proteins p75, p45, and p19 were identified as a ciliate CST complex (69, 168). Although the association of CST is transient in most other organisms, in *Tetrahymena*, it is a stable part of the holoenzyme (**Figure 1*c***) (69) and thus provides an unprecedented opportunity for structural studies of CST–telomerase interactions (22, 125).

Stn1–Ten1 Structure and Similarity to RPA

The RPA complex contains a trimeric core of three OB folds, comprising RPA14, RPA32D, and RPA70C (**Figure 7*c***). Along with a three-helix bundle, formed at the C-terminus of each participating OB fold, RPA32D bridges the interaction between RPA14 and RPA70C. RPA32 contains an additional WH domain at its C-terminus, whereas RPA70, the largest subunit, possesses three additional N-terminal OB folds (123, 153). The most well-conserved components of the CST complex, Stn1 and Ten1, also bear the most similarity to their RPA counterparts, RPA32 and RPA14, respectively. Ten1 comprises a single OB fold that binds to the Stn1N OB fold (**Figure 7*a*,*c*,*d***). Despite a lack of primary sequence similarity, structures of the human (15), *Tetrahymena* (168), *Candida*, and *Schizosaccharomyces* Ten1–Stn1N (155) complexes all superpose with high similarity to each other as well as to the structure of the human RPA14–RPA32D complex (**Figure 7*a***) (13).

Like RPA32, Stn1 contains a C-terminal domain connected to the N-terminal OB fold via a flexible linker. However, whereas RPA32 contains a single WH, Stn1 possesses a tandem WH domain (**Figure 7*b*,*c***) (15, 48, 69, 155, 168). The relative orientation of the two WH domains with respect to each other is similar between *Tetrahymena* and *Saccharomyces* but different from human (15, 48, 69, 155, 168). However, the short linker and large buried area between the tandem domains in all three organisms suggest that indeed the two WH domains in Stn1 function as a structured unit (15, 48, 69, 155, 168). Interestingly, RPA32 WH superposes with both domains but much more closely with the human Stn1 WH2 than with the WH1 (**Figure 7*b***). The same

is true for *Tetrahymena* but not for *Saccharomyces*, where its Stn1 WH2 possesses a much more divergent wing motif, comprising significantly longer β-strands (48, 69, 155, 168). Much work has shown the involvement of RPA32 WH in the recruitment of proteins for DNA repair (153); and recent work has implicated the Stn1 WH2 in the recruitment and activation of Pol α-primase for C-strand synthesis (46, 95).

Ctc1/Cdc13 Structure and Interactions

Numerous studies and the comparison to RPA suggest that Stn1 bridges the trimeric interaction between the CST proteins (22). However, a high-resolution structure of the trimeric CST or of the Ctc1/Cdc13–Stn1 detailing this interaction remains to be determined. The 9-Å cryo-EM structure of *Tetrahymena* telomerase provided the first direct structural evidence of and insight into a trimeric CST interaction (**Figure 7*d***) (69). In the model, p45N sits in between and interacts directly with p75C and p19, similar to the RPA trimeric core (13). Although p75C is based on a homology model from RPA70C, the cryo-EM map shows clear density for the three-helix bundle as well as a zinc-ribbon motif in p75C (**Figure 7*d***) (69). Primary sequence analysis of p75 suggests that the zinc-ribbon motif does indeed exist in the putative p75C (**Figure 7*c***), strongly suggesting that the C-terminal domain of p75 is homologous to RPA70C. In contrast, the C-terminal OB fold of Cdc13 is not predicted to contain a zinc ribbon, and its overall structure is different from RPA70C (**Figure 7*e***) (182). These differences highlight the apparent divergence of the large subunit of CST.

Structures of *Saccharomyces* Cdc13OB2 and *Candida* Cdc13OB4 do not superpose with their RPA counterparts. The main β-barrel of *Sacharromyces* Cdc13OB1 superposes with RPA70N and has been shown to interact with a small peptide of Pol α-primase as well as display sstDNA binding (**Figure 7*e***) (107, 154). Cdc13OB1 and OB2 are expected to facilitate Cdc13 dimerization, which is important for the proper functioning of Cdc13 as well as formation of the trimeric CST complex (103). Unlike RPA70, which displays cooperative ssDNA binding between its three C-terminal OB folds, the sstDNA-binding activity of Cdc13 is performed primarily by OB1 and OB3 (**Figure 7*e***) (107–109). *Tetrahymena* p75 and human Ctc1 have also been shown to bind sstDNA (23, 24, 55, 168), but the structural basis for this or high-resolution structures for these subunits or their subdomains have yet to be determined.

Overall, structural and functional investigations of CST proteins have revealed both similarities and differences between different organisms. There are now structures of Stnt1 and Ten1 from many organisms, but for the largest and most divergent subunit, only yeast Cdc13 has been structurally characterized. A structural basis for the large body of functional genetic and biochemical data that has been gathered for Ctc1 (human, plants, *Tetrahymena*) (23, 24, 55, 131) will be vital for understanding the role of CST in telomerase regulation and telomere maintenance.

FUTURE PROSPECTS

More than a quarter century after the discovery of telomerase, we now have a snapshot of how the components of telomerase fit and function together at telomeres. Problems of solubility, expression, and heterogeneity inherent to telomerase complexes remain a challenge for structural biologists. With recent advances in structural biology methods and biochemical characterization of telomerase, in the next few years, we can expect the first structures of human and yeast telomerase, higher-resolution structures of the telomerase RNP core with sstDNA, and details of telomerase interaction at telomeres.

DISCLOSURE STATEMENT

The authors are not aware of any affiliations, memberships, funding, or financial holdings that might be perceived as affecting the objectivity of this review.

ACKNOWLEDGMENTS

Telomerase research in the Feigon laboratory is supported by grants from NIH (RO1 GM48123) and NSF (MCB 1517629) to J.F. Additional support for UCLA-DOE X-ray and NMR facilities is provided by DOE grant DE-FC02-023463421. H.C. is partially supported by the Ruth L. Kirschstein National Research Service Award GM007185.

LITERATURE CITED

1. Akiyama BM, Gomez A, Stone MD. 2013. A conserved motif in *Tetrahymena thermophila* telomerase reverse transcriptase is proximal to the RNA template and is essential for boundary definition. *J. Biol. Chem.* 288:22141–49
2. Akiyama BM, Parks JW, Stone MD. 2015. The telomerase essential N-terminal domain promotes DNA synthesis by stabilizing short RNA–DNA hybrids. *Nucleic Acids Res.* 43:5537–49
3. Alves D, Li H, Codrington R, Orte A, Ren X, et al. 2008. Single-molecule analysis of human telomerase monomer. *Nat. Chem. Biol.* 4:287–89
4. Armanios M, Blackburn EH. 2012. The telomere syndromes. *Nat. Rev. Genet.* 13:693–704
5. Artandi SE, DePinho RA. 2010. Telomeres and telomerase in cancer. *Carcinogenesis* 31:9–18
6. Autexier C, Lue NF. 2006. The structure and function of telomerase reverse transcriptase. *Annu. Rev. Biochem.* 75:493–517
7. Bajon E, Laterreur N, Wellinger RJ. 2015. A single templating RNA in yeast telomerase. *Cell Rep.* 12:441–48
8. Berman AJ, Akiyama BM, Stone MD, Cech TR. 2011. The RNA accordion model for template positioning by telomerase RNA during telomeric DNA synthesis. *Nat. Struct. Mol. Biol.* 18:1371–75
9. Bernardes de Jesus B, Blasco MA. 2013. Telomerase at the intersection of cancer and aging. *Trends Genet.* 29:513–20
10. Blackburn EH, Collins K. 2011. Telomerase: an RNP enzyme synthesizes DNA. *Cold Spring Harb. Perspect. Biol.* 3:a003558
11. Blackburn EH, Greider CW, Szostak JW. 2006. Telomeres and telomerase: the path from maize, *Tetrahymena* and yeast to human cancer and aging. *Nat. Med.* 12:1133–38
12. Bley CJ, Qi X, Rand DP, Borges CR, Nelson RW, Chen JJ-L. 2011. RNA–protein binding interface in the telomerase ribonucleoprotein. *PNAS* 108:20333–38
13. Bochkareva E, Korolev S, Lees-Miller SP, Bochkarev A. 2002. Structure of the RPA trimerization core and its role in the multistep DNA-binding mechanism of RPA. *EMBO J.* 21:1855–63
14. Brown AF, Podlevsky JD, Qi X, Chen Y, Xie M, Chen JJ-L. A self-regulating template in human telomerase. *PNAS* 111:11311–16
15. Bryan C, Rice C, Harkisheimer M, Schultz DC, Skordalakes E. 2013. Structure of the human telomeric Stn1-Ten1 capping complex. *PLOS ONE* 8:e66756
16. Bryan TM, Goodrich KJ, Cech TR. 2003. *Tetrahymena* telomerase is active as a monomer. *Mol. Biol. Cell* 14:4794–804
17. Cash DD, Cohen-Zontag O, Kim N-K, Shefer K, Brown Y, et al. 2013. Pyrimidine motif triple helix in the *Kluyveromyces lactis* telomerase RNA pseudoknot is essential for function in vivo. *PNAS* 110:10970–75
18. Cash DD, Feigon J. Structure and folding of the *Tetrahymena* telomerase RNA pseudoknot. *Nucleic Acids Res.* 45:482–95
19. Casteel DE, Zhuang S, Zeng Y, Perrino FW, Boss GR, et al. 2009. A DNA polymerase α·primase cofactor with homology to replication protein A-32 regulates DNA replication in mammalian cells. *J. Biol. Chem.* 284:5807–18

20. Chen J-L, Blasco MA, Greider CW. 2000. Secondary structure of vertebrate telomerase RNA. *Cell* 100:503–14
21. Chen J-L, Greider CW. 2003. Template boundary definition in mammalian telomerase. *Genes Dev.* 17:2747–52
22. Chen L-Y, Lingner J. 2013. CST for the grand finale of telomere replication. *Nucleus* 4:277–82
23. Chen L-Y, Majerská J, Lingner J. 2013. Molecular basis of telomere syndrome caused by *CTC1* mutations. *Genes Dev.* 27:2099–108
24. Chen L-Y, Redon S, Lingner J. 2012. The human CST complex is a terminator of telomerase activity. *Nature* 488:540–44
25. Chen Y, Fender J, Legassie JD, Jarstfer MB, Bryan TM, Varani G. 2006. Structure of stem-loop IV of *Tetrahymena* telomerase RNA. *EMBO J.* 25:3156–66
26. Chu TW, D'Souza Y, Autexier C. 2016. The insertion in fingers domain in human telomerase can mediate enzyme processivity and telomerase recruitment to telomeres in a TPP1-dependent manner. *Mol. Cell. Biol.* 36:210–22
27. Chu TW, MacNeil DE, Autexier C. 2016. Multiple mechanisms contribute to the cell growth defects imparted by human telomerase insertion in fingers domain mutations associated with premature aging diseases. *J. Biol. Chem.* 291:8374–86
28. Churikov D, Corda Y, Luciano P, Géli V. 2013. Cdc13 at a crossroads of telomerase action. *Front. Oncol.* 3:39
29. Cohen SB, Graham ME, Lovrecz GO, Bache N, Robinson PJ, Reddel RR. 2007. Protein composition of catalytically active human telomerase from immortal cells. *Science* 315:1850–53
30. Cole DI, Legassie JD, Bonifacio LN, Sekaran VG, Ding F, et al. 2012. New models of *Tetrahymena* telomerase RNA from experimentally derived constraints and modeling. *J. Am. Chem. Soc.* 134:20070–80
31. Collins K. 2006. The biogenesis and regulation of telomerase holoenzymes. *Nat. Rev. Mol. Cell Biol.* 7:484–94
32. Cristofari G, Lingner J. 2006. Telomere length homeostasis requires that telomerase levels are limiting. *EMBO J.* 25:565–74
33. Dalby AB, Hofr C, Cech TR. 2015. Contributions of the TEL-patch amino acid cluster on TPP1 to telomeric DNA synthesis by human telomerase. *J. Mol. Biol.* 427:1291–303
34. de Lange T. 2005. Shelterin: the protein complex that shapes and safeguards human telomeres. *Genes Dev.* 19:2100–10
35. Duan J, Li L, Lu J, Wang W, Ye K. 2009. Structural mechanism of substrate RNA recruitment in H/ACA RNA-guided pseudouridine synthase. *Mol. Cell* 34:427–39
36. Eckert B, Collins K. 2012. Roles of telomerase reverse transcriptase N-terminal domain in assembly and activity of *Tetrahymena* telomerase holoenzyme. *J. Biol. Chem.* 287:12805–14
37. Egan ED, Collins K. 2010. Specificity and stoichiometry of subunit interactions in the human telomerase holoenzyme assembled in vivo. *Mol. Cell. Biol.* 30:2775–86
38. Egan ED, Collins K. 2012. An enhanced H/ACA RNP assembly mechanism for human telomerase RNA. *Mol. Cell. Biol.* 32:2428–39
39. Egan ED, Collins K. 2012. Biogenesis of telomerase ribonucleoproteins. *RNA* 18:1747–59
40. Errington TM, Fu D, Wong JM, Collins K. 2008. Disease-associated human telomerase RNA variants show loss of function for telomere synthesis without dominant-negative interference. *Mol. Cell. Biol.* 28:6510–20
41. Feigon J, Chan H, Jiang J. 2016. Integrative structural biology of *Tetrahymena* telomerase—insights into catalytic mechanism and interaction at telomeres. *FEBS J.* 283:2044–50
42. Fogarty PF, Yamaguchi H, Wiestner A, Baerlocher GM, Sloand E, et al. 2003. Late presentation of dyskeratosis congenita as apparently acquired aplastic anaemia due to mutations in telomerase RNA. *Lancet* 362:1628–30
43. Froelich-Ammon SJ, Dickinson BA, Bevilacqua JM, Schultz SC, Cech TR. 1998. Modulation of telomerase activity by telomere DNA-binding proteins in *Oxytricha*. *Genes Dev.* 12:1504–14
44. Fujii H, Shao L, Colmegna I, Goronzy JJ, Weyand CM. 2009. Telomerase insufficiency in rheumatoid arthritis. *PNAS* 106:4360–65

45. Gao H, Cervantes RB, Mandell EK, Otero JH, Lundblad V. 2007. RPA-like proteins mediate yeast telomere function. *Nat. Struct. Mol. Biol.* 14:208–14
46. Gasparyan HJ, Xu L, Petreaca RC, Rex AE, Small VY, et al. 2009. Yeast telomere capping protein Stn1 overrides DNA replication control through the S phase checkpoint. *PNAS* 106:2206–11
47. Gavory G, Symmons MF, Krishnan Ghosh Y, Klenerman D, Balasubramanian S. 2006. Structural analysis of the catalytic core of human telomerase RNA by FRET and molecular modeling. *Biochemistry* 45:13304–11
48. Gelinas AD, Paschini M, Reyes FE, Heroux A, Batey RT, et al. 2009. Telomere capping proteins are structurally related to RPA with an additional telomere-specific domain. *PNAS* 106:19298–303
49. Gillis AJ, Schuller AP, Skordalakes E. 2008. Structure of the *Tribolium castaneum* telomerase catalytic subunit TERT. *Nature* 455:633–37
50. Grandin N, Damon C, Charbonneau M. 2001. Ten1 functions in telomere end protection and length regulation in association with Stn1 and Cdc13. *EMBO J.* 20:1173–83
51. Grandin N, Reed SI, Charbonneau M. 1997. Stn1, a new *Saccharomyces cerevisiae* protein, is implicated in telomere size regulation in association with Cdc13. *Genes Dev.* 11:512–27
52. Greider CW, Blackburn EH. 1985. Identification of a specific telomere terminal transferase activity in *Tetrahymena* extracts. *Cell* 43:405–13
53. Greider CW, Blackburn EH. 1987. The telomere terminal transferase of *Tetrahymena* is a ribonucleoprotein enzyme with two kinds of primer specificity. *Cell* 51:887–98
54. Greider CW, Blackburn EH. 1989. A telomeric sequence in the RNA of *Tetrahymena* telomerase required for telomere repeat synthesis. *Nature* 337:331–37
55. Gu P, Chang S. 2013. Functional characterization of human CTC1 mutations reveals novel mechanisms responsible for the pathogenesis of the telomere disease Coats plus. *Aging Cell* 12:1100–9
56. Hamma T, Ferré-D'Amaré AR. 2004. Structure of protein L7Ae bound to a K-turn derived from an archaeal box H/ACA sRNA at 1.8 Å resolution. *Structure* 12:893–903
57. Hamma T, Ferré-D'Amaré AR. 2010. The box H/ACA ribonucleoprotein complex: interplay of RNA and protein structures in post-transcriptional RNA modification. *J. Biol. Chem.* 285:805–9
58. Harkisheimer M, Mason M, Shuvaeva E, Skordalakes E. 2013. A motif in the vertebrate telomerase N-terminal linker of TERT contributes to RNA binding and telomerase activity and processivity. *Structure* 21:1870–78
59. Hengesbach M, Kim N-K, Feigon J, Stone MD. 2012. Single-molecule FRET reveals the folding dynamics of the human telomerase RNA pseudoknot domain. *Angew. Chem. Int. Ed.* 51:5876–79
60. Hockemeyer D, Collins K. 2015. Control of telomerase action at human telomeres. *Nat. Struct. Mol. Biol.* 22:848–52
61. Hong K, Upton H, Miracco EJ, Jiang J, Zhou ZH, et al. 2013. *Tetrahymena* telomerase holoenzyme assembly, activation, and inhibition by domains of the p50 central hub. *Mol. Cell. Biol.* 33:3962–71
62. Horvath MP, Schweiker VL, Bevilacqua JM, Ruggles JA, Schultz SC. 1998. Crystal structure of the *Oxytricha nova* telomere end binding protein complexed with single strand DNA. *Cell* 95:963–74
63. Huang J, Brown AF, Wu J, Xue J, Bley CJ, et al. 2014. Structural basis for protein-RNA recognition in telomerase. *Nat. Struct. Mol. Biol.* 21:507–12
64. Jacob NK, Lescasse R, Linger BR, Price CM. 2007. *Tetrahymena* POT1a regulates telomere length and prevents activation of a cell cycle checkpoint. *Mol. Cell. Biol.* 27:1592–601
65. Jacob NK, Skopp R, Price CM. 2001. G-overhang dynamics at *Tetrahymena* telomeres. *EMBO J.* 20:4299–308
66. Jacobs SA, Podell ER, Cech TR. 2006. Crystal structure of the essential N-terminal domain of telomerase reverse transcriptase. *Nat. Struct. Mol. Biol.* 13:218–25
67. Jansson LI, Akiyama BM, Ooms A, Lu C, Rubin SM, Stone MD. 2015. Structural basis of template-boundary definition in *Tetrahymena* telomerase. *Nat. Struct. Mol. Biol.* 22:883–88
68. Jaskelioff M, Muller FL, Paik J-H, Thomas E, Jiang S, et al. 2011. Telomerase reactivation reverses tissue degeneration in aged telomerase-deficient mice. *Nature* 469:102–6
69. Jiang J, Chan H, Cash DD, Miracco EJ, Ogorzalek Loo RR, et al. 2015. Structure of *Tetrahymena* telomerase reveals previously unknown subunits, functions, and interactions. *Science* 350:aab4070

70. Jiang J, Miracco EJ, Hong K, Eckert B, Chan H, et al. 2013. The architecture of *Tetrahymena* telomerase holoenzyme. *Nature* 496:187–92
71. Kelleher C, Teixeira MT, Forstemann K, Lingner J. 2002. Telomerase: biochemical considerations for enzyme and substrate. *Trends Biochem. Sci.* 27:572–79
72. Kim N-K, Theimer CA, Mitchell JR, Collins K, Feigon J. 2010. Effect of pseudouridylation on the structure and activity of the catalytically essential P6.1 hairpin in human telomerase RNA. *Nucleic Acids Res.* 38:6746–56
73. Kim N-K, Zhang Q, Feigon J. 2014. Structure and sequence elements of the CR4/5 domain of medaka telomerase RNA important for telomerase function. *Nucleic Acids Res.* 42:3395–408
74. Kim N-K, Zhang Q, Zhou J, Theimer CA, Peterson RD, Feigon J. 2008. Solution structure and dynamics of the wild-type pseudoknot of human telomerase RNA. *J. Mol. Biol.* 384:1249–61
75. Kiss T, Fayet-Lebaron E, Jády BE. 2010. Box H/ACA small ribonucleoproteins. *Mol. Cell* 37:597–606
76. Koo B-K, Park C-J, Fernandez CF, Chim N, Ding Y, et al. 2011. Structure of H/ACA RNP protein Nhp2p reveals *cis/trans* isomerization of a conserved proline at the RNA and Nop10 binding interface. *J. Mol. Biol.* 411:927–42
77. Kupiec M. 2014. Biology of telomeres: lessons from budding yeast. *FEMS Microbiol. Rev.* 38:144–71
78. Lai CK, Miller MC, Collins K. 2002. Template boundary definition in *Tetrahymena* telomerase. *Genes Dev.* 16:415–20
79. Lai CK, Mitchell JR, Collins K. 2001. RNA binding domain of telomerase reverse transcriptase. *Mol. Cell. Biol.* 21:990–1000
80. Leehy KA, Lee JR, Song X, Renfrew KB, Shippen DE. 2013. *MERISTEM DISORGANIZATION1* encodes TEN1, an essential telomere protein that modulates telomerase processivity in *Arabidopsis*. *Plant Cell* 25:1343–54
81. Lei M, Podell ER, Baumann P, Cech TR. 2003. DNA self-recognition in the structure of Pot1 bound to telomeric single-stranded DNA. *Nature* 426:198–203
82. Lei M, Podell ER, Cech TR. 2004. Structure of human POT1 bound to telomeric single-stranded DNA provides a model for chromosome end-protection. *Nat. Struct. Mol. Biol.* 11:1223–29
83. Lewis KA, Wuttke DS. 2012. Telomerase and telomere-associated proteins: structural insights into mechanism and evolution. *Structure* 20:28–39
84. Li L, Ye K. 2006. Crystal structure of an H/ACA box ribonucleoprotein particle. *Nature* 443:302–7
85. Li S, Duan J, Li D, Ma S, Ye K. 2011. Structure of the Shq1–Cbf5–Nop10–Gar1 complex and implications for H/ACA RNP biogenesis and dyskeratosis congenita. *EMBO J.* 30:5010–20
86. Li S, Duan J, Li D, Yang B, Dong M, Ye K. 2011. Reconstitution and structural analysis of the yeast box H/ACA RNA-guided pseudouridine synthase. *Genes Dev.* 25:2409–21
87. Liang B, Xue S, Terns RM, Terns MP, Li H. 2007. Substrate RNA positioning in the archaeal H/ACA ribonucleoprotein complex. *Nat. Struct. Mol. Biol.* 14:1189–95
88. Lin J-J, Zakian VA. 1996. The *Saccharomyces CDC13* protein is a single-strand TG_{1-3} telomeric DNA-binding protein in vitro that affects telomere behavior in vivo. *PNAS* 93:13760–65
89. Lin KW, Zakian VA. 2015. 21st century genetics: mass spectrometry of yeast telomerase. *Cold Spring Harb. Symp. Quant. Biol.* 80:111–16
90. Linger BR, Morin GB, Price CM. 2011. The Pot1a-associated proteins Tpt1 and Pat1 coordinate telomere protection and length regulation in *Tetrahymena*. *Mol. Biol. Cell* 22:4161–70
91. Linger BR, Price CM. 2009. Conservation of telomere protein complexes: shuffling through evolution. *Crit. Rev. Biochem. Mol. Biol.* 44:434–46
92. Lingner J, Hughes TR, Shevchenko A, Mann M, Lundblad V, Cech TR. 1997. Reverse transcriptase motifs in the catalytic subunit of telomerase. *Science* 276:561–67
93. Liu D, Safari A, O'Connor MS, Chan DW, Laegeler A, et al. 2004. PTOP interacts with POT1 and regulates its localization to telomeres. *Nat. Cell Biol.* 6:673–80
94. Lloyd NR, Dickey TH, Hom RA, Wuttke DS. 2016. Tying up the ends: plasticity in the recognition of single-stranded DNA at telomeres. *Biochemistry* 55:5326–40
95. Lue NF, Chan J, Wright WE, Hurwitz J. 2014. The CDC13-STN1-TEN1 complex stimulates Pol α activity by promoting RNA priming and primase-to-polymerase switch. *Nat. Commun.* 5:5762

96. Lue NF, Lin Y-C, Mian IS. 2003. A conserved telomerase motif within the catalytic domain of telomerase reverse transcriptase is specifically required for repeat addition processivity. *Mol. Cell. Biol.* 23:8440–49
97. Mahmoudi S, Henriksson S, Weibrecht I, Smith S, Söderberg O, et al. 2010. WRAP53 is essential for Cajal body formation and for targeting the survival of motor neuron complex to Cajal bodies. *PLOS Biol.* 8:e1000521
98. Malyavko AN, Parfenova YY, Zvereva MI, Dontsova OA. 2014. Telomere length regulation in budding yeasts. *FEBS Lett.* 588:2530–36
99. Manival X, Charron C, Fourmann J-B, Godard F, Charpentier B, Branlant C. 2006. Crystal structure determination and site-directed mutagenesis of the *Pyrococcus abyssi* aCBF5–aNOP10 complex reveal crucial roles of the C-terminal domains of both proteins in H/ACA sRNP activity. *Nucleic Acids Res.* 34:826–39
100. Marrone A, Walne A, Dokal I. 2005. Dyskeratosis congenita: telomerase, telomeres and anticipation. *Curr. Opin. Genet. Dev.* 15:249–57
101. Martínez P, Blasco MA. 2015. Replicating through telomeres: a means to an end. *Trends Biochem. Sci.* 40:504–15
102. Mason M, Schuller A, Skordalakes E. 2011. Telomerase structure function. *Curr. Opin. Struct. Biol.* 21:92–100
103. Mason M, Wanat JJ, Harper S, Schultz DC, Speicher DW, et al. 2013. Cdc13 OB2 dimerization required for productive Stn1 binding and efficient telomere maintenance. *Structure* 21:109–20
104. Min B, Collins K. 2009. An RPA-related sequence-specific DNA-binding subunit of telomerase holoenzyme is required for elongation processivity and telomere maintenance. *Mol. Cell* 36:609–19
105. Miracco EJ, Jiang J, Cash DD, Feigon J. 2014. Progress in structural studies of telomerase. *Curr. Opin. Struct. Biol.* 24:115–24
106. Mitchell MT, Gillis A, Futahashi M, Fujiwara H, Skordalakes E. 2010. Structural basis for telomerase catalytic subunit TERT binding to RNA template and telomeric DNA. *Nat. Struct. Mol. Biol.* 17:513–18
107. Mitchell MT, Smith JS, Mason M, Harper S, Speicher DW, et al. 2010. Cdc13 N-terminal dimerization, DNA binding, and telomere length regulation. *Mol. Cell. Biol.* 30:5325–34
108. Mitton-Fry RM, Anderson EM, Hughes TR, Lundblad V, Wuttke DS. 2002. Conserved structure for single-stranded telomeric DNA recognition. *Science* 296:145–47
109. Mitton-Fry RM, Anderson EM, Theobald DL, Glustrom LW, Wuttke DS. 2004. Structural basis for telomeric single-stranded DNA recognition by yeast Cdc13. *J. Mol. Biol.* 338:241–55
110. Miyake Y, Nakamura M, Nabetani A, Shimamura S, Tamura M, et al. 2009. RPA-like mammalian Ctc1-Stn1-Ten1 complex binds to single-stranded DNA and protects telomeres independently of the Pot1 pathway. *Mol. Cell* 36:193–206
111. Nandakumar J, Bell CF, Weidenfeld I, Zaug AJ, Leinwand LA, Cech TR. 2012. The TEL patch of telomere protein TPP1 mediates telomerase recruitment and processivity. *Nature* 492:285–89
112. Nandakumar J, Cech TR. 2013. Finding the end: recruitment of telomerase to telomeres. *Nat. Rev. Mol. Cell Biol.* 14:69–82
113. Nelson AD, Shippen DE. 2015. Evolution of TERT-interacting lncRNAs: expanding the regulatory landscape of telomerase. *Front. Genet.* 6:277
114. Niederer RO, Zappulla DC. 2015. Refined secondary-structure models of the core of yeast and human telomerase RNAs directed by SHAPE. *RNA* 21:254–61
115. Nugent CI, Hughes TR, Lue NF, Lundblad V. 1996. Cdc13p: a single-strand telomeric DNA-binding protein with a dual role in yeast telomere maintenance. *Science* 274:249–52
116. O'Connor CM, Collins K. 2006. A novel RNA binding domain in *Tetrahymena* telomerase p65 initiates hierarchical assembly of telomerase holoenzyme. *Mol. Cell. Biol.* 26:2029–36
117. O'Connor CM, Lai CK, Collins K. 2005. Two purified domains of telomerase reverse transcriptase reconstitute sequence-specific interactions with RNA. *J. Biol. Chem.* 280:17533–39
118. O'Sullivan RJ, Karlseder J. 2010. Telomeres: protecting chromosomes against genome instability. *Nat. Rev. Mol. Cell Biol.* 11:171–81
119. Parks JW, Stone MD. Coordinated DNA dynamics during the human telomerase catalytic cycle. *Nat Commun.* 5:4146

120. Pfeiffer V, Lingner J. 2013. Replication of telomeres and the regulation of telomerase. *Cold Spring Harb. Perspect. Biol.* 5:a010405
121. Podlevsky JD, Bley CJ, Omana RV, Qi X, Chen JJ-L. 2008. The telomerase database. *Nucleic Acids Res.* 36:D339–43
122. Podlevsky JD, Chen JJ-L. 2016. Evolutionary perspectives of telomerase RNA structure and function. *RNA Biol.* 13:720–32
123. Prakash A, Borgstahl GE. 2012. The structure and function of replication protein A in DNA replication. *Subcell. Biochem.* 62:171–96
124. Premkumar VL, Cranert S, Linger BR, Morin GB, Minium S, Price C. 2014. The 3′ overhangs at *Tetrahymena thermophila* telomeres are packaged by four proteins, Pot1a, Tpt1, Pat1, and Pat2. *Eukaryot. Cell* 13:240–45
125. Price CM, Boltz KA, Chaiken MF, Stewart JA, Beilstein MA, Shippen DE. 2010. Evolution of CST function in telomere maintenance. *Cell Cycle* 9:3157–65
126. Qi H, Zakian VA. 2000. The *Saccharomyces* telomere-binding protein Cdc13p interacts with both the catalytic subunit of DNA polymerase α and the telomerase-associated Est1 protein. *Genes Dev.* 14:1777–88
127. Qiao F, Cech TR. 2008. Triple-helix structure in telomerase RNA contributes to catalysis. *Nat. Struct. Mol. Biol.* 15:634–40
128. Qiao F, Goodrich KJ, Cech TR. 2010. Engineering *cis*-telomerase RNAs that add telomeric repeats to themselves. *PNAS* 107:4914–18
129. Rajavel M, Mullins MR, Taylor DJ. 2014. Multiple facets of TPP1 in telomere maintenance. *Biochim. Biophys. Acta* 1844:1550–59
130. Rashid R, Liang B, Baker DL, Youssef OA, He Y, et al. 2006. Crystal structure of a Cbf5-Nop10-Gar1 complex and implications in RNA-guided pseudouridylation and dyskeratosis congenita. *Mol. Cell* 21:249–60
131. Rice C, Skordalakes E. 2016. Structure and function of the telomeric CST complex. *Comput. Struct. Biotechnol. J.* 14:161–67
132. Richard P, Darzacq X, Bertrand E, Jády BE, Verheggen C, Kiss T. 2003. A common sequence motif determines the Cajal body-specific localization of box H/ACA scaRNAs. *EMBO J.* 22:4283–93
133. Richards RJ, Theimer CA, Finger LD, Feigon J. 2006. Structure of the *Tetrahymena thermophila* telomerase RNA helix II template boundary element. *Nucleic Acids Res.* 34:816–25
134. Richards RJ, Wu H, Trantirek L, O'Connor CM, Collins K, Feigon J. 2006. Structural study of elements of *Tetrahymena* telomerase RNA stem-loop IV domain important for function. *RNA* 12:1475–85
135. Robart AR, Collins K. 2010. Investigation of human telomerase holoenzyme assembly, activity, and processivity using disease-linked subunit variants. *J. Biol. Chem.* 285:4375–86
136. Rouda S, Skordalakes E. 2007. Structure of the RNA-binding domain of telomerase: implications for RNA recognition and binding. *Structure* 15:1403–12
137. Sarek G, Marzec P, Margalef P, Boulton SJ. 2015. Molecular basis of telomere dysfunction in human genetic diseases. *Nat. Struct. Mol. Biol.* 22:867–74
138. Sauerwald A, Sandin S, Cristofari G, Scheres SH, Lingner J, Rhodes D. 2013. Structure of active dimeric human telomerase. *Nat. Struct. Mol. Biol.* 20:454–60
139. Savage SA, Bertuch AA. 2010. The genetics and clinical manifestations of telomere biology disorders. *Genet. Med.* 12:753–64
140. Schmidt JC, Cech TR. 2015. Human telomerase: biogenesis, trafficking, recruitment, and activation. *Genes Dev.* 29:1095–105
141. Schmidt JC, Dalby AB, Cech TR. 2014. Identification of human TERT elements necessary for telomerase recruitment to telomeres. *eLife* 3:e03563
142. Schnapp G, Rodi HP, Rettig WJ, Schnapp A, Damm K. 1998. One-step affinity purification protocol for human telomerase. *Nucleic Acids Res.* 26:3311–13
143. Schwartz S, Bernstein DA, Mumbach MR, Jovanovic M, Herbst RH, et al. 2014. Transcriptome-wide mapping reveals widespread dynamic-regulated pseudouridylation of ncRNA and mRNA. *Cell* 159:148–62

144. Sexton AN, Regalado SG, Lai CS, Cost GJ, O'Neil CM, et al. 2014. Genetic and molecular identification of three human TPP1 functions in telomerase action: recruitment, activation, and homeostasis set point regulation. *Genes Dev.* 28:1885–99
145. Sexton AN, Youmans DT, Collins K. 2012. Specificity requirements for human telomere protein interaction with telomerase holoenzyme. *J. Biol. Chem.* 287:34455–64
146. Shay JW. 2016. Role of telomeres and telomerase in aging and cancer. *Cancer Discov.* 6:584–93
147. Shefer K, Brown Y, Gorkovoy V, Nussbaum T, Ulyanov NB, Tzfati Y. 2007. A triple helix within a pseudoknot is a conserved and essential element of telomerase RNA. *Mol. Cell. Biol.* 27:2130–43
148. Shukla S, Schmidt JC, Goldfarb KC, Cech TR, Parker R. 2016. Inhibition of telomerase RNA decay rescues telomerase deficiency caused by dyskerin or PARN defects. *Nat. Struct. Mol. Biol.* 23:286–92
149. Singh M, Wang Z, Koo B-K, Patel A, Cascio D, et al. 2012. Structural basis for telomerase RNA recognition and RNP assembly by the holoenzyme La family protein p65. *Mol. Cell* 47:16–26
150. Stewart JA, Chaiken MF, Wang F, Price CM. 2012. Maintaining the end: roles of telomere proteins in end-protection, telomere replication and length regulation. *Mutat. Res.* 730:12–19
151. Stewart JA, Wang F, Chaiken MF, Kasbek C, Chastain PD II, et al. 2012. Human CST promotes telomere duplex replication and general replication restart after fork stalling. *EMBO J.* 31:3537–49
152. Stone MD, Mihalusova M, O'Connor CM, Prathapam R, Collins K, Zhuang X. 2007. Stepwise protein-mediated RNA folding directs assembly of telomerase ribonucleoprotein. *Nature* 446:458–61
153. Sugitani N, Chazin WJ. 2015. Characteristics and concepts of dynamic hub proteins in DNA processing machinery from studies of RPA. *Prog. Biophys. Mol. Biol.* 117:206–11
154. Sun J, Yang Y, Wan K, Mao N, Yu T-Y, et al. 2011. Structural bases of dimerization of yeast telomere protein Cdc13 and its interaction with the catalytic subunit of DNA polymerase α. *Cell Res.* 21:258–74
155. Sun J, Yu EY, Yang Y, Confer LA, Sun SH, et al. 2009. Stn1–Ten1 is an Rpa2–Rpa3-like complex at telomeres. *Genes Dev.* 23:2900–14
156. Surovtseva YV, Churikov D, Boltz KA, Song X, Lamb JC, et al. 2009. Conserved telomere maintenance component 1 interacts with STN1 and maintains chromosome ends in higher eukaryotes. *Mol. Cell* 36:207–18
157. Theimer CA, Blois CA, Feigon J. 2005. Structure of the human telomerase RNA pseudoknot reveals conserved tertiary interactions essential for function. *Mol. Cell* 17:671–82
158. Theimer CA, Feigon J. 2006. Structure and function of telomerase RNA. *Curr. Opin. Struct. Biol.* 16:307–18
159. Theimer CA, Jády BE, Chim N, Richard P, Breece KE, et al. 2007. Structural and functional characterization of human telomerase RNA processing and Cajal body localization signals. *Mol. Cell* 27:869–81
160. Townsley DM, Dumitriu B, Young NS. 2014. Bone marrow failure and the telomeropathies. *Blood* 124:2775–83
161. Tycowski KT, Shu M-D, Kukoyi A, Steitz JA. 2009. A conserved WD40 protein binds the Cajal body localization signal of scaRNP particles. *Mol. Cell* 34:47–57
162. Tzfati Y, Fulton TB, Roy J, Blackburn EH. 2000. Template boundary in a yeast telomerase specified by RNA structure. *Science* 288:863–67
163. Tzfati Y, Knight Z, Roy J, Blackburn EH. 2003. A novel pseudoknot element is essential for the action of a yeast telomerase. *Genes Dev.* 17:1779–88
164. Upton HE, Chan H, Feigon J, Collins K. 2017. Shared subunits of *Tetrahymena* telomerase holoenzyme and replication protein A have different functions in different cellular complexes. *J. Biol. Chem.* 292:217–28
165. Upton HE, Hong K, Collins K. 2014. Direct single-stranded DNA binding by Teb1 mediates the recruitment of *Tetrahymena thermophila* telomerase to telomeres. *Mol. Cell. Biol.* 34:4200–12
166. Venteicher AS, Abreu EB, Meng Z, McCann KE, Terns RM, et al. 2009. A human telomerase holoenzyme protein required for Cajal body localization and telomere synthesis. *Science* 323:644–48
167. Vogan JM, Zhang X, Youmans DT, Regalado SG, Johnson JZ, et al. 2016. Minimized human telomerase maintains telomeres and resolves endogenous roles of H/ACA proteins, TCAB1, and Cajal bodies. *eLife* 5:e18221
168. Wan B, Tang T, Upton H, Shuai J, Zhou Y, et al. 2015. The *Tetrahymena* telomerase p75–p45–p19 subcomplex is a unique CST complex. *Nat. Struct. Mol. Biol.* 22:1023–26

169. Wang F, Podell ER, Zaug AJ, Yang Y, Baciu P, et al. 2007. The POT1-TPP1 telomere complex is a telomerase processivity factor. *Nature* 445:506–10
170. Wang F, Stewart J, Price CM. 2014. Human CST abundance determines recovery from diverse forms of DNA damage and replication stress. *Cell Cycle* 13:3488–98
171. Wang Y, Yesselman JD, Zhang Q, Kang M, Feigon J. 2016. Structural conservation in the template/pseudoknot domain of vertebrate telomerase RNA from teleost fish to human. *PNAS* 113:E5125–34
172. Watson JM, Riha K. 2010. Comparative biology of telomeres: where plants stand. *FEBS Lett.* 584:3752–59
173. Wellinger RJ, Zakian VA. 2012. Everything you ever wanted to know about *Saccharomyces cerevisiae* telomeres: beginning to end. *Genetics* 191:1073–105
174. Wenz C, Enenkel B, Amacker M, Kelleher C, Damm K, Lingner J. 2001. Human telomerase contains two cooperating telomerase RNA molecules. *EMBO J.* 20:3526–34
175. Wu RA, Collins K. 2014. Human telomerase specialization for repeat synthesis by unique handling of primer-template duplex. *EMBO J.* 33:921–35
176. Wu RA, Dagdas YS, Yilmaz ST, Yildiz A, Collins K. 2015. Single-molecule imaging of telomerase reverse transcriptase in human telomerase holoenzyme and minimal RNP complexes. *eLife* 4:e08363
177. Wyatt HD, West SC, Beattie TL. 2010. InTERTpreting telomerase structure and function. *Nucleic Acids Res.* 38:5609–22
178. Xie M, Mosig A, Qi X, Li Y, Stadler PF, Chen JJ-L. 2008. Structure and function of the smallest vertebrate telomerase RNA from teleost fish. *J. Biol. Chem.* 283:2049–59
179. Xie M, Podlevsky JD, Qi X, Bley CJ, Chen JJ-L. 2010. A novel motif in telomerase reverse transcriptase regulates telomere repeat addition rate and processivity. *Nucleic Acids Res.* 38:1982–96
180. Xin H, Liu D, Wan M, Safari A, Kim H, et al. 2007. TPP1 is a homologue of ciliate TEBP-β and interacts with POT1 to recruit telomerase. *Nature* 445:559–62
181. Ye JZ-S, Hockemeyer D, Krutchinsky AN, Loayza D, Hooper SM, et al. 2004. POT1-interacting protein PIP1: a telomere length regulator that recruits POT1 to the TIN2/TRF1 complex. *Genes Dev.* 18:1649–54
182. Yu EY, Sun J, Lei M, Lue NF. 2012. Analyses of *Candida* Cdc13 orthologues revealed a novel OB fold dimer arrangement, dimerization-assisted DNA binding, and substantial structural differences between Cdc13 and RPA70. *Mol. Cell. Biol.* 32:186–98
183. Yu Y-T, Meier UT. 2014. RNA-guided isomerization of uridine to pseudouridine—pseudouridylation. *RNA Biol.* 11:1483–94
184. Zaug AJ, Podell ER, Cech TR. 2008. Mutation in TERT separates processivity from anchor-site function. *Nat. Struct. Mol. Biol.* 15:870–72
185. Zaug AJ, Podell ER, Nandakumar J, Cech TR. 2010. Functional interaction between telomere protein TPP1 and telomerase. *Genes Dev.* 24:613–22
186. Zeng Z, Min B, Huang J, Hong K, Yang Y, et al. 2011. Structural basis for *Tetrahymena* telomerase processivity factor Teb1 binding to single-stranded telomeric-repeat DNA. *PNAS* 108:20357–61
187. Zhang Q, Kim N-K, Feigon J. 2011. Architecture of human telomerase RNA. *PNAS* 108:20325–32
188. Zhang Q, Kim N-K, Peterson RD, Wang Z, Feigon J. 2010. Structurally conserved five nucleotide bulge determines the overall topology of the core domain of human telomerase RNA. *PNAS* 107:18761–68
189. Zhong FL, Batista LF, Freund A, Pech MF, Venteicher AS, Artandi SE. 2012. TPP1 OB-fold domain controls telomere maintenance by recruiting telomerase to chromosome ends. *Cell* 150:481–94